



# Hydraulic Response of Rubble Mound Breakwaters

## Scale Effects - Berm Breakwaters

Thomas Lykke Andersen

Hydraulics & Coastal Engineering  
Department of Civil Engineering  
Aalborg University

December 2006



Hydraulics & Coastal Engineering  
Department of Civil Engineering  
Aalborg University  
Sohngaardsholmsvej 57  
DK-9000 Aalborg, Denmark

ISSN 0909-4296  
SERIES PAPER No. 27

---

# Hydraulic Response of Rubble Mound Breakwaters

Scale Effects - Berm Breakwaters

by

Thomas Lykke Andersen

December 2006

Published 2006 by  
Hydraulics & Coastal Engineering  
Department of Civil Engineering  
Aalborg University

Printed in Denmark by  
Aalborg University

ISSN 0909-4296  
SERIES PAPER No. 27

## PREFACE

The present thesis *Hydraulic Response of Rubble Mound Breakwaters. Scale Effects - Berm Breakwaters* was submitted as one of the requirements set out in the Ministerial Order No. 114 of 8. March 2002 regarding Ph.D. studies. The thesis was defended publicly on 20.06.2006 at Aalborg University.

The thesis consist of the present book and an associated CD-Rom. The text book includes the main report and the CD-Rom include the main report and the appendices in pdf format.

The Ph.D. study has been performed during the period from 15. September 2002 to 15. November 2005 at Department of Civil Engineering, Hydraulics and Coastal Engineering, Aalborg University, under supervision of professor Dr. Techn. Hans F. Burcharth.

The study was partly financed by the CLASH project EVK3-CT-2001-00058 within the EESD programme of the Fifth Framework Programme of the EU. The financial contribution of the European Community is acknowledged.

As a part of the Ph.D. study the author have benefited from a three month stay at Laboratori d'Enginyeria Marítima (LIM), Universitat Politècnica de Catalunya (UPC), Barcelona, Spain. Financial support by Det Obelske Familiefond, The Faculty of Engineering and Science, Aalborg University and Department of Civil Engineering, Aalborg University made it possible to perform large scale tests in the large wave channel at LIM. Their financial support is acknowledged. The large scale tests were carried out as a joint research project between UPC and AAU. The fruitful co-operation is acknowledged very much.

In addition to the present thesis the research resulted in a number of other publications. Among these are:

- Burcharth, H. F. and Lykke Andersen, T. (2003). *Overtopping and Rear Slope Stability of Reshaping Breakwaters*. Sixth International Conference

on Coastal & Port Engineering in Developing Countries, Colombo, Sri Lanka.

- Lykke Andersen, T. and Burcharth, H. F. (2004). *Overtopping and Rear Slope Stability of Reshaping & Non-reshaping Berm Breakwaters*. The 29th International Conference on Coastal Engineering, ICCE 2004, Lisbon, Portugal.
- Lykke Andersen, T. and Burcharth, H. F. (2004). *CLACH: D24 Report on Additional Tests, Part A: Effect of Obliqueness, Short-Crested Waves and Directional Spreading*. Aalborg University.
- Lykke Andersen, T. and Burcharth, H. F. (2004). *CLACH: D24 Report on Additional Tests, Part D: Reshaping Breakwater Tests*. Aalborg University.
- Lykke Andersen, T. and Burcharth, H. F. (2005). *Overtopping of Berm Breakwaters Extension of Overtopping Formula*. Second International Coastal Symposium in Iceland, Höfn, Iceland.
- Lykke Andersen, T. (2002-2006). *WaveLab2. A software package for data acquisition and analysis* [Aalborg University, 2005b].
- Lykke Andersen, T. and Burcharth, H. F. (2006). *Landward Distribution of Wave Overtopping for Rubble Mound Breakwaters*. 1st International Conference on the Application of Physical Modelling to Port and Coastal Protection, CoasLab06, Porto, Portugal.

Last but not least the author wishes to thank his colleagues and the technical staff within the department for their support and assistance.

Aalborg, 12.12.2006

Thomas Lykke Andersen

# CONTENTS

<b>1</b>	<b>Hydraulic Response of Rubble Mound Breakwaters</b>	<b>1</b>
1.1	Types of Rubble Mound Breakwaters . . . . .	1
1.2	Failure Modes of Rubble Mound Breakwaters . . . . .	4
1.3	Wave Impact on Rubble Slopes . . . . .	5
1.4	Wave Run-up and Run-Down . . . . .	6
1.4.1	Delft Hydraulics, 1989 . . . . .	8
1.4.2	Murphy and Kingston, 1996 . . . . .	8
1.4.3	TAW, 2002 . . . . .	8
1.5	Wave Overtopping . . . . .	9
1.5.1	TAW, 2002 . . . . .	14
1.5.2	CLASH NN-Model . . . . .	14
1.6	Hydraulic Stability of Front Armour Layers . . . . .	15
1.6.1	Hudson, 1958 . . . . .	16
1.6.2	Van der Meer, 1988 . . . . .	16
1.7	Hydraulic Stability of Rear Armour Layers . . . . .	17
1.7.1	Van der Meer and Veldman, 1992 . . . . .	17
1.7.2	Andersen et al., 1992 . . . . .	18
1.7.3	Verhagen et al., 2003 . . . . .	18
1.7.4	Van Gent and Pozueta, 2004 . . . . .	19
1.8	Wave Reflection . . . . .	19
1.8.1	Seeling, 1983 . . . . .	20
1.8.2	Postma, 1989 . . . . .	20
1.8.3	Alikhani, 2000 . . . . .	21
1.9	Wave Transmission . . . . .	21
1.10	Objectives . . . . .	22
<b>2</b>	<b>The Berm Breakwater Concept</b>	<b>23</b>
2.1	Reshaping Berm Breakwaters . . . . .	24

2.2	Non-Reshaping Berm Breakwaters . . . . .	26
2.3	Multi-Layer Berm Breakwaters . . . . .	26
2.4	Redistribution of Material . . . . .	27
2.5	3-Dimensional Effects . . . . .	27
2.6	Construction Methods . . . . .	28
2.7	Quarry Material . . . . .	29
2.8	Fines . . . . .	31
2.9	Designing Berm Breakwaters . . . . .	32
<b>3</b>	<b>New Data from Present Berm Breakwater Tests</b>	<b>33</b>
3.1	Test Set-Up . . . . .	33
3.2	Data Analysis . . . . .	37
3.3	Test Series - Range of Parameters . . . . .	37
3.4	Tests in Smaller Scale to Study Scale Effects . . . . .	39
3.5	Tests with Fixed Front to Study Influence of Reshaping . . . . .	40
<b>4</b>	<b>Front Slope Stability of Berm Breakwaters</b>	<b>43</b>
4.1	Existing Methods for Estimating the Berm Recession . . . . .	44
4.1.1	Van der Meer, 1992 . . . . .	45
4.1.2	Hall and Kao, 1991 . . . . .	45
4.1.3	Tørum, 1998 . . . . .	46
4.1.4	Tørum and Krogh, 2000 . . . . .	46
4.1.5	Summary . . . . .	47
4.2	Development of Semi-Empirical Recession Formula . . . . .	47
4.2.1	Influence of Slope, Water Depth and Berm Elevation . . . . .	47
4.2.2	Influence of Wave Direction . . . . .	52
4.2.3	Influence of Number of Waves . . . . .	52
4.2.4	Influence of Stone Gradation and Shape . . . . .	53
4.2.5	Step Height $h_s$ . . . . .	54
4.2.6	Influence of Stability Numbers . . . . .	55
4.2.7	Influence of Breaking Waves . . . . .	59
4.2.8	Influence of Wave Groupiness . . . . .	61
4.2.9	Influence of a Low Berm . . . . .	62
4.2.10	Verification of Influence of Slope, Water Depth and Berm Elevation . . . . .	63
4.2.11	Verification of Influence of Wave Direction . . . . .	65
4.2.12	Verification of Influence of Number of Waves . . . . .	65
4.2.13	Verification of Influence of Stone Gradation . . . . .	66



4.2.14	Proposed Recession Formula . . . . .	66
4.2.15	A Simple Method for Estimating Wave Skewness . . . . .	68
4.3	Evaluation of Proposed and Existing Recession Formulae . . . . .	69
4.3.1	Present data . . . . .	71
4.3.2	Instones, 1987 . . . . .	73
4.3.3	Tørum et al., 1988 . . . . .	74
4.3.4	Van der Meer, 1988 . . . . .	75
4.3.5	Burcharth and Frigaard, 1990 . . . . .	76
4.3.6	Andersen and Poulsen, 1991 . . . . .	77
4.3.7	Hall, 1991 . . . . .	78
4.3.8	Lissev, 1993 . . . . .	79
4.3.9	Aalborg University, 1995 . . . . .	80
4.3.10	DHI, 1995 . . . . .	81
4.3.11	DHI, 1996 . . . . .	82
4.3.12	Porarinsson, 2004 . . . . .	83
4.3.13	Examples of measured and calculated recession and profiles	84
4.3.14	Summary . . . . .	87
4.4	Uncertainty Estimation . . . . .	89
4.5	Scale Effects . . . . .	93
4.6	Summary on Front Slope Stability of Berm Breakwaters . . . . .	96
<b>5</b>	<b>Overtopping of Berm Breakwaters</b>	<b>97</b>
5.1	TAW, 2002 . . . . .	97
5.2	CLASH NN-Model . . . . .	99
5.3	Proposed Simple Overtopping Formula . . . . .	100
5.4	Overtopping of Non-Reshaped vs. Reshaped Profiles . . . . .	104
5.5	Scale Effects . . . . .	106
5.6	Comparison with Other Overtopping Data . . . . .	107
5.6.1	Bolatti Guzzo and Marconi, 1991 . . . . .	108
5.6.2	Lissev, 1993 . . . . .	109
5.6.3	Viggosson et al., 1993 . . . . .	110
5.6.4	Kuhnen, 2000 . . . . .	112
5.6.5	Porarinsson, 2004 . . . . .	112
5.7	Summary on Overtopping of Berm Breakwaters . . . . .	113
<b>6</b>	<b>Rear Slope Stability of Berm Breakwaters</b>	<b>115</b>
<b>7</b>	<b>Reflection from Berm Breakwaters</b>	<b>121</b>

<b>8</b>	<b>Berm Breakwater Design Example</b>	<b>125</b>
8.1	Design Criteria . . . . .	125
8.1.1	Sea States . . . . .	125
8.1.2	Available Rock . . . . .	126
8.1.3	Stability Criteria for the Berm . . . . .	126
8.1.4	Allowable Overtopping . . . . .	127
8.2	Design of Breakwater . . . . .	127
8.2.1	Berm Geometry . . . . .	127
8.2.2	Top Geometry and Rear Side Armour . . . . .	129
8.2.3	Scour Protection . . . . .	132
<b>9</b>	<b>Overtopping Scale Effects, Review of Existing Knowledge</b>	<b>133</b>
9.1	Vertical Smooth Structures . . . . .	134
9.2	Rubble Mound Structures . . . . .	135
9.3	Viscosity Scale Effects . . . . .	136
9.3.1	Wave Celerity . . . . .	136
9.3.2	Porous Flow Scale Effect . . . . .	136
9.3.3	Run-Up Flow . . . . .	139
9.4	Surface Tension Scale Effects . . . . .	141
9.5	Wind Scale and Model Effects . . . . .	142
9.6	Numerical Computations . . . . .	144
9.7	Prototype Measurements . . . . .	144
9.7.1	Fukui Seawall . . . . .	145
9.7.2	Zeebrugge Breakwater . . . . .	145
9.7.3	Ostia Breakwater . . . . .	147
9.7.4	Scale/Model Effects . . . . .	148
9.8	Large Scale Measurements . . . . .	150
9.8.1	Armour Covered Seawalls . . . . .	150
9.8.2	Rock Armoured Rubble Mound Breakwater . . . . .	151
9.8.3	Accropode Armoured Rubble Mound Breakwater . . . . .	151
9.9	Summary on Existing Knowledge on Overtopping Scale Effects . . . . .	151
9.9.1	Theoretical Considerations . . . . .	151
9.9.2	Prototype Measurements . . . . .	152
9.9.3	Large Scale Measurements . . . . .	152
9.9.4	Numerical Computations . . . . .	152
9.9.5	Wind . . . . .	153
<b>10</b>	<b>Overtopping Scale Effects, New Large Scale Tests</b>	<b>155</b>

10.1	Test Set-Up & Data Analysis . . . . .	156
10.1.1	Bottom Configuration . . . . .	157
10.1.2	Breakwater Cross Sections . . . . .	157
10.1.3	Quarry Materials for the Breakwater . . . . .	159
10.1.4	Wave Measurements . . . . .	162
10.1.5	Wave Set-Up Measurements . . . . .	163
10.1.6	Overtopping Measurements . . . . .	164
10.1.7	Wave Run-Up Measurements . . . . .	166
10.1.8	Overtopping Impact Force Measurements . . . . .	167
10.2	Test Programme . . . . .	171
10.3	Comparison of Generated Waves in Large and Small Scale Experiments . . . . .	172
10.3.1	Wave Spectra and Wave Height Distributions Examples . . . . .	173
10.3.2	Wave Height Distributions from all Tests . . . . .	177
10.3.3	Wave Skewness . . . . .	178
10.3.4	Wave Groupiness . . . . .	178
10.4	Model Effects . . . . .	179
10.5	Results . . . . .	180
10.5.1	Wave Propagation and Wave Breaking . . . . .	180
10.5.2	Wave Reflection . . . . .	181
10.5.3	Wave Set-Up and Wave Transmission . . . . .	182
10.5.4	Run-Up . . . . .	184
10.5.5	Overtopping . . . . .	186
10.5.6	Influence of Surface Tension and Air Entrainment . . . . .	200
10.5.7	Spatial Distribution of Overtopping Behind the Shoreward Edge of the Breakwater Crest . . . . .	200
10.5.8	Forces from Overtopping . . . . .	209
10.6	Summary on Scale Effects related to Overtopping . . . . .	211
<b>11</b>	<b>Guidelines on Scale Effects</b>	<b>215</b>
11.1	Evaluation of Guidelines on Zeebrugge data . . . . .	217
11.2	Evaluation of Guidelines on Ostia data . . . . .	218
<b>12</b>	<b>Conclusions</b>	<b>219</b>
12.1	Berm Breakwaters . . . . .	219
12.2	Overtopping Scale Effects . . . . .	220
	<b>Bibliography</b>	<b>223</b>

Appendices (available on enclosed CD-Rom)

<b>A</b>	<b>Table with Berm Breakwater Test Results</b>	<b>233</b>
<b>B</b>	<b>Profile Measurements from Berm Breakwater Tests</b>	<b>249</b>
<b>C</b>	<b>Existing Data from Previous Berm Breakwater Tests</b>	<b>363</b>
C.1	Instanes, 1987 . . . . .	363
C.2	Tørum et al., 1988 . . . . .	364
C.3	Van der Meer, 1988 . . . . .	365
C.4	Burcharth and Frigaard, 1990 . . . . .	366
C.5	Andersen and Poulsen, 1991 . . . . .	367
C.6	Hall, 1991 . . . . .	368
C.7	Lissev, 1993 . . . . .	368
C.8	Viggosson et al., 1993 . . . . .	369
C.9	Aalborg University, 1995 . . . . .	371
C.10	DHI, 1995 . . . . .	373
C.11	DHI, 1996 . . . . .	374
C.12	Kuhnen, 2000 . . . . .	375
C.13	Porarinsson, 2004 . . . . .	376
C.14	Summary . . . . .	377
<b>D</b>	<b>Evaluation of Berm Breakwater Overtopping Formula against Dimensionless Parameters</b>	<b>379</b>
<b>E</b>	<b>Conventional Breakwater, Large Scale Test Results</b>	<b>387</b>
<b>F</b>	<b>Conventional Breakwater, Small Scale Test Results, Core 1</b>	<b>391</b>
<b>G</b>	<b>Conventional Breakwater, Small Scale Test Results, Core 2</b>	<b>395</b>
<b>H</b>	<b>Conventional Breakwater, Conventional Overtopping Plots</b>	<b>399</b>
H.1	Low Wall . . . . .	400
H.2	Normal Wall . . . . .	402
H.3	High Wall . . . . .	404
H.4	High Recurved Wall . . . . .	406

## LIST OF SYMBOLS

$\alpha$	Slope angle [°].
$\alpha_d$	Lower front slope (below berm) [°].
$\alpha_r$	Rear slope [°].
$\alpha_u$	Upper front slope (above berm) [°].
$\beta$	Mean wave direction [°].
$\delta = \frac{\sigma}{\mu}$	Coefficient of variation.
$\Delta = \frac{\rho_s}{\rho_w} - 1$	Relative reduced mass density.
$\Delta R$	Movement of profile at bottom [m].
$\Delta h$	Difference in hydraulic head [m].
$\epsilon_2 = \sqrt{\frac{m_0 \cdot m_2}{m_1^2} - 1}$	Spectral width parameter (narrowness parameter).
$\epsilon_4 = \sqrt{1 - \frac{m_2^2}{m_0 \cdot m_4}}$	Spectral width parameter (broadness factor).
$\eta$	Surface elevation [m].
$\gamma$	Peak enhancement factor in JONSWAP spectrum.
$\gamma_\beta$	Reduction factor for wave direction.
$\gamma_b$	Reduction factor for a berm.
$\gamma_f$	Reduction factor for roughness and permeability.
$\gamma_s$	Reduction factor for scale effects. $\gamma_s = 1.0$ for prototype conditions.
$\gamma_v$	Reduction factor for a vertical or nearly vertical crown wall.
$\mu$	Average value.
$\nu$	Kinematic viscosity of fluid [m <sup>2</sup> /s]
$\rho$	Density [kg/m <sup>3</sup> ].
$\rho_s$	Mass density of stone material [kg/m <sup>3</sup> ].
$\rho_w$	Mass density of water [kg/m <sup>3</sup> ].

$\sigma$	Standard deviation.
$\sigma$	Surface tension ( $\sigma \approx 0.073$ N/m for fresh water) [N/m].
$\varphi$	Angle of repose [ $^{\circ}$ ].
$\xi = \frac{\tan(\alpha)}{\sqrt{s}}$	Surf similarity parameter.
$\xi_{0m} = \frac{\tan(\alpha)}{\sqrt{s_{0m}}}$	Surf similarity parameter based on mean deep water steepness.
$\xi_{0p} = \frac{\tan(\alpha)}{\sqrt{s_{0p}}}$	Surf similarity parameter based on peak deep water steepness.
$\xi_0 = \frac{\tan(\alpha)}{\sqrt{s_0}}$	Surf similarity parameter based on deep water steepness.
$\zeta$	Damping ratio.
$a$	Acceleration [ $\text{m/s}^2$ ].
$A_c$	Armour crest freeboard which is the vertical distance from the armour crest to SWL. Defined in Fig. 1.6 [m].
$A_e$	Eroded cross-section area [ $\text{m}^2$ ].
$b$	Shortest side of stone [m].
$b_1 = \frac{1}{N} \sum_{j=1}^N \left( \frac{\eta_j - \bar{\eta}}{\sigma(\eta)} \right)^3$	Skewness of surface elevation.
$b_2 = \frac{1}{N} \sum_{j=1}^N \left( \frac{\eta_j - \bar{\eta}}{\sigma(\eta)} \right)^4$	Kurtosis of surface elevation.
$B$	Berm width [m].
$B_{\star} = \frac{B}{H_{m0}}$	Dimensionless berm width.
$c = \frac{L}{T}$	Wave celerity [m/s].
$C_r = \frac{H_{m0,r}}{H_{m0,i}}$	Reflection coefficient.
$C_t = \frac{H_{m0,t}}{H_{m0,i}}$	Transmission coefficient.
$D$	Diameter [m].
$D_{15}$	Sieve diameter exceeded by 85% of a sample [m].
$D_{50}$	Sieve diameter exceeded by 50% of a sample [m].
$D_{85}$	Sieve diameter exceeded by 15% of a sample [m].
$D_n = \left( \frac{W}{\rho_s} \right)^{1/3}$	Nominal diameter/Equivalent cube length [m].
$D_{n,15} = \left( \frac{W_{15}}{\rho_s} \right)^{1/3}$	Equivalent cube length exceeded by 85% of a sample (by weight) [m].
$D_{n,50} = \left( \frac{W_{50}}{\rho_s} \right)^{1/3}$	Equivalent cube length exceeded by 50% of a sample (by weight) [m].
$D_{n,85} = \left( \frac{W_{85}}{\rho_s} \right)^{1/3}$	Equivalent cube length exceeded by 15% of a sample (by weight) [m].
$D_{s,50} = \left( \frac{6 \cdot W_{50}}{\pi \cdot \rho_s} \right)^{1/3}$	Equivalent sphere diameter exceeded by 50% of a sample (by weight) [m].

$E_i$	Incident wave energy [J].
$E_r$	Reflected wave energy [J].
$E_t$	Transmitted wave energy [J].
$f$	Frequency [Hz].
$f_0$	Eigenfrequency [Hz].
$f_{H0}$	Factor accounting for the influence of stability numbers.
$f_N$	Factor accounting for the influence of number of waves.
$f_\beta$	Factor accounting for the influence of wave direction.
$f_d$	Factor accounting for the influence of depth.
$f_g = \frac{D_{n,85}}{D_{n,15}}$	Gradation factor of rock material.
$f_{grading}$	Factor accounting for the influence of stone gradation.
$f_{hb}$	Factor accounting for the influence of berm elevation.
$f_p$	Peak frequency [Hz].
$f_{scale}$	Multiplikation factor on small scale overtopping measurements to take into account scale effects.
$f_{skewness}$	Factor accounting for the influence of wave skewness.
$F$	Force [N].
$F_D$	Drag force [N].
$F_G$	Gravity force [N].
$F_L$	Lift force [N].
$g \approx 9.82 \text{ m/s}^2$	Acceleration due to gravity [ $\text{m/s}^2$ ].
$GF$	Wave groupiness factor.
$G_\star = \frac{G_c}{H_{m0}}$	Dimensionless armour crest width.
$G_c$	Width of armour in front of eventual crest element [m].
$h$	Water depth [m].
$h_b$	Water depth above berm (negative if berm is elevated above SWL) [m].
$h_{b\star} = \frac{3 \cdot H_{m0} - h_b}{3 \cdot H_{m0} + R_c}$	Dimensionless berm elevation.
$h_f$	Water depth above point of intersection of initial and reshaped profile [m].
$h_s$	Water depth above step [m].
$H$	Wave height [m].
$H_0 = \frac{H_{m0}}{\Delta \cdot D_{n,50}}$	Stability number.
$H_0 T_0 = H_0 \cdot T_0$	Stability number including mean wave period.

$H_{1/n}$	Average height of waves exceeded by n% of the waves in a record [m].
$H_m$	Mean wave height calculated from the time domain analysis [m].
$H_{m0} = \sqrt{4 \cdot m_0}$	Significant wave height based on frequency domain analysis [m].
$H_{m0,i}$	Incident significant wave height based on frequency domain analysis [m].
$H_{m0,r}$	Reflected significant wave height based on frequency domain analysis [m].
$H_{m0,t}$	Transmitted significant wave height based on frequency domain analysis [m].
$H_{max}$	Maximum wave height based on time domain analysis [m].
$H_s = H_{1/3}$	Significant wave height based on time domain analysis [m].
$H_{xx\%}$	Wave height with xx% exceedance probability based on time domain analysis [m].
$I = \frac{\Delta h}{L}$	Hydraulic gradient.
$I_c$	Hydraulic gradient transition point from Forchheimer to fully turbulent regime.
$K$	Compressibility [ $\frac{kg}{m \cdot s^2}$ ].
$KC = \frac{u_{max} \cdot T}{D}$	Keulegan-Carpenter number.
$K_D$	Stability coefficient in the Hudson formula.
$l$	Longest side of stone [m].
$L$	Length [m].
$L$	Wave length [m].
$L_{0m} = \frac{g \cdot T_m^2}{2 \cdot \pi}$	Mean deep water wave length [m].
$L_{0p} = \frac{g \cdot T_p^2}{2 \cdot \pi}$	Peak deep water wave length [m].
$m_n = \int S_\eta(f) \cdot f^n df$	n order moment of spectra [ $m^2/s^n$ ].
$MWL$	Mean water level [m].
$N$	Number of waves.
$N_F$	Scaling ratio for forces.
$N_K$	Scaling ratio for compressibility.
$N_L$	Scaling ratio for lengths.
$N_\nu$	Scaling ratio for viscosity.
$N_\rho$	Scaling ratio for densities.
$N_\sigma$	Scaling ratio for surface tensions.
$N_a$	Scaling ratio for accelerations.



$N_p$	Scaling ratio for pressures.
$N_q$	Scaling ratio for overtopping discharges per meter width.
$N_t$	Scaling ratio for time.
$N_u$	Scaling ratio for velocities.
$P$	Notational permeability as defined in Van der Meer, 1988.
$P_R$	Fraction of rounded stones in a sample.
$q$	Mean overtopping discharge per meter structure width [m <sup>3</sup> /m/s].
$q^* = \frac{q}{\sqrt{g \cdot H_{m0}^3}}$	Dimensionless mean overtopping discharge.
$q_{SS}$	Overtopping discharge measured in small scale, but scaled to prototype scale [m <sup>3</sup> /m/s].
$Q$	Discharge [m <sup>3</sup> /s].
$R_* = \frac{R_c}{H_{m0}}$	Dimensionless crest freeboard.
$R_c$	Crest freeboard which is the vertical distance from SWL to the point where the overtopping is measured. This is not always equal to the highest point of the structure, cf. Fig. 1.6 [m].
$R_u$	Run-up height [m].
$R_{u,2\%}$	Run-up height with 2% exceedance probability [m].
$Re = \frac{u \cdot L}{\nu}$	Reynolds number.
$Re_D = \frac{D_{n,50} \cdot \sqrt{g \cdot H_{m0}}}{\nu}$	Reynolds number for armour elements.
$Rec$	Recession of the berm [m].
$Rec^{50\%}$	Recession of the berm with 50% non-exceedance probability [m].
$Rec^{5\%}$	Recession of the berm with 5% non-exceedance probability [m].
$Rec^{95\%}$	Recession of the berm with 95% non-exceedance probability [m].
$Rec_{SWL}$	Recession of berm but measured at still water level [m].
$s = \frac{H}{L}$	Wave steepness.
$s_{0m} = \frac{H_{m0}}{L_{0m}}$	Deep water mean wave steepness.
$s_{0p} = \frac{H_{m0}}{L_{0p}}$	Deep water peak wave steepness.
$s_0 = \frac{H_{m0}}{L_{0m}}$	Deep water wave steepness.
$S = \frac{A_e}{D_{n,50}^2}$	Damage parameter.
$SWL$	Still water level [m].
$S_\eta$	Spectral density [m <sup>2</sup> ·s].
$T$	Wave period [s].

$T_{-1,0} = \frac{m-1}{m_0}$	Wave period based on frequency domain analysis [s].
$T_{0,1} = \frac{m_0}{m_1}$	Mean wave period based on frequency domain analysis [s].
$T_{0,2} = \sqrt{\frac{m_0}{m_2}}$	Mean wave period based on frequency domain analysis [s].
$T_0 = \sqrt{\frac{g}{D_{n,50}}} \cdot T_{0,1}$	Dimensionless wave period.
$T_0^*$	Dimensionless wave period transition point.
$T_m$	Mean wave period [s].
$T_p$	Peak wave period [s].
$T_z$	Mean wave period based on zero-down crossing analysis [s].
$u$	Flow velocity [m/s].
$u_{1\%}$	Run-up velocity with 1% exceedance probability [m/s].
$u_c$	Velocity transition point from Forchheimer to fully turbulent regime [m/s].
$Ur = \frac{H}{2 \cdot h \cdot (k \cdot h)^2}$	Ursell number.
$V_{max}$	Maximum single wave overtopping volume [m <sup>3</sup> /m].
$W$	Weight [kg].
$W_{15}$	Weight exceeded by 85% of a sample [kg].
$W_{50}$	Weight exceeded by 50% of a sample [kg].
$W_{85}$	Weight exceeded by 15% of a sample [kg].

## SUMMARY

Rubble mound breakwaters have been extensively investigated in the last decades. Nevertheless, there still exists some white spots where only little knowledge and only poor design rules are available. Some of these white spots are due to new types of structures developed in recent years.

In this thesis is presented results from two experimental studies, in which the focus has been on overtopping of berm breakwaters and scale effects related to overtopping of conventional rubble mound breakwaters.

The berm breakwater is a fairly new type of structure considered in harbour protection. The present experimental test programme with berm breakwaters, has not only resulted in an enormous amount of overtopping data, but also establishment of a design formula to calculate average overtopping discharges. Further, the test programme led to an improved design rule for front side stability of berm breakwaters, which was not actually identified as a white spot, but still there was room for big improvements. Rear slope stability and wave reflection has been discussed briefly.

The conventional rubble mound breakwater has been investigated for many decades. Anyhow, there is still room for improvements in some areas. One very important white spots is the uncertainty related to overtopping measured in a small scale model. There are some indications of rather large scale effects, which seems especially pronounced for low overtopping discharges, with unsafe results obtained in the model. This was investigated in the CLASH project, where comparisons of prototype and model data were performed. However, the problem was not completely solved in the CLASH project as many possible model effects were identified. In the present project small and large scale tests have been performed. These tests led to the conclusion that overtopping scale effects are most pronounced for structures with a low crown wall, where scale effect may go up to a factor of 20. For a crown wall higher than the armour crest, only small scale effects were identified.



## SUMMARY IN DANISH

Stenkastningsbølgebrydere har været undersøgt i stor udstrækning i de sidste årtier. Ikke desto mindre findes der stadig nogle delområder, hvor kun lidt viden og kun design formler af tvivlsom kvalitet er til rådighed. Nogle af disse hvide pletter skyldes nye konstruktionstyper udviklet inden for de sidste år.

I denne afhandling er der præsenteret resultater fra to eksperimentelle studier, hvor fokus har været på overskyl af banketmoler og skalaeffekter relateret til overskyl af konventionelle stenkastningsmoler.

Banketmolen er en forholdsvis ny type konstruktion anvendt som bølgebryder i forbindelse med havne. Nærværende test program har ikke kun ledt til en enorm mængde overskyldsdata, men også til etablering af en design formel til bestemmelse af middelloverskyls mængder. Derudover førte test programmet til forbedrede design formler for forside stabilitet af banketmoler, hvilket egentlig ikke i første omgang blev identificeret som en hvid plet, men der var alligevel plads til store forbedringer. Bagside stabilitet og refleksion er i mindre omfang også diskuteret.

Den konventionelle stenkastnings mole har været undersøgt i mange årtier. Alligevel er der i visse områder plads til forbedringer og brug for ny viden. En meget vigtig hvid plet er uklarheden omkring skalering af overskyl bestemt ved modelforsøg i lille skala. Der er visse indikationer på forholdsvis store skalaeffekter, særlig udpræget for små overskylsmængder, hvor resultater på den usikre side opnås i lille skala. Dette blev undersøgt i CLASH projektet, hvor målinger i prototype og lille skala blev sammenlignet. Problemet blev dog ikke fuldstændig løst i CLASH projektet, da mange mulige modeffekter blev identificeret. I nærværende projekt er der blevet udført små- og storskala forsøg. Disse forsøg førte til konklusionen at skalaeffekter på overskyl er mest udpræget for moler med en lav overbygning, hvor skalaeffekter op til en faktor 20 på overskylsmængden er fundet. I tilfælde hvor moleoverbygningen er højere end kronen af dæklaget blev der kun identificeret små skalaeffekter.



## CHAPTER 1

# Hydraulic Response of Rubble Mound Breakwaters

Rubble mound breakwaters have for more than a century been used worldwide to protect harbour basins against the violent forces of the surrounding sea. Breakwaters are constructed to create sufficiently calm waters for safe mooring and loading operations, handling of ships and protection of harbor facilities.

Until the late 1960'ties rubble mound breakwaters were used in relatively shallow water wave conditions only. However, since that time the need for bigger ships and harbors has resulted in many breakwaters now are located in deeper water, where no previous experience was available at that time. This development resulted in the failure of several large rubble mound breakwaters in the 1970'ties. The research since then has resulted in much more knowledge and new generally accepted design rules and concepts has been developed.

In this chapter is given an introduction to hydraulic response of rubble mound breakwaters, with the purpose to define white spots and select some of these for further investigations in the present project. Moreover, fundamental background knowledge and formulae to be used in the rest of the thesis are presented.

## 1.1 Types of Rubble Mound Breakwaters

The rubble mound breakwater is the most commonly applied type of breakwater. A rubble mound breakwater dissipates the main part of the incoming wave energy by wave breaking on the slope and partly by porous flow in the mound. The remaining energy is partly reflected back to the sea and partly transmitted into

## 1.1 Types of Rubble Mound Breakwaters

---

the harbour area by wave penetration and wave overtopping.

Various kinds of rubble mound breakwaters have been constructed depending on the purpose of the breakwater, cf. Fig. 1.1.

The most simple rubble mound breakwater consist only of a mound of stones (Fig. 1.1-a). However, this type of structure is very permeable and will cause heavy penetration of waves and sediment. Moreover, large stones are expensive because most quarries yield a lot of finer material and relatively few large stones.

Fig. 1.1-b and 1.1-c are the two most common types of rubble mound breakwaters and are known as conventional rubble mound breakwaters with and without a superstructure. Even though the two types of structures appear different the structures have several points of resemblance. Both breakwaters consists of a core of fine material covered by layers of larger units preventing the fine core material from being washed out. The outer seaward layer, the armour layer, consist of units of rock or concrete, large and heavy enough to remain in their position during design wave conditions. The inclination of the the front slope is one of the parameters that determines the required mass of the armour unit. Concrete armour units are typically more expensive than rock, but in some cases large enough rock is not available near by, unless a very flat front slope of the breakwater is applied. Using a flat front slope increases the needed volume of material, and hence the construction costs, dramatically. The maximum size of rocks that quarries can yield and handle is at the moment 20-30 tons. For rock typical front slope inclinations are in the range 1:1.5 to 1:4 depending on the available rock and the soil conditions. In case of concrete armour units a steep front slope is for most types of units used, as the weight of the above lying units has a stabilizing effect. Typically 1:1 to 1:2 is used for concrete units depending on the interlocking of the units. Unless the breakwater is located on a rock bottom, a toe is constructed to provide a safe base for the armour layer. On the rear side an armour layer is constructed to protect the breakwater against overtopping waves and waves in the harbour basin. Fig. 1.1-b shows a structure primary used in relatively shallow water, where berthing along the breakwater and access on the breakwater is not required. In these cases relatively large amounts of wave overtopping are typically allowed. In Fig. 1.1-c is shown a breakwater with a concrete superstructure, which works as a shelter for the overtopping waves and an access road for repairment and traffic to and from the breakwater. For similar overtopping conditions a structure with a crown wall needs significant smaller volume of material.



## Hydraulic Response of Rubble Mound Breakwaters

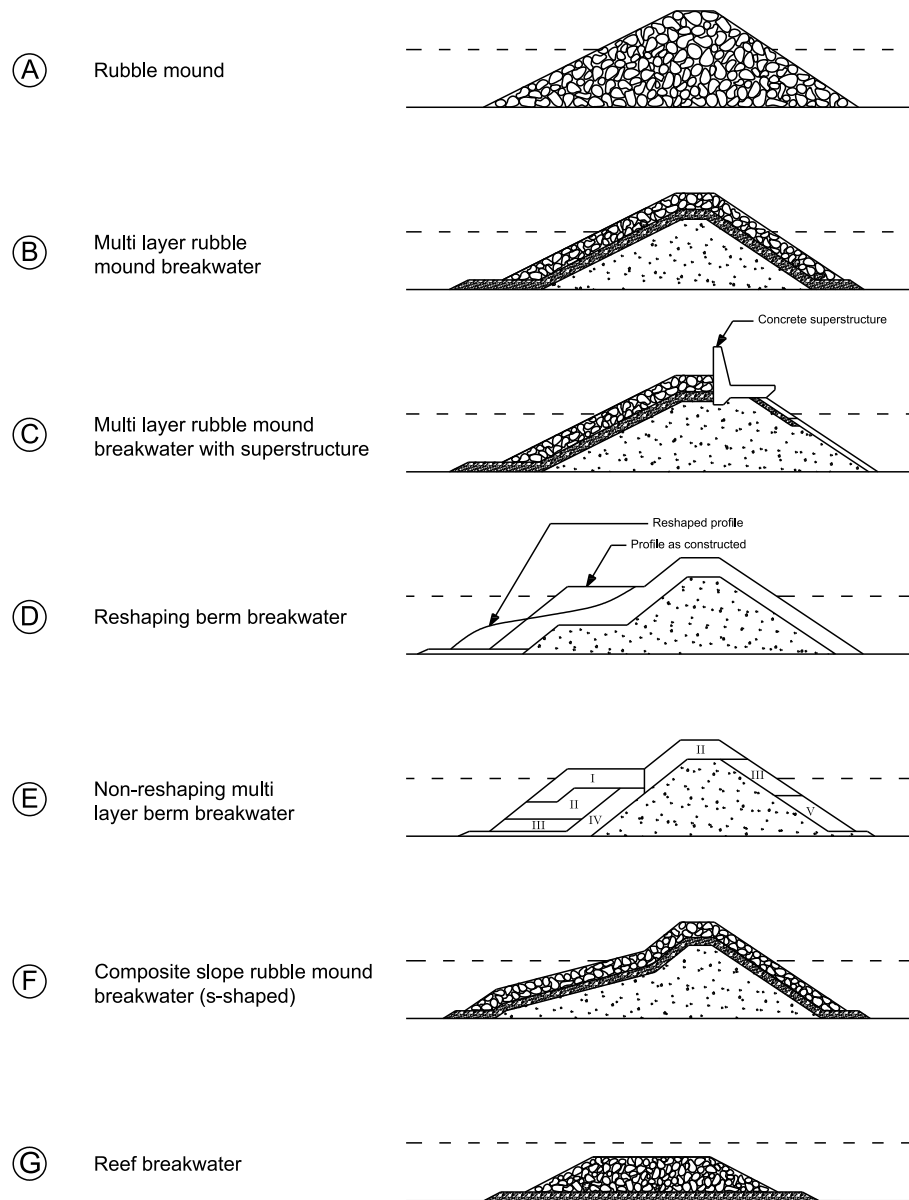


**Figure 1.1**  
*Types of rubble mound breakwaters.*

## 1.2 Failure Modes of Rubble Mound Breakwaters

---

Since the 1980'ties a design based on natural reshaping of the front rock armour during wave action has gained more attention (Fig. 1.1-d). This type of breakwater is known as berm breakwaters or reshaping breakwaters. The main advantage of this structure is that simpler construction methods can be applied. In most cases this type of structure is built with no superstructure as shown in Fig. 1.1.

Furthermore, the berm breakwater is considered as a more durable structure with much easier and cheaper repair methods as compared to the conventional rubble mound breakwater. The berm breakwater is typically built with a very steep front slope and with relatively smaller armour units. The profile self-adjusts to the wave climate leading to a profile stable for the given climate. The berm breakwater concept is described in details in chapter 2.

Lately also non-reshaping berm breakwaters have been considered, often with several stone classes to maximize the total stability and quarry utilization, as indicated in Fig. 1.1-e. Especially in Iceland this structure is widely used, and is therefore also known as the Icelandic type of berm breakwater. This type of structure is also described in details in chapter 2.

Structures constructed with an S-shaped profile are typically used in large water depths to reduce the volume of material, but construction costs are in most cases significantly larger than for the reshaping berm breakwater, resulting in approximately the same profile.

Fig. 1.1-f shows a reef breakwater which is a submerged breakwater mainly used for protecting beaches.

## 1.2 Failure Modes of Rubble Mound Breakwaters

The possible failure modes of a conventional rubble mound breakwater are shown in Fig. 1.2. Failure will here be defined as any exceedence of prespecified structural or functional property. This definition implies that not only any partial or total collapse of one or more structural elements is regarded as damage, but also for instance large overtopping events which can lead to improper use of the breakwater and lead to damage on installations and equipment on or behind the breakwater, persons, ships etc.

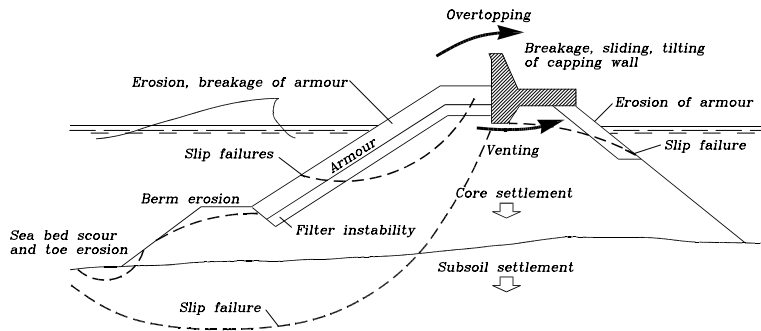


**Figure 1.2**

*Possible failure modes for a rubble mound breakwater [Burcharth, 1993].*

The many different failure modes and the high complexity of the structure has made the design of rubble mound breakwaters quite a task. The failure modes can be separated in geotechnical, hydraulic and structural failure modes. Many different design formulae has been developed for the different failure modes. The verification of the hydraulic stability is most often based on small scale physical model tests. The geotechnical and structural stability is not further dealt with in this thesis, as these cannot be assessed from small scale hydraulic model tests. In some cases the hydraulic model tests can be used to assess the loadings on the structural elements (e.g. pressure measurements on a superstructure), and then base the design on these loads. For other elements it is more difficult and other design methods have to be used (e.g. breaking of armour units).

### 1.3 Wave Impact on Rubble Slopes

The calculation of wave impacts on rubble mound breakwaters involves very complex physical phenomenas as wave breaking and porous flow. When the waves face a sloping structure wave breaking will be triggered due to the reduced water depth and increased wave steepness. The flow past armour units and the wave breaking process cause air to be entrained in the water. Due to these complex physics involved, design of rubble mound breakwaters are most often based on small scale hydraulic model results, where the breakwater is tested in a wave laboratory, typically in scale 1:30 to 1:100. Results from such small scale model tests have led to much more insight in the physics involved and have also resulted in development of design rules.

Several types of wave breaking processes have been observed. The type of wave breaking can be characterized by the surf similarity parameter ( $\xi$ ), which is also

## 1.4 Wave Run-up and Run-Down

---

known as Irribarren number or breaker parameter. In deep water conditions it is defined as:

$$\xi_0 = \frac{\tan(\alpha)}{\sqrt{s_0}} \quad (1.1)$$

where  $\alpha$  is the slope angle and  $s_0$  is the deep water wave steepness. In case of irregular waves various wave parameters can be used to calculate the wave steepness in Eq. 1.1. The significant wave height is most often used in combination with the mean wave period ( $\xi_{0m}$ ) or the peak wave period ( $\xi_{0p}$ ). Fig. 1.3 shows the type of wave breaking depending on the surf similarity parameter for regular waves.

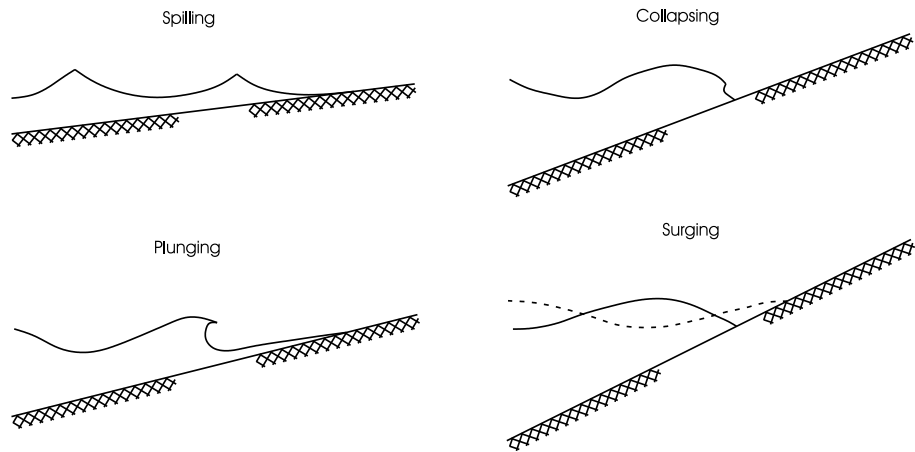


**Figure 1.3**

*Types of wave breaking observed for regular waves depending on the surf similarity parameter.*

## 1.4 Wave Run-up and Run-Down

The wave action and breaking on the slope cause wave run-up and run-down. Run-up and run-down heights are defined as the vertical distance from the still water level to the crest and trough of the up- and downrushing wave.

## Hydraulic Response of Rubble Mound Breakwaters

On an impermeable and less permeable slope the up- and downrush will only take place on the top of the slope and in the outer most permeable layers (if such exists). The more permeable and rough the structure is, the lower run-up heights and velocities, as a larger proportion of the flow takes place inside the structure. The wave action on a slope will cause an increase in the internal water level compared to the still water level. This set-up is a result of larger inflow period and larger surface during the run-up process compared to the run-down process.

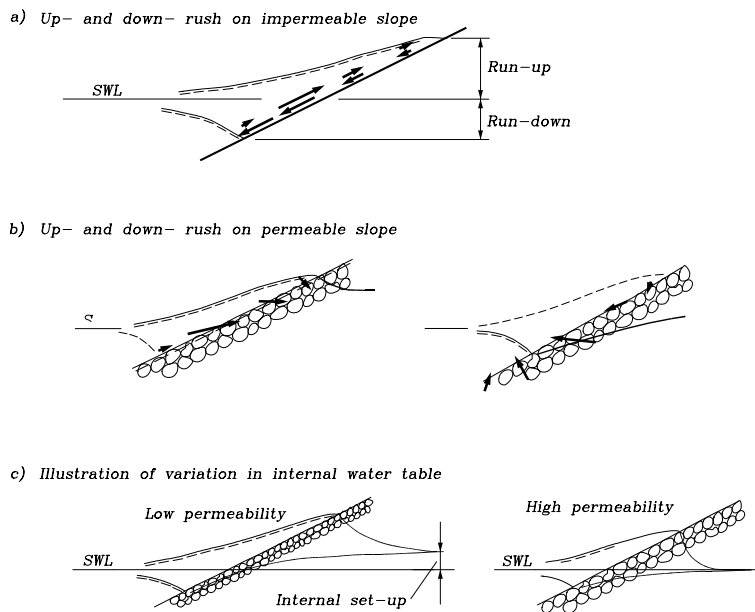


**Figure 1.4**

*Illustration of up- and down-rush on a slope [Burcharth, 1993].*

The run-up and run-down heights depends on the wave climate, the geometry of the slope including permeability, porosity and surface roughness.

There are some indications that run-up on rough slopes may be underestimated by up to 20% in a small scale model. However, only few large and prototype scale investigations are available for rubble mound breakwaters. This is further discussed in chapter 9.

Several empirical formulae that mainly are based on small scale model data, have been developed for run-up heights and velocities for different kinds of straight

## 1.4 Wave Run-up and Run-Down

---

slopes (smooth/rough and permeable/impermeable). In the following some of the formulae for rubble mound structures are presented.

### 1.4.1 Delft Hydraulics, 1989

Results of a large test programme were presented by Delft Hydraulics, 1989. The test programme covers the influence of slope angle, spectral shape, permeable and impermeable core, wave height and wave steepness. The central fit to the obtained data is given in Eq. 1.2 for permeable structures. Differences in 2% run-up heights ( $R_{u,2\%}$ ) between permeable and impermeable structures were only observed for  $\xi_{0m} > 3.1$ .

$$\frac{R_{u,2\%}}{H_{m0}} = \begin{cases} 0.96 \cdot \xi_{0m} & \text{for } 1.0 < \xi_{0m} \leq 1.5 \\ 1.17 \cdot \xi_{0m}^{0.46} & \text{for } 1.5 < \xi_{0m} \leq 3.1 \\ 1.97 & \text{for } 3.1 < \xi_{0m} < 7.5 \end{cases} \quad (1.2)$$

### 1.4.2 Murphy and Kingston, 1996

Murphy and Kingston, 1996 fitted a formula of the type given in Eq. 1.3 to experimental data from 3 different laboratories for the Zeebrugge breakwater, which is an antifer cube armoured rubble mound breakwater. This type of formula was first introduced by Losada and Gimenez-Curto, 1981 for regular waves. Murphy and Kingston, 1996 give  $A = 1.76$  and  $B = -0.28$  valid for irregular waves on rough slopes and run-up heights measured with a wave gauge along the slope. Murphy and Kingston, 1996 observed during the tests that using a wave probe along the slope, will due to the thin layer thickness in the run-up wedge lead to an underestimation of the run-up heights. The wave period used in the formula to calculate the surf similarity parameter is not mentioned.

$$\frac{R_{u,2\%}}{H_{m0}} = A \cdot (1 - \exp(B \cdot \xi)) \quad (1.3)$$

### 1.4.3 TAW, 2002

The TAW, 2002 guidelines are used for safety assessment and design of dikes in the Netherlands. In the report are given guidelines on how to calculate wave run-up heights and wave overtopping discharges for not only dikes, but also for other kinds of structures as reduction factors are given to take into account roughness and permeability. TAW, 2002 gives Eq. 1.4 for 2% run-up height, which is a

central fit to the data. To take into account the scatter of the data another set of recommended equations is given in the TAW, 2002 guidelines.

$$\frac{R_{u,2\%}}{H_{m0}} = \min \begin{cases} 1.65 \cdot \gamma_b \cdot \gamma_f \cdot \gamma_\beta \cdot \xi_0 \\ \gamma_f \cdot \gamma_\beta \cdot (4.0 - 1.5/\sqrt{\xi_0}) \end{cases} \quad (1.4)$$

$\xi_0$  is calculated using  $T_{-1,0}$  and the average slope from  $1.5 \cdot H_{m0}$  below still water level to  $R_{u,2\%}$  above still water level, but ignoring any berm as the influence of this is treated separately in  $\gamma_b$ . Since  $R_{u,2\%}$  is unknown an iterative procedure has to be used. With the TAW, 2002 guidelines comes the computer program PC-OVERSLAG to perform the calculations (in dutch).

The TAW, 2002 formulae give for straight rough slopes similar results as Eq. 1.2, but takes into account the influence of a berm, roughness and wave direction.  $\gamma_b = 1.0$  is applied for no berm,  $\gamma_f = 0.55$  for a two layer rock armour and  $\gamma_\beta = 1.0$  for perpendicular wave attack. For other structures the reduction factors can be estimated using the TAW, 2002 guidelines.

## 1.5 Wave Overtopping

In most situations, it is not economically feasible to construct coastal structures high enough to prevent wave overtopping and as a consequence most coastal structures suffer a certain degree of overtopping. Certain functions of the breakwater set restrictions to the allowable overtopping discharge, as it might damage the breakwater itself and objects located behind the breakwater. Extreme overtopping events results in water and spray thrown over the crest with considerable velocities. These events can be extremely dangerous and previously people, cars and even trains have been washed into the sea. Small buildings have been destroyed and people drowned from various structures. The amount of overtopping on a breakwater is mainly determined by the water level, wave climate and the top geometry of the structure (mainly the crest level). Thus the allowable overtopping discharge determines the top geometry and crest level of the structure and hence the volume of the structure. Due to the ongoing sea level rise and increasing storm intensity and frequency, coastal protection will become even more important. Areas that at the moment are safe, will become more and more critical as the structures will suffer higher floods and waves and consequently more wave overtopping. The increased overtopping may at first not be important for the safety of the structure against failure, but the safety of people and installations during normal service will be lower.

Many people worldwide are living near the coastlines, and the areas near the

coastline are being used for more and more public activities. Due to aesthetic reasons this has resulted in a wish for designs of breakwaters, dikes and seawalls with low crest levels, for which new types of structures have been developed, to give overtopping discharges in the acceptable range.

Overtopping can occur as spray before the highest run-up levels exceed the crest freeboard, but green water wave overtopping occurs first when the highest run-up levels exceed the crest freeboard. Overtopping is therefore a phenomena highly related to run-up. However, whereas run-up is a close to linear phenomenon, overtopping is an extremely non-linear phenomenon and the overtopping discharge varies considerably from wave to wave, and the overtopping discharge is very unevenly distributed both in time and space. The major part of the overtopping water during a storm is due to a small fraction of the waves, the ones with the highest (fictitious) run-up levels. In fact, the local overtopping discharge from a single wave can be more than 100 times the average overtopping discharge during the storm peak. The discharge intensity of the individually overtopping waves is important because most damaging impacts on persons, vehicles and structures are caused by overtopping of large single waves. Nevertheless, the amount of allowable overtopping is normally based on the time average overtopping discharge as shown in Fig. 1.5. Only limited information exists on the probability distribution of the volume of overtopping. However, lately some new guidelines for critical overtopping have been presented which also includes single wave peak volumes [De Rouck, 2005]. The De Rouck et al., 2005 guidelines for mean discharges are quite similar to those given in Fig. 1.5. The landward distance the overtopping water travel is also very important because it put restrictions to the use of these areas.



## Hydraulic Response of Rubble Mound Breakwaters

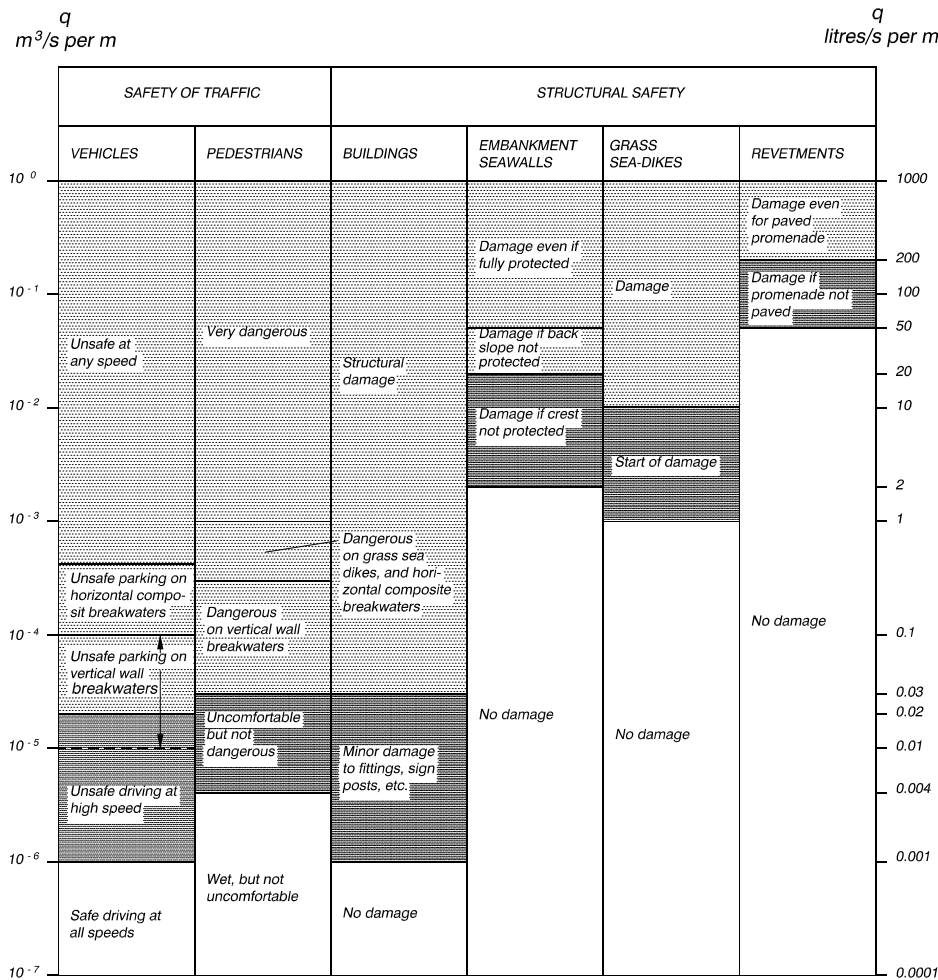


**Figure 1.5**

*Critical average overtopping discharges [Burcharth and Hughes, 2003, Table VI 5-6].*

The overtopping discharges depend, as the run-up height, not only on the environmental conditions, but also on the structure geometry and the layout of the breakwater. The large number of geometrical parameters and the complicated hydrodynamics involving breaking waves and porous flow makes calculation of overtopping discharges difficult. The research on overtopping of conventional rubble mound breakwaters and dikes has led to some widely used simple regression models that are based on empirical expressions fitted to hydraulic model

## 1.5 Wave Overtopping

---

test results. For more complex kinds of structures much less is known on the overtopping discharge, e.g. for berm breakwaters only very little data on wave overtopping is available.

Most of the regression formulae are fitted to a limited number of tests with a specific type of structure, and no universal formula exists. As a consequence, the overtopping discharge estimated by different formulae varies tremendously, especially for small overtopping rates (a factor of 10 to 100 is common). The advantage of these regression models is that they are very easy to use. Most of the simple regression models follow one of the two types of mathematical expressions:

$$q_{\star} = a \cdot \exp(-b \cdot R_{\star}) \quad (1.5)$$

$$q_{\star} = a \cdot R_{\star}^{-b} \quad (1.6)$$

where  $a$  and  $b$  are empirical fitted coefficients that depend on the geometry of the structure,  $q_{\star}$  is a dimensionless average discharge per meter and  $R_{\star}$  is a dimensionless crest freeboard.

The crest freeboard ( $R_c$ ) and the armour crest freeboard ( $A_c$ ) is defined in Fig. 1.6.  $R_c$  is the crest freeboard of the structure, which is the vertical distance from SWL to the point of the structure where overtopping is measured. This is in not always the highest point of the structure.  $A_c$  is the armour crest freeboard of the structure. It is the vertical distance from SWL to the upper limit of the armour layer.  $A_c$  may be used together with  $R_c$  and  $G_c$  to describe the crest of the structure more detailed, cf. Fig. 1.6. In a lot of cases  $A_c$  and  $R_c$  are identical.

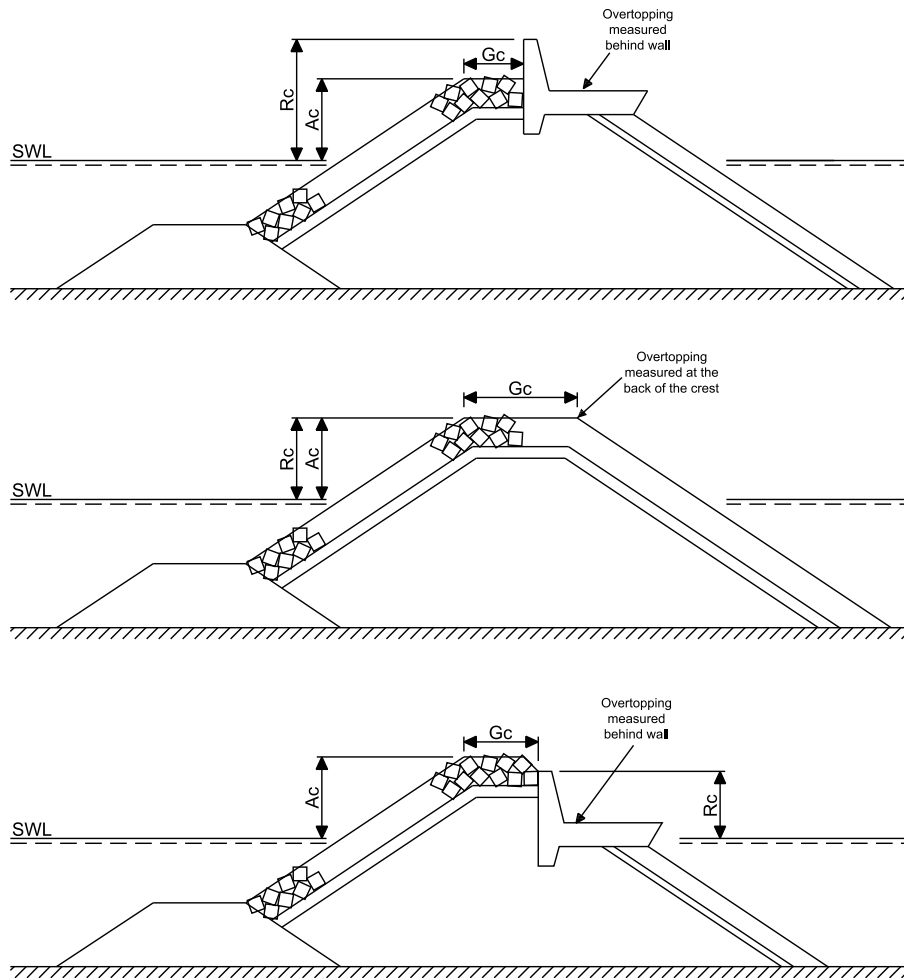


**Figure 1.6**  
 Definition of crest freeboard ( $R_c$ ) and armour crest freeboard ( $A_c$ ).

The crest freeboard ( $R_c$ ) is often related to the significant wave height ( $H_s$ ) or the  $H_{m0}$  wave height to give the dimensionless freeboard  $R_* = R_c/H_{m0}$ . The significant wave height is used even though only a small fraction of the waves contributes to the main part of the overtopping.

Within the CLASH project (De Rouck, 2005) a neural network model was developed to cover all kinds of structures.

### 1.5.1 TAW, 2002

Van der Meer and Janssen, 1994 gives a widely used set of formulae to calculate the overtopping discharge, including reduction factors to account for roughness, the presence of a berm, the shallowness of the foreshore and the obliqueness of the wave attack. These formulae were later slightly modified and included in the TAW, 2002 manual. The central fit to the data is given in Eq. 1.7. TAW, 2002 give another set of recommended equations to take into account the scatter of the data. Because the formulae initially were developed for dikes they give the overtopping discharge at the outer crest line. The freeboard at this point has to be used in the formulae. The influence of a permeable armour crest has to be taken into account afterwards. This could e.g. be done by the method of Besley, 1999. The influence of a superstructure could be taken into account by  $\gamma_v$  or preferably by a more accurate method.

$$\frac{q}{\sqrt{g \cdot H_{m0}^3}} = \min \left\{ \begin{array}{l} \frac{0.067}{\sqrt{\tan(\alpha)}} \cdot \gamma_b \cdot \xi_o \cdot \exp \left( -4.75 \cdot \frac{R_c}{H_{m0}} \cdot \frac{1}{\xi_o \cdot \gamma_b \cdot \gamma_f \cdot \gamma_\beta \cdot \gamma_v} \right) \\ 0.2 \cdot \exp \left( -2.6 \cdot \frac{R_c}{H_{m0}} \cdot \frac{1}{\gamma_f \cdot \gamma_\beta} \right) \end{array} \right. \quad (1.7)$$

The upper formula corresponds to breaking waves on the slope ( $\gamma_b \cdot \xi_o \lesssim 2$ ) and the lower to non-breaking waves ( $\gamma_b \cdot \xi_o \gtrsim 2$ ). When calculating the surf similarity parameter the method mentioned in section 1.4.3 has to be used. The  $\gamma$ -values take into account the influence of a berm, roughness, angle of wave attack and a vertical wall (superstructure).

### 1.5.2 CLASH NN-Model

In the CLASH project a neural network model for wave overtopping was developed [De Rouck, 2005]. The neural network model must be regarded as state of the art in estimating average overtopping discharges, as it is based on approximately 10,000 overtopping tests with all kinds of structures. The reliability of this model is very much dependent on the amount of data available for the specific structure in the training process of the neural network. Consequently, very accurate estimations are given for most conventional rubble mound breakwaters, but much less reliable for complex geometries with fewer available data, as berm breakwaters etc.

To use the CLASH NN-model the user should specify 3 sea state parameters and 12 geometrical parameters.

## 1.6 Hydraulic Stability of Front Armour Layers

The hydraulic stability of the main armour layer on the front slope has been extensively investigated for many years. The most common failure mode of the armour layer is failure of single units when the wave exerted dislocating force is greater than the stabilizing force. The dislocation of units starts around the still water line. After a stone has been drawn out of the armour layer the dominant mode of motion is rolling. The armour stone is then deposited below the still water line. The amount of damage is then calculated either from the number of units moved or from the eroded surface profile. The counting method is typically used for concrete units, while the eroded profile is typically used for rock armour. Broderick, 1983 defined the following dimensionless damage parameter ( $S$ ) for rock armoured structures:

$$S = \frac{A_e}{D_{n,50}^2} \quad (1.8)$$

where  $A_e$  is the eroded cross-section area.

For calculating the necessary armour unit weight several empirical design formulae have been developed. Most of these formulae is based on the stability index  $H_0$ , which can be derived from a simple quantitative ratio between driving forces (drag and lift) and stabilizing forces (gravity):

$$\frac{F_D + F_L}{F_G} \approx \frac{\rho_w \cdot D_{n,50}^2 \cdot u^2}{g \cdot (\rho_s - \rho_w) \cdot D_{n,50}^3} \cdot K = \frac{u^2}{g \cdot \Delta \cdot D_{n,50}} \cdot K \quad (1.9)$$

where  $K$  is a dimensionless calibration function. Taking the velocity as  $u = \sqrt{2 \cdot g \cdot H}$  leads to the well known stability index ( $H_0$ ):

$$\frac{F_D + F_L}{F_G} \approx \frac{2 \cdot g \cdot H}{g \cdot \Delta \cdot D_{n,50}} \cdot K = \frac{H}{\Delta \cdot D_{n,50}} \cdot K_2 = H_0 \cdot K_2 \quad (1.10)$$

Now a days the most widely used are the Hudson, 1958 formula and the Van der Meer, 1988 formulae for static stability.

For reshaping berm breakwater where much more damage is accepted, another way of defining the amount of damage has been introduced. For these structures the damage assessment is always done from the reshaped profile. A good single parameter describing the amount of damage is the recession of the berm. There exists some methods for calculating the entire profile, but also some simple empirical formula for estimating the recession of the berm have been developed. Front slope stability of berm breakwaters are further described in details in chapter 4.

In addition to the hydraulic stability it is important to investigate the structural strength of the armour units. This is especially important for reshaping berm breakwaters and for cases where relatively slender concrete armour units are used. It is important to be aware that this cannot be assessed from a hydraulic model test study.

### 1.6.1 Hudson, 1958

Hudson, 1958 found from his model tests that the stability could be described by Eq. 1.11.

$$H_0 = \frac{H_{m0}}{\Delta \cdot D_{n,50}} = (K_D \cdot \cot(\alpha))^{1/3} \quad (1.11)$$

The value of  $K_D$  depends mainly on the type of armour used. However, the value of  $K_D$  should be selected with great caution as it also depends on the wave steepness, the wave breaking process, the number of waves, the amount of damage allowed, the permeability etc. For this reason it is not possible to give definite values of  $K_D$ , but as a rule of thumb  $K_D = 1.0 - 4.0$  can be used for rock armour.

### 1.6.2 Van der Meer, 1988

Van der Meer has proposed several empirical formulae for hydraulic stability of different kind of armour units. The formula for static stability of a rock armoured slope is given in Eq. 1.12. Van der Meer, 1988 also gives a set of equation to calculate dynamic stability of reshaping berm breakwaters. However, the dynamic stability formulae are complex to apply and requires a computer program to perform the calculations.

$$\frac{H_{m0}}{\Delta \cdot D_{n,50}} = \begin{cases} 6.2 \cdot \xi_{0m}^{-0.5} \cdot P^{0.18} \cdot \left(\frac{S}{\sqrt{N}}\right)^{0.2} & \text{for plunging waves} \\ \xi_{0m}^P \cdot \cot(\alpha) \cdot P^{-0.13} \cdot \left(\frac{S}{\sqrt{N}}\right)^{0.2} & \text{for surging waves} \end{cases} \quad (1.12)$$

where  $N$  is the number of waves.  $P$  is the notational permeability, which is a parameter introduced by Van der Meer, 1988 to describe the permeability of the entire structure. This parameter has later been included in several formulae by Van der Meer and others. The value of the notational permeability are presented in Van der Meer, 1988 for some standard structures. The value of the damage

parameter ( $S$ ) is also given in Van der Meer, 1988 for different slope angles and damage levels (initial damage, intermediate damage and failure).

The transition from plunging to surging waves is described by the interaction of the two formulae, given as:

$$\xi_{0m,transition} = \left(6.2 \cdot P^{0.31} \cdot \sqrt{\tan(\alpha)}\right)^{1/(P+0.5)} \quad (1.13)$$

### 1.7 Hydraulic Stability of Rear Armour Layers

For breakwaters subjected to a considerable amount of overtopping it is important to check the stability of the rear side armour, as overtopping waves can damage the rear side of a berm breakwater and an erosion process may start which quickly causes a breach in the breakwater. However, no good and simple design rules are available, not even for conventional breakwaters.

Walker et al., 1976, Vidal et al., 1990, Andersen et al., 1992, Van der Meer and Veldman, 1992 and Kudale and Kobayashi, 1996 have all presented methods to assess the stability of the rear armour. These methods use the wave height at the toe of the structure and some few geometrical parameters to calculate the rear side stability. However, in that case not only the wave parameters should be included, but also a large number of parameters describing the breakwater cross section.

Recently Verhagen et al., 2003 and Van Gent and Pozueta, 2004 linked the rear side stability to the velocity of the water overtopping the crest, which is a much more logical approach, as the overtopping water is the main cause for the rear side damage. However, only for the very simple structures information is available of how to calculate the velocity of the overopping water, and in every case much less information is available than for overtopping discharges.

#### 1.7.1 Van der Meer and Veldman, 1992

Van der Meer and Veldman, 1992 performed test series on two different berm breakwater designs with no superstructure ( $R_c = A_c$ ). A first design rule was assessed on the relationship between damage to the rear side of a reshaping breakwater and the crest height, the wave steepness and the rock size. They concluded that longer waves, higher waves and lower crest gives more overtopping and thus more damage to the rear side of the breakwater. Their suggestions for

designs are:

$$\text{Start of damage: } \frac{R_c}{H_s} \cdot s_{0p}^{1/3} = 0.25 \quad (1.14)$$

$$\text{Moderate damage: } \frac{R_c}{H_s} \cdot s_{0p}^{1/3} = 0.21 \quad (1.15)$$

$$\text{Severe damage: } \frac{R_c}{H_s} \cdot s_{0p}^{1/3} = 0.17 \quad (1.16)$$

However these guidelines are based on a very limited number of tests and must only be regarded as very rough guidelines, i.e. the crest and berm width are not included which are two very important parameters for the overtopping discharge.

### 1.7.2 Andersen et al., 1992

Rear slope stability of berm breakwaters with no superstructure ( $R_c = A_c$ ) was also studied by Andersen et al., 1992.

Even though the crest width has an enormous influence on the overtopping rate Andersen et al., 1992 found surprisingly no visible influence of the crest width on rear side stability of berm breakwaters within the tested range being 0.175 - 0.30 m in a model with water depths in the range 0.77 - 0.97 m and  $H_{m0}$  in the range 0.176 - 0.279 m. Andersen et al., 1992 concluded that a wider range of crest widths were needed to examine the variation of the rear side stability with this parameter.

Andersen et al., 1992 give, based on a specific test program, the following criterion for the rear side stability of a berm breakwater (start of damage):

$$R_c \geq \tan(\alpha) \cdot \frac{H_{m0}}{\sqrt{s_{0m}}} - \Delta \cdot D_{n,50} \cdot \frac{\mu \cdot \cos(\beta) - \sin(\beta)}{C_D + \mu \cdot C_L} \quad (1.17)$$

Where  $\alpha$  and  $\beta$  are the front and the rear side slope respectively,  $\mu$  is the resistance against rolling and sliding and can be calculated as  $\mu = \tan(\varphi)$  where  $\varphi$  is the natural angle of repose. Andersen et al., 1992 used  $T_{0,2}$  for calculating the mean wave steepness ( $s_{0m}$ ). Andersen et al., 1992 optimized the value of the expression  $C_D + \mu \cdot C_L$  to give the best fit to the experiments. They found that a value of 0.08 gave the best agreement.

### 1.7.3 Verhagen et al., 2003

Verhagen et al., 2003 used a special device to simulate single wave overtopping



plunges on a breakwater with no superstructure. This study resulted in the rear side mobility parameter ( $\theta$ ) given in Eq. 1.18. The number of displace units are proportional to  $\theta$ .

$$\theta = \frac{(u_{char} \cdot \cos(\beta - \alpha))^2}{\Delta \cdot g \cdot D_{n,50}} \cdot \frac{R_c}{D_{n,50}} \cdot \sin(\alpha) \cdot \sqrt{N} \quad (1.18)$$

The characteristic velocity  $u_{char}$  is the time averaged velocity during the single wave overtopping event (maximum instaneous discharge divided by layer thickness).  $\alpha$  is the rear slope angle and  $\beta - \alpha$  is the angle between the rear slope and the flow direction of the overtopping water (which is unknown).  $N$  is the number of waves.

#### 1.7.4 Van Gent and Pozueta, 2004

Eq. 1.19 is a relation between damage level and the stone size which was recently presented by Van Gent and Pozueta, 2004 and based on a hydraulic model test study. For a given acceptable damage level the required stone size on the rear slope can be calculated from the velocity of the overtopping water.

$$\frac{S}{\sqrt{N}} = 2.62 \cdot 10^{-13} \cdot \left( \frac{u_{1\%} \cdot T_{-1,0}}{\Delta^{0.5} \cdot D_{n,50}} \right)^6 \cdot (\cot(\alpha))^{-2.5} \cdot \left( 1 + 10 \cdot \exp\left(-\frac{R_c}{H_{m0}}\right) \right) \quad (1.19)$$

$u_{1\%}$  is the maximum overtopping velocity that is exceeded by 1% of the waves.  $S$  is the damage level as defined in Eq. 1.8 and  $\alpha$  is the rear slope angle.

## 1.8 Wave Reflection

The incident wave energy can be reflected, dissipated and/or transmitted into the harbour area. If reflection is significant, the interaction of incident and reflected waves can create an extremely chaotic sea with very steep, standing and breaking waves. This makes maneuvering difficult in front of the harbour entrance for smaller vessels. Reflected waves can also contribute to scour at the toe of the structure and erosion at adjacent beaches. Therefore it is often preferred that a significant part of the incident energy is dissipated. The incident energy can be dissipated by wave breaking, porous flow and friction at rough surfaces. Wave breaking is the main contributor to wave dissipation for sloping rubble mound structures.

## 1.8 Wave Reflection

---

Smooth and impermeable vertical walls reflect almost all the incident energy in case they are non-overtopped. Rubble mound structures absorb a significant part of the incident energy and are therefore well suited for use in harbour basins. For rubble mound structures a part of the incident energy can be transmitted into the harbour area due to penetration and wave overtopping, the amount of transmitted energy depends on the top geometry and the permeability of the structure.

Wave reflection can be quantified by the reflection coefficient  $C_r$ :

$$C_r = \frac{H_{m0,r}}{H_{m0,i}} = \left( \frac{E_r}{E_i} \right)^{1/2} \quad (1.20)$$

where  $H_{m0,r}$  and  $H_{m0,i}$  is respectively reflected and incident significant wave height calculated from the spectra.  $E_r$  and  $E_i$  is reflected and incident wave energy.

The reflection coefficient ( $C_r$ ) is normally related to the breaker parameter ( $\xi_0$ ) as wave breaking is the main contributor to wave dissipation on sloping coastal structures. In shallow water wave condition also the water depth to wave height ratio may be important as it influences the characteristics of the incoming waves and the breaking on the slope.

Several formulae to calculate wave reflection coefficients have been proposed for perpendicular wave attack, some of these are presented in the following.

### 1.8.1 Seeling, 1983

Seeling, 1983 presented the following empirical relation:

$$C_r = \frac{a \cdot \xi_0^2}{b + \xi_0^2} \quad (1.21)$$

Based on tests with regular waves on impermeable, smooth, straight slopes Seeling, 1983 give  $a=1.0$  and  $b=5.5$ . Various researchers have proposed different values for  $a$  and  $b$  for regular and irregular waves on different types of slopes.

### 1.8.2 Postma, 1989

Some alternative formulae to the formula of Seeling, 1983 were presented by Postma, 1989, who analysed Van der Meer, 1988 reflection data for non-overtopped

rock slopes. For a first estimate Postma, 1989 proposed the simple formula:

$$C_r = 0.140 \cdot \xi_{0p}^{0.73} \quad (1.22)$$

For a more accurate approach Postma, 1989 proposed Eq. 1.23 in which he included the notational permeability ( $P$ ) as introduced by Van der Meer, 1988, the slope angle ( $\alpha$ ) and the peak wave steepness ( $s_{0p}$ ).

$$C_r = 0.071 \cdot P^{-0.082} \cdot (\cot(\alpha))^{-0.62} \cdot s_{0p}^{-0.46} \quad (1.23)$$

### 1.8.3 Alikhani, 2000

Alikhani, 2000 presented the formula given in Eq. 1.24 valid for reshaping berm breakwaters. He found that for reshaping berm breakwaters the slope of the structure has no influence on the reflection coefficient, because higher waves causes flatter slope and compensate the wave energy.

$$C_r = 0.044 \cdot s_{0p}^{-0.46} \quad (1.24)$$

## 1.9 Wave Transmission

Waves behind a rubble mound breakwater are caused by wave penetration and wave overtopping. The amount of wave penetration is dependent on the permeability of the structure. Waves generated by overtopping tend to have shorter periods than the incident waves. The amount of energy transmitted through the breakwater can be quantified by the wave transmission coefficient ( $C_t$ ) defined as:

$$C_t = \frac{H_{m0,t}}{H_{m0,i}} = \left( \frac{E_t}{E_i} \right)^{1/2} \quad (1.25)$$

where  $H_{m0,t}$  is the transmitted wave height and  $H_{m0,i}$  is the incident wave height, both calculated from the surface elevation spectrum.

The amount of wave transmission is important as it is preferable to minimize waves in the harbour area, as it can cause ship maneuver problems.

No general formula to calculate wave transmission coefficients has been established yet.

### 1.10 Objectives

The objective of the present project is to experimentally investigate white spots related to hydraulic response of rubble mound breakwaters. Two important white spots are selected:

1. Hydraulic response of berm breakwaters, with the main focus on wave overtopping, which is an enormous white spot for this type of structure. This is a very important white spot as this type of structure has gained much more attention in recent years. This white spot was also defined during the CLASH project, and a part of the present tests were carried out as a part of the CLASH project and included in the CLASH database. An introduction to the berm breakwater concept is given in chapter 2. The test set-up and programme is given in chapter 3. The results related to front slope stability, wave overtopping, rear slope stability and wave reflection are given in chapter 4, 5, 6 and 7. An example of application of the developed design rules is given in chapter 8.
2. As the author got the opportunity to perform large scale tests in the CIEM flume in Barcelona, it was logical to select the overtopping scale effect problem as the second objective. An introduction to the overtopping scale effect problem is given in chapter 9, where some theoretical considerations and results of some of the previous investigations are presented. The new tests and the results of these are presented in chapter 10.

## CHAPTER 2

# The Berm Breakwater Concept

The berm breakwater concept is basically rather old, but was not used very much until it was "reinvented" in the early 1980'ties, when a slope protection for an airfield runway extending into the sea in the Alutian Islands, Alaska was designed [Rauw, 1987]. Since then, many berm breakwaters have been built, especially in Iceland. The design and construction of berm breakwaters is described in the PIANC, 2003 report "State-of-the-Art of Designing and Constructing Berm Breakwaters".

Conventional rubble mound breakwaters are designed to withstand wave action without significant displacement of material. Therefore, each armour unit has to be put into its final position during the construction phase. The thickness of the armour layer is typically two stone diameters.

The berm breakwater is a rubble mound breakwater initially constructed with a large porous berm above or at still water level at the seaward side. During wave attack the berm breakwater will typically reshape into a s-shaped profile. Lately also more stable berm breakwaters have been considered. The berm breakwater is designed to optimize the utilization of the quarry material for the available construction equipment. This is obtained by separating the quarry material in stone classes. For a berm breakwater with a homogeneous berm, two stone classes are typically used (core and armour). The stone gradations will typically be rather wide to get 100% utilization of the quarry material. In multi-layer berm breakwaters more stone classes are used, typically around 5. In this way a more stable structure is obtained by placing the largest stones where they add most to the stability, i.e. on the top and in front of the berm.

## 2.1 Reshaping Berm Breakwaters

---

The berm breakwater concept is relevant to many hot climate port locations where only relative small size rocks are available due to rock degradation. In many of these cases the necessary armour stone weight on a conventional two layer rubble mound breakwater is so large that concrete armour blocks are required or the slope has to be very flat. In these cases the berm breakwater is a good alternative. It is clear that even a non-reshaped berm breakwater requires cover stones with less weight than required for a conventional rubble mound breakwater due to the voluminous permeable berm. In many cases the total construction and repair costs are significantly lower for a berm breakwater compared to a conventional rubble mound breakwater, especially in hot climate locations and in large water depths.

Due to the large porosity in the berm the structure is very stable as the down-rush is much smaller than on a conventional rubble mound breakwater. A berm breakwater is considered to be a very tough structure as it is very difficult to destroy even a dynamically stable berm breakwater by incoming head-on-waves, unless the structure is overtopped or the berm is too narrow. A conventional rubble mound breakwater is more brittle and repair operations more difficult.

Overtopping waves can easily damage the rear side of a berm breakwater and an erosion process may start which quickly causes a breach in the breakwater. Therefore, rear side stability of a berm breakwater is closely related to overtopping.

## 2.1 Reshaping Berm Breakwaters

The concept of a reshaping berm breakwater involves the use of relatively smaller armour stones which will be transported by the waves from the position where they were placed or dumped by the use of low cost land based equipment. During exposure to wave action of a certain intensity, the berm reshapes until, eventually, an equilibrium profile is reached. For a given sea state, an equilibrium profile exists provided that there is enough material. Berm breakwaters have traditionally been allowed to reshape into a static or dynamic stable profile and are therefore also known as reshaping breakwaters.

A berm breakwater is dynamically stable when the profiles have stabilized after deformation, although up and down movements of the stones continuously occur during each run-up and run-down of the waves. This continuously up and down movements could cause a longshore net transport in oblique waves, which could lead to increased maintenance costs and maybe even failure of some parts of the breakwater. In case of perpendicular wave attack an equilibrium profile is

reached when the net transport has become zero.

If the berm breakwater is reshaping but statically stable, the stones will mainly move downward the slope and the breakwater will reshape into a stable profile where movements occur in very severe and rare conditions only. Therefore, longshore transport is of much less importance in this case. However, it is important to investigate the longshore transport anyway, especially during the reshaping phase where the longshore transport is greatest. The longshore transport problems and other 3D problems are further discussed in section 2.5.

Some designers favour the statically stable reshaping berm breakwaters due to its safety, reliability and lower risk of longshore transport and stone breakage. Others argue that a reshaping statically stable berm breakwater is a too costly design and that the client may be prepared to accept some maintenance costs for a reduced initial investment. There seems to be a drive towards designing most berm breakwaters to be statically stable. However, in many cases the dynamically stable berm breakwater becomes attractive due to a too small amount of large stones to design a statically stable berm breakwater. In these cases the dynamically stable berm breakwater becomes very attractive.

A typical reshaping berm breakwater profile, before and after reshaping has taken place, is shown in Fig. 2.1. Just below water level, the reshaped profile typically has a slope of about 1:4. In front of this slope, stones are deposited with a steeper slope approaching the natural angle of repose.

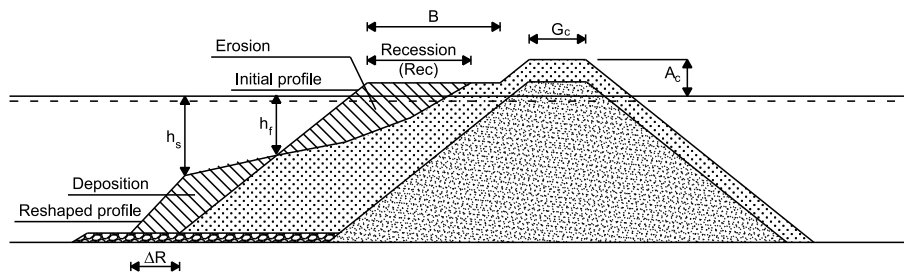


Figure 2.1

Typical initial and reshaped profile for a berm breakwater with homogeneous berm.

Wave energy is dissipated by wave breaking over the berm and by porous flow in the mound. The flat slope around the water level and a highly energy absorbing porous medium give little reflection from a berm breakwater, thus better maneuvering conditions in front of the entrance and less scour in front of the structure. Further run-up and overtopping are generally smaller than for a conventional

straight and steeper breakwater slope.

## 2.2 Non-Reshaping Berm Breakwaters

In recent years there has been a drive to design the berm breakwater in such a way that it will not reshape at all (non-reshaping statically stable berm breakwater), where only a few stones are allowed to move similar to what they are allowed in a conventional rubble mound breakwater. The reason for considering the non-reshaping berm breakwater is the possibility of longshore transport and that the reshaping process might lead to excessive breaking and abrasion of individual stones. However many of the old reshaped berm breakwaters have functioned quite well, without excessive breaking and abrasion of the stones [PIANC, 2003, p. 6]. In some projects, model tests have due to possible breaking and abrasion of armour stones been carried out with smaller stones compared to the actual planned stone size. A disadvantage with the non-reshaping berm breakwater is more wave reflection from the structure due to the steeper front slope, but an advantage is that overtopping is, as demonstrated in chapter 5, generally smaller on a non-reshaped berm breakwater compared to a reshaped.

## 2.3 Multi-Layer Berm Breakwaters

The multi-layer berm breakwater is also known as the Icelandic type berm breakwater, as this type of berm breakwater has been very much used in Iceland, where more than 20 has been built up to now. The Icelandic type berm breakwater is a multi-layer statically stable berm breakwater, with only very limited reshaping accepted. The stones are placed in layers to give a higher total stability of the structure. The largest stones are placed on the top of the berm and sometimes also at the front of the berm, where they will be most effective in reinforcing the structure. Smaller stones are used in the innerlayers of the berm, even smaller than on a reshaping berm breakwater consisting of two stone classes. For a multi-layer berm breakwater the advantage of using simple construction methods is still archived, as experiences from many berm breakwater projects have shown that working with several stone classes and placement of stones only increases the construction cost insignificantly, while leading to a better utilization of the quarry material, thus lowering the total costs [PIANC, 2003, p. 46]. The stone classes are selected to optimize the utilization of the quarry material for the construction equipment available. The optimization often leads to several stone classes with different gradations. One disadvantage with the Icelandic type of berm breakwaters is that they also give significantly more reflection than the



reshaping berm breakwaters.

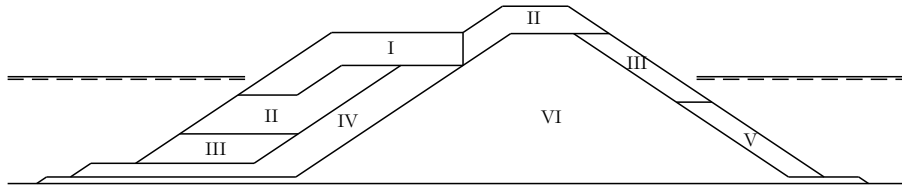


**Figure 2.2**

*Typical initial profile for an Icelandic multi-layer berm breakwater. In this case 6 stone classes is used.*

## 2.4 Redistribution of Material

On a reshaping berm breakwater a significant redistribution of stone material along the slope takes place, resulting in larger stones at the bottom and smaller stones on the berm. At the bottom  $W_{50}$  may be around 2-3 times larger than at the berm, of course depending on the stone gradation. The redistribution might result from:

- The rotation velocity for the larger stones may be the same as for the smaller stones, resulting in larger movement over a wave period [PIANC, 2003, p. 21]. Even if this is not true, the larger stones may have more inertia, so they are not as easily stopped moving downward by the next wave.
- The larger stones roll more easily on a rough surface compared to smaller stones.

If the breakwater is built with a "reshaped" profile, the redistribution will be less resulting in increased stability of the profile. However, this requires different and more complex construction methods, leading to higher construction costs and probably higher total costs.

## 2.5 3-Dimensional Effects

The recession of the berm is for an infinite long berm breakwater generally lower for oblique waves than for head-on waves. Nevertheless, oblique waves could be the worst case due to longshore transport which might cause unacceptable removal and transport of stones along the structure and lead to failure of some

parts of the structure. The reason for longshore transport being so important for reshaping berm breakwaters is the less stable armour stones compared to a conventional rubble mound breakwater. The less stable the armour stones are the more longshore transport could be expected.

For statically stable reshaping berm breakwaters longshore transport is only of little importance after the reshaping phase. However, during the reshaping phase there could be a significant amount of longshore transport.

In case of dynamically stable profiles the longshore transport is very important due to the continuously armour stone movements on the reshaped berm during wave attack. The longshore transport increases very non-linearly with the wave height [Burcharth and Frigaard, 1990]. Some existing methods for calculating the longshore transport is summarized in PIANC, 2003.

The longshore transport could be increased by a 3-dimensional foreshore or a bending breakwater as this can lead to focusing of the waves and cause a net longshore transport of armour material towards the focus point. The higher waves at the focus point causes more reshaping and more overtopping. Therefore it could be necessary to increase the volume of the structure near the focus point.

What has to be treated with great care is roundheads and corners as they are generally more exposed than a straight stretch. Furthermore the stones on the roundhead are not allowed to move into the areas behind the breakwater head in order not to block shipping lanes or otherwise be a hazard to navigation [PIANC, 2003].

All these 3-dimensional problems are not dealt with further in this thesis. However, it is important to emphasize that this is a very important analysis to perform when designing a berm breakwater.

## 2.6 Construction Methods

One of the primary benefits of berm breakwaters compared to conventional rubble mound breakwaters is their greater acceptable stone gradation and placement tolerances, which lead to simpler construction and repair methods, offering substantial savings over the more rigorous approach normally adopted for conventional rubble mound breakwaters [PIANC, 2003, p. 45]. The usual construction equipment consists of a drilling rig, two or more backhoe excavators, one or more front end loaders and several trucks. In addition stones may be dumped from barges. Large cranes have been used instead of backhoe excavators in some projects, but are usually considered more expensive [Sigurdarson et al., 1999].

The backhoe excavator can crawl on a uneven stone layer where a crane needs a much finer and more stable workpad.



**Figure 2.3**

*Backhoe excavator placing stones at the Sirevåg berm breakwater [PIANC, 2003, Fig. 11.1].*

When the first berm breakwaters were built, bulldozers were used to push the stones to the berm, which resulted in breakage of stones and dispersal of too many fines that plugged the voids [PIANC, 2003, p. 45]. To what extent the berm stones could be dropped or thrown by the backhoe excavator without breaking depends on the stone quality.

## 2.7 Quarry Material

Design of a rubble mound breakwater should start with inspection of near by existing commercial rock quarries and/or inspection of geological maps to find new promising sites. The most important difference between a berm breakwater and the conventional breakwater is the utilization of the quarry material. In the design of a berm breakwater the designer will try to maximize the yield of the quarry material, which is typically based on a forecast for a quarry using surface or core samples. To get the amount of armour stones needed for a conventional rubble mound breakwater an overproduction of core material will typically be required, cf. Fig. 2.4. However, the results given in Fig. 2.4 for the conventional breakwater is the worst case where the cross section is identical in the entire breakwater. In most cases the entire breakwater do not have the same cross-section and the same needed armour stone weight. Moreover, inner breakwaters are in many cases constructed at the same time for which some of the wasted

material can be used.

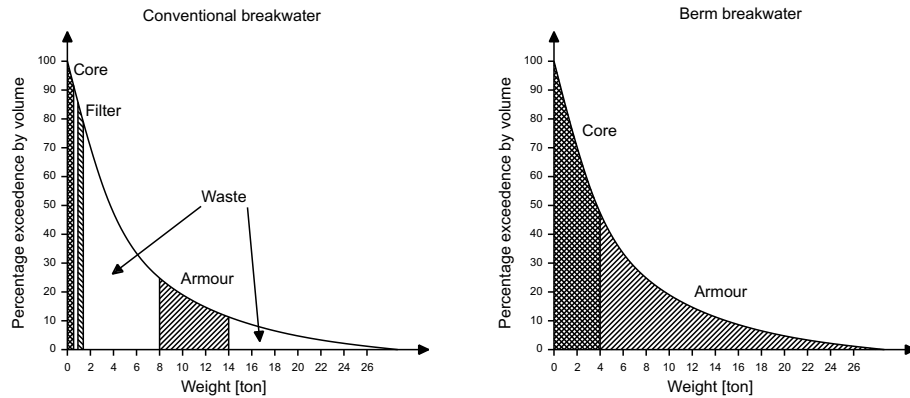


**Figure 2.4**

*Quarry yield and stone weights required by conventional breakwaters and a reshaping berm breakwater.*

In most cases the needed volume for a berm breakwater is approximately the same as for a conventional breakwater. In shallow water wave conditions the volume is typically larger for the berm breakwater, but smaller in deeper waters. The total costs to construct a breakwater is very dependent on the transportation volume and distance. For the berm breakwater to be an economical better solution than the conventional breakwater a short transportation distance from the quarry is needed in most cases. However, when the transport distance of concrete armour units is not significant smaller the berm breakwater could still be an attractive solution. When the transportation distance of the quarry material is 10 km the transportation cost is about 50% of the total construction costs [Sigurdarson et al., 1995]. An example of the cost of construction is given in Delft Hydraulics, 1985, where it is mentioned that the construction costs of the St. George Berm Breakwater was found to be between 50 and 70% of the cost of an equivalent traditional structure.

For a reshaping berm breakwater it is important to examine the rolling resistance of the stones, as these movements can result in breaking and abrasion of the stones. The armour stones can break when they hit other stones, and are primarily dependent on the impact energy and the ability of the stones to resist this energy. Abrasion results in rounding of the armour stones due to rolling back and forth which chips off small fragments. Drop tests are frequently used to evaluate the durability of the quarry material. An indicative measure of the durability is the rock density, as this is highly correlated with the strength. The

lower density of the stones the poorer inner bindings of minerals and the more water absorption which result in less freeze/thaw resistance. If good quality rock is not available near by, poorer rocks can be accepted for the core to reduce transportation costs.

In many cases the total cost of a berm breakwater is less than of a conventional breakwater, especially if the much better repair possibilities are taken into account. If some of the following criteria are fulfilled a berm breakwater could be considered to be a very attractive solution:

- Good quality quarry material is available within a short distance from the construction site.
- Not enough large stones available from the quarry to construct a conventional rubble mound breakwater unless a very flat slope is used. This will typically result in using concrete type armour units as armour of a conventional breakwater, which in many cases is far more expensive than using rock.
- Non-depth limited design conditions at the toe of the structure. In these cases the total volume of quarry needed to construct a berm breakwater could even be smaller than for a conventional breakwater.
- Little reflection from the breakwater is wanted to give less disturbance outside the harbour entrance and hence better maneuvering conditions.

## 2.8 Fines

It is very important that the pores in the berm are not filled with fines either during construction or during use as the performance of the breakwater may decrease significantly. Smaller material can enter the berm in one of the following ways [Gilman, 2001]:

- Running heavy tracked equipment on the berm.
- Deliberately pushing small material onto the berm in order to build pads for the equipment to work on the berm.
- Breaking of armour stones when dropped.
- Dispersal of small material when picked up a long with larger armour stones for placement in the berm.

The design must take this potential contamination into account and field inspections must stress the minimization of contamination through proper education of construction personal and monitoring of the work [PIANC, 2003, p. 45].

## 2.9 Designing Berm Breakwaters

Very limited information on stability and overtopping of berm breakwaters exist. Therefore designs are more or less always based on small scale model tests, and several iterations could be required to obtain a good design that meets the required design criteria with respect to overtopping and stability without being too conservative.

Although overtopping is an extremely important breakwater design parameter, the available information on overtopping of berm breakwaters is very limited, and no systematic study seems to exist. Therefore the present systematic model test study was initiated and resulted in an overtopping design formula for berm breakwaters, cf. chapter 5.

On front slope stability there exist some methods for calculating the reshaped profile, but non of them are universal and further most of them are, as shown in chapter 4, very uncertain. In chapter 4 a new, simple and reliable method to evaluate front slope stability is developed.

Some results on rear slope stability and reflection are presented in chapter 6 and 7.

## CHAPTER 3

# New Data from Present Berm Breakwater Tests

Overtopping, reflection, front and rear slope stability were studied for statically and dynamically stable berm breakwaters as well as non-reshaping statically stable berm breakwaters, all with homogenous berms. The test programme with a total of 695 tests covers influence of crest freeboard, crest width, berm width and elevation, sea state (wave height and steepness), stone size and water depth.

### 3.1 Test Set-Up

Physical model tests with head-on waves were performed in a wave flume of dimensions  $21.5 \times 1.2 \times 1.5$  m (length  $\times$  width  $\times$  depth) at Aalborg University. Oblique waves may cause longshore transport which can be an important factor for the stability of singular points of the breakwater and the maintenance needed, cf. section 2.5. For an infinite long trunk section recession and overtopping is normally larger for head-on waves than for oblique waves.

Besides few metres of horizontal bottom the flume bed had a slope of 1:20, giving a 0.60 m larger water depth at the wavemaker than at the toe of the structure, cf. Fig. 3.1. Arrays of three resistance type wave gauges were placed both at the deep end and at the toe of structure to separate incident and reflected waves. Because the bottom is sloping at the toe and the waves are more non-linear at the toe it is expected that the separation is more reliable at the deep end than at the toe. Nevertheless, the incident waves calculated at the toe are used in the present analysis as little reflection is observed in most tests and large changes in wave parameters due to breaking and shoaling could be expected. The position of the

### 3.1 Test Set-Up

wave gauges very close to the breakwater was chosen even though the reflection analysis is less reliable here. This was chosen because the waves in some cases were breaking close to the structure and thus the wave characteristics changes significantly within a short distance. The reflected waves are expected to be better estimated at the deep end.

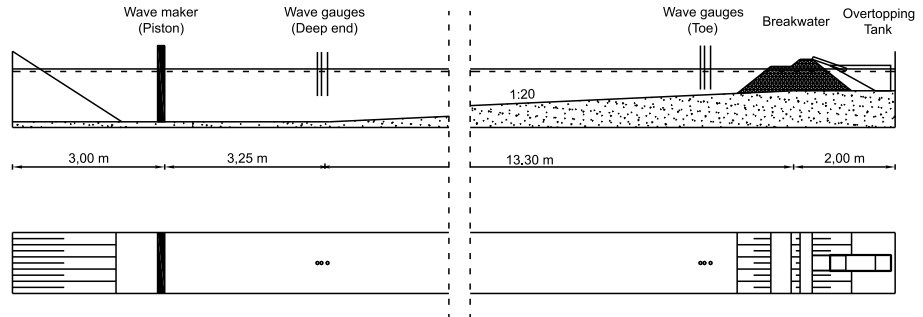


**Figure 3.1**

*Layout in flume (side and top view).*

Due to the construction method, the initial front and rear slopes of a reshaping breakwater are close to the natural angle of repose of the material. Slopes between 1:1 and 1:1.5 are typical. In all the present experiments, the slopes were 1:1.25 which was close to the natural angle of repose for the armour materials tested.

The crest level of the core was 2 cm below SWL, cf. Fig. 3.2.

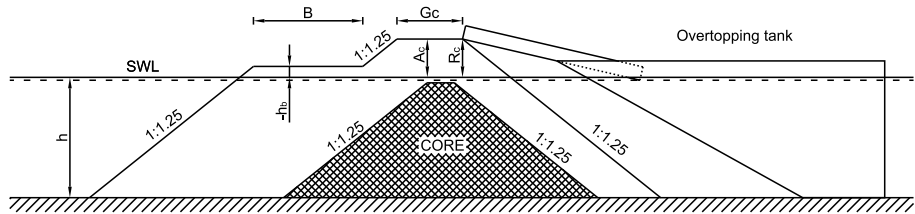


**Figure 3.2**

*Initial geometry of breakwater. Note  $h_b$  is negative when the berm initially is above SWL. Note that  $R_c = A_c$  in all tests due to the position of the overtopping ramp.*

The properties of the materials are given in Table 3.1.



**New Data from Present Berm Breakwater Tests**

	<b>Armour 1 (Largest)</b>	<b>Armour 2 (Medium)</b>	<b>Armour 3 (Smallest)</b>	<b>Core</b>
$W_{50}$ [kg]	0.175	0.0882	0.0202	0.0069
Mass density $\rho_s$ [kg/m <sup>3</sup> ]	3000	2630	2610	2700
$D_{n,50}$ [m]	0.0388	0.0323	0.0198	0.0137
$f_g = D_{n,85}/D_{n,15}$	1.35	1.35	1.45	1.59
Length to width ratio, $l/b$	1.98	1.96	2.01	2.04

**Table 3.1**  
*Material properties.*

The smallest armour stones (Armour 3) correspond in almost all tests to a dynamically stable reshaping berm breakwater. The largest armour stones (Armour 1) correspond to a non-reshaping berm breakwater. The grain size distribution curves are given in Fig. 3.3.

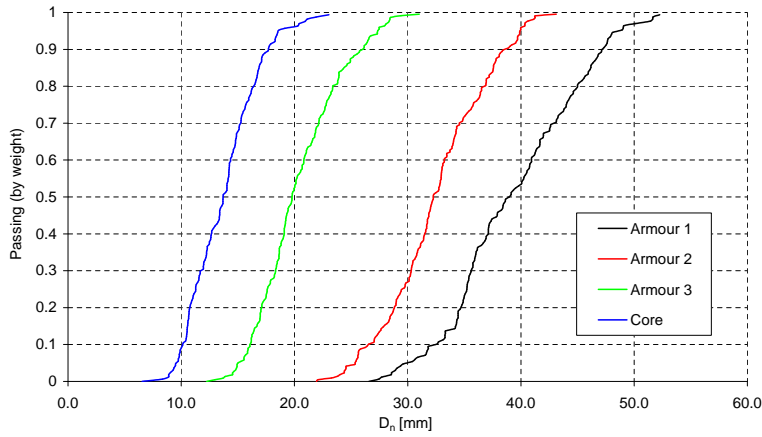


**Figure 3.3**  
*Gradation curves.*

Overtopping volumes were measured with a water surface amplitude gauge in a tank placed behind a ramp extending from the back of the crest ( $R_c = A_c$ ) as shown in Fig. 3.1 and 3.2. The measured overtopping volume is very dependent on the placement of the ramp. The uncertainty of the ramp placement is estimated to be  $\pm 2$  mm. The ramp and the tank was 0.297 m wide and placed in the middle of the flume. Prototype overtopping discharges between 0.05 l/m/s and 10 l/m/s were the target for the tests. The overtopping tank was constructed so both small and large overtopping volumes could be measured with good accuracy. A water surface elevation gauge was installed behind the breakwater to

### 3.1 Test Set-Up

---

measure the water level set-up.

After each test the reshaped profile was measured with a non-contact laser profiler (see upper right corner of Fig. 3.4) [Aalborg University, 2005a]. The profiler was setup to measure the profile in a grid with spacing  $1 \times 1$  cm. The profiles given in Appendix B are average profiles over the width discarding 10 cm at each side due to wall effects. The rear side erosion was visually observed at each side of the overtopping ramp as the ramp prevented erosion of the middle of the structure.



**Figure 3.4**

*Picture of test set-up viewed from the side.*

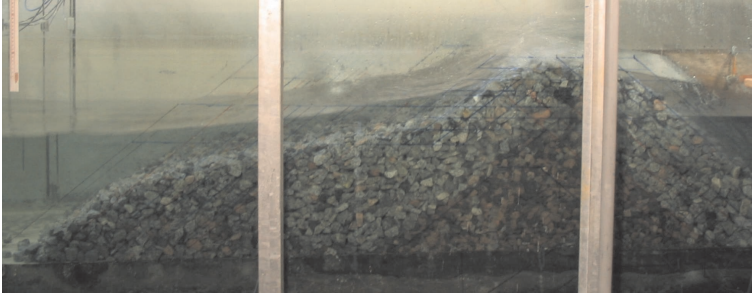


**Figure 3.5**

*Picture of breakwater from a test with Armour 3 (viewed from the side through the windows).*

### 3.2 Data Analysis

All signals were filtered using an analog lowpass filter with a cut-off frequency of 8 Hz. A digital filter with cut-off frequencies of  $1/3 \cdot f_p$  and  $3 \cdot f_p$  was applied to the wave signals. The method of Mansard and Funke, 1980 was applied to calculate the incident wave spectrum, and the SIRW method of Frigaard and Brorsen, 1995 was used to calculate the incident wave trains. All signal analysis was performed with the WaveLab2 software package [Aalborg University, 2005b].

### 3.3 Test Series - Range of Parameters

In each test series the wave height was gradually increased in steps with constant wave steepness. For each sea state the overtopping was recorded after the deformation of the breakwater had stabilized (at least 1500 waves used). The number of waves used after the reshaping to determine the average overtopping discharge was more than 1500.

The breakwater was only rebuilt when changing the initial geometry or the wave steepness, i.e. 150 times. Two tests have been performed with lower wave heights than the breakwater had reshaped to. Some experiments were carried out where the front was fixed with a net in order to determine how much the overtopping discharge differs between reshaped and non-reshaped profiles.

All tests were carried out with irregular waves generated from a JONSWAP spectrum with a peak enhancement factor ( $\gamma$ ) of 3.3 using a white noise filtering method. The tested range of wave steepness ( $s_{0p}$ ) was 0.01 - 0.054 with most of the tests close to 0.035 as illustrated in Fig. 3.6.

### 3.3 Test Series - Range of Parameters

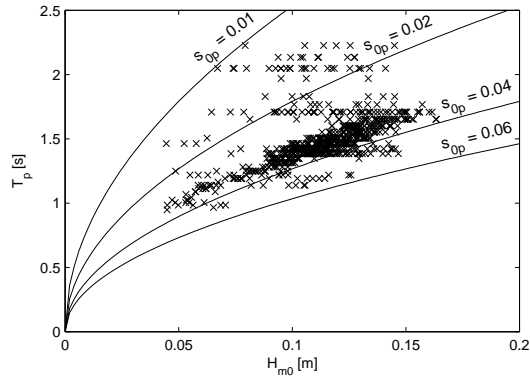


**Figure 3.6**  
*Tested sea states.*

The ranges of parameters covered in the tests are listed in Table 3.2:

Peak wave steepness ( $s_{op}$ )		0.010 - 0.054
Wave height at toe of structure ( $H_{m0}$ )	[m]	0.064 - 0.164
Water depth at toe of structure ( $h$ )	[m]	0.24, 0.34 and 0.44
Crest and armour crest freeboard ( $R_c/A_c$ )	[m]	0.08, 0.11, 0.14 and 0.17
Crest width ( $G_c$ )	[m]	0.17, 0.24, 0.31 and 0.38
Berm width ( $B$ )	[m]	0.00, 0.20, 0.30, 0.40, 0.50, 0.65
Berm elevation ( $h_b$ )	[m]	-0.04, 0.00, 0.04 and 0.12
Front slope below berm		1:1.25
Front slope above berm		1:1.25
Rear slope		1:1.25
Stability number ( $H_0$ )		0.96 - 4.86
Stability index incl. wave period ( $H_0T_0$ )		16.8 - 163
Reynolds number for berm stones ( $Re_D$ )		Armour 1: $3.32 \cdot 10^4$ to $4.92 \cdot 10^4$ Armour 2: $3.13 \cdot 10^4$ to $3.91 \cdot 10^4$ Armour 3: $1.60 \cdot 10^4$ to $2.44 \cdot 10^4$

**Table 3.2**  
*Range of parameters tested.*

594 tests have been performed with reshaped profiles to cover the ranges of parameters listed in Table 3.2. In addition, 59 tests were performed with fixed front geometry, cf. section 3.5. Moreover 42 tests with parameters given in section 3.4 have been performed in a smaller scale to study scale effects.

The main test results including the measured profiles are presented in Appendix

A and B.

### 3.4 Tests in Smaller Scale to Study Scale Effects

It was preferred to perform large scale tests to study influence of scale effect. This was however not possible at Aalborg University. Therefore 42 tests have been performed in smaller scale (Froude scaling) by using Armour size 4 given in Table 3.3, which however will give only a rough guess on scale effects. The small scale tests correspond to a length scale of approximately 1:1.9 of the tests with Armour 3, see Table 3.1. The Reynolds number varied from  $6.85 \cdot 10^3$  to  $8.80 \cdot 10^3$  in the tests with Armour 4. Due to the small difference in grain size between Armour 4 and the scaled core material, no core was present in the smaller scale tests.

	<b>Armour 4 (Scaled Armour 3)</b>
$W_{50}$ [kg]	0.0028
Mass density $\rho_s$ [kg/m <sup>3</sup> ]	2580
$D_{n,50}$ [m]	0.0103
$f_g = D_{n,85}/D_{n,15}$	1.36
Length to width ratio, $l/b$	1.88

**Table 3.3**  
*Material properties for model in smaller scale.*

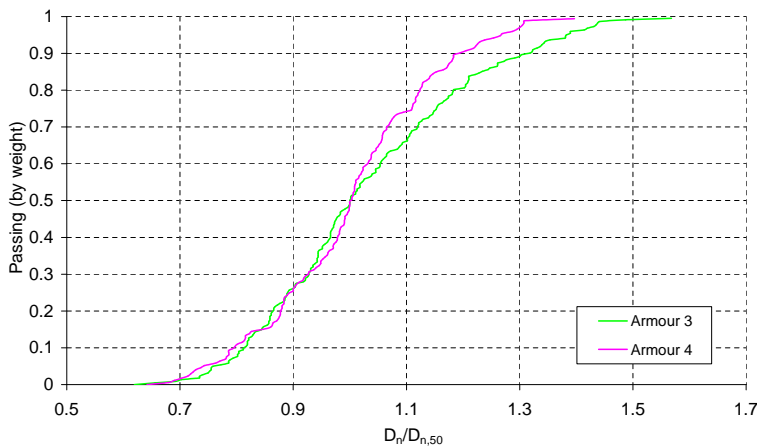


**Figure 3.7**  
*Comparison of gradation curves for Armour 3 and 4.*

### 3.5 Tests with Fixed Front to Study Influence of Reshaping

---

The gradation factor for Armour 3 and 4 are not identical as Armour 3 contains more large stones, cf. Fig. 3.7. The effect of this model effect was not quantified.

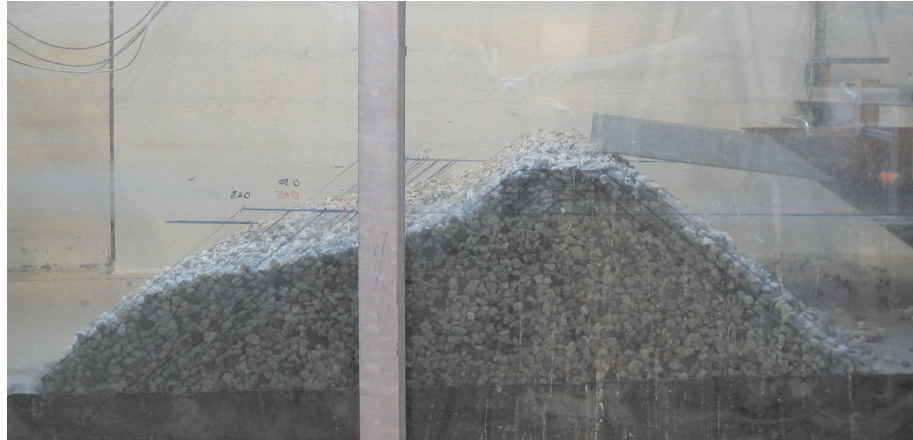


**Figure 3.8**  
*Scaled model with Armour 4 after reshaping.*

### 3.5 Tests with Fixed Front to Study Influence of Reshaping

To study the influence of reshaping on reflection and overtopping 59 tests were performed with fixed front geometry. The front was fixed with a net and steelbars as shown in Fig. 3.9. In this way the breakwater had almost unchanged roughness and was almost fully prevented in reshaping, although a little reshaping occurred mainly due to compaction.



**Figure 3.9**

*Picture showing test setup for tests with fixed front.*





## CHAPTER 4

# Front Slope Stability of Berm Breakwaters

The breakwater can be characterized by the stability parameter  $H_0$  defined as:

$$H_0 = \frac{H_{m0}}{\Delta \cdot D_{n,50}} \quad (4.1)$$

$\Delta = \frac{\rho_s}{\rho_w} - 1$  is the relative reduced mass density. It is common to include  $\Delta$  in this way in the stability number. Nevertheless discussions on this way of treating the density is still under investigation, cf. Helgason, 2006. In the present analysis it is assumed that the influence of the density can be described as in Eq. 4.1.

$H_0$  does not include the influence of the wave period, and a modified stability number which includes the effect of the wave period as well can be used instead. Van der Meer, 1988 introduced the dimensionless parameter  $H_0 T_0$  defined in Eq. 4.2, containing the mean wave period which was found to be the governing period for the reshaping, at least for large values of  $H_0$ .

$$H_0 T_0 = \frac{H_{m0}}{\Delta \cdot D_{n,50}} \cdot \sqrt{\frac{g}{D_{n,50}}} \cdot T_{0,1} \quad (4.2)$$

where  $T_{0,1} = m_0/m_1$  is a spectral mean wave period.

Table 4.1 shows the mobility criterion for the three types of berm breakwaters.

## 4.1 Existing Methods for Estimating the Berm Recession

---

Type of breakwater	$H_0$	$H_0T_0$
Statically stable non-reshaped berm breakwater	$< 1.5-2$	$< 20-40$
Statically stable reshaped berm breakwater	$1.5 - 2.7$	$40 - 70$
Dynamically stable reshaped berm breakwater	$> 2.7$	$> 70$

**Table 4.1**

*Mobility criterion (the criterion depends on stone gradation) [PIANC, 2003].*

Typical ranges of stability indices for berm breakwater trunk sections are  $2.5 < H_0 < 4$  and  $60 < H_0T_0 < 100$  for reshaping berm breakwaters.

The most important measure for the reshaping is the recession of the berm ( $Rec$ ) as failure typically is defined as  $Rec > B$ , but also the step height ( $h_s$ ) is of some importance, both parameters defined in Fig. 2.1. The depth at which the reshaped profile intersects with the initial profile ( $h_f$ ) is a measure also used to describe the reshaped profile (see Fig. 2.1). The movement of the profile at the bottom  $\Delta R$  can be important for design of scour protection. The parameters  $Rec$  and  $h_f$  are only good measures for the reshaped profile when the berm initially is located above or at mean water level. In case the berm initially is placed below SWL damage can occur even when the recession is 0%. For these structures damage/stability has to be defined otherwise.

In addition to ensuring that  $Rec \leq B$  for the design situation the designer has to look into longshore transport caused by oblique and/or short crested waves. It is important also to take into account the breaking and abrasion of armour stones which can occur due to stone movements, this is especially important for dynamically stable structures where stone movements continuously occur.

## 4.1 Existing Methods for Estimating the Berm Recession

As mentioned above the recession of the berm is the most important parameter describing the reshaping of berm breakwaters as front slope damage is normally defined as occurring when the entire berm is eroded ( $Rec > B$ ). Therefore it is important to have a reliable method to calculate the recession. For calculating the recession of the berm a number of methods exists, i.e:

- Van der Meer, 1992
- Van Gent, 1995
- Archetti and Lamberti, 1996

- Hall and Kao, 1991
- Tørum, 1998
- Tørum et al., 1999
- Tørum and Krogh, 2000

The first three methods give the entire profile, but a computer program is really needed to perform the calculations. The last methods are simple empirical formulae, which validity however are questionable as a number of important parameters are not included.

#### **4.1.1 Van der Meer, 1992**

As demonstrated in appendix B the method of Van der Meer, 1992 can with reasonable accuracy be used to calculate the reshaped profile for dynamically stable profiles ( $H_0T_0 > 70$ ). However, the method of Van der Meer (1992) has the following limitations:

- The method predicts too much damage for statically stable reshaped and non-reshaped breakwaters ( $H_0T_0 < 70$ ).
- The method assumes conservation of the total volume of the breakwater. However, it has been observed both during the present test programme and by other researchers that some compaction can occur.
- In principle the method could use the reshaped profile as input and then continuing from this profile with another sea state. However, in the present study it was observed that this resulted in less damage than always starting with the initial profile and worse agreement with measurements. Unless the water level varies a lot it is therefore suggested always to start with the initial profile in the calculations.

#### **4.1.2 Hall and Kao, 1991**

Hall and Kao, 1991 investigated the influence of rounded stones and stone gradation on reshaping of berm breakwaters. They give the following formula to calculate the recession of the berm:

$$\frac{Rec}{D_{n,50}} = -10.4 + 0.51 \cdot H_0^{2.5} + 7.52 \cdot f_g - 1.07 \cdot f_g^2 + 6.12 \cdot P_R \quad (4.3)$$

## 4.1 Existing Methods for Estimating the Berm Recession

---

$P_R$  is the fraction of rounded stones in the armour. Breaking and abrasion of armour stones can occur during reshaping leading to an increase of the fraction of rounded stones.

### 4.1.3 Tørum, 1998

Tørum, 1998 and Tørum et al., 1999 give a formula (Eq. 4.4) to calculate the recession of the berm based on small scale model test results from different projects and laboratories.

$$\frac{Rec}{D_{n,50}} = 7.39 \cdot 10^{-4} \cdot (H_0 T_0)^2 + 4.99 \cdot 10^{-2} \cdot H_0 T_0 + 0.604 \quad (4.4)$$

### 4.1.4 Tørum and Krogh, 2000

Menze, 2000 and Tørum and Krogh, 2000 modified the equation of Tørum, 1998 to take into account the effect of stone gradation and water depth respectively. Hence PIANC, 2003 gives the following formula to calculate the recession of the berm of a homogenous berm:

$$\begin{aligned} \frac{Rec}{D_{n,50}} = & 2.7 \cdot 10^{-6} \cdot (H_0 T_0)^3 + 9 \cdot 10^{-6} \cdot (H_0 T_0)^2 + 0.11 \cdot H_0 T_0 \\ & - f_{grading} - f_d \end{aligned} \quad (4.5)$$

where  $f_{grading}$  is a factor depending on the stone gradation  $f_g$  and  $f_d$  is a depth factor.

$$f_{grading} = -9.9 \cdot f_g^2 + 23.9 \cdot f_g - 10.5 \quad \text{for } 1.3 < f_g < 1.8 \quad (4.6)$$

$$f_d = -0.16 \cdot \frac{h}{D_{n,50}} + 4.0 \quad \text{for } 12.5 < h/D_{n,50} < 25 \quad (4.7)$$

The depth at which the reshaped profile intersects with the initial profile ( $h_f$ ) can within the range  $12.5 < h/D_{n,50} < 25$  be estimated from [PIANC, 2003, Eq. 4.4]:

$$\frac{h_f}{D_{n,50}} = 0.2 \cdot \frac{h}{D_{n,50}} + 0.5 \quad \text{for } 12.5 < h/D_{n,50} < 25 \quad (4.8)$$

### **4.1.5 Summary**

The formula of Hall and Kao, 1991 and Tørum and Krogh, 2000 do not include the influence of berm elevation and front slope which are two important parameters for the recession. The reshaped profile will for identical volumes of stones be approximately independent on the front slope, but much more material has to be moved for the steep slope which therefore leads to much more recession. As shown in section 4.3 the present data and other researchers' data show that these formulae are not generally valid. Tørum, 1998 concluded that the deviations between the measurements and his formula was due to a random scatter mechanism. However, many of the deviations observed by Tørum, 1998 was not present in the method of Van der Meer, 1992. This shows that the need for a simple and reliable method to calculate the amount of recession at least as accurately as the method of Van der Meer, 1992.

Many of the deviations observed by Tørum, 1998 has also been addressed by the formula derived in section 4.2, which seems to be superior to the other methods tested, including the method of Van der Meer, 1992.

## **4.2 Development of Semi-Empirical Recession Formula**

A formula to calculate berm recession is derived in this section. The recession formula is based on some theoretical considerations on the influence of front slope, water depth and berm elevation, cf. section 4.2.1. The formula is calibrated mainly using the present data with Armour 1-3, but also data of other researchers is used to cover ranges/parameters not covered in the present test programme.

### **4.2.1 Influence of Slope, Water Depth and Berm Elevation**

The reshaped profile has generally the following characteristics:

- In case of dynamically stable profiles the final reshaped profiles are for the same volume of material approximately independent of the initial lower front slope. Therefore the recession is less for a flatter initial front slope (larger volume).
- If the breakwater is not located in very shallow water wave conditions, the slope of the reshaped profile approaches the natural angle of repose on the

## 4.2 Development of Semi-Empirical Recession Formula

---

lower part. The distance from SWL to this transition is called the step height  $h_s$  (see Fig. 2.1 on page 25).

- Between SWL and the step the slope is flat with a slope around 1:5 and slightly curved.
- In case of a high berm the slope approaches the natural angle of repose a small distance above SWL.

Based on the above observations the change in recession due to change in front slope, water depth and berm elevation is investigated. Two situations are considered and an approximate formula for the difference in recession between the two situations is derived based on the observed geometry of the reshaped profiles listed above and some geometrical considerations.

The initial profile in situation 1 has the following parameters:

- Water depth is equal to the step height ( $h_1 = h_s$ ).
- Berm is located at SWL ( $h_{b1} = 0$ ).
- The front slope is equal to the natural angle of repose ( $\cot(\alpha_{d1}) \approx 1.05$ )

Situation 2 has a water depth  $h_2 \geq h_s$ , a berm elevation  $h_{b2} \leq 0$  (berm initially above or at SWL) and an arbitrary initial front slope  $\alpha_{d2}$ . An important assumption in the following is that the step height does not change from situation 1 to situation 2, which seems quite reasonable as the incident waves are the same. The idea is that a much simpler formula for calculating the recession of the berm can in situation 1 can be derived compared to situation 2 as the initial geometry is fixed in situation 1.

The two initial and reshaped profiles are shown in Fig. 4.1. Note in situation 2 the reshaped profile from situation 1 has been used between the step and SWL. Above SWL and below the step a slope of 1:1.05 has been assumed which is based on the general profile observations listed above. The profile was then moved horizontally so the total volume was conserved. A formula for the amount of movement needed is derived in the following.

## Front Slope Stability of Berm Breakwaters

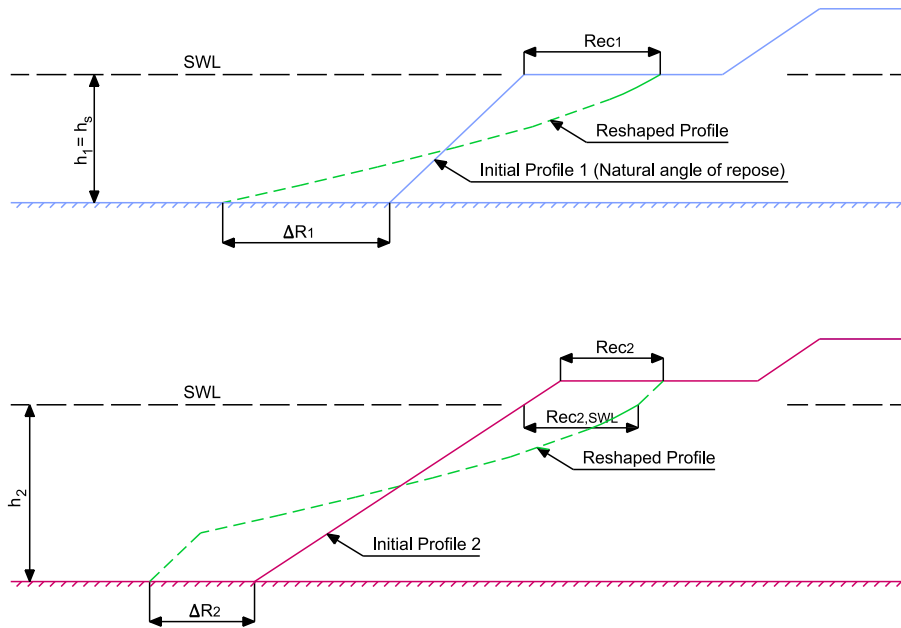


**Figure 4.1**  
*Situation 1 (blue) and 2 (red).*

In Fig. 4.2 the initial and reshaped profiles in situation 1 and 2 are shown in the same figure. In this figure the volume conservation is fulfilled for situation 1 but not for situation 2. It is now calculated how much the profile has to be moved in situation 2 to fulfill the volume conservation criteria. This is done by horizontally moving the profile until  $A1 + A2 = A3$ .

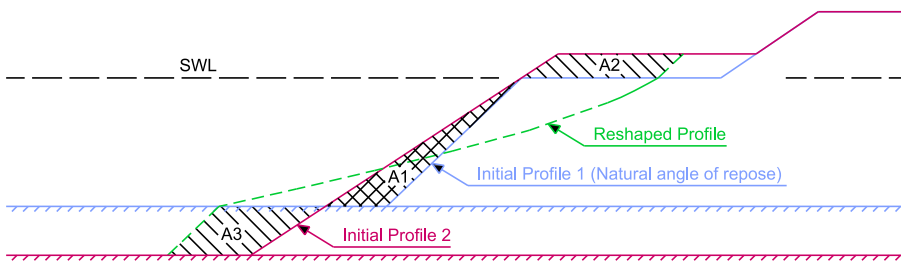


**Figure 4.2**  
*Situation 1 (blue) and 2 (red). Note that in situation 2 the volume conservation is not fulfilled. This is taking into account later by moving the profile forward or backward.*

## 4.2 Development of Semi-Empirical Recession Formula

---

The three areas  $A_1$ ,  $A_2$  and  $A_3$  defined in Fig. 4.2 can be calculated as:

Area in slope:

$$A_1 = \frac{h_1^2}{2} \cdot (\cot(\alpha_{d2}) - \cot(\alpha_{d1})) \quad (4.9)$$

Inserting  $\alpha_{d1} = 1.05$  gives:

$$A_1 = \frac{h_s^2}{2} \cdot (\cot(\alpha_{d2}) - 1.05) \quad (4.10)$$

Area in berm:

$$A_2 = Rec_1 \cdot (-h_{B2} + h_{B1}) - \frac{(-h_{B2} + h_{B1})^2}{2} \cdot (\cot(\alpha_{d2}) - 1.05) \quad (4.11)$$

Inserting  $h_{B1} = 0$  gives:

$$A_2 = -Rec_1 \cdot h_{B2} - \frac{h_{B2}^2}{2} \cdot (\cot(\alpha_{d2}) - 1.05) \quad (4.12)$$

Area at bottom:

$$A_3 = (h_2 - h_1) \cdot (\Delta R_1 - (\cot(\alpha_{d2}) - \cot(\alpha_{d1})) \cdot (h_1 - h_{B1})) - \frac{(h_2 - h_1)^2}{2} \cdot (\cot(\alpha_{d2}) - 1.05) \quad (4.13)$$

Inserting  $h_1 = h_s$ ,  $\cot(\alpha_{d1}) = 1.05$  and  $h_{B1} = 0$  gives:

$$A_3 = (h_2 - h_s) \cdot (\Delta R_1 - (\cot(\alpha_{d2}) - 1.05) \cdot h_s) - \frac{(h_2 - h_s)^2}{2} \cdot (\cot(\alpha_{d2}) - 1.05) \quad (4.14)$$

In general the reshaped profile is slightly curved between SWL and the step. If a straight line is used as an approximation, it leads to that the movement of the profile at the bottom in situation 1 ( $\Delta R_1$ ) is equal to the recession of the berm ( $Rec_1$ ). In reality the movement at the bottom  $\Delta R_1$  is slightly larger than  $Rec_1$  (see Fig. 4.2) and  $\Delta R_1 = c_1 \cdot Rec_1$  is used, where  $c_1$  is a constant with a value around 1.2. The reshaped profile is now moved forward or backward until



the mass balance is fulfilled, which is an approximation as some compaction can occur. This leads to:

$$\begin{aligned}
 (Rec_{2,SWL} - Rec_1) \cdot (h_2 - h_{B2}) &= A_3 - A_1 - A_2 \\
 &= (h_2 - h_s) \cdot [c_1 \cdot Rec_1 - (\cot(\alpha_{d2}) - 1.05) \cdot h_s] - \\
 &\quad \frac{(h_2 - h_s)^2}{2} \cdot (\cot(\alpha_{d2}) - 1.05) - \\
 &\quad \frac{h_s^2}{2} \cdot (\cot(\alpha_{d2}) - 1.05) + \\
 &\quad Rec_1 \cdot h_{B2} + \frac{h_{B2}^2}{2} \cdot (\cot(\alpha_{d2}) - 1.05)
 \end{aligned} \tag{4.15}$$

The change in recession due to a higher point of measuring the recession when  $h_{B2} < 0$  is taking into account later. Therefore the parameter  $Rec_{2,SWL}$  in Eq. 4.15 is not actually the recession in situation 2 but the recession at the still water level in situation 2. Eq. 4.15 can be rewritten as:

$$\begin{aligned}
 Rec_{2,SWL} - Rec_1 &= \frac{c_1 \cdot (h_2 - h_s) + h_{B2}}{h_2 - h_{B2}} \cdot Rec_1 + \\
 &\quad [\cot(\alpha_{d2}) - 1.05] \cdot \left[ \frac{\frac{1}{2}h_{B2}^2 - \frac{1}{2}h_s^2}{h_2 - h_{B2}} \right]
 \end{aligned} \tag{4.16}$$

The change in recession due to the higher measuring point for the recession in situation 2 ( $h_{B2} < 0$ ) could be expressed as:

$$Rec_2 - Rec_{2,SWL} = (h_{B2} - h_{B1}) \cdot [\cot(\alpha_{d2}) - 1.05] \tag{4.17}$$

Inserting  $h_{B1} = 0$  gives:

$$Rec_2 = Rec_{2,SWL} + h_{B2} \cdot [\cot(\alpha_{d2}) - 1.05] \tag{4.18}$$

Combining Eq. 4.16 and 4.18 leads to:

$$\begin{aligned}
 Rec_2 - Rec_1 &= \frac{c_1 \cdot (h_2 - h_s) + h_{B2}}{h_2 - h_{B2}} \cdot Rec_1 + \\
 &\quad [\cot(\alpha_{d2}) - 1.05] \cdot \left[ \frac{\frac{1}{2}h_{B2}^2 - \frac{1}{2}h_s^2}{h_2 - h_{B2}} + h_{B2} \right]
 \end{aligned} \tag{4.19}$$

Which could be rewritten as:

$$Rec_2 = \frac{(1 + c_1) \cdot h_2 - c_1 \cdot h_s}{h_2 - h_{B2}} \cdot Rec_1 + [\cot(\alpha_{d2}) - 1.05] \cdot \frac{1}{2} \cdot [h_{B2} - h_2] \quad (4.20)$$

The recession is made dimensionless with the stone size:

$$\frac{Rec_2}{D_{n,50}} = \frac{(1 + c_1) \cdot h_2 - c_1 \cdot h_s}{h_2 - h_{B2}} \cdot \frac{Rec_1}{D_{n,50}} + \frac{\cot(\alpha_{d2}) - 1.05}{2 \cdot D_{n,50}} \cdot (h_{B2} - h_2) \quad (4.21)$$

As mentioned earlier  $c_1$  is a constant equal to approximately 1.2. With Eq. 4.21 it is possible to calculate the recession in situation 2, when the recession in situation 1 ( $Rec_1$ ) and the step height ( $h_s$ ) are known. Situation 1 has an initial profile with  $\cot(\alpha_{d1})=1.05$ ,  $h_{b1}=0$  and  $h_1 = h_s$ . The dimensionless recession in situation 1 is assumed to be a function of the wave direction ( $\beta$ ), the number of waves ( $N$ ), the grading of the armour stones represented by the gradation factor ( $f_g$ ) and a stability index ( $H_0$ ,  $T_0$  and  $s_{0m}$ ). A product of 4 functions is used:

$$\begin{aligned} \frac{Rec_1}{D_{n,50}} &= f(\beta, N, f_g, H_0, T_0, s_{0m}) \\ &= f_\beta(\beta) \cdot f_N(N) \cdot f_{grading}(f_g) \cdot f_{H0}(H_0, T_0, s_{0m}) \end{aligned} \quad (4.22)$$

### 4.2.2 Influence of Wave Direction

The influence of the wave direction has not been studied in the present tests, but Van der Meer, 1988 states that all profile parameters except the crest height is reduced by a factor  $\cos(\beta)$ , where  $\beta$  is the angle of wave attack ( $\beta = 0$  for head-on waves). On this basis the following reduction factor is introduced:

$$f_\beta = \cos(\beta) \quad (4.23)$$

In Fig. 4.21 this expression is verified for the trunk section. Clearly at singular points the recession could be bigger due to longshore transport which is not studied in this project. Therefore, eq. 4.23 is valid for a straight breakwater that is infinite long or where material is added at the singular point corresponding to the longshore transport.

### 4.2.3 Influence of Number of Waves

Damage of reshaping berm breakwaters is expected to develop much faster than on a conventional rubble mound breakwater due to much smaller resistance to

wave action. From Van der Meer, 1988 it is known that the reshaped profile parameters are proportional to  $N^a$  where  $a$  is a constant. For conventional rubble mound breakwaters  $a$  is around 0.5, whereas a much lower value is found for reshaping berm breakwaters [Van der Meer, 1988]. Van der Meer, 1992 found for large stability numbers that the step height and length was proportional to  $N^{0.07}$  corresponding to  $a = 0.07$  for dynamically stable structures ( $H_0 > 5$ ).

The resistance to wave action depends on the slope angle and the stability number. It is expected that damage develops faster on a steep slope and for large stability numbers. Limited data is available on the combined influence of slope, stability number and number of waves. Therefore, the slope angle is not included in the following equation to describe the influence of the number of waves:

$$f_N = \begin{cases} (N/3000)^{-0.046 \cdot H_0 + 0.3} & \text{for } H_0 < 5 \\ (N/3000)^{0.07} & \text{for } H_0 \geq 5 \end{cases} \quad (4.24)$$

3000 waves is used as the reference value as this is the value used in the present tests, which the formula mainly is fitted to. The expression is verified in section 4.2.12. During the present physical model tests it was visually observed that after 500 waves only minor change in the profile occurs, which is in good agreement with the formula. It should be noted that the crest still increases in height even after a fairly long duration of wave attack [Van der Meer, 1992].

#### 4.2.4 Influence of Stone Gradation and Shape

The shape of a stone can be characterized by the ratio between the length of the longest and shortest side ( $l/b$ ). Frigaard et al., 1996 tested four types of stone shapes, round ( $l/b = 1.0 - 1.5$ ), normal ( $l/b = 1.5 - 2.5$ ), flat ( $l/b = 2.5 - 3.5$ ) and a mix of these three ( $l/b = 1.0 - 3.5$ ). The four stone types had exactly identical gradation curves. Any measurable difference in the profiles for the four stone types were not observed. However, the longshore transport rates were 3-5 times higher for the flat stones compared to the round stones.

Hall, 1991 performed physical model tests to study the influence of stone gradation and the percentage of rounded stones in the armour stones. He tested 4 different gradings with  $f_g$  in the range 1.35 to 5.4 with 30% rounded stones, further 2 gradations were tested with respectively 0% and 15% rounded stones. Hall, 1991 found increasing recession of the berm with increasing grading factor and increasing percentage of rounded stones. A wider grading typically decrease the porosity resulting in less energy disipation in the berm. However, for a very wide grading Hall, 1991 found increasing stability, which he explained by the

## 4.2 Development of Semi-Empirical Recession Formula

---

larger stones dominating over the decrease in energy dissipation. Another reason for the decreased stability for a wide gradation could be the redistribution of material along the slope, resulting in smaller  $W_{50}$  on the berm for a wide gradation compared to a narrow gradation for identical overall  $W_{50}$ .

Lissev and Daskalov, 2000 performed physical model tests with regular waves and 5 different stone gradations ( $f_g$ ) in the range 1.2 to 3.92. Lissev and Daskalov, 2000 found no difference in recession for the two stone gradations  $f_g = 1.2$  and  $f_g = 1.5$ , while for higher values of  $f_g$  the recession is significantly larger with maximum for  $f_g \approx 2.5$ .

Van der Meer, 1988 found almost no difference in the profiles when comparing  $f_g = 1.25$  and  $f_g = 1.50$ , whereas the wide grading with  $f_g = 2.5$  gave a much longer profile below SWL.

DHI, 1996 performed tests with the two gradings  $f_g = 1.38$  and  $f_g = 1.79$  and found more recession for the wide grading.

Thus all available data on the influence of the stone gradation factor seems to be in good agreement, and the following factor is introduced in the recession formula.

$$f_{grading} = \begin{cases} 1 & \text{for } f_g \leq 1.5 \\ 0.43 \cdot f_g + 0.355 & \text{for } 1.5 < f_g < 2.5 \\ 1.43 & \text{for } f_g > 2.5 \end{cases} \quad (4.25)$$

The increase in stability for  $f_g > 2.5$  is not taken into account, which is on the safe side. The expression is verified in section 4.2.13 for all available data.

### 4.2.5 Step Height $h_s$

The expression given in Eq. 4.26 is used for  $h_s$ , which is based on curve fitting by hand to the present experiments. The step height is assumed independent on the initial geometries, which was also an assumption when deriving Eq. 4.21. That this assumption is quite good can be seen from Fig. 4.3 where the expression is evaluated against the present data.

$$h_s = 0.65 \cdot H_{m0} \cdot s_{0m}^{-0.3} \cdot f_N \cdot f_\beta \quad (4.26)$$

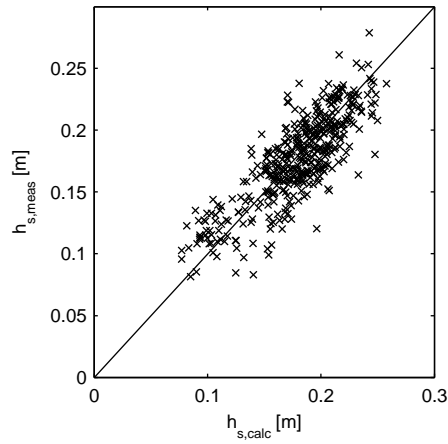


**Figure 4.3**  
Evaluation of Eq. 4.26 against present data.

### 4.2.6 Influence of Stability Numbers

For large values of  $H_0$  Van der Meer, 1992 found that the governing parameter was  $H_0T_0$ , which will say equal influence of wave height and period. For smaller values of  $H_0$  it was observed that the period may have little or no influence as found by Kao and Hall, 1990.

The influence of the stability numbers is evaluated by rearranging Eq. 4.21 and 4.22, which leads to:

$$f_{H0} = \left[ \frac{Rec_2}{D_{n,50}} - \frac{\cot(\alpha_{d2}) - 1.05}{2 \cdot D_{n,50}} \cdot (h_b - h) \right] \cdot \frac{h_2 - h_{b2}}{(1 + c_1) \cdot h_2 - c_1 \cdot h_s} \cdot \frac{1}{f_N \cdot f_{grading}} \quad (4.27)$$

By plotting the right handside of Eq. 4.27 against  $H_0$  and  $H_0T_0$  the variation of  $f_{H0}$  is evaluated.

## 4.2 Development of Semi-Empirical Recession Formula

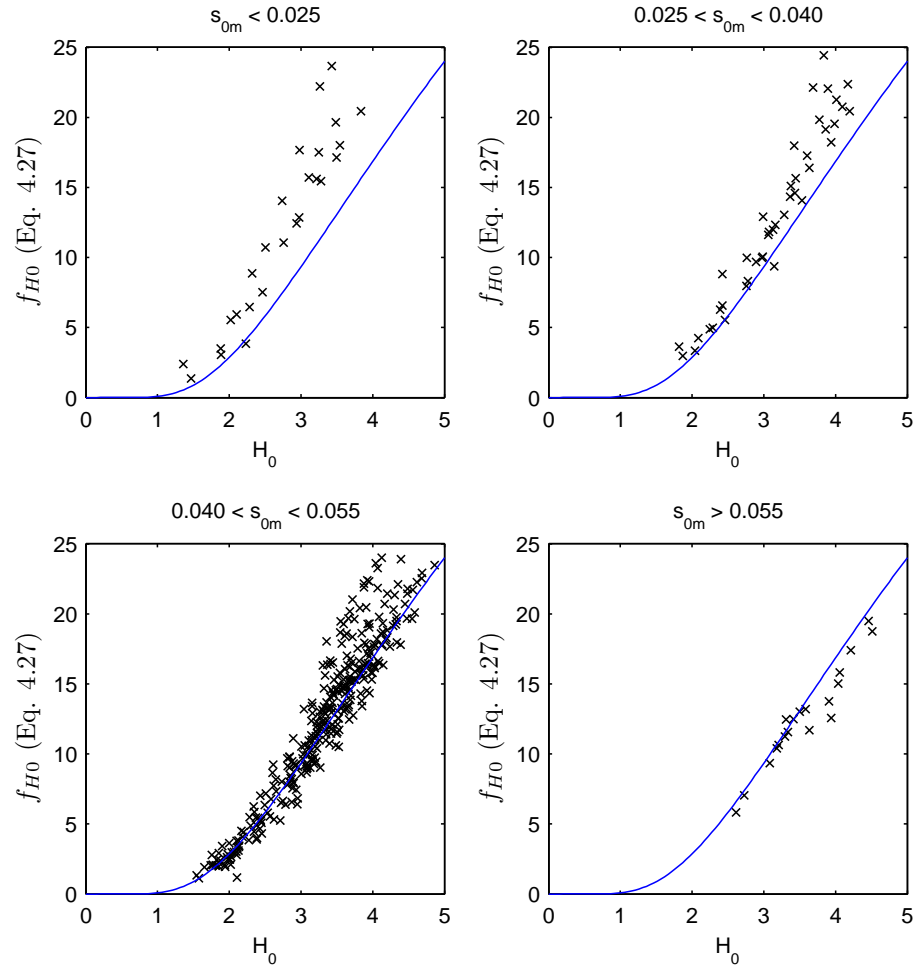


**Figure 4.4**  
Variation of  $f_{N_s}$  with  $H_0$  (present data with  $h_b \leq 0$ ).

The present tests confirm the finding of Kao and Hall, 1990 as only minor influence of the wave steepness was found for  $H_0 < 3.5$ . The recession is proportional to  $s_{0m}^{-0.5}$  for  $H_0 < 3.5$  and the recession could be expressed as an exponential function of  $1/H_0$ :

$$f_{H_0} = 19.8 \cdot \exp\left(-\frac{7.08}{H_0}\right) \cdot s_{0m}^{-0.5} \quad \text{for } H_0 < 3.5 \quad (4.28)$$

Fig. 4.5 shows the evaluation of Eq. 4.28.

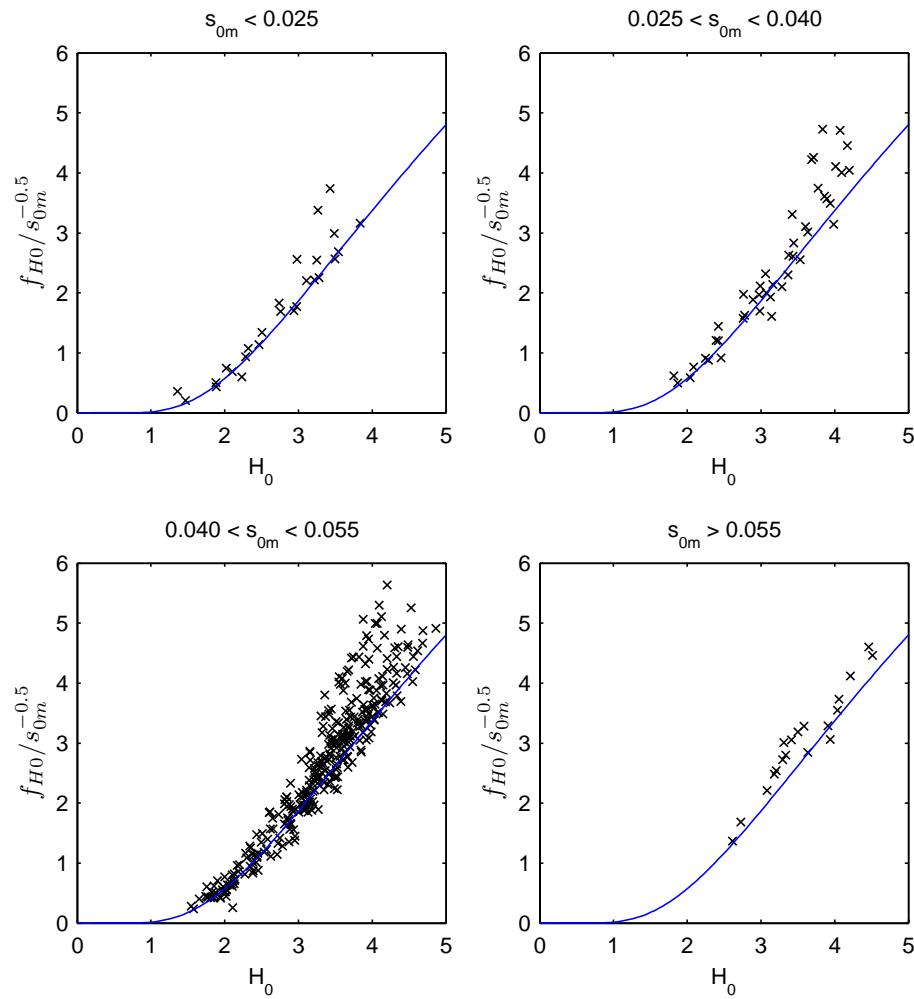


**Figure 4.5**  
Evaluation of  $f_{N_s}$  (present data with  $h_b \leq 0$ ).

For  $H_0 > 5$  the recession is assumed to be a function of  $H_0 T_0$  which means equal influence of the wave height and the wave period. This is based on the data of Van der Meer, 1988 and Burcharth and Frigaard, 1990, as only limited data

## 4.2 Development of Semi-Empirical Recession Formula

exists for very large values of  $H_0T_0$ , as this is outside the area normally used for berm breakwaters. Fig. 4.6 shows the variation with  $H_0T_0$ . The blue line is the formula used for large  $H_0T_0$  values (Eq. 4.29), which does not seem to fit the data that well, but this is due to an additional factor introduced later to take into account wave skewness.

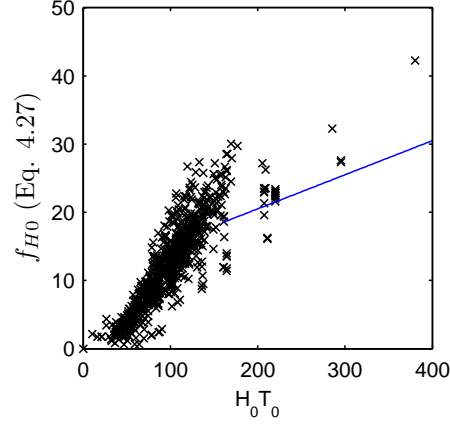


**Figure 4.6**  
 *$f_{H_0}$  plotted against  $H_0T_0$  (all available data).*

$$f_{H_0} = 0.05 \cdot H_0T_0 + 10.5 \quad \text{for } H_0 > 5.0 \quad (4.29)$$

Between  $H_0 = 3.5$  and  $H_0 = 5$  there is more scatter than for lower and higher values. It is nevertheless proposed simply to use the intersection between the two formula as the transition point, which can be expressed analytical as:

$$T_0^* = \frac{19.8 \cdot \exp\left(-\frac{7.08}{H_0}\right) \cdot s_{0m}^{-0.5} - 10.5}{0.05 \cdot H_0} \quad (4.30)$$

Eq. 4.28 is used for  $T_0 \geq T_0^*$  and Eq. 4.29 is used for  $T_0 < T_0^*$ , yielding:

$$f_{H_0} = \begin{cases} 19.8 \cdot \exp\left(-\frac{7.08}{H_0}\right) \cdot s_{0m}^{-0.5} & \text{for } T_0 \geq T_0^* \\ 0.05 \cdot H_0T_0 + 10.5 & \text{for } T_0 < T_0^* \end{cases} \quad (4.31)$$



### 4.2.7 Influence of Breaking Waves

Breaking waves seem to have an effect on the stability of a berm breakwater, as there are several indications of more damage for breaking and broken waves. Hedar, 1960 comes to more or less the same result from tests with regular waves on rock fill slopes, as he found waves breaking around one half wave length from the structure gave significantly more damage.

In Fig. 4.7 - 4.12 is the deviation in calculated (using Eq. 4.21 and 4.22 with the proposed equations for  $h_s$ ,  $f_\beta$ ,  $f_N$ ,  $f_{grading}$  and  $f_{H0}$ ) and measured berm recession plotted against some parameters which are influenced by wave breaking.

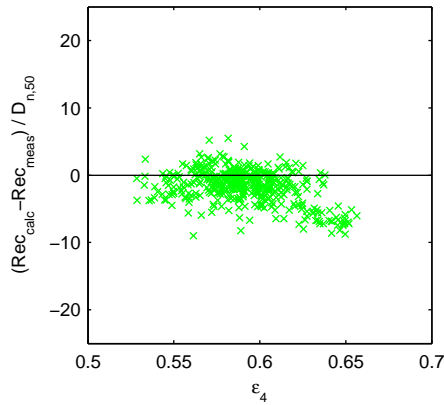


**Figure 4.7**  
Variation with spectral width  $\epsilon_4$  (broadness factor) for present data.

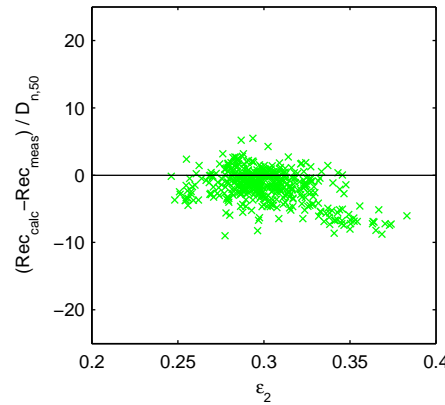


**Figure 4.8**  
Variation with spectral width  $\epsilon_2$  (narrowness parameter) for present data.

A JONSWAP spectrum with  $\gamma = 3.3$  and cut-off frequencies  $f_p/3$  and  $3 \cdot f_p$  has  $\epsilon_2 = 0.295$  and  $\epsilon_4 = 0.588$ . Much higher values of the spectral width parameter indicates breaking and broken waves as this leads to a wider spectrum. For high values of  $\epsilon$  more damage is observed, cf. Fig. 4.7 and 4.8

For a Gaussian process the skewness is zero and the kurtosis is 3. A kurtosis larger than 3 implies that the distribution of the wave height (from trough to crest) is broader than the Gaussian distribution, leading to a higher estimate of the extreme wave height in a sea state. The kurtosis does not seem to have any significant influence on the recession. A positive skewness means that the crest height is larger than the trough and vice versa. The skewness of the waves is an important parameter for the stability as larger skewness give more damage, cf. Fig. 4.10. Nearly breaking waves have a large skewness.

## 4.2 Development of Semi-Empirical Recession Formula

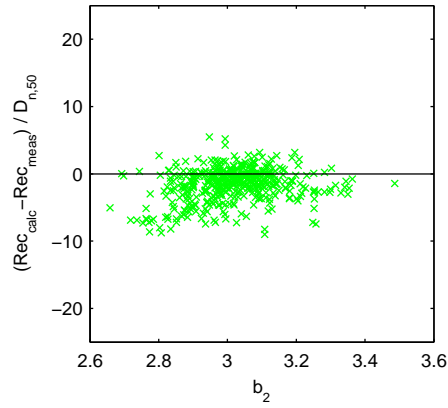


**Figure 4.9**  
Variation with kurtosis  $b_2$  (present data).

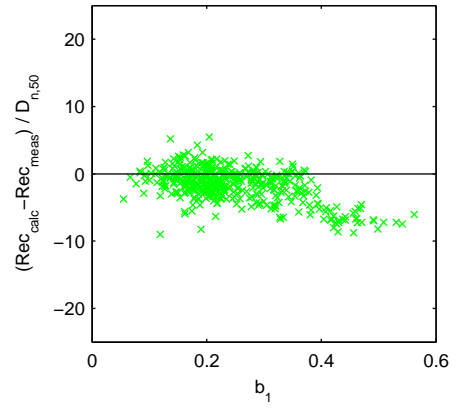


**Figure 4.10**  
Variation with skewness  $b_1$  (present data).

It was found that the kurtosis which is a measure for the wave height distribution had only minor or no influence on the recession. The same is the case for  $H_{1/100}/H_{m0}$  (see Fig. 4.11) which is another measure for the wave height distribution from which it can be concluded that the wave height distribution has only minor influence on the reshaping, cf. Fig. 4.11. However, it is worth mentioning that a small kurtosis and a small value of  $H_{1/100}/H_{m0}$  seems to give an underprediction of the recession. This is an indication of more recession for small values of  $H_{1/100}/H_{m0}$  compared to bigger values, but could also be an effect of other parameters indirectly influencing the wave height distribution. The findings is maybe opposite of what one expect, but low values of  $H_{1/100}/H_{m0}$  indicates depth limited breaking and broken waves, which seems to give more damage than none breaking waves.

$T_{-1,0}$  is a wave period which gives more weight to the lower frequencies in the spectrum as compared to the average period  $T_{0,1}$ . For single peaked spectra this period is close to the peak period. Breaking waves result in a wider spectrum and hence  $T_{-1,0}/T_{0,1}$  will be larger.

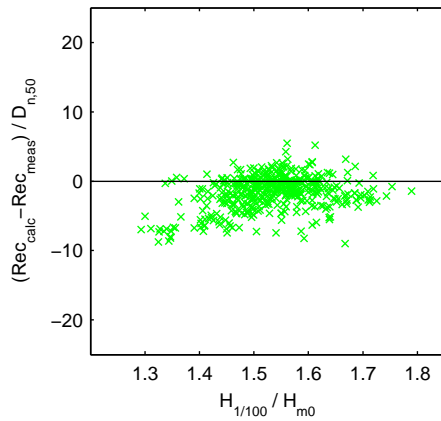


**Figure 4.11**  
Variation with wave height distribution  
 $H_{1/100}/H_{m0}$  (present data).

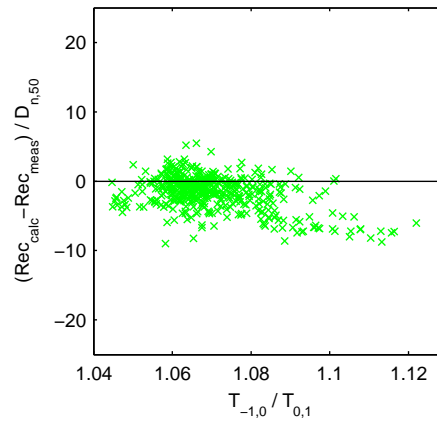


**Figure 4.12**  
Variation with  $T_{-1,0}/T_{0,1}$  (present data).

It can be concluded that there are several indication of larger damage for breaking waves. The best way to characterize this seems to be from the skewness of the waves and the following factor is introduced:

$$f_{skewness} = exp(1.5 \cdot b_1^2) \quad (4.32)$$

After introducing this parameter the data shows no systematic variation with  $\epsilon_4$ ,  $\epsilon_2$ , kurtosis, skewness,  $H_{1/100}/H_{m0}$  and  $T_{-1,0}/T_{0,1}$ .

#### 4.2.8 Influence of Wave Groupiness

The groupiness factor of a completely Gaussian signal can be shown to be equal to 1.0 independent of the spectrum shape. The actual values for time signals generated from a JONSWAP spectrum using random uncorrelated phases including approximately 500 waves are approximately 1.0 in mean with a standard deviation of approximately  $\sigma = 0.13$ , and of course less spreading when the signal contains more than 500 waves. Nothing was in the present test programme done to test a large interval of the groupiness factor as a standard white noise filtering generation method was used. From the present data it can be observed that the wave groupiness has no significant influence on the stability of a berm breakwater, Hall, 1994 arrived at the same conclusion from his data.

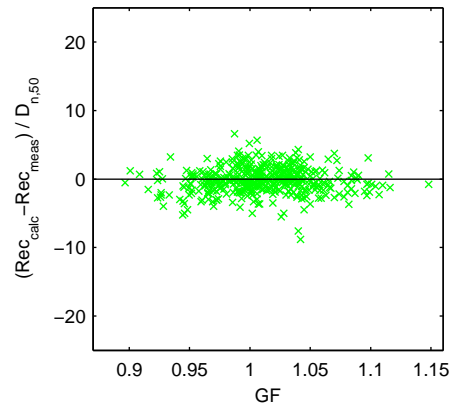


**Figure 4.13**  
Variation with wave groupiness  $GF$  (present data).

### 4.2.9 Influence of a Low Berm

When the initial berm is located below SWL (not really a berm breakwater) the recession is much lower as shown in Fig. 4.14. This is taken into account by the reduction factor given in Eq. 4.33, which variation is also shown in Fig. 4.14.

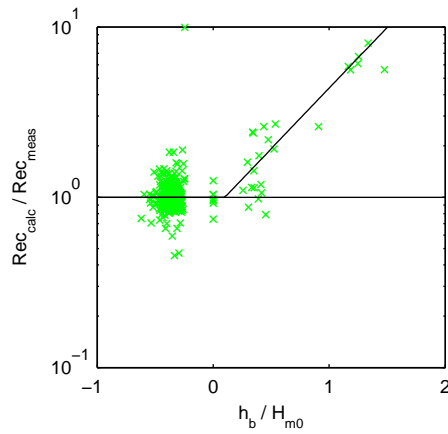


**Figure 4.14**  
Influence of a low berm (present data).

$$f_{h_b} = \begin{cases} 1.18 \cdot \exp\left(-1.64 \cdot \frac{h_b}{H_{m0}}\right) & \text{for } \frac{h_b}{H_{m0}} > 0.1 \\ 1 & \text{for } \frac{h_b}{H_{m0}} \leq 0.1 \end{cases} \quad (4.33)$$

It is important to be aware that when the berm is located below SWL ( $h_b > 0$ ) the breakwater could observe severe damage much before  $Rec = B$ .

#### 4.2.10 Verification of Influence of Slope, Water Depth and Berm Elevation

In this section the validity of Eq. 4.21 is evaluated. Eq. 4.21 was based on some geometrical considerations only, and includes the influence of initial lower front slope, water depth and berm elevation.

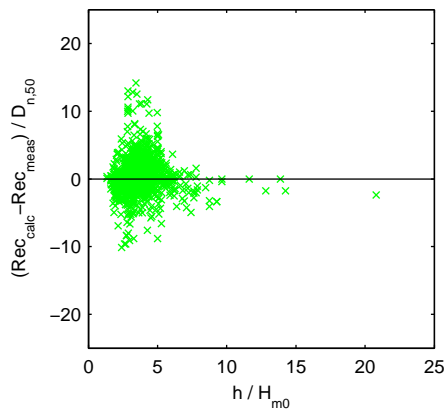


**Figure 4.15**  
Variation with  $h/H_{m0}$  (all available data).

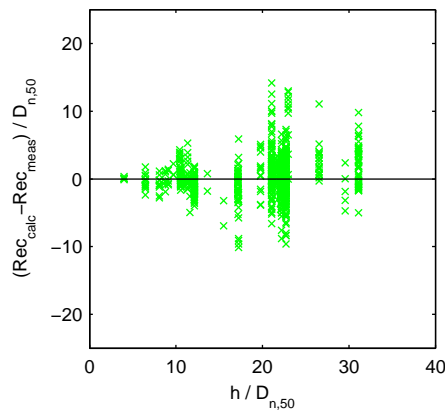


**Figure 4.16**  
Variation with  $h/D_{n,50}$  (all available data).

The water depth seems to be included in a proper way in the recession formula as no systematic scatter is observed in Fig. 4.15 and 4.16.

## 4.2 Development of Semi-Empirical Recession Formula

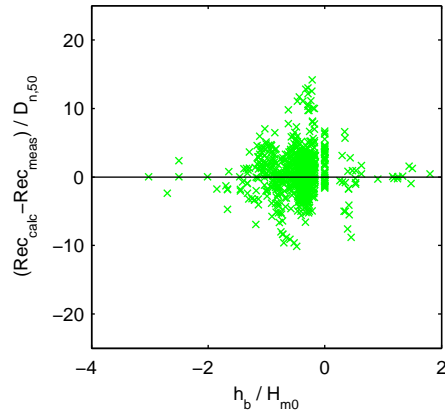


**Figure 4.17**  
*Variation with  $h_b/H_{m0}$  (all available data).*

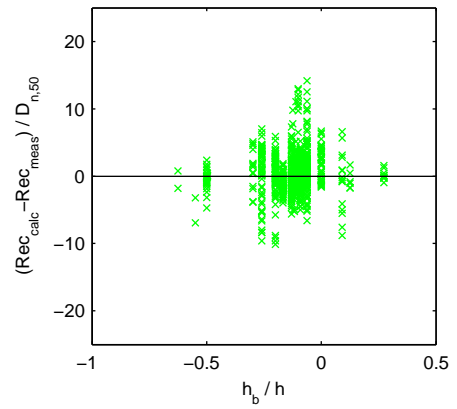


**Figure 4.18**  
*Variation with  $h_b/h$  (all available data).*

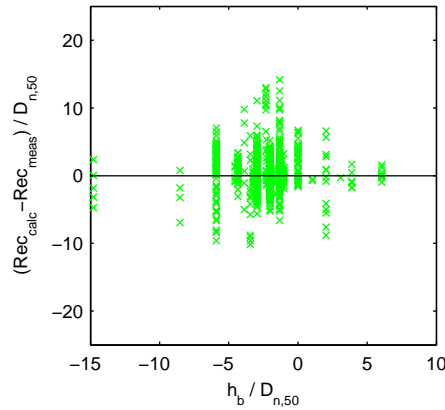


**Figure 4.19**  
*Variation with  $h_b/D_{n,50}$  (all available data).*

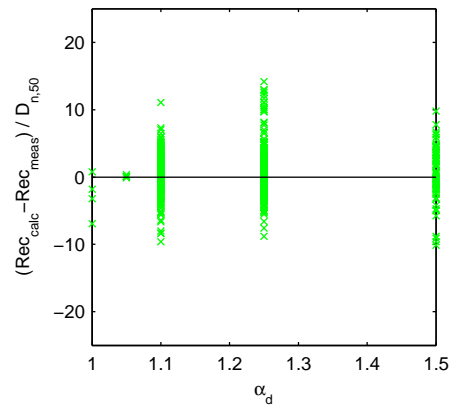


**Figure 4.20**  
*Variation with down slope  $\alpha_d$  (all available data).*

The berm elevation seems to have been included in a proper way even for very high and very low berms, cf. Fig. 4.17 - 4.19. The front slope seems also to be included in a proper way as no systematic scatter is observed in Fig. 4.20.

### 4.2.11 Verification of Influence of Wave Direction

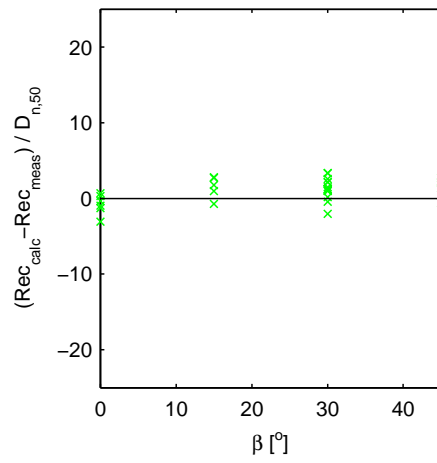


**Figure 4.21**  
Variation with angle of wave attack  $\beta$  (DHI, 1995 data).

The angle of wave attack seems to have been included in a proper way.

### 4.2.12 Verification of Influence of Number of Waves

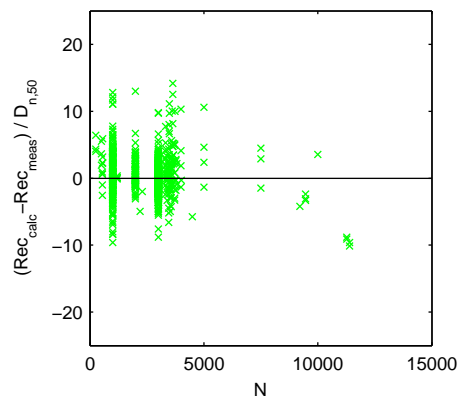


**Figure 4.22**  
Variation with number of waves  $N$  (all available data).

## 4.2 Development of Semi-Empirical Recession Formula

For a small number of waves it is expected more scatter due to sample variability. It is difficult to judge if the number of waves could have been included in a better way. One thing that could be expected, but is not included in the formula, is a faster profile development on a steep slope compared to a flatter slope.

### 4.2.13 Verification of Influence of Stone Gradation

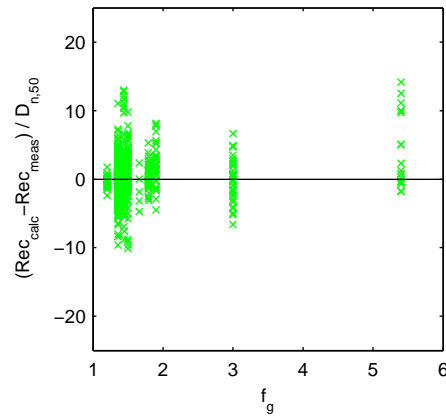


**Figure 4.23**  
Variation with stone gradation factor  $f_g$  (all available data).

Only the data set of Hall, 1991 has data above  $f_g = 1.80$ . For  $f_g \leq 3$  the stone gradation seem to have been included in a proper way. For the very wide gradation ( $f_g = 5.4$ ) there is some conservative scatter.

### 4.2.14 Proposed Recession Formula

The recession formula can now be written as:

$$\frac{Rec}{D_{n,50}} = f_{h_b} \cdot \left[ \frac{(1 + c_1) \cdot h - c_1 \cdot h_s}{h - h_B} \cdot f_N \cdot f_\beta \cdot f_{H0} \cdot f_{skewness} \cdot f_{grading} + \frac{\cot(\alpha_d) - 1.05}{2 \cdot D_{n,50}} \cdot (h_b - h) \right] \quad (4.34)$$



where

$$f_{hb} = \begin{cases} 1.18 \cdot \exp\left(-1.64 \cdot \frac{hb}{H_{m0}}\right) & \text{for } \frac{hb}{H_{m0}} > 0.1 \\ 1 & \text{for } \frac{hb}{H_{m0}} \leq 0.1 \end{cases} \quad (4.35)$$

$$c_1 = 1.2 \quad (4.36)$$

$$f_\beta = \cos(\beta) \quad (4.37)$$

$$f_N = \begin{cases} (N/3000)^{-0.046 \cdot H_0 + 0.3} & \text{for } H_0 < 5 \\ (N/3000)^{0.07} & \text{for } H_0 \geq 5 \end{cases} \quad (4.38)$$

$$h_s = 0.65 \cdot H_{m0} \cdot s_{0m}^{-0.3} \cdot f_N \cdot f_\beta \quad (4.39)$$

$$T_0 = \sqrt{\frac{g}{D_{n,50}}} \cdot T_{0,1} \quad (4.40)$$

$$T_0^* = \frac{19.8 \cdot \exp\left(-\frac{7.08}{H_0}\right) \cdot s_{0m}^{-0.5} - 10.5}{0.05 \cdot H_0} \quad (4.41)$$

$$H_0 = \frac{H_{m0}}{\Delta \cdot D_{n,50}} \quad (4.42)$$

$$f_{H0} = \begin{cases} 19.8 \cdot \exp\left(-\frac{7.08}{H_0}\right) \cdot s_{0m}^{-0.5} & \text{for } T_0 \geq T_0^* \\ 0.05 \cdot H_0 T_0 + 10.5 & \text{for } T_0 < T_0^* \end{cases} \quad (4.43)$$

$$f_{skewness} = \exp(1.5 \cdot b_1^2) \quad (4.44)$$

$$f_{grading} = \begin{cases} 1 & \text{for } f_g \leq 1.5 \\ 0.43 \cdot f_g + 0.355 & \text{for } 1.5 < f_g < 2.5 \\ 1.43 & \text{for } f_g > 2.5 \end{cases} \quad (4.45)$$

In some cases the formula predicts negative recession in these cases the recession should be zero. The negative value just indicates that the breakwater could resist even a harder wave attack without recession of the berm.

If a toe which is wide enough to support the entire reshaped profile is present, then the water depth above the toe should be used in the formulae. If the toe is not wide enough to support the entire profile then one has to use a water depth between the water depth above the toe and the water depth without the toe. This could be based on an estimation of the movement of the profile at the bottom, and then use the mean water depth over the distance the profile moves.

If the structure has no berm the recession is measured at the crest, hence  $h_b = -R_c$  should be used in the formula, as  $h_b$  is negative when the berm is above SWL.

### 4.2.15 A Simple Method for Estimating Wave Skewness

For applying Eq. 4.34 the wave skewness has to be estimated. It is investigated if a simple correlation with the Ursell number ( $Ur$ ), which is used as a measure of the relative importance of non-linearity, could be applied.

$$Ur = \frac{H}{2 \cdot h \cdot (k \cdot h)^2} = \frac{H \cdot L_p^2}{8 \cdot \pi^2 \cdot h^3} \quad (4.46)$$

For irregular waves is used the  $H_{m0}$  wave height and the peak wave length calculated from the linear dispersion relation.  $Ur > 1$  indicates strong non-linearities. A correlation analysis resulted in Eq. 4.47 to estimate wave skewness.

$$b_1 = 0.54 \cdot Ur^{0.47} \quad (4.47)$$

Fig. 4.24 shows the evaluation of Eq. 4.47 against the present data.

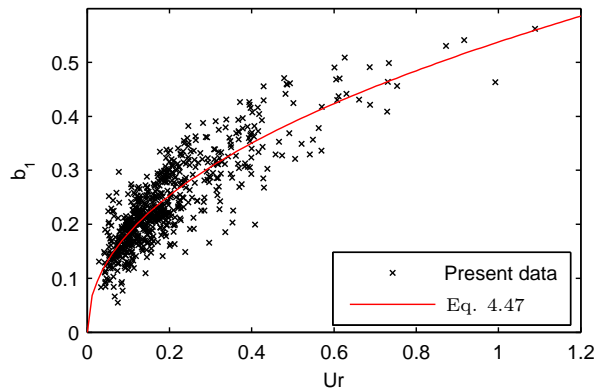


**Figure 4.24**  
Correlation between wave skewness and Ursell number.

### 4.3 Evaluation of Proposed and Existing Recession Formulae

In this section the proposed recession formula given in 4.34 is compared to the method of Hall and Kao, 1991, Van der Meer, 1992 and Tørum and Krogh, 2000.

An input parameter to the formula of Hall and Kao, 1991 is the fraction of rounded stones ( $P_r$ ). Hall and Kao, 1991 used  $P_r = 0.30$  for the main part of their tests, but also some tests with  $P_r = 0$  and  $P_r = 0.15$  were performed. It favors their formula to use  $P_r = 0.30$  for all tests, which is therefore applied even though the amount of rounded stones in the other tests is neglectable. The difference in recession between applying  $P_r = 0$  and  $P_r = 0.3$  is only 1.8 stone diameters.

If  $f_g$  or  $f_d$  is outside the interval of validity of the Tørum and Krogh, 2000 formula, the limit value is applied.

The present derived recession formula depends on the wave skewness, which is only available for the present data. For all other data Eq. 4.47 is used to estimate the wave skewness.

In case of multi-layer berm breakwaters the largest stone size is applied in the formulae.

The following data is used for the comparison and described in Chapter 3 and Appendix C:

### 4.3 Evaluation of Proposed and Existing Recession Formulae

---

- Present data.
- Instanes, 1987
- Tørum et al., 1988
- Van der Meer, 1988
- Burcharth and Frigaard, 1990
- Andersen and Poulsen, 1991
- Hall, 1991
- Lissev, 1993
- Aalborg University, 1995
- DHI, 1995
- DHI, 1996
- Porarinsson, 2004

### 4.3.1 Present data

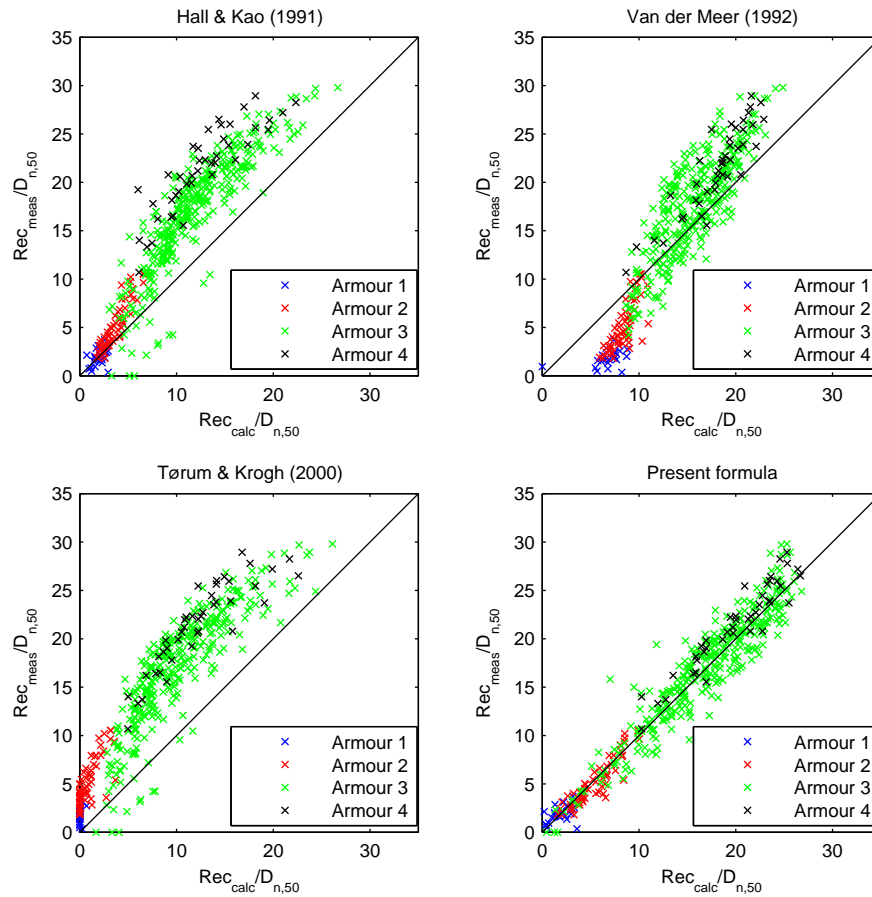


**Figure 4.25**

*Comparison of measured and calculated recession for Present data.*

For the present data the present derived recession formula fits the data very well and much better than the other three models. The largest deviations for the present formula, both above and below the prediction line, is found for tests with the berm some few stone diameters below SWL which is not really a berm breakwater. When the berm is above SWL or far below SWL the predictions seem very reliable.

### 4.3 Evaluation of Proposed and Existing Recession Formulae

---

With the present method it is actually possible to calculate start of damage within very few stone diameters, however the scatter is maybe too big for using this method for designing multi-layer berm breakwaters as only very limited reshaping is allowed. An alternative approach for these structures could be to use the method of Van der Meer, 1988 for static stability as there is only allowed damage which is comparable to what is allowed on a conventional breakwater with a armour thickness equal to two stone diameters.

The method of Van der Meer, 1992 give the second best fit to the present data, but this method has shown to be very conservative for  $H_0T_0 < 70$ .

The formulae of Hall and Kao, 1991 and Tørum and Krogh, 2000 give similar results and are both somewhat on the unsafe side for the present data. A little less scatter for the Hall and Kao, 1991 method compared to the method of Tørum and Krogh, 2000 is observed.

There is a tendency that slightly more recession is measured for Armour 4 compared to Armour 3, but only minor differences exists. The difference could be due to a scale effect or the model effect that Armour 3 contains more large stones than Armour 4, cf. Fig 3.7. Therefore it could only be concluded that the results indicate only small or no scale effects. Scale effects related to front slope stability of berm breakwaters are further discussed in section 4.5.

4.3.2 Instanes, 1987

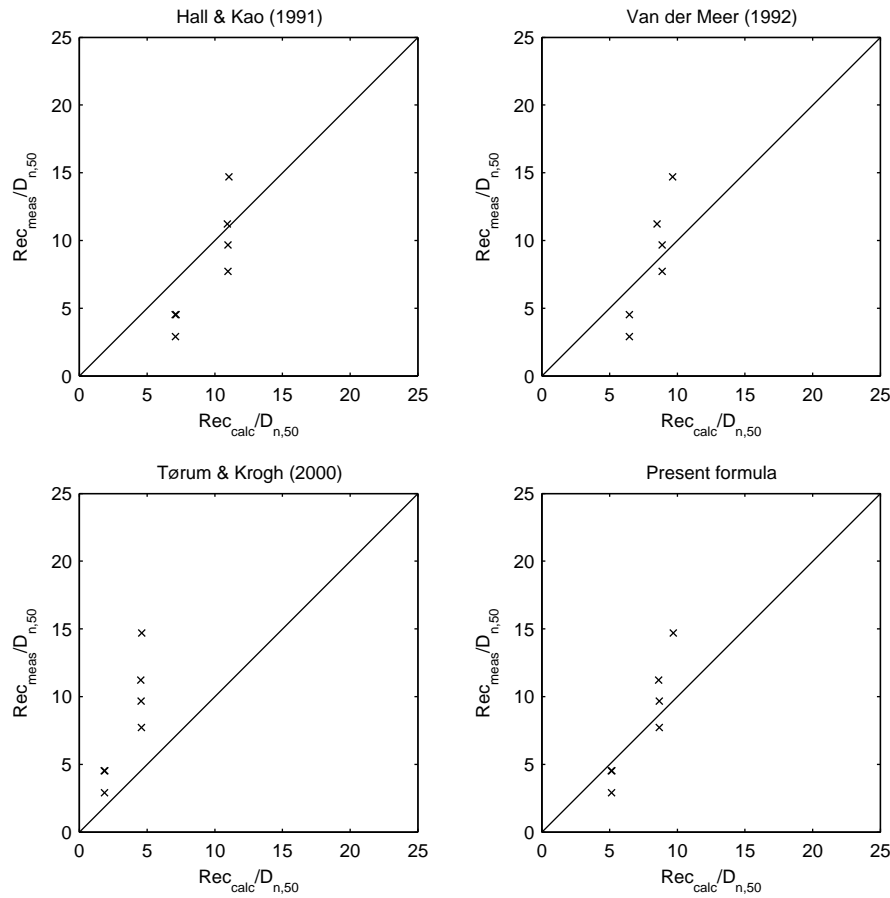


**Figure 4.26**  
Comparison of measured and calculated recession for Instanes, 1987 data.

In spite of the waves in these tests consist of broken waves which parameters were calculated from the SWAN method the agreement is fair for the Van der Meer, 1992, Hall and Kao, 1991 and the present method. The formula of Tørum and Krogh, 2000 is more on the unsafe side. The present method and the Van der Meer, 1992 method give almost identical results for this data set.

4.3.3 Tørum et al., 1988

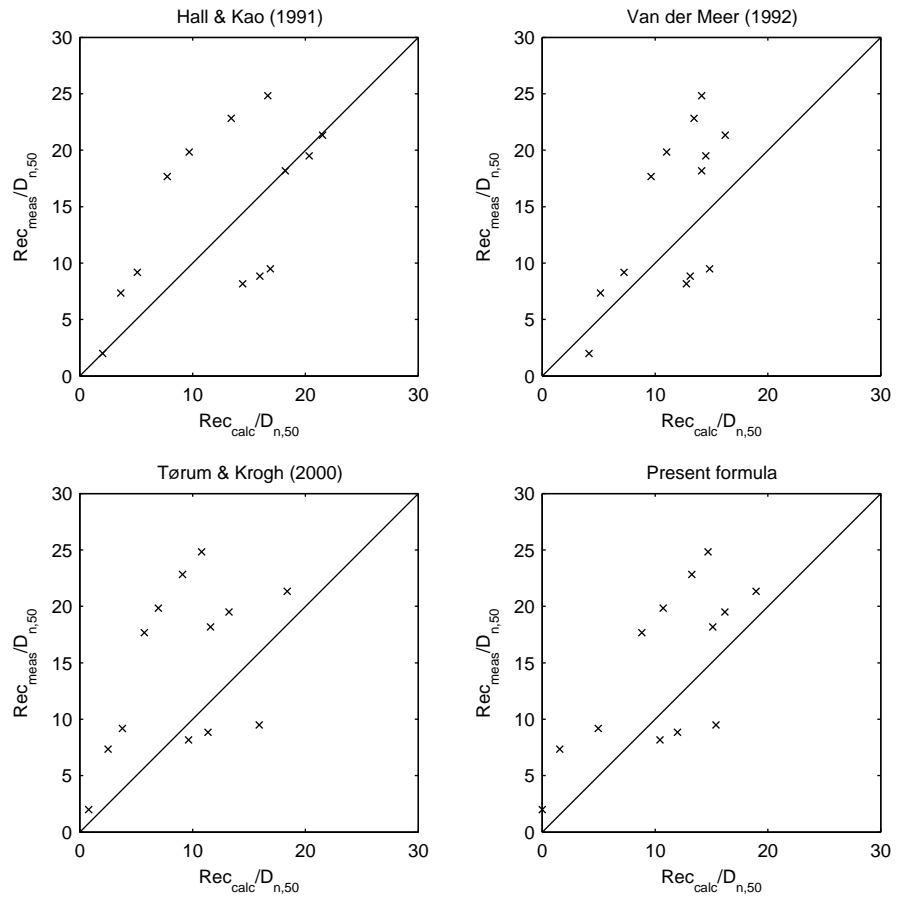


**Figure 4.27**  
 Comparison of measured and calculated recession for Tørum et al., 1988 data.

A huge amount of scatter is observed for this data set for all 4 methods. The wave parameters at the toe were calculated by the SWAN method, which maybe can explain some of the scatter.



4.3.4 Van der Meer, 1988

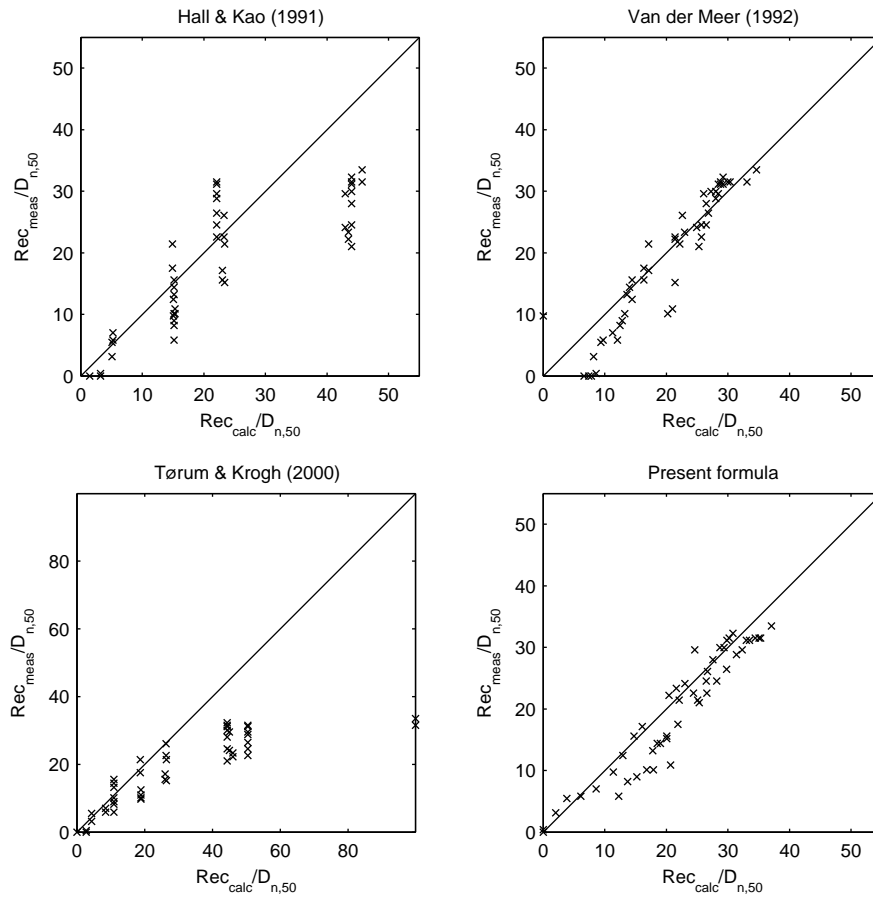


**Figure 4.28**  
 Comparison of measured and calculated recession for Van der Meer, 1988 data.

For the Van der Meer, 1988 data the present formula and the Van der Meer, 1992 method predicts the recession very well. A huge amount of scatter is observed for the other two formulae, especially for large values of the stability index.

4.3.5 Burcharth and Frigaard, 1990

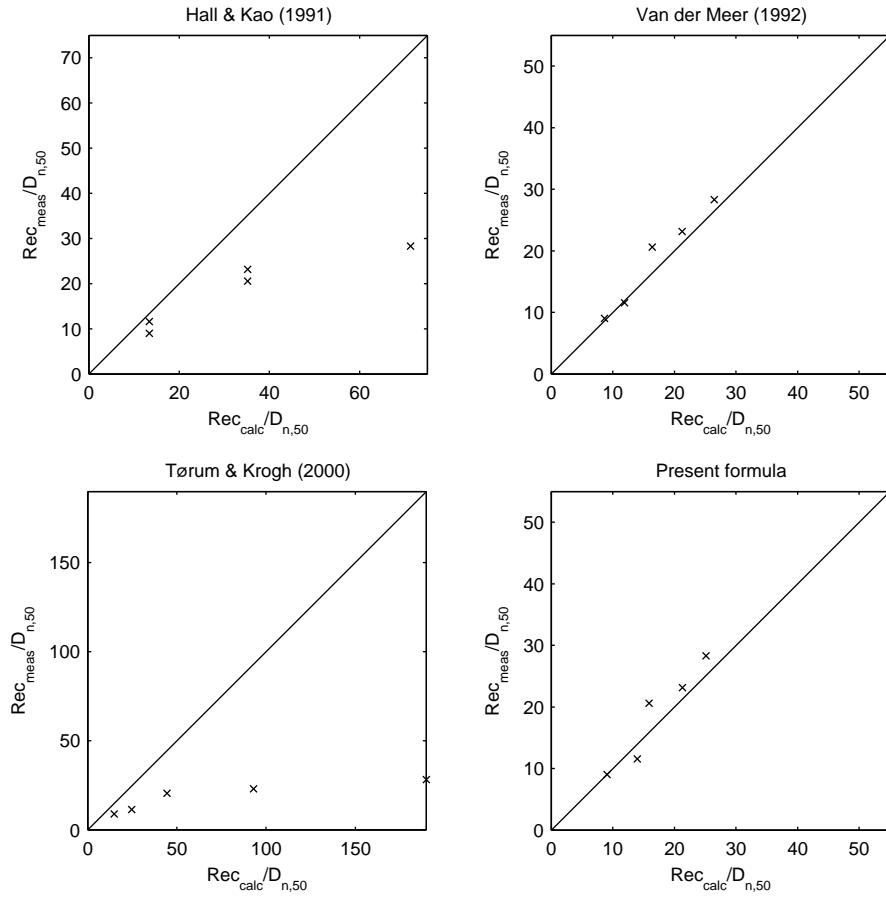


**Figure 4.29**  
 Comparison of measured and calculated recession for Burcharth and Frigaard, 1990 data.

For the Burcharth and Frigaard, 1990 data both the method of Van der Meer, 1992 and the present formula predicts the recession very well. The other two methods overestimate the recession for large  $H_0T_0$  values.

4.3.6 Andersen and Poulsen, 1991

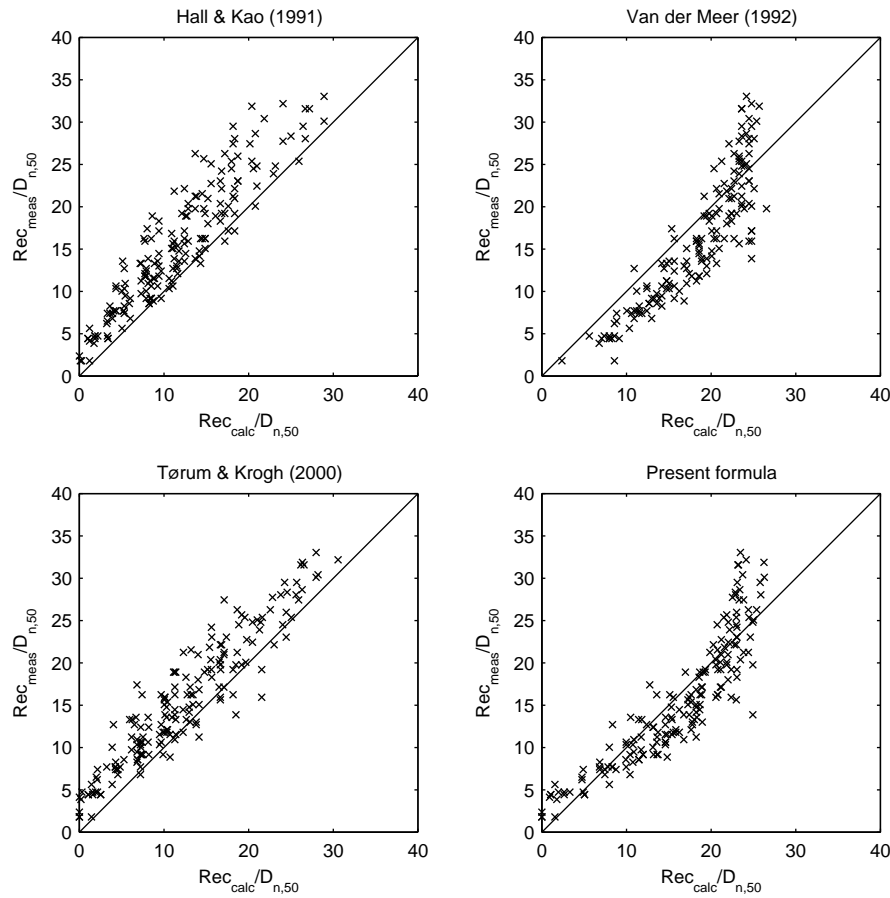


**Figure 4.30**  
 Comparison of measured and calculated recession for Andersen and Poulsen, 1991 data.

The present formula fits the data of Andersen and Poulsen, 1991 very good and better than the other three methods. The formula of Tørum and Krogh, 2000 is mainly fitted to the data of Andersen and Poulsen, 1991, and therefore it fits these data well.

4.3.7 Hall, 1991

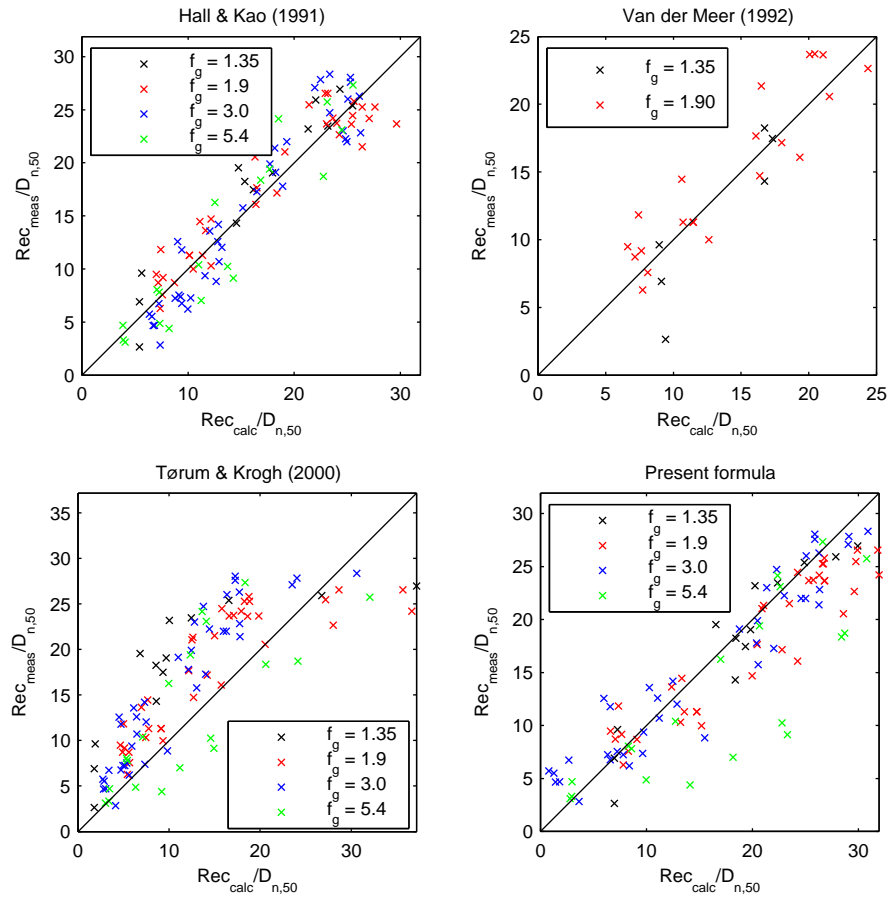


**Figure 4.31**  
Comparison of measured and calculated recession for Hall, 1991 data.

For the Hall, 1991 data the formula of Hall and Kao, 1991 performs best as it is fitted to these results only. The present method predicts also the recession in these experiments with reasonable accuracy. However, for the very wide grading some conservative scatter is observed. A gradation factor of 5.4 is however very seldom even for homogeneous berm breakwaters. Further non-uniform recession can be expected for such a wide grading due to the large variation in stone sizes. The method of Van der Meer, 1992 is limited to  $f_g < 2.5$ .

4.3.8 Lissev, 1993

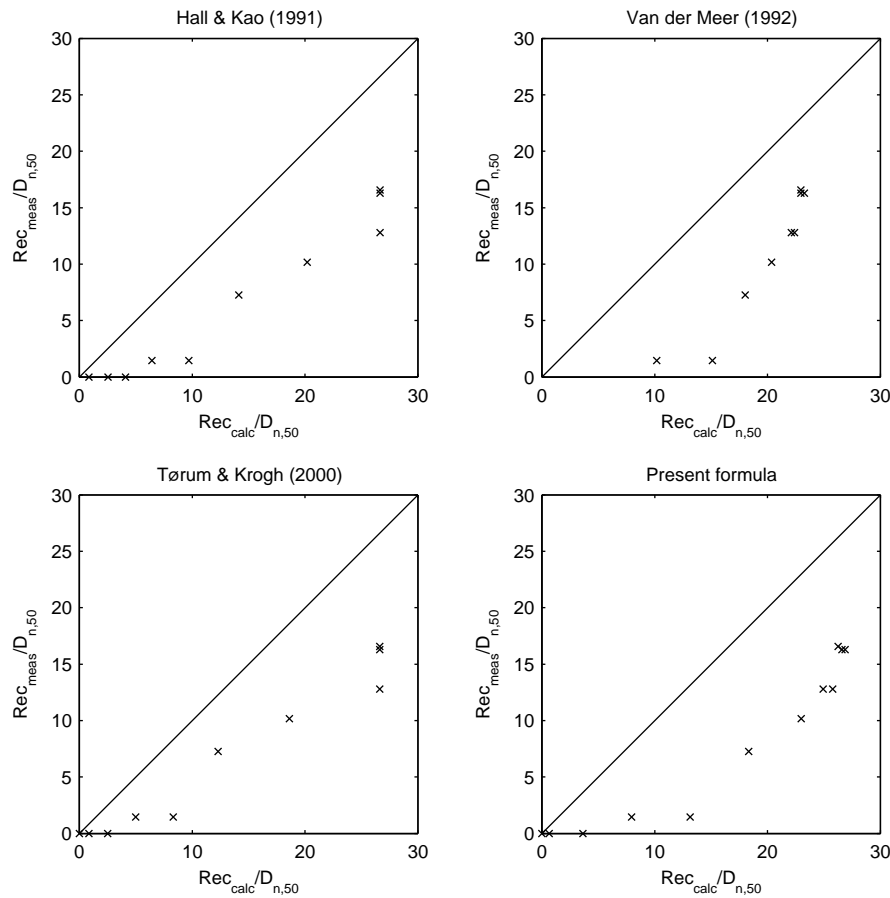


**Figure 4.32**  
Comparison of measured and calculated recession for Lissev, 1993 data.

The tests of Lissev, 1993 are performed on a cross-section very similar to the present tests with Armour 3, but in 1.7 times larger scale. Therefore it is very surprising that the data shows that different results. All 4 methods overestimate the recession for this data set. A scale effect on armour stability would lead to too much damage in small scale due to viscous effects. Nevertheless, the deviations for this data set are not expected to be due to scale effects, as other data in the same range of Reynolds numbers fits well with the present formula.

### 4.3 Evaluation of Proposed and Existing Recession Formulae

Scale effects on armour stability are further discussed in section 4.5.

#### 4.3.9 Aalborg University, 1995

For the Aalborg University, 1995 data the water depth in the calculations is lowered due to the influence of a high toe, cf. Fig. C.15.

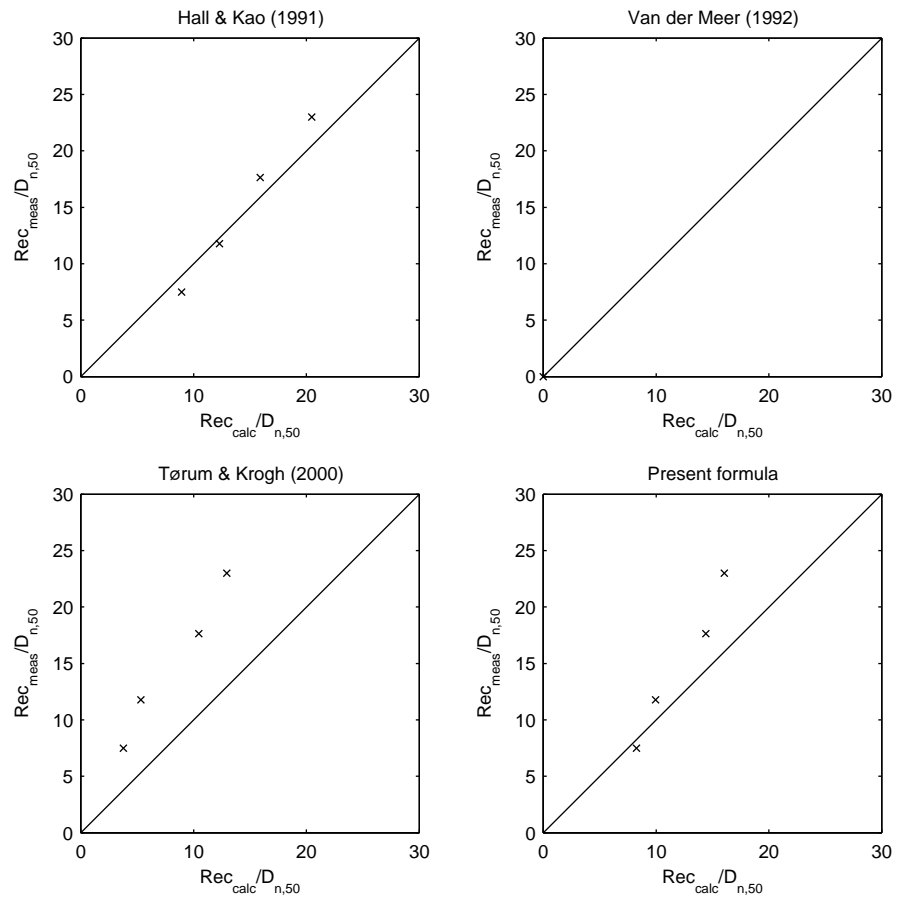


**Figure 4.33**  
*Comparison of measured and calculated recession for Aalborg University, 1995 data.*

For these data the method of Van der Meer, 1992 did not give a profile. The

three other methods give reasonable results.

4.3.10 DHI, 1995

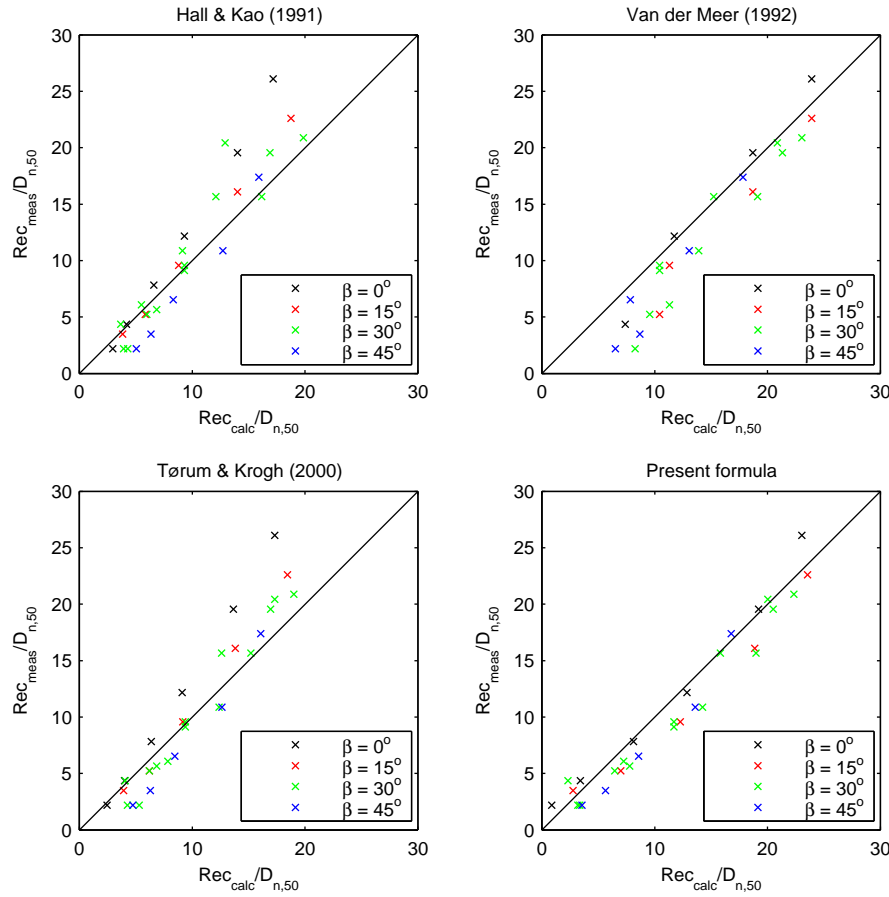


**Figure 4.34**  
Comparison of measured and calculated recession for DHI, 1995 data (trunk section).

The Van der Meer, 1992 method and the present proposed formula predicts both the recession in the DHI, 1995 tests very well both for head-on and oblique waves. In the method of Hall and Kao, 1991 and Tørum and Krogh, 2000 the influence of wave direction is not included. However, the influence of the wave direction

### 4.3 Evaluation of Proposed and Existing Recession Formulae

is not that important for  $\beta < 45^\circ$  and it is on the safe side not to take it into account. However, the two methods are on the unsafe side for data from tests with head-on waves for this data set.

#### 4.3.11 DHI, 1996

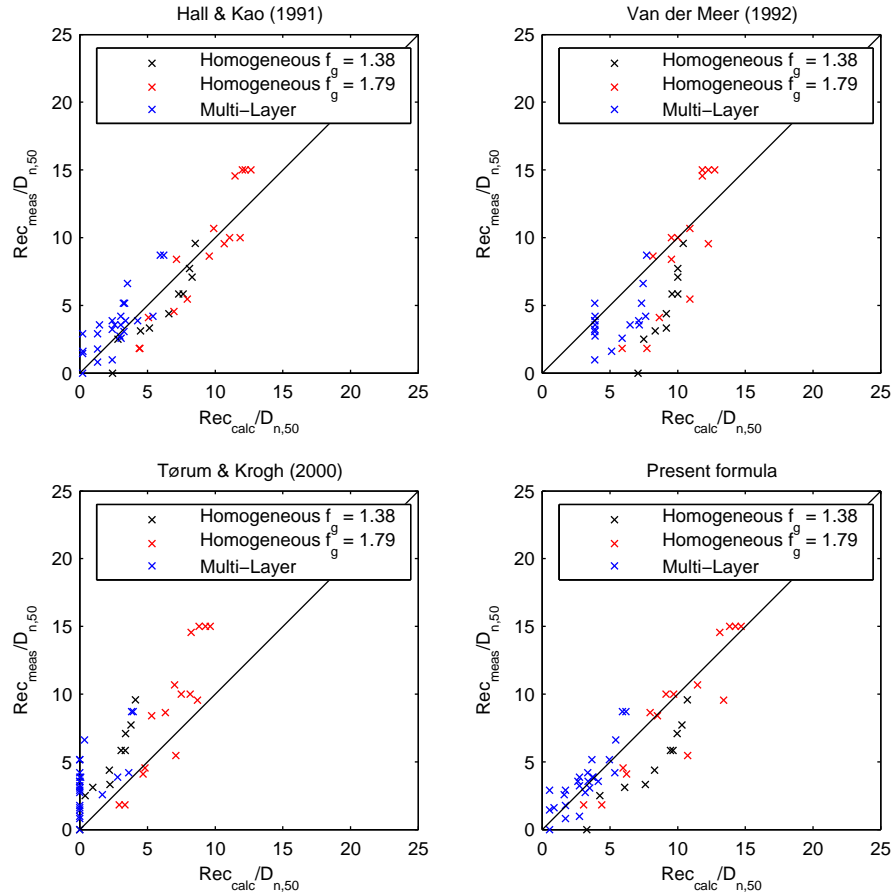


**Figure 4.35**  
*Comparison of measured and calculated recession for DHI, 1996 data.*

For the DHI, 1996 data the present formula and the formula of Hall and Kao, 1991 predicts the recession well.



4.3.12 Porarinsson, 2004

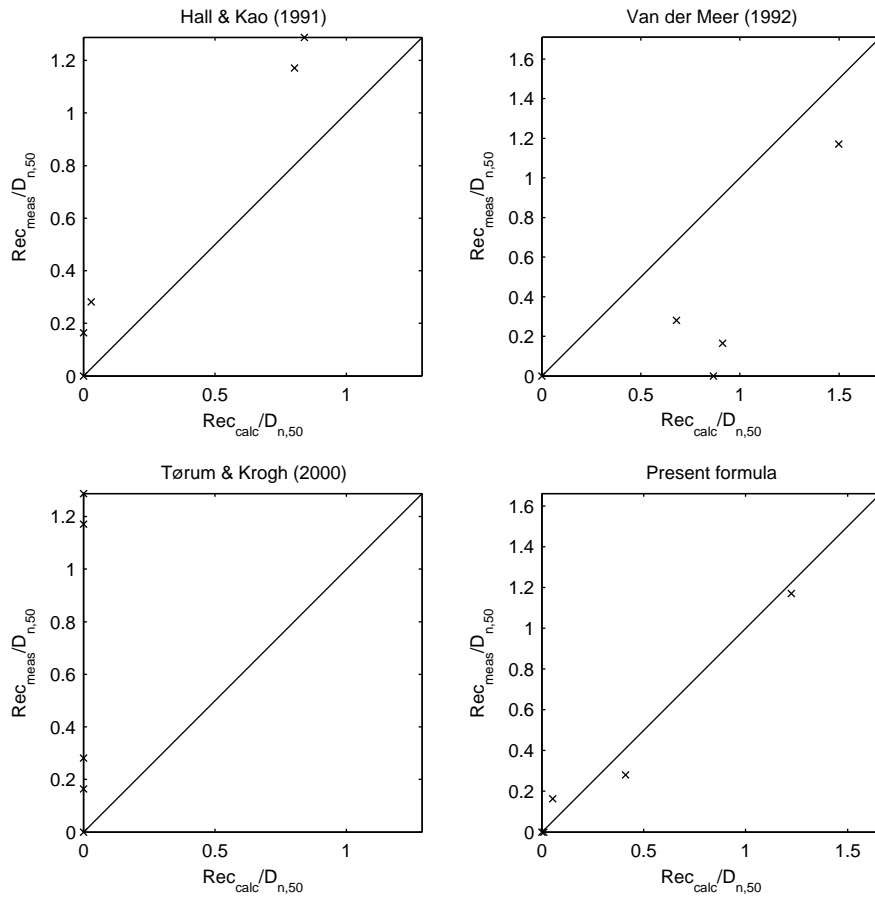


**Figure 4.36**

*Comparison of measured and calculated recession for Porarinsson, 2004 data (multi-layer berm breakwater).*

Even though the recession is less than 1.5 stone diameters reasonable agreement could be observed between calculated recession by present formula and measured recession for the Porarinsson, 2004 data. This confirms the findings from the present data, that start of damage could be accurately predicted by the present formula.

4.3.13 Examples of measured and calculated recession and profiles

In this section some few examples of the measured profiles in the present tests are given. In the same figure is showing the profile predicted by the method of Van der Meer, 1992 and the recession predicted by the present proposed formula. In appendix B on the CD-Rom such a figure is given for every single test. It can be seen that for tests with Armour 3 the method of Van der Meer, 1992 gives very reliable predictions of the reshaped profile. In most tests with Armour 3 the breakwater corresponds to a dynamically stable breakwater. In tests with Armour 2 the method slightly overpredicts the deformation and for armour 1 the predictions are very bad. It should be mentioned that this limitation is mentioned by Van der Meer, 1992 as the method has been developed for dynamically stable profiles. The predicted recession by the present formula gives very reliable predictions for all three armour configurations.

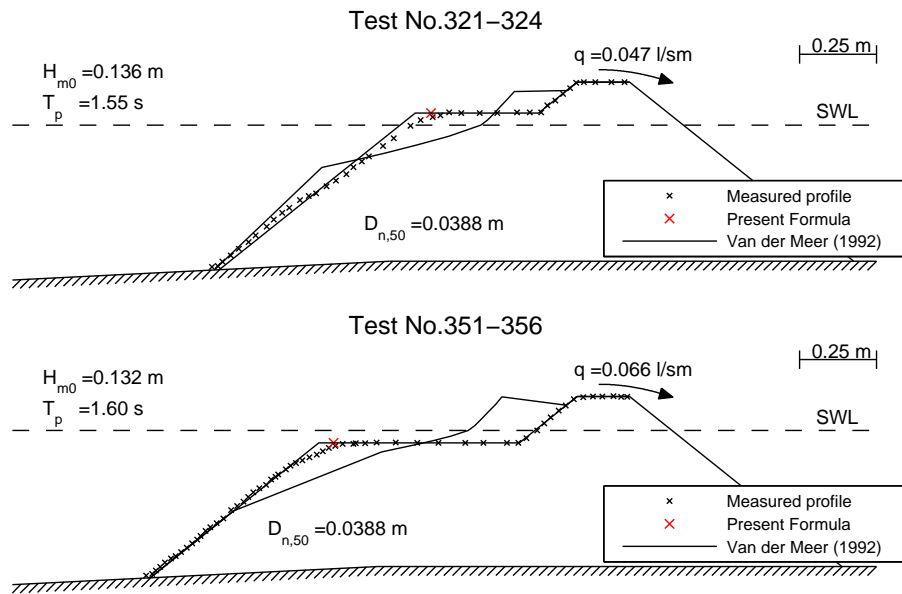
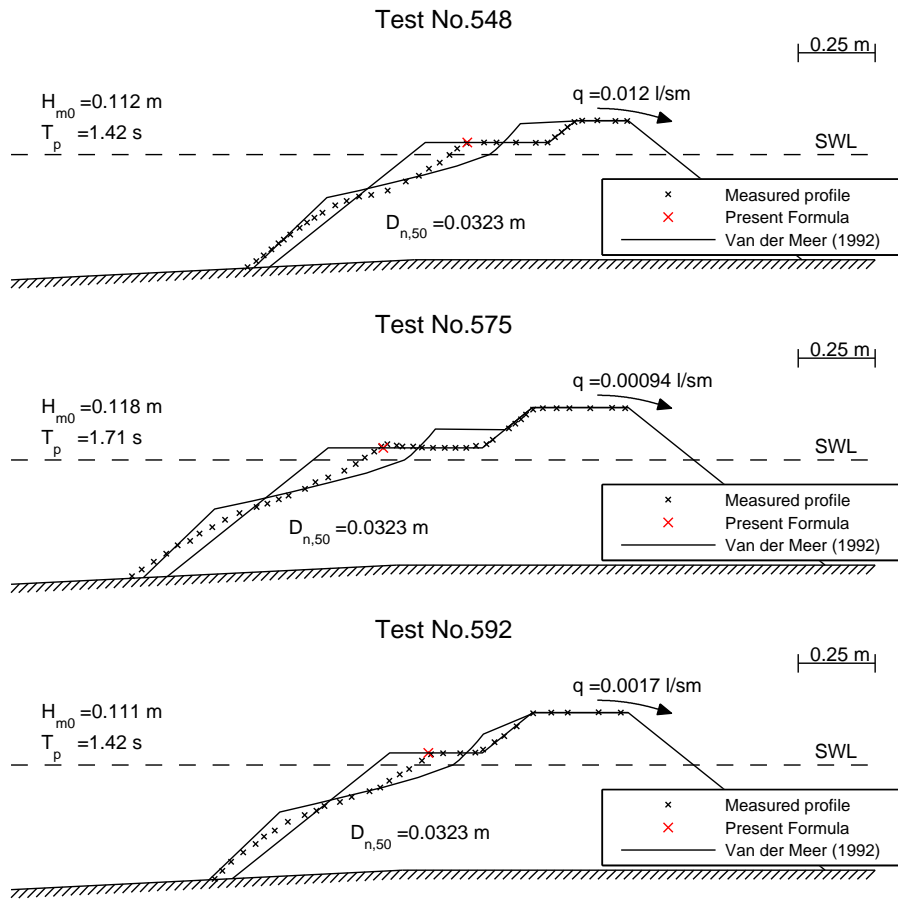
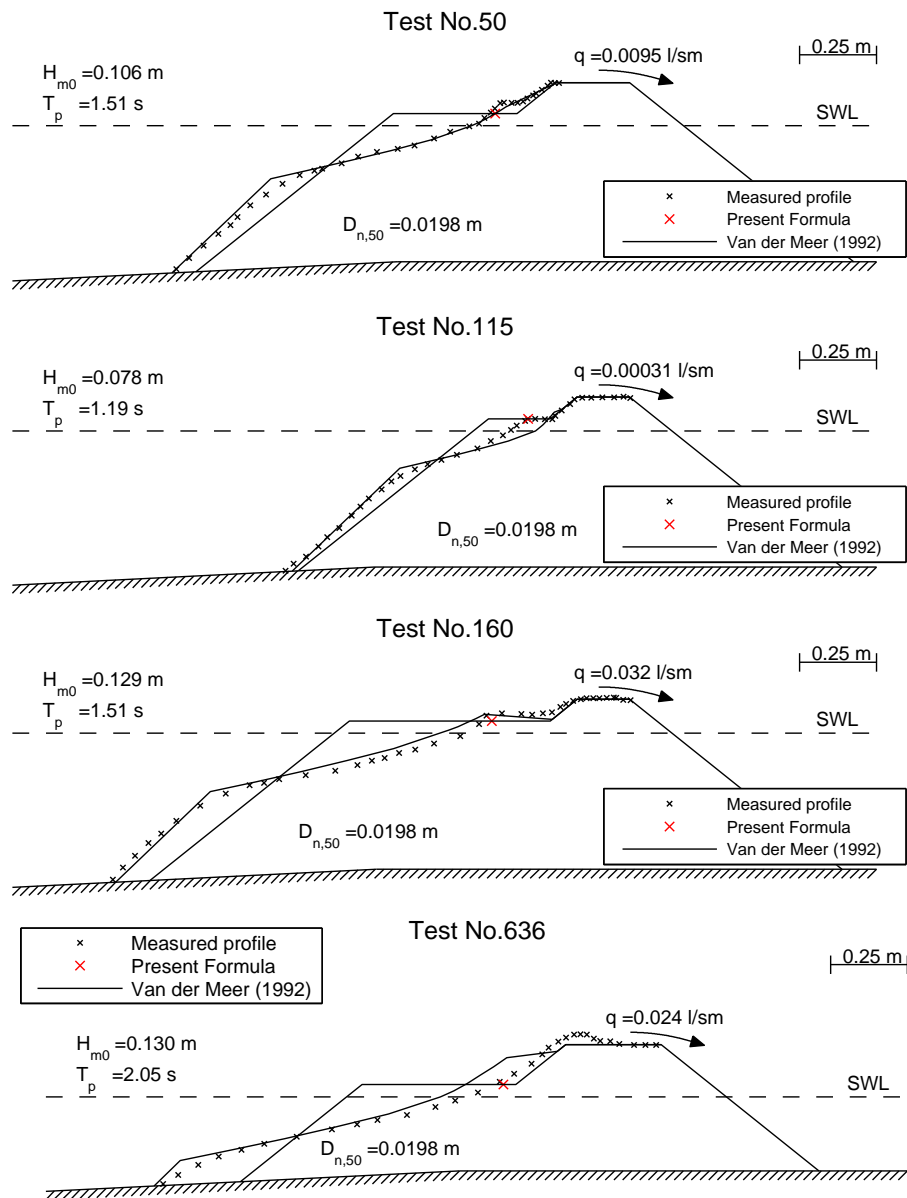


Figure 4.37  
Examples of profiles for armour 1.



**Figure 4.38**  
Examples of profiles for armour 2.

### 4.3 Evaluation of Proposed and Existing Recession Formulae



**Figure 4.39**  
Examples of profiles for armour 3.

#### 4.3.14 Summary

The present derived formula has shown to be able to predict the recession in the present experiments with very good accuracy and much better than the three other existing methods tested.

When comparing to data of other researchers the agreement with the present formula is for the main part of the data sets very good. Largest deviations is observed for the data set of Lissev, 1993 and Tørum et al., 1988. The three other methods tested, also predict the recession for these two data sets very bad. Lissev, 1993 measured much less recession than observed in the present tests even though the parameters tested are very close to the present ones, but in 1.7 times larger scale. It is not believed to be a scale effect as tests of other researchers in the same range of Reynolds numbers as the Lissev, 1993 tests give similar results as the present tests.

In Fig. 4.40 the 4 methods are evaluated against all available data, and it can be seen that the present formula predicts the recession much better than the other 3 methods. The plots are limited at  $Rec/D_{n,50} = 55$ , even though the formula of Tørum and Krogh, 2000 in some cases give recession up to 200 stone diameters in cases where there are measured less than 40 (see Fig. 4.28 and 4.29). This deviation is due to calibration of this formula within the area  $H_0T_0 < 180$  and  $Rec/D_{n,50} < 35$  only, which are also the typical ranges for berm breakwaters. Actually it was found that the formula by Tørum, 1998 performed better than the modified formula by Tørum and Krogh, 2000 for all data sets except two, but it must be stated that also this formula is not generally valid and some of the important parameters which are included in the present formula are missing in the formula, i.e. front slope, water depth and berm elevation.

### 4.3 Evaluation of Proposed and Existing Recession Formulae

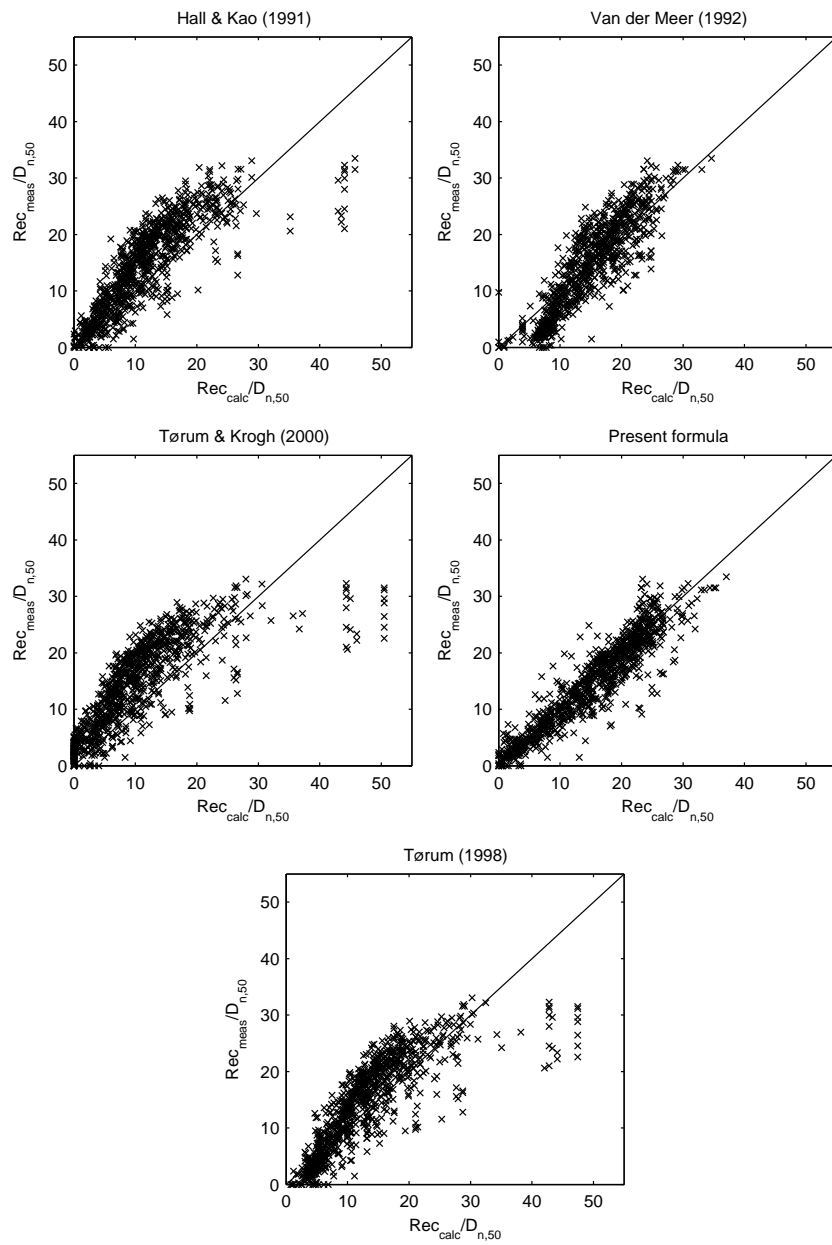


**Figure 4.40**  
*Comparison of measured and calculated recession for all available data.*

## 4.4 Uncertainty Estimation

In this section are the uncertainties of the 5 recession methods evaluated, with a special focus on the present derived formula. The uncertainty of the formulae has to be taken into account in probabilistic design.

In the following two tables are the error on the recession estimations given for the 5 methods tested. Two error measures are considered:

1. The standard deviation of the errors on the dimensionless recession predictions.
2. The mean relative error on the recession predictions.

In the present case method 1 is considered to be the best, because method 2 gives too high weight on small errors for tests where almost no damage has been measured. Nevertheless, the conclusion from both error measures is that the present method is superior to the four other existing methods tested, cf. Table 4.2 and 4.3. This confirms the conclusions drawn from Fig. 4.40.

However, the ranking of the other 4 methods tested is different for the two different error measures. This is mainly because the method of Van der Meer, 1992 overpredicts the damage a lot for very stable structures, but performs better for less stable structures. Therefore, the mean relative error measure unfavours this method.

For the Van der Meer, 1992 the errors given in Table 4.2 and 4.3 are based on a smaller amount of data as the method did not give a profile in some situations.

Data	Present formula	Hall & Kao, 1992	Van der Meer, 1992	Tørnum & Krogh, 2000	Tørnum, 1998
Present data	1.91	5.73	3.79	7.18	4.41
Instanes, 1987	2.36	2.84	2.79	5.31	2.79
Tørnum et al., 1988	6.12	6.39	6.15	8.27	6.60
Van der Meer, 1988	3.53	9.67	4.12	18.83	15.43
Burcharth and Frigaard, 1990	2.89	21.09	2.23	79.68	51.04
Andersen and Poulsen, 1991	3.38	4.83	4.31	4.09	2.63
Hall, 1991	4.06	2.61	2.68	6.12	5.56
Lissev, 1993	9.60	8.96	9.40	8.46	10.56
Aalborg University, 1995	3.96	1.72	-	7.20	3.51
DHI, 1995	1.84	2.93	3.04	2.72	2.66
DHI, 1996 homogeneous	2.56	1.91	3.80	3.31	2.67
DHI, 1996 multi-layer	1.21	1.53	2.15	3.35	1.59
Porarinsson, 2004	0.16	0.25	0.50	0.67	1.48
Overall	2.98	5.60	3.96	9.53	6.69

**Table 4.2**

Standard deviation between calculated and measured dimensionless recession ( $Rec/D_{n,50}$ ) for five methods and for

different data sets. The standard deviation ( $\sigma$ ) is calculated as: 
$$\sigma = \sqrt{\frac{1}{N} \cdot \sum_{i=1}^N \left( \frac{Rec_{meas}}{D_{n,50}} - \frac{Rec_{calc}}{D_{n,50}} \right)_i^2}$$



Data	Present formula	Hall & Kao, 1992	Van der Meer, 1992	Tørum & Krogh, 2000	Tørum, 1998
Present data	14.4%	34.9%	48.7%	50.9%	36.4%
Instanes, 1987	26.2%	48.7%	41.3%	53.7%	40.4%
Tørum et al., 1988	44.2%	39.9%	43.3%	48.5%	46.4%
Van der Meer, 1988	23.4%	54.8%	68.1%	72.1%	84.1%
Burcharth and Frigaard, 1990	12.7%	67.8%	8.4%	233.1%	174.1%
Andersen and Poulsen, 1991	22.0%	28.8%	32.6%	27.9%	15.2%
Hall, 1991	26.7%	18.7%	19.5%	34.0%	31.6%
Lissev, 1993	212.4%	167%	228.7%	141.3%	199.5%
Aalborg University, 1995	18.6%	11.2%	-	47.2%	17.1%
DHI, 1995	24.6%	27.0%	48.6%	28.0%	28.3%
DHI, 1996 homogeneous	45.0%	33.7%	76.3%	41.2%	46.0%
DHI, 1996 multi-layer	35.6%	42.3%	63.5%	86.7%	55.8%
Porarinsson, 2004	36.9%	64.0%	164.9%	100.0%	423.7%
Overall	21.9%	34.0%	48.4%	46.9%	38.4%

**Table 4.3**

Mean relative error of calculated recession lengths for five methods and for different data sets. Tests with  $Rec_{meas} = 0$  has been excluded in the calculations. The mean relative error ( $E$ ) is calculated as:

$$E = \frac{1}{N} \cdot \sum_{i=1}^N \left( \frac{|Rec_{calc} - Rec_{meas}|}{Rec_{meas}} \right)_i$$

#### 4.4 Uncertainty Estimation

Fig. 4.41 shows that the deviations for the present formula is approximately Gaussian distributed.

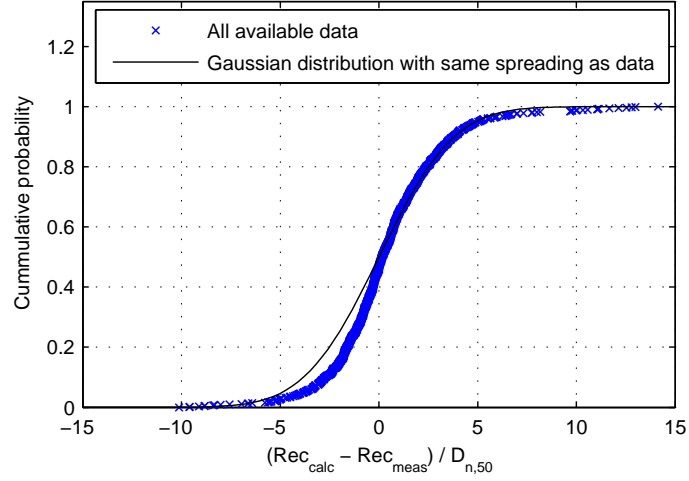


**Figure 4.41**  
Cumulative distribution of  $(Rec_{calc} - Rec_{meas})/D_{n,50}$ .

It could be expected that the spreading increases with increasing recession which is also what is observed from Fig. 4.42. This was verified by calculating the standard deviation of the residuals within 7 intervals of  $Rec_{meas}/D_{n,50}$ . Assuming Gaussian distributed residuals the upper and lower 95% confidence levels could be estimated as 1.645 times the standard deviation. This resulted in the following equations for the 90% confidence band on all data, i.e. only 10% of the data are outside this band:

$$\begin{aligned} \frac{Rec_{calc}^{95\%}}{D_{n,50}} &= 1.080 \cdot \frac{Rec_{calc}^{50\%}}{D_{n,50}} + 4.00 \\ \frac{Rec_{calc}^{5\%}}{D_{n,50}} &= 0.909 \cdot \frac{Rec_{calc}^{50\%}}{D_{n,50}} - 2.95 \end{aligned} \quad (4.48)$$

For the present data a much more narrow 90% confidence band is observed:

$$\begin{aligned} \frac{Rec_{calc}^{95\%}}{D_{n,50}} &= 1.028 \cdot \frac{Rec_{calc}^{50\%}}{D_{n,50}} + 2.38 \\ \frac{Rec_{calc}^{5\%}}{D_{n,50}} &= 0.961 \cdot \frac{Rec_{calc}^{50\%}}{D_{n,50}} - 2.10 \end{aligned} \quad (4.49)$$

In addition to this there could be a non-uniform distribution along the breakwater which should be taken into account.

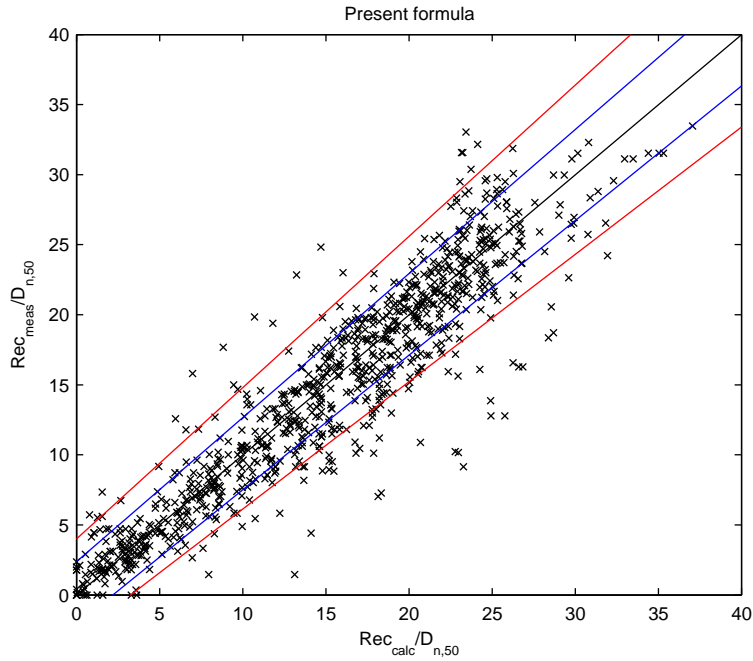


**Figure 4.42**

*Evaluation of present recession formula. Red and blue lines show the 90% confidence band on respectively all data and present data.*

## 4.5 Scale Effects

A general introduction to scale effects related to hydraulic response of rubble mound breakwaters, with special reference to overtopping, is given in chapter 9. In this section some considerations on stability scale effects are presented.

## 4.5 Scale Effects

---

The Reynolds number, defined in Eq. 4.50, is commonly used to evaluate viscous scale effects in rubble mound breakwater model tests.

$$Re = \frac{u \cdot L}{\nu} \quad (4.50)$$

$u$  is characteristic velocity often calculated as  $\sqrt{g \cdot H_s}$  and  $L$  is a characteristic length of the armour unit often taken as  $D_{n,50}$ , hence we arrive at:

$$Re_D = \frac{\sqrt{g \cdot H_s} \cdot D_{n,50}}{\nu} \quad (4.51)$$

The Reynolds number in the present experiments is given in section 3.3 for Armour size 1, 2 and 3 and in section 3.4 for Armour 4. Tests with Armour 4 corresponds to a length scale 1,9 times smaller than tests with Armour 3.

When tests performed with Armour 3 and 4 are compared it can be observed that there is a little more recession in tests in smaller scale (Armour 4). This could be due to the model effect that Armour 3 contains more large stones and/or a scale effect. Anyhow it can be concluded that if there is a scale effect when comparing  $Re_D \approx 2 \cdot 10^4$  with  $Re_D \approx 7 \cdot 10^3$  it is very small. However, from this it cannot be concluded that there is no scale effect when comparing to prototype data.

Many authors refer to the tests of Dai and Kamel, 1969 when discussing scale effects on stability of rubble mound breakwaters. Their tests with regular waves and armour stone sizes in the range  $20 \text{ mm} < D_{n,50} < 300 \text{ mm}$  showed no scale effects on stability when the Reynolds number ( $Re_D$ ) exceeds  $3 \cdot 10^4$ . For lower values of the Reynolds number the small scale tests leads to conservative results.

Scale effects related to armour stability in irregular waves were studied experimentally by Tørum et al., 1977, Brodertick and Ahrens, 1982, Mol et al., 1983 and Van der Meer, 1988. No significant scale effects on armour stability was found for  $1 \cdot 10^4 < Re_D < 4 \cdot 10^4$ .

Sharp and Khader, 1984 proposed a critical Reynolds number  $Re_{D,crit} = 4 \cdot 10^5$ , whereas Kajima and Sakakiyama, 1994 proposed  $Re_{D,crit} = 3 \cdot 10^5$ .

From theoretical considerations Jensen and Klinting, 1983 argued that  $Re_{D,crit} > 0.7 \cdot 10^4$ .

Model tests with conventional rubble mound breakwaters are typically performed with  $Re_D > 4 \cdot 10^4$ . However, model tests with berm breakwaters are typically performed in the range  $1.0 \cdot 10^4 < Re_D < 5.0 \cdot 10^4$ , which is a bit lower than many authors seems to recommend. This is due to the relatively smaller armour stones

used in a berm breakwater, which makes it difficult to get Reynolds numbers above  $3 \cdot 10^4$  due to physical limitations of the typical flumes.

From prototype experiences with berm breakwaters, the following can be found in the literature:

- **Racine berm breakwater:** Montgomery et al., 1987 reported that the breakwater had behaved similar to the model tests with respect to berm reshaping.
- **Bakkafjordur multi-layer berm breakwater:** Viggosen, 1990 found reasonable agreement between model tests and prototype measurements of reshaped profile. Only poor quality stones were available and the effect of possible rounding and breakage of the armour stones was included in the model tests by using a reduced stone size.
- **Sirevåg Berm Breakwater:** Tørum et al., 2003 give a detailed analysis of the behavior of the breakwater during the storm 28-29 January 2002. The wave heights during the storm exceeded the 100 year design wave height, but nil reshaping of the berm was observed. The model tests indicate recession of 2-4 m for this sea state. Tørum et al., 2003 did not rule scale effects out, but considered model effects more likely. In prototype the stones were placed orderly whereas they were placed randomly in the model. Further there are many model effects and uncertainties related to the wave measurements. The shallow water waves were in prototype measured with a wave rider, these results indicate a gaussian sea surface, whereas the model results show strong skewness of the waves. This indicate that the bouy somehow linearise the non-linear waves which makes the reliability of the prototype measurements questionable. In prototype the waves have an obliquity of approximately 35 degrees and model tests were performed with head-on waves, further the duration of the storm was shorter and the wave steepness bigger than during the model tests. The conclusion must be that there are several model effects that maybe could explain the differences in recession.
- **Funchal Airport Extension Berm Breakwater:** Abecasis and Ferreira da Costa, 2004 found that in prototype the reshaping was not uniform over the length of the structure, but on the whole with some small local variations the profile reshaping has been in accordance with the model tests. Full profile reshaping has not yet occurred as the design situation has not yet taken place and it is expected that further reshaping will take place within the next years leading to further knowledge on scale effects.

All in all it seems reasonable to assume that only small and insignificant scale effects on berm breakwater reshaping are present when  $Re_D > 3 \cdot 10^4$  and maybe also for lower values as the present tests indicate.

The strength of the armour stones are not scaled in a physical model test. Therefore, one has to put special attention to the influence of stone breaking and abrasion. If breaking and abrasion can take place in prototype, model tests and recession calculations can be done using a reduced armour size, compared to the one actually used in prototype.

## 4.6 Summary on Front Slope Stability of Berm Breakwaters

A new empirical formula for calculating berm recession, which was found to be superior to any other method tested, has been presented in this chapter.

The uncertainty of the formula has been discussed and should be taken into account for design purposes. For the main part of the data sets used to evaluate the derived formula performs very well. However, the scatter on the data from some few researchers was found to be much greater than for the main part of the data sets. The reason for this scatter could not be addressed. Scale effects on reshaped profiles seems not to be a major problem and are probably neglectable for  $Re_D > 3 \cdot 10^4$  as found for static stable rubble mound breakwaters.

## CHAPTER 5

# Overtopping of Berm Breakwaters

Two existing methods to calculate wave overtopping are tested on the data from the present berm breakwater test programme:

- TAW, 2002
- CLASH neural network model (De Rouck, 2005)

For both methods the reshaped profile is needed to calculate some reshaped profile input parameters. Therefore, a reliable method to calculate the reshaped profile is needed to apply these two methods.

### 5.1 TAW, 2002

It might be expected that the overtopping discharge on reshaped berm breakwater profiles should be well predicted by the overtopping formulae of Van der Meer and Janssen, 1994 developed for dikes. These formulae were later slightly modified and presented in TAW, 2002, which are shortly presented in section 1.5.1.

TAW, 2002 give the overtopping discharge at the outer crest line, and it is assumed that this overtopping also reaches the rear of the crest, which is a very rough assumption. Besley, 1999 presented a reduction factor due to a permeable crest berm to be applied to the formula of Owen, 1980, but because this formula

is very similar to the TAW, 2002 formulae it would be expected that the same reduction factor could be applied also to the TAW, 2002 formulae.

Due to the flat slope around SWL the waves are breaking on the structure ( $\xi < 2$ ). The formulae given in TAW, 2002 can take into account a berm from slope 1:15 to horizontal. The berm on a reshaped berm breakwater profile is steeper (around 1:5). Thus the berm is taken into account by the average slope in the TAW, 2002 formulae. A roughness factor ( $\gamma_f$ ) of 0.45 is applied for reshaping berm breakwaters (Armour 2-3) and 0.40 for non-reshaping berm breakwaters (Armour 1), which are the values recommended in De Rouck, 2005.

As shown in Fig. 5.1 the average prediction seems okay, but a lot of scatter is observed. From this it can be concluded that these formulae does not cover this kind of structure.

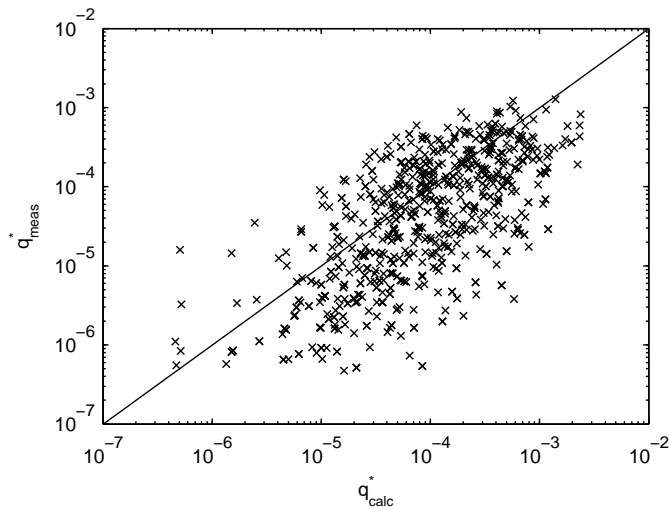


**Figure 5.1**

*Comparison of present data for Armour 1, 2 and 3 and TAW, 2002 overtopping formula.*

Inclusion of the reduction factor by Besley, 1999 to take into account the permeable crest berm resulted only in a little less scatter, cf. Fig. 5.2. When including the reduction factor of Besley, 1999 a roughness factor of 0.55 was applied as a value of 0.40 resulted in way too low overtopping discharges. Hence it can be concluded that the scatter of the data in these plots are at least a factor 100 on the overtopping discharge.



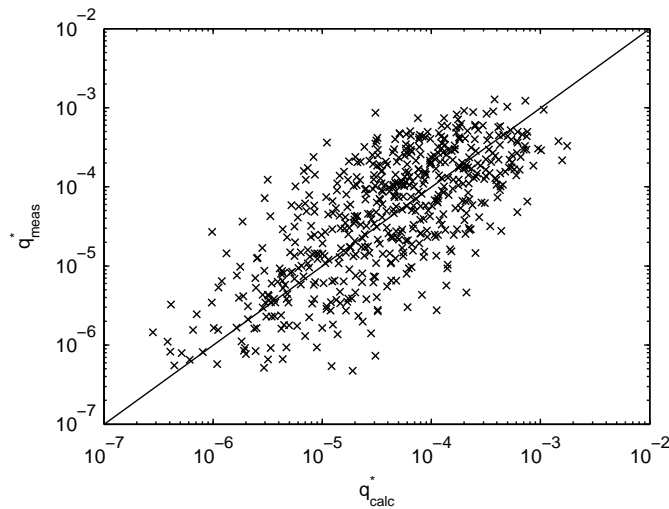


**Figure 5.2**

*Comparison of present data for Armour 1, 2 and 3 and TAW, 2002 overtopping formula with inclusion of the Besley, 1999 reduction factor to take into account a permeable crest.*

## 5.2 CLASH NN-Model

Recently a prediction method based on a neural network model based on a large database with overtopping test results has been developed [De Rouck, 2005]. To use the CLASH NN-model for a reshaping berm breakwater the user should specify some sea state parameters and some geometrical parameters related to the reshaped profile. In the CLASH model reshaping berm breakwaters are given a roughness/permeability factor ( $\gamma_f$ ) of 0.45 and non-reshaping berm breakwaters are given a value of 0.40.

In Fig. 5.3 the model test results are compared to the predictions by the CLASH NN-model when profile parameters are related to actual measured reshaped profiles. It can be seen that the CLASH NN-model is a step forward compared to the TAW, 2002 model, but too little amount of data for berm breakwaters were included in the fitting of the model, to give reliable predictions for berm breakwaters. 82 of the present tests were included in the training process and for these tests the CLASH NN-model predicts the overtopping discharge with very good accuracy. This show some degree of overlearning for berm breakwaters. It is expected that inclusion of the rest of the present data in the learning process of the neural network, would lead to much improved neural network predictions

of overtopping on berm breakwaters.

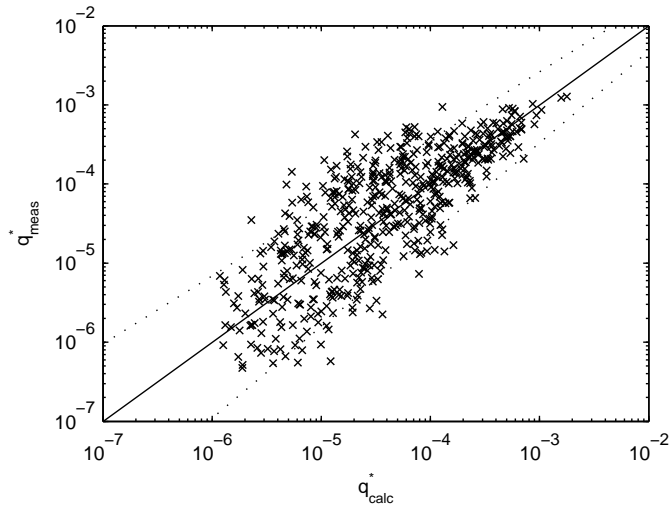


**Figure 5.3**

*Comparison of present data for Armour 1, 2 and 3 and CLASH NN-model. Dashed lines show the 95% confidence band, i.e. only 5% of the data used for the NN development are outside this band.*

### 5.3 Proposed Simple Overtopping Formula

Multiparameter fitting using the Curve Fitting component in the WaveLab2 software package resulted in the overtopping formula given in Eq. 5.1. The curve fitting routine is based on a non-linear least square algorithm utilizing the Levenberg-Marquardt method for optimizing the coefficients in order to minimize the merit function. In the present case the square on the errors of  $\log(Q_*)$  were minimized, which is also the most common parameter used when plotting overtopping discharges. The following data was used for fitting:

- Present data with Armour 1-3 and reshaped profiles (565 tests).
- Lissev, 1993 data (11 tests).
- Bolatti Guzzo and Marconi, 1991 data (3 tests).
- Kuhnen, 2000 data (3 tests).

- Viggosson et al., 1993 data (39 tests).
- Porarinnsson, 2004 data (13 tests).

The formula given in Eq. 5.1 is valid for berm breakwaters with no superstructure and gives the overtopping discharge at the back of the crest ( $R_c = A_c$ ).

$$Q_\star = 1.79 \cdot 10^{-5} \cdot (f_{H0}^{1.34} + 9.22) \cdot s_{0p}^{-2.52} \cdot \exp[-5.63 \cdot R_\star^{0.92} - 0.61 \cdot G_\star^{1.39} - 0.55 \cdot h_{b\star}^{1.48} \cdot B_\star^{1.39}] \quad (5.1)$$

where

$$Q_\star = \frac{q}{\sqrt{g \cdot H_{m0}^3}} \quad (5.2)$$

$q$  is the average overtopping discharge per meter structure width.  $H_{m0}$  is the significant wave height at the toe of the structure (frequency domain parameter).

$$R_\star = \frac{R_c}{H_{m0}} \quad (5.3)$$

$$G_\star = \frac{G_c}{H_{m0}} \quad (5.4)$$

$$B_\star = \frac{B}{H_{m0}} \quad (5.5)$$

$$h_{b\star} = \begin{cases} \frac{3 \cdot H_{m0} - h_b}{3 \cdot H_{m0} + R_c} & \text{for } h_b < 3 \cdot H_{m0} \\ 0 & \text{for } h_b \geq 3 \cdot H_{m0} \end{cases} \quad (5.6)$$

$$T_0 = \sqrt{\frac{g}{D_{n,50}}} \cdot T_{0,1} \quad (5.7)$$

$$T_0^\star = \frac{19.8 \cdot \exp(-\frac{7.08}{H_0}) \cdot s_{0m}^{-0.5} - 10.5}{0.05 \cdot H_0} \quad (5.8)$$

### 5.3 Proposed Simple Overtopping Formula

$$H_0 = \frac{H_{m0}}{\Delta \cdot D_{n,50}} \quad (5.9)$$

$$f_{H0} = \begin{cases} 19.8 \cdot \exp\left(-\frac{7.08}{H_0}\right) \cdot s_{0m}^{-0.5} & \text{for } T_0 \geq T_0^* \\ 0.05 \cdot H_0 T_0 + 10.5 & \text{for } T_0 < T_0^* \end{cases} \quad (5.10)$$

In order to make design easier only the non-reshaped geometrical parameters, defined in Fig. 3.2, are included in the overtopping formula. As the formula does not contain geometrical parameters which describe directly the reshaping the stability parameter  $f_{H0}$  introduced in chapter 4 (Eq. 5.10 is identical to Eq. 4.31 used in the recession formula), is used as an indicative measure of the reshaping. The actual reshaping can be estimated by Eq. 4.34.

The present tests are all performed with initial slopes 1:1.25. For other initial down slopes one could still use the formula because the reshaped profiles are almost identical for the same volume of stones independent on the lower slope. This is valid at least for dynamically stable profiles, and leads to the conclusion that  $B$  has to be enlarged by  $0.5 \cdot (h - h_b) \cdot (\cot(\alpha_d) - 1.25)$  in the formula for a slope different from 1.25. For a very stable structure with very little damage it is believed that the down slope has very little influence on the overtopping discharge. Therefore, the correction should not be done in such cases as it could lead to unsafe results for  $\cot(\alpha_d) > 1.25$ .

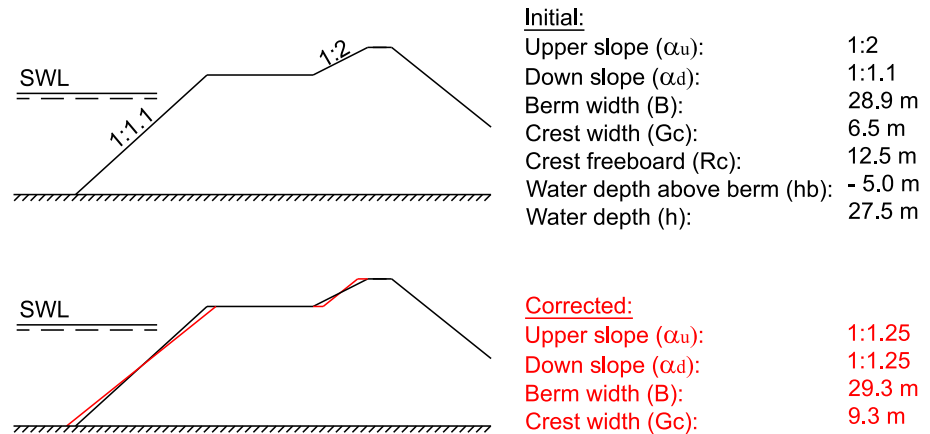


**Figure 5.4**  
Initial cross-section (black) and modified initial cross-section (red) to use in the present proposed overtopping formula (Eq. 5.1).

For initial front slopes above the berm different from 1:1.25, it is proposed to enlarge/reduce  $B$  and  $G_c$ , so the distance to the back of the crest is the same as for a slope 1:1.25. This means increasing both  $B$  and  $G_c$  with the distance  $0.5 \cdot (R_c + h_b) \cdot (\cot(\alpha_u) - 1.25)$  as shown in the example in Fig. 5.4.

The modified cross-section yields the following modified formulae for  $G_\star$  and  $B_\star$ :

$$G_\star = \frac{G_c + 0.5 \cdot (R_c + h_b) \cdot (\cot(\alpha_u) - 1.25)}{H_{m0}} \quad (5.11)$$

$$B_\star = \frac{B + 0.5 \cdot (R_c + h_b) \cdot (\cot(\alpha_u) - 1.25) + 0.5 \cdot (h - h_b) \cdot (\cot(\alpha_d) - 1.25)}{H_{m0}} \quad (5.12)$$

For probabilistic design one should take into account the scatter of the data. Coefficient of variation ( $\delta = \sigma/\mu$ ) on the factor  $1.79 \cdot 10^{-5}$  is 2.22.

Some dependency on the overtopping discharge with the water depth was found for  $h/H_{m0} < 2.5$  due to wave breaking which influences the wave height distribution. For flatter foreshores the influence of the water depth will start for higher values of  $h/H_{m0}$ . However, these two parameters are not included in the formula as the main part of the tests were performed with non-breaking waves on the foreshore and only one foreshore slope was tested. Thus the validity of the formula needs to be verified for cases where heavy wave breaking is not taking place on the foreshore. In cases with heavy wave breaking the formula is expected to give conservative results. Also in very deep water situations ( $h/H_{m0} > 7$ ), additional data is needed to verify the formula.

The grading of the armour stones can have an influence on the overtopping discharge, as it influences the reshaping and the porosity of the structure. This was however not investigated in the present study where  $f_g \approx 1.4$  was used for all tests.

More tests are needed to conclude if the formula, as expected, can be used also in cases where the breakwater has reshaped corresponding to higher waves. The highest  $f_{H0}$  value the breakwater has observed should then be used in the formula.

In Fig. 5.5 the overtopping formula given in Eq. 5.1 is evaluated against data from the present tests with reshaped profiles and Armour 1, 2 and 3.

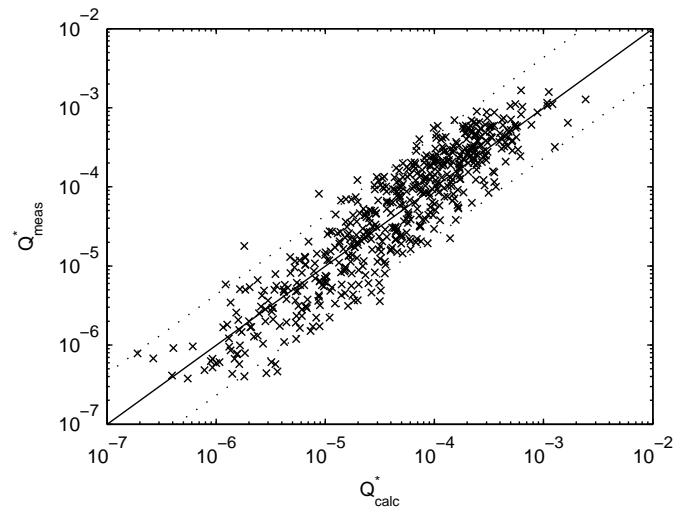


**Figure 5.5**

*Evaluation of proposed overtopping formula (Eq. 5.1) against data related to reshaped profiles for Armour 1, 2 and 3. Dashed lines show the 95% confidence band, i.e. only 5% of the data are outside this band.*

The performance of the formula seems good considering the amount of scatter normally related to overtopping formulae.

## 5.4 Overtopping of Non-Reshaped vs. Reshaped Profiles

59 tests were, as described in section 3.5, performed with the front geometry fixed with a net. More overtopping on the reshaped profile compared to the non-reshaped profile was observed, cf. Fig. 5.6

However, the overtopping formula predicts the overtopping of non-reshaped profiles very well if  $f_{H0} = 0$  (corresponding to no reshaping) instead of the actual  $f_{H0}$  values (corresponding to the structure was not fixed  $f_{H0} = 5.1$  to 18) are used in the formula, cf. Fig. 5.7.

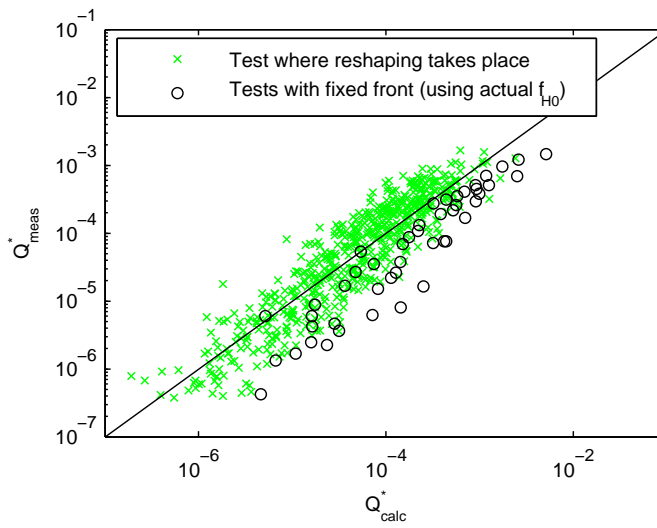


**Figure 5.6**

*Influence of reshaping on overtopping discharge (applying actual  $f_{H0}$  in Eq. 5.1).*

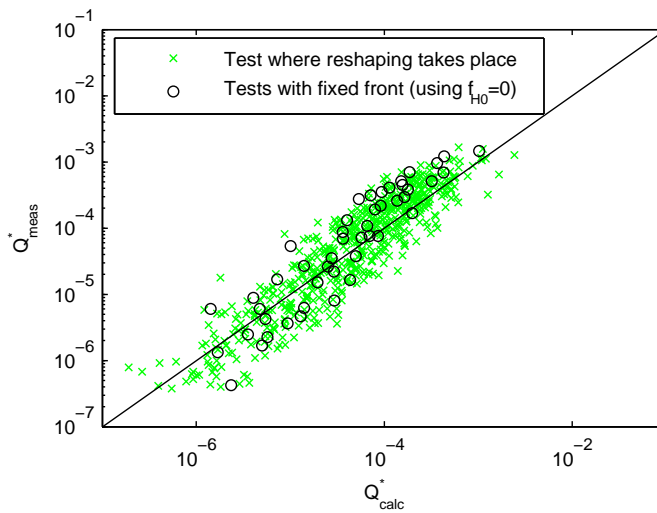


**Figure 5.7**

*Evaluation of Eq. 5.1 for non-reshaped profiles applying  $f_{H0} = 0$ .*

## 5.5 Scale Effects

As discussed in section 4.5 a safe value for the critical Reynolds number ( $Re_{D,crit}$ ) seems to be  $3 \cdot 10^4$  for armour stability. For overtopping there is only very limited documentation on the critical value, cf. chapter 9. There are some indications of scale effects on overtopping of porous and/or rough structures also for  $Re_D > 3 \cdot 10^4$ , causing too little overtopping to be measured in a small scale model of a rubble mound structure, which seems especially pronounced for low overtopping discharges and flat front slopes. However, there are many possible model effects mainly due to different measurements methods in small and prototype scale. New investigations in overtopping scale effects for a conventional rubble mound breakwater with a 1:2 slope and a superstructure, were carried out in the present study and presented in chapter 10. The slope of a reshaping berm breakwater is flat around the water level and could thus be subjected to larger scale effects than observed for a conventional rubble mound structure with a slope around 1:2.

No differences in overtopping in the tests with Armour 1,2 and 3 were observed when comparing to the overtopping formula. However, it can not be concluded that no scale effects were present for these three armour configurations as the overtopping formulae is fitted to all these tests, implying that compensation for a possible scale effect might be included in the  $f_{H0}$  parameter in the overtopping formula.

To study scale effects on overtopping of berm breakwaters, it was preferable to perform comparisons to large scale or prototype data with berm breakwaters. This was however not possible and tests in 1.9 times smaller scale using Armour 4 were performed instead. In Fig. 5.8 overtopping from tests with Armour 3 is compared to overtopping in tests with Armour 4. The small scale experiments are within the cloud of the other data points. However, in average there is measured 1.66 times less overtopping in the small scale compared to the predictions by the overtopping formula. The difference is small, but the probability that the tests with Armour 4 is belonging to the same population as Armour 1-3 with respect to mean value of  $q_{calc}/q_{meas}$  is only  $2.8 \cdot 10^{-5}$  calculated by the method given in Ayyub and McCuen, 1997, p. 219ff. This method is a hypothesis test of whether the mean of two independent samples are equal. Model effects could also be the reason for this small difference.



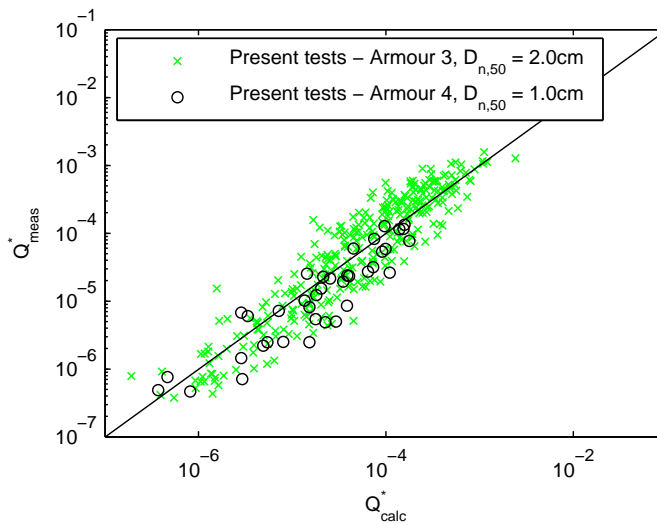


**Figure 5.8**  
*Comparison of overtopping in larger and smaller scales.*

## 5.6 Comparison with Other Overtopping Data

The present tests were performed due to lack of knowledge on overtopping of berm breakwaters. Therefore, the available data from other researchers on overtopping of berm breakwaters is very scarce. The following data of other researchers was used for comparison with the present data and formula:

- Bolatti Guzzo and Marconi, 1991 tested two cross-sections, but measurements at the crest are only available for one cross-section (3 tests), other measurements are performed at the wharf alongside the inner part of the breakwater (7 tests).
- Lissev, 1993 tested a reshaping berm breakwater with homogeneous berm (11 tests on one cross-section).
- Viggosson et al., 1993 performed model tests measuring wave overtopping on a multi-layer berm breakwater cross-section (39 tests).
- Kuhnen, 2000 tested one cross section of a multi-layer berm breakwater (3 tests).

## 5.6 Comparison with Other Overtopping Data

- Porarinnsson, 2004 performed 13 model tests with a multi-layer berm breakwater proposed for the Þorlákshöfn breakwater (one cross-section tested).

The comparison of their results and the present obtained results is made using the present formula and the CLASH NN-model. In appendix D is the proposed overtopping formula evaluated against some dimensionless parameters for the above given data sets.

### 5.6.1 Bolatti Guzzo and Marconi, 1991

Fig. 5.9 shows a comparison of the present test results and the test results of Bolatti Guzzo and Marconi, 1991 where a different down and upper slope as compared to the present tests were taken into account in the present formula as recommended in section 4.3.

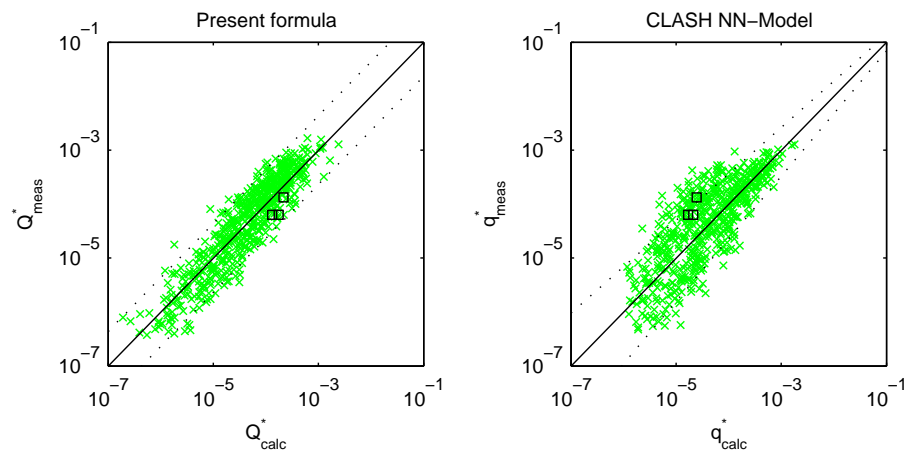


**Figure 5.9**

*Comparison of present overtopping data with data of Bolatti Guzzo and Marconi, 1991.*

The present formula predicts between 1.6 and 2.8 times the measured overtopping discharge for their tests with all results within the 90% confidence band of the formula. These data was not included in the training process of the CLASH NN-Model, and the predictions by the CLASH NN-Model is good, but slightly worse than the present formula.

### 5.6.2 Lissev, 1993

Fig. 5.10 shows a comparison of the present test results and the test results of Lissev, 1993, the latter performed with  $D_{n,50}$  approximately 1.7 times larger than for Armour 3. Lissev, 1993 performed the overtopping measurements after the stability tests with stepwise increasing waves. Consequently, the breakwater had reshaped corresponding to the highest waves in the series and the highest stability index was used in the overtopping formula given in Eq. 5.1. The different upper slope was taking into account as described in section 5.3.

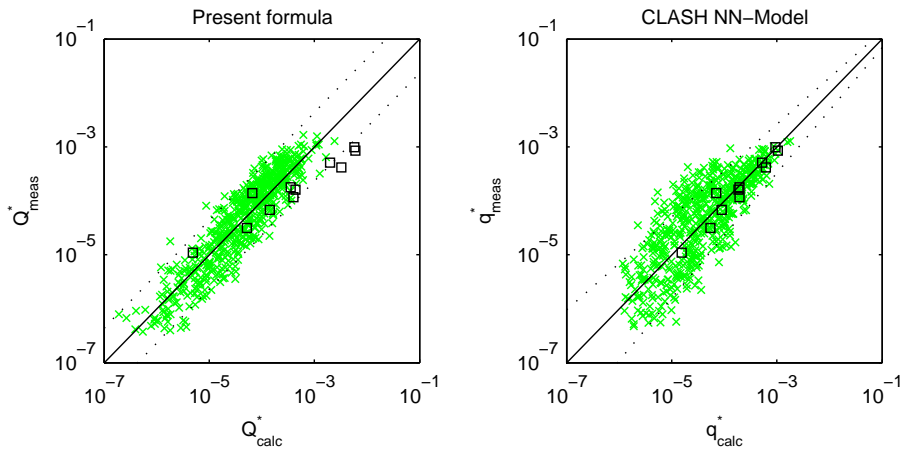


**Figure 5.10**

*Comparison of present overtopping data with data of Lissev, 1993.*

The formula predicts between 0.45 and 7.8 times the measured overtopping discharge for his tests with the main part within the 90% confidence band. The deviation for larger overtopping discharges may be due to less recession of the berm compared to the present tests as shown in section 4.3. A different wave spectra was tested by Lissev, 1993 as his tests are performed with the Pierson-Moskowitz and the present tests are performed with a JONSWAP spectra with a peak-enhancement factor ( $\gamma$ ) of 3.3.

The Lissev, 1993 data was also included for fitting the CLASH NN-model, and this model predicts the overtopping extremely well. In contrast to the present formula the CLASH NN-model uses the actual reshaped profile as input.

## 5.6.3 Viggooson et al., 1993

The different upper slope used in Viggooson et al., 1993 compared to present tests was taken into account in the present formula as recommended in section 4.3. The flatter down slope was not taken into account as it was a very stable structure that was tested, further it will lead to only an insignificant change in overtopping discharge in this case. In these tests overtopping is not measured at the crest but further down the rear slope ( $R_c < A_c$ ), cf. Fig. C.13. The influence of this is unknown but expected to be quite small even though the crest is rather permeable.

For this data set only total (incident + reflected) waves are given as no reflection analysis was performed. Due to very low wave steepness and a very stable steep structure, reflection coefficients ( $C_r$ ) around 40% could be expected (cf. Fig. 7.1) giving an incident significant wave height of 92.8% of the total recorded significant wave height. The latter compensation was made in the present analysis (Fig. 5.12), but not made in the analysis of Viggooson et al., 1993.  $A_c$  is inserted in the formula instead of  $R_c$  and thus ignoring the lower position of the overtopping measurements.

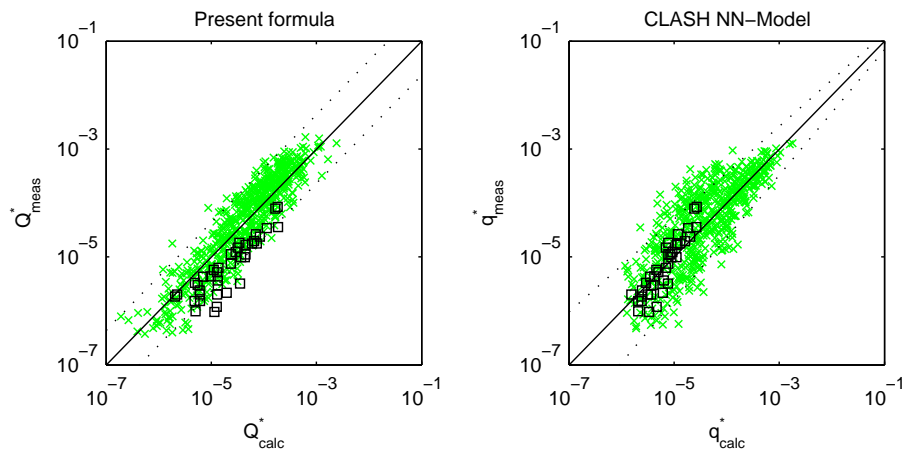


**Figure 5.11**

*Comparison of present overtopping data and data of Viggooson et al., 1993 (assuming 0% reflection).*

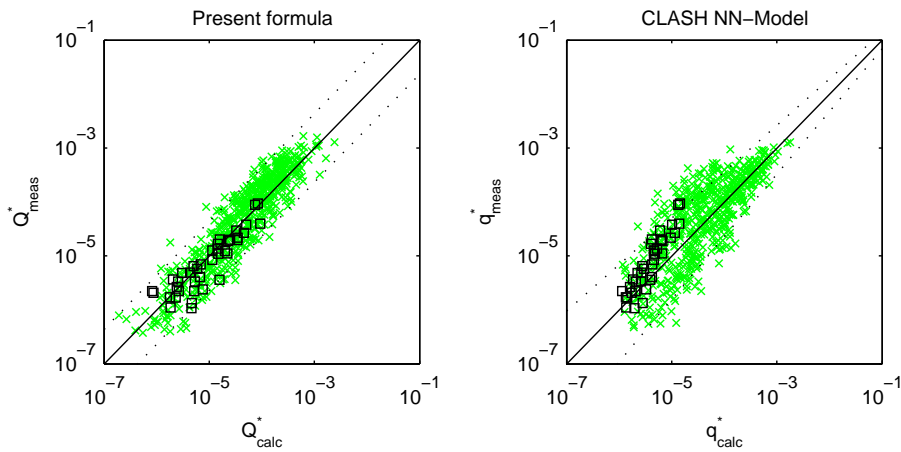


**Figure 5.12**

*Comparison of present overtopping data and data of Viggosson et al., 1993 (assuming 40% reflection).*

The present formula predicts between 0.37 and 4.4 times the measured overtopping discharge in their experiments when  $C_r = 40\%$  is assumed, which is very good considering that the way the tests were carried out were completely different to the present tests. Their test are 3D basin tests with a specific 3D bottom configuration. The waves were measured offshore using no reflection analysis, and 40% reflection was assumed due to low steepness waves. The influence of the rather high toe on the cross-section tested by Viggosson et al., 1993 is not known.

The CLASH neural network model give very good predictions for this data set when  $C_r = 0\%$  is assumed, but the data was also included in the fitting process of the NN without correcting the wave heights due to reflection. Some calculations were performed using the CLASH NN-model on the same cross section but with no toe berm, which resulted in 1.1 to 3 times less overtopping, which seems doubtful and probably is due to limited data for berm breakwaters which could have resulted in overlearning of the neural network. When  $C_r = 40\%$  is assumed the data show similar behavior as the present tests with armour 1 with slightly underprediction of the overtopping discharge.

5.6.4 Kuhnen, 2000

For this data set the different upper slope compared to the present data was included in the present formula as recommended in section 4.3. The different down slope was not taken into account.

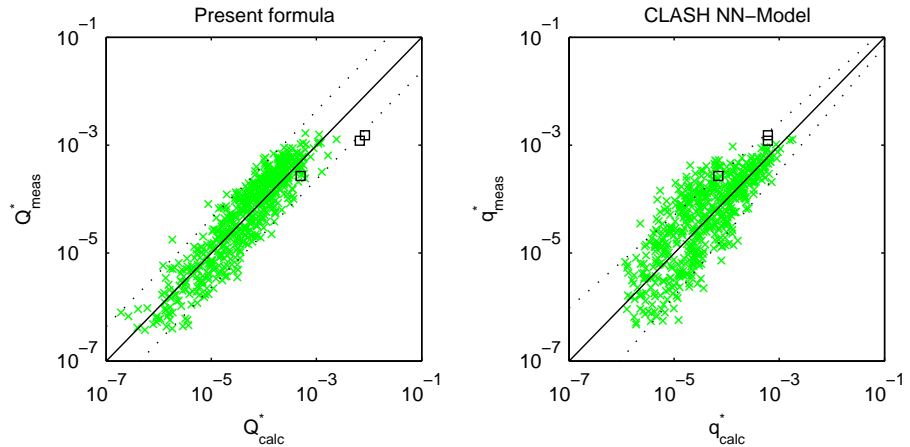


**Figure 5.13**  
*Comparison of present overtopping data with data of Kuhnen, 2000.*

The data of Kuhnen, 2000 shows results close to those obtained by Lissev, 1993. The measured overtopping discharges are between 1.9 and 5.5 times lower than predicted by the formula. All three data points are outside the calibrated area of the formula for one parameter, due to a more narrow crest than tested in the present tests, cf. Fig. D.2. The CLASH NN-model gives good predictions for this data set.

5.6.5 Porarinsson, 2004

The upper slope was for the present formula taken into account as mentioned in section 4.3. The different down slope compared to the present tests was not taken into account due to very limited reshaping.

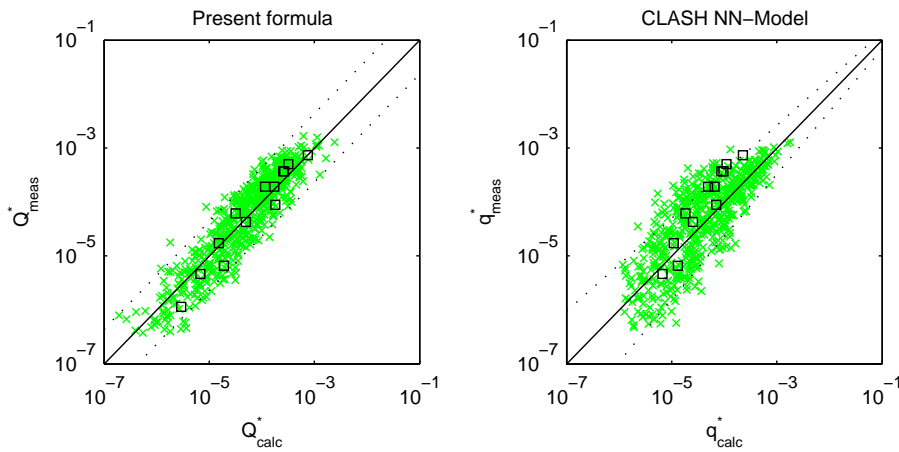


**Figure 5.14**

*Comparison of present overtopping data with data of Porarinsson, 2004.*

Very good agreement between the present derived formula and the tests by Porarinsson, 2004, also performed at Aalborg University, is observed. All tests are within the 90% confidence band which show that the formula could be used for multi-layer berm breakwaters with the same accuracy as for reshaping berm breakwaters. This demonstrates that overtopping discharges on a multi-layer berm breakwater are similar to those on a homogeneous one with the largest stone class used in the entire berm. This corresponds well to the results obtained in chapter 10, where no differences were found between two different sizes of core material.

## 5.7 Summary on Overtopping of Berm Breakwaters

A design formula to calculate average overtopping discharges on berm breakwaters has been developed. The design formula uses only non-reshaped geometrical parameters, which makes design easier. The design formula has been verified for homogeneous and multi-layer berm breakwaters. In case of a homogeneous berm breakwater the formula covers the entire area from non-reshaping to dynamically stable profiles.

In general the agreement between the derived formula and data of other researchers is very good. The best agreement is found between the present tests

and the test of Porarinnsson, 2004, both performed at Aalborg University.

From SINTEF there are two data set available published by Lissev, 1993 and Kuhnen, 2000. These two data are also well predicted by the formula but there is a tendency that the formula overestimates the overtopping discharge for large overtopping discharges. The difference in overtopping discharges for the Lissev, 1993 data set could alone be explained by the deviation in recession.

For the data set of Viggosson et al., 1993 the present formula predicts the overtopping discharge very well, eventhough the tests are performed in a completely different way as it is three dimensional tests where the waves are measured offshore with no reflection analysis (in this comparison  $C_r = 40\%$  was assumed due to low steepness tests). Also a high toe is present which could have an influence on the amount of overtopping.

All in all it can be concluded that the formula gives extremely accurate estimates of overtopping discharges and seems superior to the existing methods for overtopping discharge calculations, including the CLASH NN-model, which however performed reasonable. It is expected that inclusion of all of the present data in the fitting of the NN will lead to more accurate predictions. However, the CLASH NN model still need an accurate prediction of the reshaped profile to give the geometrical input parameters.

For large overtopping discharges ( $q > 5$  l/sm in prototype) it is for some data sets observed some conservative bias on the developed overtopping formula. These deviations were discussed in appendix D, and could partly be addressed by some parameters being outside the calibrated area.



## CHAPTER 6

# Rear Slope Stability of Berm Breakwaters

In this chapter are the results on rear slope stability obtained in the present tests with berm breakwaters presented. If the rear side damage is related to the overtopping velocity at the crest, it is expected that design rules developed for conventional breakwaters could be applied also to berm breakwaters. The validity of the model of Van Gent and Pozueta, 2004 can however not from the present test results be checked for berm breakwaters, as overtopping velocities were not measured.

Even though some authors state that rear slope stability is better correlated to the overtopping velocity than to the discharge, a logical approach would be to link rear side stability to the average overtopping discharge, as much more information is available on the discharge. High correlation between overtopping velocity and discharge is also expected, maybe also dependent on the wave steepness or breaker parameter as different types of overtopping events have visually been observed for breaking and non-breaking waves on the slope. In case of waves breaking on the slope, it can easily be observed that the overtopping water is thrown over with considerable higher velocities than for non-breaking waves, which indicates that the critical overtopping discharge is less for higher steepness. However, what points in the opposite direction is that for higher wave steepness the overtopping is also much more evenly distributed in time, leading to smaller single wave overtopping volumes than for lower steepness (for identical average discharge). These two effects might perhaps balance each other.

It seems reasonable to assume that the rear slope stability, can be calculated from the overtopping discharge, in combination with the rear slope angle, the

---

natural angle of repose, the stone size and density and the crest freeboard only.

In the present tests it was observed that the rear slope damage typically starts with a few stones being displaced downwards during wave overtopping from a position just above still water level. This has been observed by several other researchers. If the damage development continues it will reach the crest both due to direct impact and due to missing support as a result of movements of stones further down. Below the waterline the damage decreases rapidly and the eroded stones are deposited here.

Fig. 6.1 shows the definition of rear side damage and the variation in the probability distribution of rear side damage observed in the present tests with mean overtopping discharge. The results are based on visual observations done after each test, where the rear side damage was characterized by one of the following six categories:

- No damage
  
- Initial damage
  
- Initial/moderate damage
  
- Moderate damage
  
- Moderate/severe damage
  
- Severe damage

The probability distributions shown on the bottom of Fig. 6.1 is the probability distributions of all tests with no damage for the three different armour types defined in Table 3.1. It can be seen that no damage has been measured for overtopping discharges between  $5 \cdot 10^{-8} \text{ m}^3/\text{m/s}$  and  $8 \cdot 10^{-5} \text{ m}^3/\text{m/s}$ . However, there is a large overlap in overtopping discharges with the higher rear slope damage categories (shown above in Fig. 6.1). Nevertheless, the figure shows as expected reasonable correlation between rear slope stability and mean overtopping discharge for the three tested stone sizes.

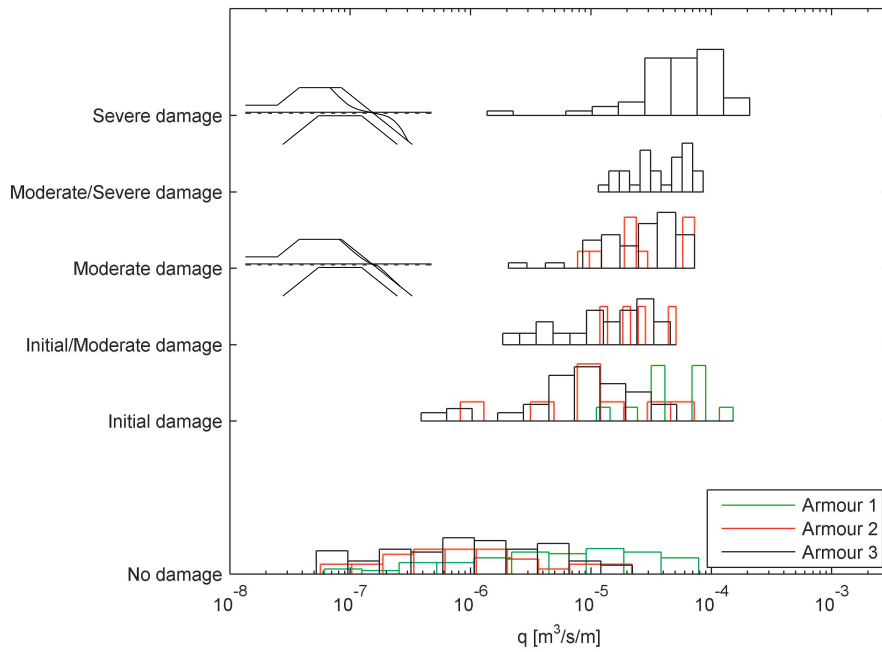


**Figure 6.1**

*Definition of rear slope damage and probability distribution of rear slope stability against measured mean overtopping for Armour sizes 1, 2 and 3.*

As expected the larger stones, Armour 1, shown in green on Fig. 6.1 are more stable than the smaller ones for the same overtopping discharges. A dimensionless mobility parameter  $\theta$  depending on the overtopping discharge, the stone density and stone diameter is introduced.

$$\theta = \frac{q}{\sqrt{g \cdot \Delta \cdot D_{n,50}^3}} \quad (6.1)$$

Fig. 6.2 shows the probability distribution of rear side damage against  $\theta$ . After introducing  $\theta$  there are no clear differences between the three armour configurations. Hence, it seems reasonable to conclude that it is possible to use this parameter to calculate rear side erosion. However, this conclusion is a little dangerous as Armour 1 has a significant larger density than Armour 2 & 3. With this parameter there still remains a lot of scatter and only some conservative design rules can be developed.

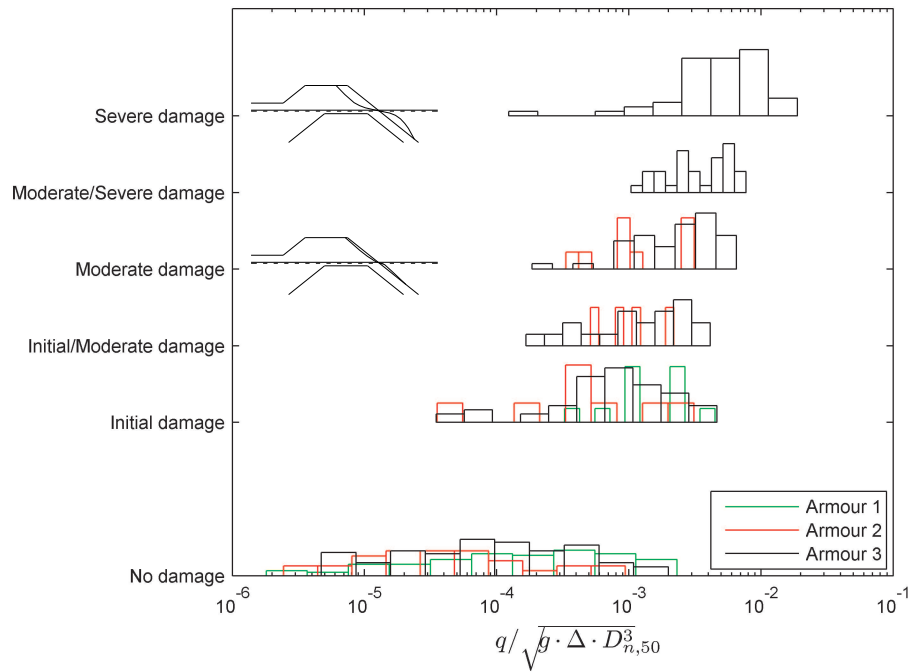


**Figure 6.2**

*Definition of rear slope damage and probability distribution of rear slope stability against measured dimensionless parameter defined in Eq. 6.1 for Armour sizes 1, 2 and 3.*

Due to only one slope angle tested, it has not been possible to include this parameter in a design formula. The following conservative limits can be identified from Fig. 6.2 valid for 1:1.25 rear slope:

$$\begin{aligned}
 \text{No damage:} & \quad \frac{q}{\sqrt{g \cdot \Delta \cdot D_{n,50}^3}} < 4 \cdot 10^{-5} \\
 \text{Start of damage:} & \quad 4 \cdot 10^{-5} \leq \frac{q}{\sqrt{g \cdot \Delta \cdot D_{n,50}^3}} < 3 \cdot 10^{-4} \\
 \text{Moderate damage:} & \quad 3 \cdot 10^{-4} \leq \frac{q}{\sqrt{g \cdot \Delta \cdot D_{n,50}^3}} < 7 \cdot 10^{-4} \\
 \text{Severe damage:} & \quad 7 \cdot 10^{-4} \leq \frac{q}{\sqrt{g \cdot \Delta \cdot D_{n,50}^3}}
 \end{aligned} \tag{6.2}$$

It is expected that these values conservatively can be applied on flatter rear slopes.



## CHAPTER 7

# Reflection from Berm Breakwaters

Reflection from berm breakwaters is generally smaller than for a conventional steeper rubble mound breakwater. This is mainly due to the flatter slope at the water level which promotes wave breaking, but also due to the greater porosity of the voluminous berm of armour stones. Reflection from non-reshaping berm breakwaters is significantly higher due to the steeper slope.

The existing formulae account for the effects of wave steepness and structure slope, which are the main parameters for a straight slope. For a reshaping berm breakwater the slope and hence the surf similarity parameter ( $\xi$ ) vary continuously along the slope making it difficult to give a single value of  $\xi$  representing the breaking on the structure and the phase lag between reflections from different parts of the structure.

By analysing the data from the present tests, it was found that when the slope ( $\tan(\alpha)$ ) was calculated as the average slope between SWL and  $1.5 \cdot H_{m0}$  below SWL, it gave reasonable correlation between reflection coefficient and the surf similarity parameter  $\xi_{op}$ . The slope above SWL is of less importance. For a horizontal berm this gives a singularity when berm the berm is located around the water level. The influence of this was not studied further.

In Fig. 7.1 the reflection coefficients from the present tests are plotted against the breaker parameter calculated as recommended above. The reflection coefficients are based on reflected waves from the deep end and incident waves at the toe. In the figure the equations by Seeling, 1983 and Postma, 1989 are given. They are based on conventional straight slopes. As the slope on the part from SWL

and  $1.5 \cdot H_{m0}$  below SWL is typically around 1:2 to 1:4.5 for a reshaping berm breakwater, it can be seen that a reshaping berm breakwater gives the same amount of reflection as a very flat conventional structure with a constant slope in the same range. However, as a very flat slope is very uncommon for conventional breakwaters, it can be concluded that reshaping berm breakwaters usually give less reflection than observed on a typical conventional straight rubble round breakwater.

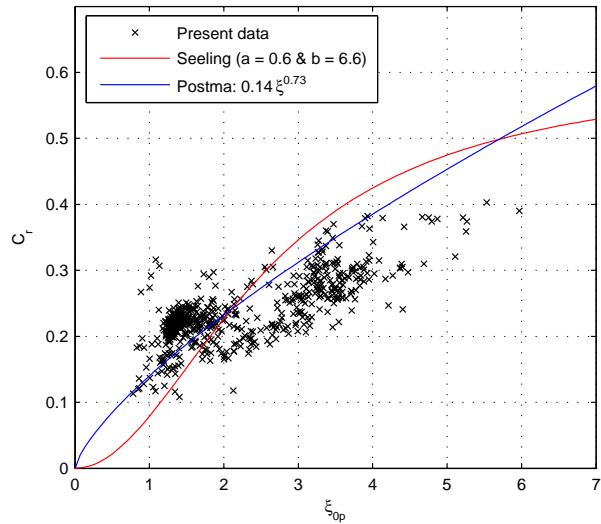


**Figure 7.1**

*Empirical formulae for wave reflection and present data. The slope is calculated as the average slope between SWL and  $1.5 \cdot H_{m0}$  below SWL.*

In Fig. 7.2 the existing formulae are evaluated against the present data. It can be concluded that a lot of scatter is present for most formulae. However, the improved formula of Postma, 1989 (Eq. 1.23) gives quite good estimations when it is taken into account it has been developed for non-overtopping straight slopes. The other existing formulae can only give a rough guess on the reflection coefficient. It was found that all formulae were less reliable for a very stable berm breakwater compared to a reshaping berm breakwater. This especially applies to the formula of Alikhani, 2000 which was also expected as this formula does not include the slope angle as it is developed for reshaping berm breakwaters.



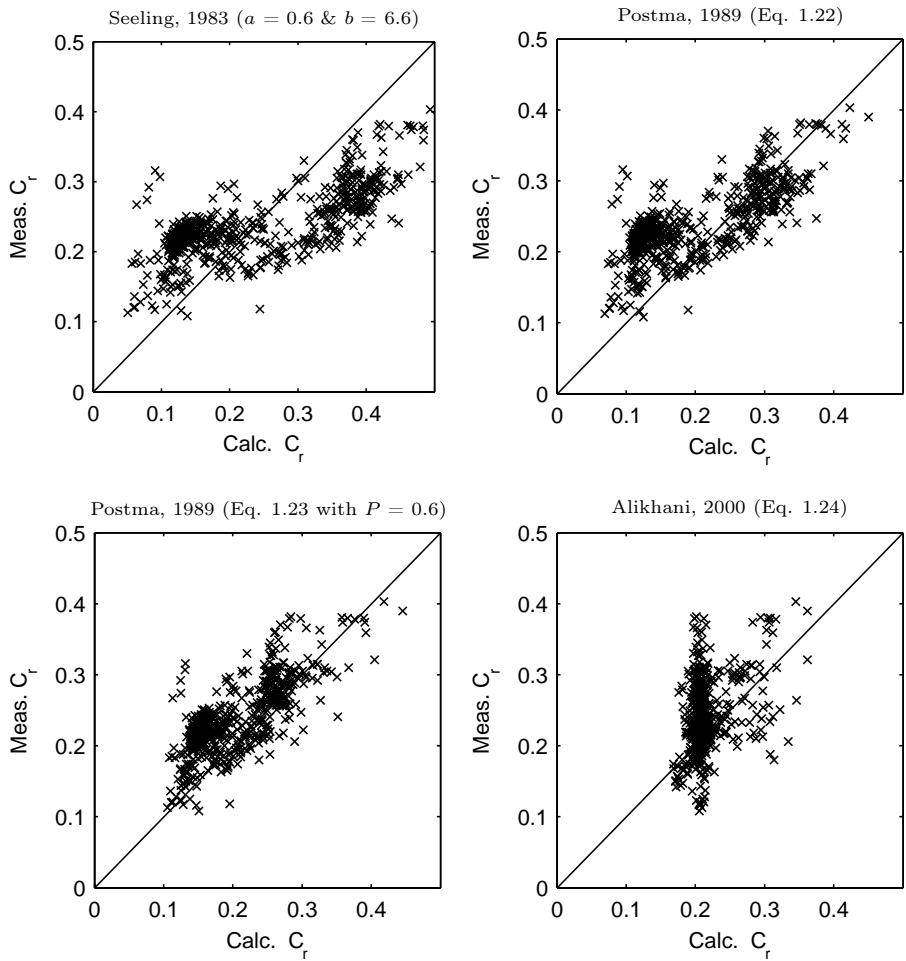


**Figure 7.2**

*Evaluation of existing formulae for wave reflection and present data. The slope is calculated as the average slope between SWL and  $1.5 \cdot H_{m0}$  below SWL.*

Fig. 7.3 shows that the formula of Alikhani, 2000 gives good estimations of the reflection coefficient for dynamically stable profiles ( $H_0 > 2.7$ ).

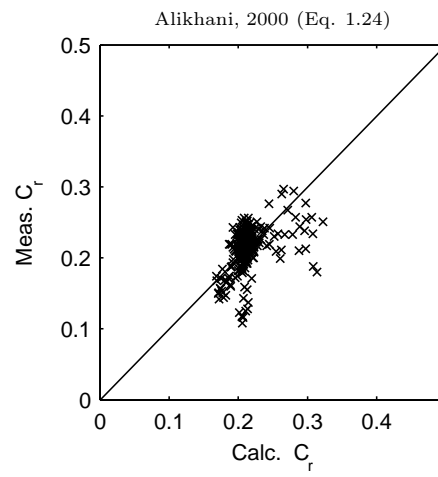


**Figure 7.3**

*Evaluation of Alikhani, 2000 formulae and present data with  $H_0 > 2.7$ .*

## CHAPTER 8

# Berm Breakwater Design Example

In this chapter an example is given on the application of the derived formulae for designing a berm breakwater. First the fictitious design conditions for the breakwater are given. Afterwards the design procedure is given and discussed.

### 8.1 Design Criteria

#### 8.1.1 Sea States

The breakwater should be designed for the following sea states, which is a result of a long term wave statistical analysis:

	1 year return period	50 year return period
Water depth $h$ [m]	14.0	15.0
Sign. wave height $H_{m0}$ [m]	4.2	6.0
Peak period $T_p$ [s]	9.0	10.0
Wave direction $\beta$ [°]	0	0

**Table 8.1**  
*Design sea states.*

The duration of these wave attacks is assumed to be equal to 3000 waves. The uncertainty of these parameters should be taken into account for probabilistic design, but is not dealt with in this short example, where they are assumed deterministic.

## 8.1 Design Criteria

---

The wave spectrum is assumed to be similar to the JONSWAP spectrum with a peak enhancement factor ( $\gamma$ ) of 3.3, which makes it possible to calculate all other frequency domain wave periods from the peak period from the formulae given in Eq. 8.1.

$$\begin{aligned}T_{-1,0} &\approx 0.91 \cdot T_p \\T_{0,1} &\approx 0.85 \cdot T_p \\T_{0,2} &\approx 0.82 \cdot T_p\end{aligned}\tag{8.1}$$

As no information is available on wave skewness ( $b_1$ ), Eq. 4.47 is used to estimate the skewness to  $b_1 = 0.14$  for the 1-year event and  $b_1 = 0.17$  for the 50-year event.

### 8.1.2 Available Rock

The design should be based on maximizing the utilization of the available rock material for the available construction equipment. This adds an additional iteration process to the design procedure, as this depends on the proportion between volume of armour material and volume of core material. In the following it is simply assumed that the armour stones have the following properties, which include the effect of stone breaking and abrasion that might take place during reshaping.

- $W_{50} = 5 \text{ t}$
- $\Delta = 1.65$
- $f_g = \frac{D_{n,85}}{D_{n,15}} = 1.5$

These stone parameters result in a stability index ( $H_0$ ) of 2.9 for the 50 year event, which indicates a dynamically stable profile in this situation. Further, it indicates that if a rock armoured conventional rubble breakwater has to be constructed a slope around 1:3 has to be applied for the available quarry material, taking into account the larger  $W_{50}$  for a smaller amount of needed armour stones.

### 8.1.3 Stability Criteria for the Berm

The recession of the berm should with a 95% confidence level be less than the initial berm width for the sea state with a 50 year return period. For the 1-year event no significant motions of the stones are allowed.

### 8.1.4 Allowable Overtopping

The allowable overtopping discharge depends on the function of the breakwater and the areas behind it. In the present case it is assumed that there is no public access to the breakwater for neither pedestrians or vehicles. No vessels are moored behind the breakwater. Therefore the following rather large overtopping discharges are allowed:

- 50 year return period:  $q = 5 \text{ l/s/m}$
- 1 year return period:  $q = 0.5 \text{ l/s/m}$

Further, it should be checked that the sea state with a 50 year return period does not cause overtopping events which may damage the rear side armour. Very limited damage of the rear armour is allowed for the 50 year event (corresponding to start of damage in Eq. 1.25).

## 8.2 Design of Breakwater

The rear slope, the lower and upper front slope are selected to 1:1.25, which is close to the natural angle of repose for the material. If the contractor prefer to place the armour stones with a steeper front slope, then the berm width should just be increased accordingly, as the most important is that the volume of material in the berm is correct and that the longshore profile is not too non-uniform.

The berm elevation is chosen to 1.0 m above the 50-year high water level, which corresponds to 1.8 m above the 1-year event.

### 8.2.1 Berm Geometry

The necessary berm width for the 50-year ultimate limit state event, can be calculated from Eq. 4.34 as follows:

$$H_0 = \frac{H_{m0}}{\Delta \cdot D_{n,50}} = \frac{6.0 \text{ m}}{1.65 \cdot 1.24 \text{ m}} \approx 2.94 \quad (8.2)$$

$$T_0 = \sqrt{\frac{g}{D_{n,50}}} \cdot T_{0,1} = \sqrt{\frac{9.82 \text{ m/s}^2}{1.24 \text{ m}}} \cdot 8.5 \text{ s} \approx 24.1 \quad (8.3)$$

## 8.2 Design of Breakwater

---

$$\begin{aligned}
 T_0^* &= \frac{19.8 \cdot \exp\left(-\frac{7.08}{H_0}\right) \cdot s_{0m}^{-0.5} - 10.5}{0.05 \cdot H_0} \\
 &= \frac{19.8 \cdot \exp\left(-\frac{7.08}{2.9}\right) \cdot 0.053^{-0.5} - 10.5}{0.05 \cdot 2.9} = -18.4
 \end{aligned} \tag{8.4}$$

$$\begin{aligned}
 f_{H0} &= 19.8 \cdot \exp\left(-\frac{7.08}{H_0}\right) \cdot s_{0m}^{-0.5} \quad (T_0 \geq T_0^*) \\
 &= 19.8 \cdot \exp\left(-\frac{7.08}{2.94}\right) \cdot 0.053^{-0.5} = 7.79
 \end{aligned} \tag{8.5}$$

$$f_\beta = \cos(\beta) = \cos(0^\circ) = 1 \tag{8.6}$$

$$f_{skewness} = \exp(1.5 \cdot b_1^2) = \exp(1.5 \cdot 0.17^2) = 1.044 \tag{8.7}$$

$$f_N = (N/3000)^{-0.046 \cdot H_0 + 0.3} = (3000/3000)^{-0.046 \cdot 2.94 + 0.3} = 1 \quad (H_0 < 5) \tag{8.8}$$

$$h_s = 0.65 \cdot H_{m0} \cdot s_{0m}^{-0.3} \cdot f_N \cdot f_\beta = 0.65 \cdot 6.0 \text{ m} \cdot 0.053^{-0.3} \cdot 1 \cdot 1 = 9.4 \text{ m} \tag{8.9}$$

$$f_{grading} = 1 \quad (f_g \leq 1.5) \tag{8.10}$$

$$f_{hb} = 1 \quad \left( \frac{h_b}{H_{m0}} \leq 0.1 \right) \tag{8.11}$$

$$\begin{aligned}
 \frac{Rec}{D_{n,50}} &= f_{hb} \cdot \left[ \frac{(1 + c_1) \cdot h - c_1 \cdot h_s}{h - h_B} \cdot f_N \cdot f_\beta \cdot f_{H0} \cdot f_{skewness} \cdot f_{grading} + \right. \\
 &\quad \left. \frac{\cot(\alpha_d) - 1.05}{2 \cdot D_{n,50}} \cdot (h_b - h) \right] \\
 &= 1 \cdot \left[ \frac{(1 + 1.2) \cdot 15.0 \text{ m} - 1.2 \cdot 9.4 \text{ m}}{15.0 \text{ m} - (-1.0 \text{ m})} \cdot 1 \cdot 1 \cdot 7.79 \cdot 1.044 \cdot 1 + \right. \\
 &\quad \left. \frac{1.25 - 1.05}{2 \cdot 1.24 \text{ m}} \cdot (-1.0 \text{ m} - 15.0 \text{ m}) \right] = 9.7
 \end{aligned} \tag{8.12}$$

$$Rec_{50\%} = 9.7 \cdot D_{n,50} = 9.7 \cdot 1.24 \text{ m} = 12.0 \text{ m} \quad (8.13)$$

The uncertainty of the estimation is taken into account by Eq. 4.48 and 4.49:

$$\begin{aligned} Rec_{95\%,\text{present data}} &= 1.028 \cdot Rec_{50\%} + 2.38 \cdot D_{n,50} = 15.3 \text{ m} \\ Rec_{95\%,\text{all data}} &= 1.080 \cdot Rec_{50\%} + 4.00 \cdot D_{n,50} = 17.9 \text{ m} \end{aligned} \quad (8.14)$$

Whether the confidence level identified for all data or for the present data is used depends on the philosophy of the designer. The design conditions are well covered in the present data, from which one can argue to use the 95% confidence level on these data. However, in the following a minimum berm width of 18 m is applied, as it has only a small impact on the total volume of the structure due to the requirements on the overtopping discharge, cf. Fig. 8.2.

For the 1-year event no significant motions of the armour stones are allowed as this can cause breakage of armour stones and for just a small wave obliquity also a longshore transport of armour stones. This is fulfilled if  $H_0$  is significant smaller than 2.7, which is the limit for dynamic stability. In the present case we have:

$$H_0 = \frac{H_{m0}}{\Delta \cdot D_{n,50}} = \frac{4.2 \text{ m}}{1.65 \cdot 1.24 \text{ m}} \approx 2.06 \quad (8.15)$$

which corresponds to a static stable reshaped profile. For the 1-year event the expected recession can be calculated using Eq. 4.34 and given in the following Table 1.25.

	<i>Rec</i> <sub>5%</sub> [m]	<i>Rec</i> <sub>50%</sub> [m]	<i>Rec</i> <sub>95%</sub> [m]
<b>1-year</b>	1.0	3.7	6.8
<b>50-year</b>	9.0	12.0	15.3

**Table 8.2**

*Expected recession for the 1-year and 50-year event, using the uncertainty identified for the present data.*

## 8.2.2 Top Geometry and Rear Side Armour

The allowable overtopping discharge determines the top geometry of the structure. The limit on the overtopping discharge for start of damage of the rear side

## 8.2 Design of Breakwater

damage can conservatively be calculated from Eq. 6.2 to:

$$q < 3 \cdot 10^{-4} \cdot \sqrt{g \cdot \Delta \cdot D_{n,50}^3}$$

$$\Downarrow$$

$$q < 3 \cdot 10^{-4} \cdot \sqrt{9.82 \text{ m/s}^2 \cdot 1.65 \cdot (1.24 \text{ m})^3} \approx 1.7 \text{ l/s/m}$$
(8.16)

Thus rear side damage for the applied stone size is the parameter determining the allowable overtopping discharge during the 50-year event.

It is now investigated for which combinations of the initial geometrical parameters  $B$ ,  $R_c$  and  $G_c$  defined in Fig. 3.2 this criteria is fulfilled with a 95% confidence level. This can be calculated from Eq. 5.1, if  $1.645 \cdot \sigma$  is added to the estimations. As the coefficient of variation ( $\sigma/\mu$ ) is 2.22, the factor  $1.79 \cdot 10^{-5}$  in Eq. 5.1 has to be substituted by  $1.79 \cdot 10^{-5} \cdot 1.64 \cdot 2.22 = 6.54 \cdot 10^{-5}$ . The validity of the overtopping formula has been verified for  $1 < G_* < 4$  and  $0.6 < R_* < 2$ , this area is indicated in Fig. 8.1.

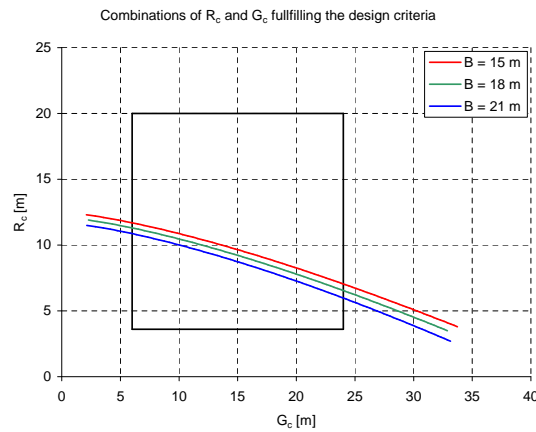


**Figure 8.1**

Figure showing combinations of  $R_c$  and  $G_c$  fulfilling the requirements of  $q < 1.7 \text{ l/s/m}$  for a 95% confidence level. The black box indicate the area in which the overtopping formula has been verified.

It can be seen from Fig. 8.2 that any combination of  $B$ ,  $R_c$  and  $G_c$  that fulfill the overtopping requirement lead to a maximum of 10% difference in total volume of the structure. In many cases there is a wish for a low crest level which can be archived without a significant increase in total volume of the structure by



## Berm Breakwater Design Example

increasing the crest width and/or berm width instead. A wide but low crest and a wide berm result probably in a more durable structure compared to a structure with a narrow and high crest.

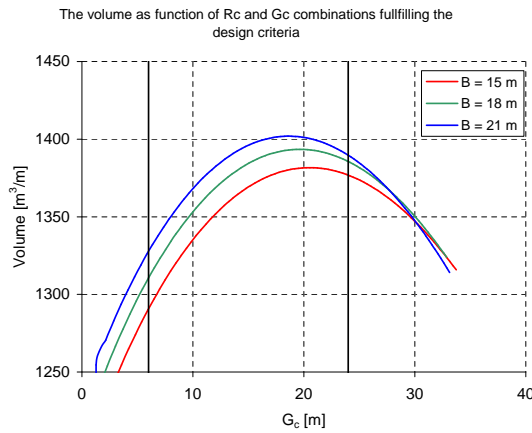


**Figure 8.2**

*Volume of breakwater as function of  $G_c$  and  $B$ , when  $R_c$  is calculated so the requirement in Eq. 8.16 is fulfilled.*

It is worth mentioning that a conventional rubble mound breakwater with a 1:3 front slope, 1:1.25 rear slope, a crest freeboard of 11 m and a crest width of 3 stone diameters has a volume of approximately  $1550 \text{ m}^3/\text{m}$ , which is actually larger than the volume needed for the berm breakwater.

On the basis of Eq. 8.14, Fig. 8.1 and 8.2 is selected  $B = 18.0 \text{ m}$ ,  $G_c = 8.0 \text{ m}$  and  $R_c = 11.0 \text{ m}$ . This result in expected overtopping discharges as given in Table 8.3. It can be seen the 50-year value for the 95% confidence level is close to the limit for causing rear side damage calculated to  $q \approx 1.7 \text{ l/s/m}$  in Eq. 8.16.

	$q_{5\%}$ [l/s/m]	$q_{50\%}$ [l/s/m]	$q_{95\%}$ [l/s/m]
1-year	0.0001	0.0004	0.002
50-year	0.12	0.42	1.5

**Table 8.3**

*Expected overtopping discharges for the 1-year and 50-year event.*

Table 8.3 shows almost no overtopping can be expected during the 1-year event. If moderate rear side damage was allowed the crest freeboard could be reduced

by 1.2 m and the volume by 8.6%. However, there is a risk of higher repair costs if the structure is designed for moderate rear slope damage.

### 8.2.3 Scour Protection

A scour protection is most probably needed at the breakwater toe, especially if the breakwater is placed on a sand bottom. Otherwise a deep scour hole can develop where a large volume of armour stones can be lost before the scour stops developing. Clearly a berm breakwater is less sensitive to toe scour than a conventional rubble mound breakwater, but if a design based on no scour protection is considered, it is important that the volume of lost armour stones is investigated. A design based on no scour protection will probably not be economical feasible.

The needed stone size, thickness and extension of the scour protection can most probably be based on design rules developed for conventional breakwaters, but taking into account the movement of the profile.

First it is checked if the method of Van der Meer, 1992 to estimate the entire reshaped profile, gives similar amount of recession as calculated using the method derived in the present thesis for the present case. Fig. 8.3 shows the profile calculated by the Van der Meer, 1992 method. The recession is 14.4 m which is in between the 50% and 95% confidence level for the present formula. Therefore it seems trustworthy to use this profile for selecting the extension of the scour protection.

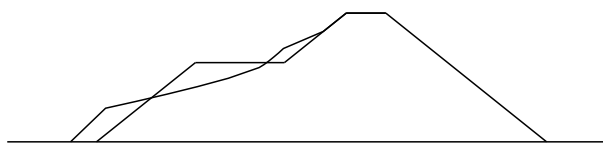


**Figure 8.3**

*Initial and calculated profile using the Van der Meer, 1992 method.*

The movement of the profile at the sea bottom calculated by Van der Meer, 1992 is 5.2 m. On this basis an extension of the scour protection of 10 m is selected, which is between 3 and 4 armour stone diameters more than the expected maximum movement (95% confidence value). The stone size needed in the toe protection could probably be calculated from the formulae developed for conventional breakwaters.

## CHAPTER 9

# Overtopping Scale Effects, Review of Existing Knowledge

Wave overtopping has traditionally been estimated from laboratory tests. The tests have for practical and economically reasons traditionally been performed in small scale, typically between 1:30 and 1:100. These tests might be subjected to model and scale effects. In this chapter a review of available information on scale effects related to wave overtopping tests is given.

In hydraulic models for the study of physical phenomae related to waves one has to use Froude scaling which assures that the ratio between inertia and gravity forces is maintained in the model. This is fundamental for a scale reproduction of waves, as the gravity and inertia forces will always be present in flows related to waves. In various models the inertia force is balanced by other forces. The ratios between the other single forces and the inertia force appear as independent dimensionless coefficients in the non-dimensional equations of motion (see e.g. Hughes, 1993).

A consequence of Froude-scaling of wave dominated hydraulic models is, as shown in Table 9.1, a disproportion of viscosity forces (Reynolds law), surface tension forces (Weber law) and elasticity forces (Cauchy law). All effects and errors resulting from incorrect reproduction of these forces are called scale effects. The consequence of Froude scaling is that viscous forces, surface tension forces and elastic forces are too large in the model, when identical fluids are used in prototype and model.

For the physical modeller scale effects can be interpreted as what decreased accuracy due to complex physical processes modeled by simplified mathematical

## 9.1 Vertical Smooth Structures

formulations is for the numerical modeller [Kamphuis, 1975]. In both cases it can be difficult to assess the size of the error. However, it is very important to be able to quantify the influence of overtopping scale effects on small scale physical model tests, as this is needed to correct existing and new small scale measurements and empirical calculation models based on small scale model results.

Parameter	Froude	Cauchy	Weber	Reynolds
Force ratio	$\frac{Inertia}{Gravity}$	$\frac{Inertia}{Elasticity}$	$\frac{Inertia}{Surface\ tension}$	$\frac{Inertia}{Viscosity}$
Equation	$\frac{u}{\sqrt{g \cdot L}} = const.$	$\frac{\rho \cdot u^2}{K} = const.$	$\frac{\rho \cdot L \cdot u^2}{\sigma} = const.$	$\frac{u \cdot L}{\nu} = const.$
Length [m]	$N_L$	$N_L$	$N_L$	$N_L$
Time [s]	$N_t = \sqrt{N_L}$	$N_t = \sqrt{\frac{N_\rho}{N_K}} \cdot N_L$	$N_t = \sqrt{\frac{N_\rho}{N_\sigma}} \cdot N_L^{1.5}$	$N_t = \frac{N_L^2}{N_\nu}$
Velocity [m/s]	$N_u = \sqrt{N_L}$	$N_u = \sqrt{\frac{N_K}{N_\rho}}$	$N_u = \sqrt{\frac{N_\sigma}{N_\rho \cdot N_L}}$	$N_u = \frac{N_\nu}{N_L}$
Acceleration [m/s <sup>2</sup> ]	$N_a = 1$	$N_a = \frac{N_K}{N_\rho \cdot N_L}$	$N_a = \frac{N_\sigma}{N_\rho \cdot N_L^2}$	$N_a = \frac{N_\nu^2}{N_L^3}$
Pressure [Pa]	$N_p = N_\rho \cdot N_L$	$N_p = N_K$	$N_p = \frac{N_\sigma}{N_L}$	$N_p = \frac{N_\rho \cdot N_\nu^2}{N_L^2}$
Force [N]	$N_F = N_\rho \cdot N_L^3$	$N_F = N_K \cdot N_L^2$	$N_F = N_\sigma \cdot N_L$	$N_F = N_\rho \cdot N_\nu^2$
Overtopping discharge [ $\frac{m^3}{s \cdot m}$ ]	$N_q = N_L^{1.5}$	$N_q = \sqrt{\frac{N_K}{N_\rho}} \cdot N_L$	$N_q = \sqrt{\frac{N_\sigma \cdot N_L}{N_\rho}}$	$N_q = N_\nu$

**Table 9.1**

*Scaling laws.  $N$  is defined as the scaling ratio of prototype and model, e.g.*

*$N_L = L_{prototype}/L_{model}$ .  $\nu$  is the viscosity of the fluid,  $\rho$  is the density of the fluid,  $K$  is the compressibility of the fluid,  $\sigma$  is the surface tension of the fluid and  $g$  is the gravitational acceleration.*

## 9.1 Vertical Smooth Structures

For vertical and nearly vertical walls, where roughness and porosity has only minor influence several investigations have shown no measurable scale effects on overtopping discharges. In the VOWS project (Violent Wave Overtopping of Waves at Seawalls) comparisons of large scale and small scale measurements for a nearly vertical (10:1) seawall were performed [Pearson et al., 2002]. The large scale overtopping tests were conducted in the CIEM flume at LIM/UPC in Barcelona. The  $H_{m0}$  wave height in these large scale tests was in the range 0.22 - 0.67 m. The small scale tests were conducted at the School of Engineering, University of Edinburgh. The  $H_{m0}$  wave height in the small scale tests were in the range 0.062 - 0.105 m. The small scale model tests were not an exactly reproduction of the large scale, as some differences in foreshore and wave conditions exists. However, it seems reasonable to assume no significant scale effects, as both large and small scale tests are in good agreement with the prediction formula by Besley, 1999. The results of the VOWS project are supported by the

findings within the CLASH project, as no overtopping scale effects were identified by comparing prototype and small scale test results for the Sampire Hoe seawall [De Rouck, 2005]. Shiraishi et al., 1968 performed also prototype overtopping measurements on a vertical wall. These results agreed roughly with the small scale laboratory results.

## 9.2 Rubble Mound Structures

For rubble mound structures, roughness and porous flow plays an important role. Therefore, scale effects are more likely to be present for this type of structure compared to the smooth impermeable vertical wall.

There have been some previous investigations in overtopping scale effects for rubble mound structures. Both theoretical and experimental investigations have shown that there probably is a scale effect on overtopping of rubble mound structures, leading to more overtopping in large scale than in small scale model tests (unsafe results obtained in the model). This scale effect seems especially pronounced for flatter slopes. However, from the previous investigations it has been impossible to distinguish between differences due to model/wind and scale effects.

Armour stability model tests are in principle subjected to the same viscous, surface tension and elastic scale effects as run-up and overtopping. Investigations has shown that there exists a critical value of the Reynolds number, and above this critical value armour stability scale effects are small. A safe value for the critical Reynolds number seems to be  $3 \cdot 10^4$  for armour stability. Lower Reynolds numbers will lead to too much damage (conservative results are obtained in the model).  $Re_D > 3 \cdot 10^4$  is fulfilled in most small scale model tests for determining armour stability and overtopping. For run-up and overtopping much less knowledge exists on the critical Reynolds number. However the critical Reynolds number could be much higher than observed for stability due to the very thin upper part of the run-up wedge. This is further discussed in the following sections.

The flow domain related to the action of incoming waves on a sloping porous structure changes in space and time. During the run-up phase the flow domain can be separated in a jet like surface flow domain and a porous flow domain [Burcharth, 2004]. Froude-scaling, which imply linear scaling of material diameters has different influence on scale effects in the two domains. Besides viscosity also surface tension and wind cause scale effects in Froude scale models.

### 9.3 Viscosity Scale Effects

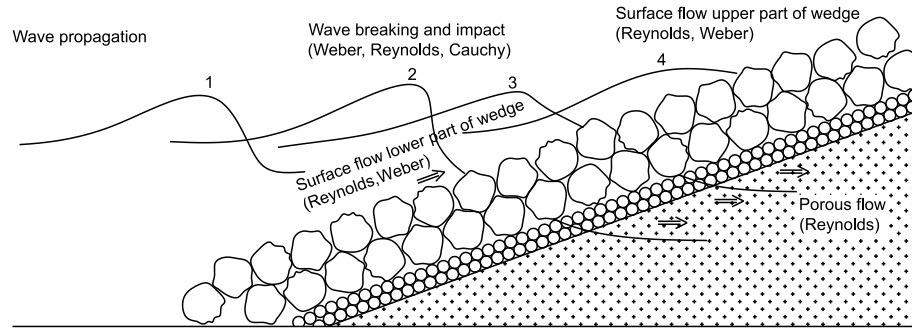


Figure 9.1

Sketch of flow domains and additional scaling laws that have to be fulfilled in a Froude model to avoid wave/structure scale effects.

### 9.3 Viscosity Scale Effects

In this section viscosity scale effects related to overtopping tests are discussed. Viscosity scale effects are due to not fulfilling the Reynolds scaling criteria.

#### 9.3.1 Wave Celerity

Biesel, 1949 calculated the influence of viscosity on the wave celerity. Schüttrumpf, 2002 arrived at a critical Reynolds number  $Re_{crit} = \frac{c \cdot h}{\nu} = 10^4$  by assuming shallow water conditions. This is fulfilled if the water depth is larger than 2-3 cm. Therefore, this scale effect is not important for small scale overtopping tests.

#### 9.3.2 Porous Flow Scale Effect

Porous flow scale effects arise from not having identical flow fields in the prototype and model core. The main problem is that the hydraulic gradient in the core is varying in time and space, which makes it impossible to perform a complete correction for porous flow scale effects. Stationary porous flows can be characterized by three different types of regimes with transition zones in between [Burcharth and Andersen, 1995].

Creeping / Darcy flow regime ( $Re < 1$ )

In this regime the flow is dominated by viscous forces and the well know Darcy expression can be applied, which is a linear relationship between hydraulic gradient ( $I$ ) and flow velocity ( $u$ ).

$$I = A'' \cdot u \quad (9.1)$$

At  $Re = \frac{u \cdot D}{\nu} \approx 1$  boundary layers start to develop at the grains.

Forchheimer flow regime ( $10 < Re < 150$ )

In this flow regime the boundary layers are more pronounced and an "inertial core" appears. The development of these core flows outside the boundary layers is the reason for non-linear relationship between flow velocity and hydraulic gradient given by the Forchheimer expression:

$$I = A \cdot u + B \cdot u^2 \quad (9.2)$$

The application of Eq. 9.2 is complicated by  $A$  and  $B$  dependency on the Reynolds number. Further,  $A$  and  $B$  are not dimensionless and are dependent on porosity, grain shape and grading. Burcharth and Andersen, 1995 rewrote the equation in the following dimensionless correct form:

$$I = \alpha \cdot \left( \frac{1-n}{n} \right) \cdot \frac{\nu}{g \cdot D^2} \cdot \frac{u}{n} + \beta \cdot \frac{1-n}{n} \cdot \frac{1}{g \cdot D} \cdot \left( \frac{u}{n} \right)^2 \quad (9.3)$$

where  $\alpha$  and  $\beta$  are coefficients that depends on the Reynolds number, grain shape and grading, which can be estimated from Burcharth and Andersen, 1995. In the upper end of the Forchheimer equation the  $\beta$  coefficient further depends on the surface roughness of the grains. As grain diameter ( $D$ ) is in case of irregular grains used the sieve diameter ( $D_{50}$ ) or the equivalent sphere diameter ( $D_{s,50}$ ).  $u$  is the discharge velocity and  $u/n$  is the pore velocity.

Fully turbulent (rough turbulent) flow regime ( $Re > 300$ )

It is not entirely correct to use both a linear and a quadratic term for fully turbulent flow as the quadratic term is dominating. However, this is the conventional approach:

$$I = A' \cdot u + B' \cdot u^2 \quad (9.4)$$

A different approach was given by Burcharth and Christensen, 1991 who proposed the following equation without the linear term which is insignificant:

$$I = I_c + b \cdot (u - u_c)^2 \quad (9.5)$$

Where  $I_c, u_c$  is the transition point from the Forchheimer regime to the fully turbulent regime and  $b$  is a coefficient.

In non-stationary flows an inertia term should be added to the equations 9.1 - 9.5. In the porous flow case it is not possible to merge the local and convective acceleration terms into one term. However, the local accelerations are usually dominating over the convective accelerations and thus the inertia term is often taken as  $c \cdot \frac{\partial u}{\partial t}$ , where  $c$  then is calibrated to match this equation. However, Burcharth and Andersen, 1995 showed that this term can be neglected for porous flows in breakwater cores.

The prototype porous flow will in conventional structures be rough turbulent in the filter layers and in most of the core. This is not the case in small scale models, which can be characterized by significant wave heights in the range  $H_s = 0.05 - 0.30$  m, filter grain diameters in the range  $0.01 - 0.03$  m and core material diameters of  $0.001 - 0.005$  m, if scaled linearly. The flow in the model core and filter layers will not be rough turbulent except for the largest models for which only limited parts of the filters and the core can have this type of flow, only for a fraction of the wave period. The consequence of this is that kinematic similarity between flow in prototype and model cannot exist, as the flow resistance will be relatively too large and velocities too small in the model. This effects the surface flow as less water penetrates into the porous structure leaving a larger proportion of the incoming water to remain on the surface. The consequence is less energy transmitted through the structure, relatively more energy reflected from the structure, more damage to armour, higher run-up heights and velocities and more overtopping water. A complete correction for this scale effect is not possible as the Reynolds number varies in time and space. However, a practical engineering compensation for this blocking effect can be dealt with by enlarging



the grain sizes, for example as proposed by Burcharth et al., 1999. This method involves determination of a characteristic time and space averaged flow velocity characterizing the interior velocity field, calculated from the Forchheimer equation (Eq. 9.3).

If in the prototype the core is completely saturated during wave action then it is expected that the model core grain size has less influence on overtopping as long as the model core is also saturated. Moreover, for flatter slopes with relatively thick armour and filter layers there will only be a small influence of core permeability on the overtopping discharge.

The influence of core material is further dealt with in section 10.5.2 - 10.5.5.

### **9.3.3 Run-Up Flow**

The character of the run-up surface flow changes considerably in space and time during the run-up phase. Where and when the thickness of the run-up wedge is several times the roughness of the armour units, the flow has sectionwise similarities with the bottom part of flow in a wide rectangular conduct. But when and where the wedge thickness is less than the roughness, as is the case in the upper part of the run-up wedge, the flow has similarities to flow around obstacles [Burcharth, 2004].

In order to avoid viscous scale effects in the run-up flow in Froude models it is a necessity that the type of flow is similar to that in prototype. In the prototype the run-up flow will be rough turbulent, but in the model that is not necessarily the case, especially for small overtopping rates where the run-up velocity and layer thickness is smaller, it is possible that the turbulent boundary does not exist in the upper part of the run-up wedge. This leads to increased flow resistance on the slope and increased energy loss, cf. Fig. 9.2.

For the surface flow in the lower part of the run-up wedge, Burcharth, 2004 showed that, it seems reasonable to assume that the flow is rough turbulent both in prototype and in the small scale model. This was based on two calculations assuming the flow in the lower part of the run-up wedge to be a steady flow and an oscillatory flow respectively. The flow is neither a steady flow nor an oscillatory flow, but as they both point to the same conclusion it seems trustworthy.

The flow resistance in the region of small water depth is dominated by the drag force exerted upon the armour units (inertia forces are of minor importance). In prototype the Reynolds number, even in the very upper part of the run-up wedge, will be larger than  $Re = 5 \cdot 10^5$ . In a Froude model the Reynolds number scale with the length scale in a power of 1.5 (assuming  $N_\nu = 1$ ), leading to a

### 9.3 Viscosity Scale Effects

Reynolds number in the very upper run-up wedge in a 1:50 model is larger than  $Re = 1.4 \cdot 10^4$ . This reduction in Reynolds numbers has a significant influence on the drag coefficient ( $C_D$ ). Although not the same flow, it is useful to consider the drag coefficients for flow past single cylinders or arrays of cylinders.

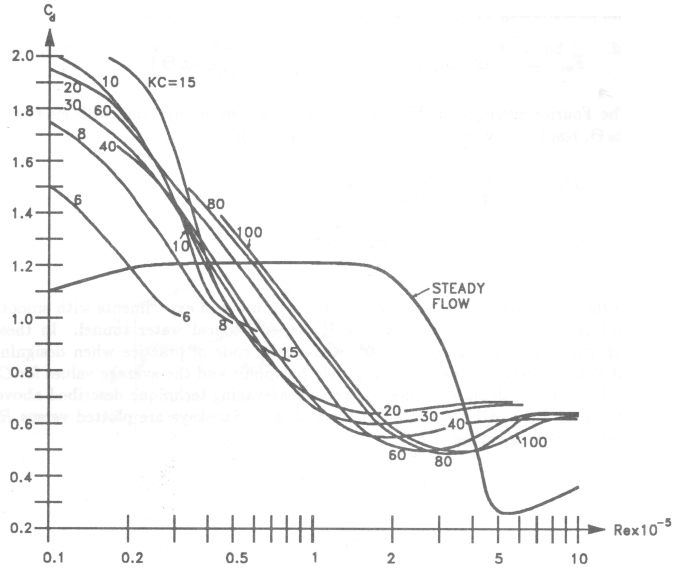


**Figure 9.2**

Variation of drag coefficient  $C_D$  with Reynolds number for a smooth cylinder and different values of the Keulegan-Carpenter number ( $KC = \frac{u_{max} \cdot T}{D}$ ) [Sarpkaya and Isaacson, 1981].

For circular or rounded cross sections the variation of  $C_D$  with  $Re$  is large, typically a 50% to 100% increase in  $C_D$  when  $Re$  is reduced from  $5 \cdot 10^5$  to  $1 \cdot 10^4$ . For flat sided objects with sharp corners the increase in  $C_D$  is less, but still significant. For objects of small length to width ratio there is a general reduction in the drag coefficients compared to those for cylinders (infinite length to width ratio). Although this reduction factor is smaller for supercritical flow ( $Re \geq 10^6$ ) than for sub critical flow ( $Re \leq 10^5$ ) there is still a difference in  $C_D$  for the flow in prototypes and small scale models [Burcharth, 2004]. The effect of this is smaller run-up heights and less overtopping in small scale Froude models than in prototypes. Due to decreasing layer thickness and run-up velocities for decreasing overtopping discharges, this scale effect is expected to be much more significant for small overtopping rates than for the larger ones.

## 9.4 Surface Tension Scale Effects

Based on the extended dispersion equation, that includes the surface tension, Le Mehauté, 1976 and others have found that the influence of surface tension on non-breaking wave propagation is insignificant when the water depth is greater than 2 cm and the wave period is greater than 0.35 s. Lower values lead to dampening of the waves.

In breaking and close to breaking waves the surface tension plays a role causing surface tension scale effects. This is partly due to the decreased curvature radius in the crest and partly due to air entrainment. Entrained air escapes from the water either as rising bubbles or by dissolving into the water. The different sizes of the bubbles influence their rise velocity, their capillary excess pressure and dissolution rate. A result of this surface tension scale effect is that the entrained air bubbles are relatively larger in the model, as the bubble sizes are mainly determined by the surface tension, but also partly because of the saline water in prototype compared to the fresh water in the model. Slauenwhite and Johnson, 1996 found that there is 4-5 times more bubbles in sea water compared to fresh water for similar generation conditions, and thereby bubbles also were generally smaller in sea water. Fresh water bubbles have a greater tendency to coalesce and escape, as the smaller bubbles rise and escape more slowly than the larger bubbles. The result of this is that the air content will be relatively smaller in the model. Bullock et al., 2001 found from small scale tests that in his tests air content in sea water could be up to 3.9%, while with fresh water it was one order of magnitude lower. In field breaking waves Bullock et al., 2001 found up to 8.4% air content and concluded also that the amount of foam generated in the field is higher than in the model, even if sea water is used in the model tests. This indicate clearly a surface tension scale effect.

Le Mehauté, 1976 argued that even though the fine details of the breaking wave process are different in small scale and prototype, the process of energy dissipation during wave breaking will be similar. The momentum equations express the total rate of energy dissipation as a balance of the external forces irrespective of the internal dissipation mechanisms. This means that even if the proportions of energy dissipated by various mechanisms are different in the model compared to the prototype, the total energy budget remains in similitude by virtue of the momentum theorem.

Stive, 1985 verified Le Méhautés statement by performing small and large scale tests with regular and irregular breaking waves. He found no significant differences in wave heights, wave set-up and vertical profiles of maximum seaward, shoreward and time-mean horizontal velocities between large and small scale

tests. The tests were performed with wave heights in the range 0.1 m to 1.5 m.

Miller, 1972 did model investigations with both fresh water and with additives added. The additives reduce the surface tension, and he showed that this reduction in the surface tension increased the possible wave height before breaking and hence shifted the breaker point landward. When fresh water is used in the model the surface tension is not scaled correctly and according to the findings of Miller, 1972 too much wave breaking on the foreshore will take place in a small scale model. Thus the experiments of Stive, 1985 and Miller, 1972 point in different directions.

Wave breaking on a rubble slope and the front wedge flow past the armour units cause air to be enclosed in the flowing water. Due to the above mentioned surface tension effect relatively more air will be enclosed in prototype flow than in the model flow. The total effect of this is that due to differences in relative air contents, the average mass density of the uprushing water is smaller in prototype than in the model - disregarding the difference in mass density of salt and fresh water [Burcharth, 2004].

Assuming the impulse of the water approaching the slopes to be correctly scaled in the Froude model the effect of the differences in air entrainment would be higher run-up and thus larger overtopping in the prototype than in a small scale model - provided that the air entrainment process in the model does not involve relatively larger energy dissipation (which seems unlikely) [Burcharth, 2004].

A reduction in average mass density of say 5% will cause an approximately 5% higher run-up. Although the overtopping water contains more air in the case of prototype structures the volume of solid water will be larger due to the non-linearity between the theoretical run-up level and overtopping volume.

The influence of surface tension on run-up heights and velocities on a smooth slope was investigated by Schüttrumpf, 2002. He found that an increase in surface tension will increase the run-up height and velocity on a smooth surface. The influence is negligible if  $We = \frac{uL}{\sigma_0} > 10$ , where  $u$  is the run-up velocity,  $L$  is the layer thickness and  $\sigma_0$  is the surface tension which for fresh water equals 0.073 N/m at 20°C.

## 9.5 Wind Scale and Model Effects

During design conditions the wind is typically strong and in many cases also onshore. Therefore, wind may have a significant influence on the overtopping discharge, especially for low overtopping rates (wind carried spray). Resio, 1987

give two effects that cause increased overtopping due to wind (1 and 2). Ward, 1994 mention a third action that may increase overtopping due to wind.

1. Increased wave run-up and overtopping due to wind energy input during the run-up flow. This effect is most pronounced for flat slopes.
2. Advection by wind of water spray and splashing resulting from wave impact on coastal structures. This effect is most pronounced for steep slopes.
3. Onshore wind generated onshore surface currents may increase initial run-up speed.

No information is available on how to scale the drag dominated wind velocity field in a Froude model, which makes it impossible to reproduce prototype wind field in the model correctly. Further, the generated spray and drop sizes is not correctly reproduced in a Froude model and the effect of wind carried spray is very difficult to assess from small scale model tests. In addition to this only few laboratories have the possibility to add wind in the model. As a result of all these limitations most model tests are performed with no wind.

As the wind also generates water level set-up it is important to compensate for this when comparing wind and no wind model tests.

Ward et al., 1996 performed model tests in a wave flume with regular waves ( $H = 2-10$  cm in model scale and without wind) and different wind conditions. Smooth and rough slopes in the range 1:1.5 to 1:5 were tested. The wind adds energy to the waves so with wind we get  $H_s = 2 - 20$  cm at the toe. The measured waves which are both mechanically and wind generated were reproduced mechanically with no wind. The waves were measured at the toe and separated in incident and reflected waves by the method of Goda and Suzuki, 1976. The wind generated set-up was measured and taken into account in the data analysis. The analysis of the run-up measurements showed that a wind speed of 6.5 m/s in model scale has no influence on run-up heights, while 12 and 16 m/s in the model led to significant higher run-up levels. For the rough slopes the increase in run-up due to wind is largest for the steep 1:1.5 slope. Overtopping discharges were compared for the conditions that resulted in overtopping. The conclusions drawn from the run-up measurements also apply to the overtopping measurements.

Model tests with wind in the wave-wind facility at Universidad Politécnic de Valencia (UPV) has shown that in a small scale model (1:30) wind velocities of 5-7 m/s may easily have an influence of more than a factor of 10 on the overtopping discharge, cf. Fig. 9.4. However, it is not known what wind speed this corresponds to in prototype.

The main problem with the small scale model tests with wind is the unknown scaling procedure of the wind field. From prototype measurements at Ostia with very similar hydraulic conditions but different wind speeds it was found that a wind speed of around 9-11 m/s compared to a wind speed of 4-6 m/s increase the overtopping discharge by a factor 5 for rather low overtopping discharges in the range  $0.006 \text{ l/s/m} < q < 0.07 \text{ l/s/m}$ .

## 9.6 Numerical Computations

A subtask of the CLASH project was to use numerical models to simulate wave overtopping in order to solve the problem of suspected scale effects. Two numerical models were developed in the CLASH project, the MMU Amazon code and the UGhent VOF code. Both models are two-dimensional and have free surface capturing, porous flow calculations and surface friction calculations. Both models use idealised incompressible fresh water, rather than aerated, compressible, salt water. Because both models are very computational heavy to run, each computation consists only of some few regular waves.

The UGhent VOF code has been used to simulate the Ostia breakwater in scale 1:20, 1:10 and 1:1 keeping gravity and viscosity constant. The Ostia breakwater is a rubble mound breakwater with a front slope of approximately 1:4. The numerical results show up to a factor of 2 in difference in overtopping discharges between the three scales, with the smallest overtopping discharge in prototype scale, which is a scale effect in the opposite direction of what many other studies has suggested. However, a factor of two in difference on overtopping discharge is very little, which means the calculations indicate no significant scale effects. In the simulations the core was completely saturated, so porous flow scale effects is expected to be small.

The MMU Amazon code has been used to model overtopping of a structure in four different scales, keeping gravity and viscosity constant. The structure is a vertical wall with a porous rubble mound with a slope of 1:3 in front of the wall. The results of these computations showed that for hydraulic independence of the scale, the Reynolds number should be above  $10^5$ . However, smaller Reynolds numbers result only in slightly different overtopping velocities and volumes.

## 9.7 Prototype Measurements

Very little literature has been published on prototype overtopping measurements, which is probably due to the high costs involved. The following prototype in-

vestigations on run-up and overtopping scale effects for rubble mound structures are available:

- Sakakiyama et al., 1997: Fukui seawall covered with tetrapods.
- De Rouck et al., 2001: Run-up measurements at the Zeebrugge breakwater performed during the OPTICREST project.
- De Rouck, 2005: Overtopping measurements at Ostia and Zeebrugge breakwaters performed during the CLASH project.

### 9.7.1 Fukui Seawall

Sakakiyama and Kajima, 1998 compared model tests and prototype measurements obtained for the Fukui seawall, which is a caisson covered with tetrapod armour units. The prototype results show very different results compared to results from 2D model tests performed in scale 1:11.3 and 1:50. Sakakiyama and Kajima, 1998 concluded that the differences were due to 3D effects in prototype, wind effects and other uncertainties in prototype. Even for very large overtopping discharges the prototype results show a very different trend than the model results, which makes it reasonable to assume that the differences is due to large model effects.

### 9.7.2 Zeebrugge Breakwater

The Zeebrugge breakwater is a rubble mound structure armoured with grooved cubes and front slope of approximately 1:1.4.

Within OPTICREST comparisons of prototype and small scale wave run-up results for the Zeebrugge breakwater were performed. The small scale tests were performed in three different laboratories: Aalborg University (AAU), Flemish Community Flanders Hydraulics (FH) and Universidad Politécnica de Valencia (UPV). The analysis resulted in different run-up values for the three laboratories and the prototype investigation, cf. Fig. 9.3. Results showed that average values of  $R_{u2\%}/H_{m0}$  varied in between 1.46 (FH) to 1.79 (UPV) together with a large scatter of the data points around the mean values. Furthermore, the spectral width parameter  $\epsilon_4$  and the wave height  $H_{m0}$  were observed to be different in the tests thus resulting in different wave run-up heights. These differences can be due to differences between the spectra in the model and the field. However, with this in mind still there is a tendency that prototype measurements are in average at least 10% larger than the model results.

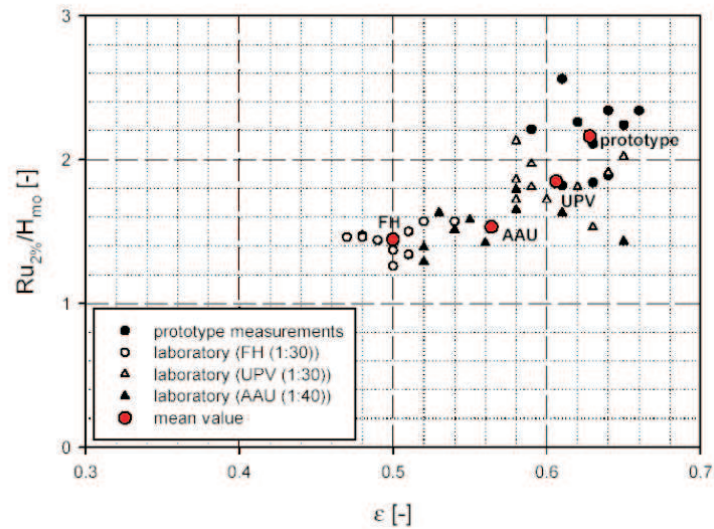


**Figure 9.3**

*Run-up measurements obtained within the OPTICREST project plotted against the spectral width parameter  $\epsilon_4$  [De Rouck et al., 2000].*

Fig. 9.4 shows the overtopping results obtained within the CLASH project. The prototype measurements were reproduced in two laboratories, Leichtweiss-Institute for Hydraulics (LWI) and Universidad Politécnic de Valencia (UPV). In these tests the measured prototype spectra were reproduced as accurately as possible, but not matching the complex spectrum (time series). At UPV only three of the prototype storms with most overtopping were reproduced. Two of these three resulted in no overtopping in the model. LWI reproduced all of the prototype storms and the model results are very similar to prototype measurements, cf. Fig. 9.4.

For very small overtopping discharges ( $q^* < 10^{-5} - 10^{-6}$ ) the CLASH NN model generally overpredicts the overtopping discharge. It should further be noticed that for the Zeebrugge breakwater the armour crest is higher than the wall of the superstructure ( $A_c > R_c$ ), and in these cases the CLASH NN-model is inaccurate due to a very limited number of data used for the development of the model in this area. It seems that for the Zeebrugge overtopping data there is only little differences between LWI model and prototype results. However, UPC model results are clearly lower than prototype and LWI results. Adding wind of 5 - 7 m/s in the UPC model resulted in significant more overtopping, cf. Fig. 9.4.



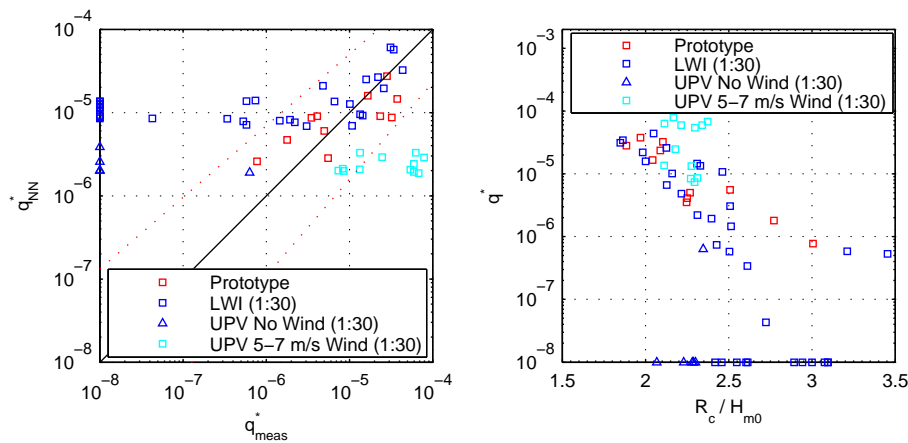


**Figure 9.4**

Overtopping measurements obtained at Zeebrugge within the CLASH project plotted against the CLASH NN-model and the Van der Meer and Janssen, 1994 plot for non-breaking waves. No overtopping measured is plotted at  $q^* = 10^{-8}$

### 9.7.3 Ostia Breakwater

The Ostia breakwater is a rock armoured rubble mound structure with a front slope around 1:4.

Within the CLASH project 8 prototype storms have been measured. These have been reproduced in 2D at Ghent University and in 3D at Flanders Hydraulics. All 2D prototype reproductions resulted in no overtopping, which was explained by a significant 3D effect, which was also observed from the prototype video recordings. Some overtopping was observed in the 3D tests, but clearly much lower than prototype results, cf. Fig. 9.5. This can be due to scale effects or large model effects, which is further discussed in section 9.7.4. The results show in average a 15% lower roughness coefficient ( $\gamma_f$ ) in the model compared to the prototype results, which has a large impact on the overtopping discharge.

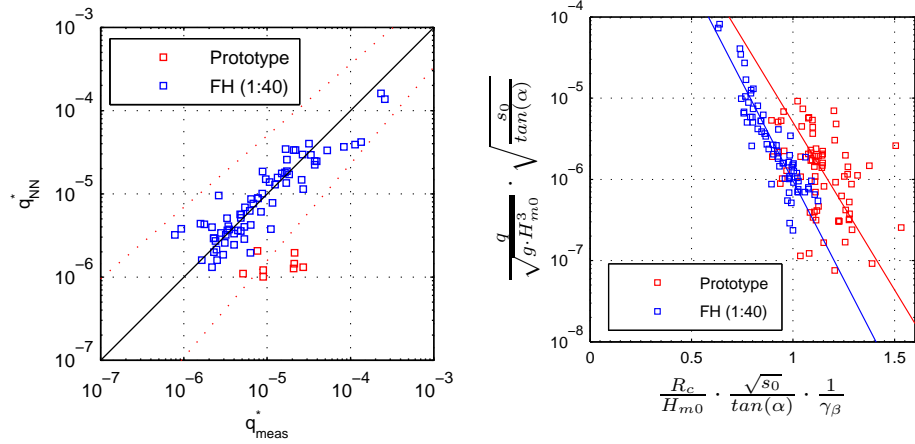


**Figure 9.5**  
*Overtopping measurements obtained at Ostia within the CLASH project plotted against the CLASH NN-model and the Van der Meer and Janssen, 1994 plot for breaking waves using  $T_{-1,0}$  for the calculation of the wave steepness.*

### 9.7.4 Scale/Model Effects

One may think that prototype studies provide the best data on scale effects, but they are usually expensive and too many of the nature's variables are present, which make data interpretation difficult. During the OPTICREST and CLASH project several possible model effects were identified, the most important ones seem to be:

- Making accurate measurements at a prototype site is very difficult and for practical reasons the model instrumentation always differs from the prototype. Especially measuring the wave conditions with good accuracy is extremely difficult. 10% uncertainty on the wave height may have a huge impact on the overtopping discharge and hence the conclusion on overtopping scale effects. Moreover, it is impossible to separate the measured waves in incident and reflected waves. In many cases the total wave height measured offshore is used both for the prototype and model results instead. However, this makes it impossible to distinguish between overtopping scale effects, wave propagation and breaking scale effect, wave structure interaction scale effects, bed changes in prototype under storm conditions. Especially for Ostia where the breakwater is located in very shallow water and wave breaking continuously occurs on the foreshore, model effects related to

bed changes and wave breaking could be very important.

- The absence of wind in the model tests and strong wind in the prototype may also be a very important effect, especially for low overtopping rates (wind carried spray). The wind might also have an influence on the wave propagation from deeper water to the toe of the structure, which is important as waves often are measured offshore in prototype.

Due to the above mentioned possible model effects, it was impossible to distinguish between differences due to model and scale effects. Nevertheless, based on the data from Zeebrugge and Ostia the following conservative multiplication factors were suggested in the CLASH project for a rough structure ( $\gamma_f \leq 0.7$ ):

No wind conditions:

$$q_{prototype} = q_{SS} \cdot f_{scale}$$

$$f_{scale} = \begin{cases} 16.0 & \text{for } q_{SS} < 0.01 \text{ l/sm} \\ 1.0 + 15 \cdot \left( \frac{-\log(q_{SS}) - 2}{3} \right)^3 & \text{for } 0.01 \text{ l/sm} \leq q_{SS} < 10 \text{ l/sm} \\ 1.0 & \text{for } q_{SS} \geq 10 \text{ l/sm} \end{cases} \quad (9.6)$$

Onshore wind conditions:

$$q_{prototype} = q_{SS} \cdot f_{scale \& wind}$$

$$f_{scale \& wind} = \begin{cases} 24.0 & \text{for } q_{SS} < 0.01 \text{ l/sm} \\ 1.0 + 23 \cdot \left( \frac{-\log(q_{SS}) - 2}{3} \right)^3 & \text{for } 0.01 \text{ l/sm} \leq q_{SS} < 10 \text{ l/sm} \\ 1.0 & \text{for } q_{SS} \geq 10 \text{ l/sm} \end{cases} \quad (9.7)$$

where  $q_{SS}$  is based on small scale tests but scaled to prototype. After the CLASH project the scaling factors were revised by reanalyzing the data, which resulted in using Eq. 9.6 and 9.7 for flat slopes around 1:4 and using Eq. 9.8 and 9.9 for steep slopes around 1:1.4 [De Rouck et al., 2005].

$$f_{scale} = \begin{cases} 6.0 & \text{for } q_{SS} < 0.1 \text{ l/sm} \\ 1.0 + 5 \cdot \left( \frac{-\log(q_{SS}) - 2}{2} \right)^3 & \text{for } 0.1 \text{ l/sm} \leq q_{SS} < 10 \text{ l/sm} \\ 1.0 & \text{for } q_{SS} \geq 10 \text{ l/sm} \end{cases} \quad (9.8)$$

$$f_{scale \& wind} = \begin{cases} 8.0 & \text{for } q_{SS} < 0.1 \text{ l/sm} \\ 1.0 + 7 \cdot \left( \frac{-\log(q_{SS}) - 2}{2} \right)^3 & \text{for } 0.1 \text{ l/sm} \leq q_{SS} < 10 \text{ l/sm} \\ 1.0 & \text{for } q_{SS} \geq 10 \text{ l/sm} \end{cases} \quad (9.9)$$

## 9.8 Large Scale Measurements

In contrast to prototype studies, the large scale wave facilities allow for control of input conditions, and allow more systematic studies to be performed. Further the differences between small scale and large scale due to model effects can be kept at a minimum.

Comparison of small and large scale run-up measurements on an impermeable rough slope was presented by Van der Meer, 2004. Different slope angles were used in small and large scale, as a 1:4 slope was used in large scale and 1:3 in small scale. The large scale tests performed in the Deltaflume gave approximately 25% higher run-up levels than those in small scale. Eventhough the roughness facor is slope dependent it seems unlikely that the difference in slope angle alone could lead to that different run-up levels. Therefore, these results indicate a scale effect on run-up of rough structures.

For rubble mound structures the previous investigations on overtopping scale effects is due to:

- Overtopping measurements on armour covered seawalls in the CRIEPI flume [Kajima and Sakakiyama, 1994 and Sakakiyama and Kajima, 1998].
- Overtopping and run-up measurements on a rock armoured rubble mound breakwater in GWK [Van de Walle, 2003 & Helgason, 2006].
- Overtopping measurements on an accropode armoured rubble mound breakwater [Archetti et al., 1995].

### 9.8.1 Armour Covered Seawalls

Kajima and Sakakiyama, 1994 and Sakakiyama and Kajima, 1998 performed large and small scale overtopping tests with seawalls covered with armour units. Both studies shows larger overtopping discharges in large scale. In average the overtopping discharge is around 3 times larger in large scale, but up to a factor of 10 in some cases.

### 9.8.2 Rock Armoured Rubble Mound Breakwater

Large scale tests with a rubble mound breakwater were performed in GWK, Hannover by Van de Walle, 2003 and Helgason, 2006 and repeated in small scale. The main focus in the tests was on front slope stability, but also run-up heights and overtopping discharges were measured. Preliminary analyses have shown no or only small overtopping scale effects [Helgason and Burcharth, 2006].

### 9.8.3 Accropode Armoured Rubble Mound Breakwater

Archetti et al., 1995 performed large scale overtopping tests with an accropode armoured rubble mound breakwater with a 1:2 front slope. The tests were performed in GWK, Hannover. The focus was on regular waves, but some short tests (164 peak periods) with irregular waves were performed as well. The significant wave height were in the range 0.90 - 1.30 m. Any comparison to small scale tests was not performed.

## 9.9 Summary on Existing Knowledge on Overtopping Scale Effects

Several previous studies have shown no significant overtopping scale effects for vertical or nearly vertical smooth impermeable structures. For rough permeable structures there are some indications of overtopping scale effects, which will be summarized in the following.

### 9.9.1 Theoretical Considerations

1. Porous flow: The porous flow field in the core will be different in the model compared to prototype. If the size of the core material is scaled according to Froude the flow resistance in the model core will be too large and hence overtopping discharge too large.
2. Run-up flow: The lower part of the run-up flow seems not to be subjected to viscous scale effects. However, the upper part of the run-up flow where the layer thickness is small compared to the roughness, significant viscosity scale effects may exist. The different Reynolds numbers in large and small scale, may have a large influence on the drag coefficient and hence the flow resistance. The resistance in the model will be too large and result in too little overtopping.

## 9.9 Summary on Existing Knowledge on Overtopping Scale Effects

---

3. Surface tension: In a Froude model the surface tension will be too high, which will effect the air content in the fluid during breaking and during the run-up flow. In the model the air bubbles will be too big and escape more easily. The influence of this may be too little overtopping in the model.

The effect of item 1 could maybe be balanced by the effect of item 2 and 3. When compensating item 1 by enlarging the grain size in the core as proposed by Burcharth et al., 1999 and others, the items 2 and 3 will lead to too little overtopping in the model. However, it is not known how big an influence these scale effects have on the overtopping discharge, but it is expected that the effect is much more pronounced for small overtopping discharges than for larger ones.

### 9.9.2 Prototype Measurements

Prototype measurements have been performed at Ostia and Zeebrugge breakwaters. The comparison of prototype and small scale model data for the Zeebrugge case has shown only small scale effects. In contrast to this the data from Ostia show much more overtopping in prototype compared to the model (larger than a factor 10). The Ostia breakwater is very different from the Zeebrugge breakwater, as it has a much flatter front slope and is located in very shallow water. However, also much larger model effects are possible in the Ostia case.

### 9.9.3 Large Scale Measurements

Only few large scale overtopping measurements have been performed so far for rubble mound structures and these studies points in different directions regarding scale effects. For most of the large scale tests performed there is still missing a comparison to identical small scale model tests with model effects kept at a minimum.

### 9.9.4 Numerical Computations

The two numerical models developed within the CLASH project both show no significant scale effects on overtopping discharges for regular waves on a rough structure. Numerical models are still too computationally heavy to simulate more than a few wave periods, but maybe in the future this will be an alternative to physical models.

### **9.9.5 Wind**

The influence of the wind is difficult to quantify as it has to be studied in prototype. Wind speeds of 5-7 m/s in a small scale model gave more than 10 times the overtopping compared to no wind. However, it is not known what wind speed this corresponds to in prototype scale. Prototype measurements at Ostia showed that an increase in wind speed from 5 m/s to 10 m/s, increased the overtopping discharge by a factor five for low overtopping discharges ( $q \approx 0.01 \text{ l/ms}$ ).





## CHAPTER 10

# Overtopping Scale Effects, New Large Scale Tests

As shown in the previous chapter there are both theoretical and experimental indications of overtopping scale effects for rubble mound structures, but other investigations show no significant overtopping scale effects. Only few experimental results are available and there are many possible model effects. This has made it important to be able to distinguish between model/wind effects and scale effects. The best way to draw clear conclusions on overtopping scale effects without wind effects is probably to perform a systematic comparison of large and small scale model tests with as identical set-ups as possible. This is because incident waves can much better be determined in the laboratory compared to conditions in the field. On this background a comparative study of overtopping measurements was planned, with small scale tests at Aalborg University and large scale tests at Universitat Politècnica de Catalunya in Barcelona. The large scale tests were performed in the CIEM flume, where the maximum wave height is 1.6 m. To ensure as identical set-ups as possible the author was involved in the model building, calibration and testing in both small scale and large scale. These tests do not include wind, which has to be studied in prototype.

The comparison of large and small scale test results will lead to conclusions on overtopping scale effects. It is preferable that in the future more comparisons of small and large scale tests are performed, to verify the results obtained in the present tests. This is because for some unknown reasons there could be large differences on overtopping measured in different laboratories. These tests could advantageously be performed with the same cross-sections as used in the present tests, so the present results could be used as a reference.

## 10.1 Test Set-Up & Data Analysis

Average overtopping discharges, single wave overtopping volumes and spatial distribution of overtopping was measured. Run-up, forces from overtopping on an obstacle and wave set-up are all overtopping related quantities that were measured as well. This was done by using the layout shown in Fig. 10.1.

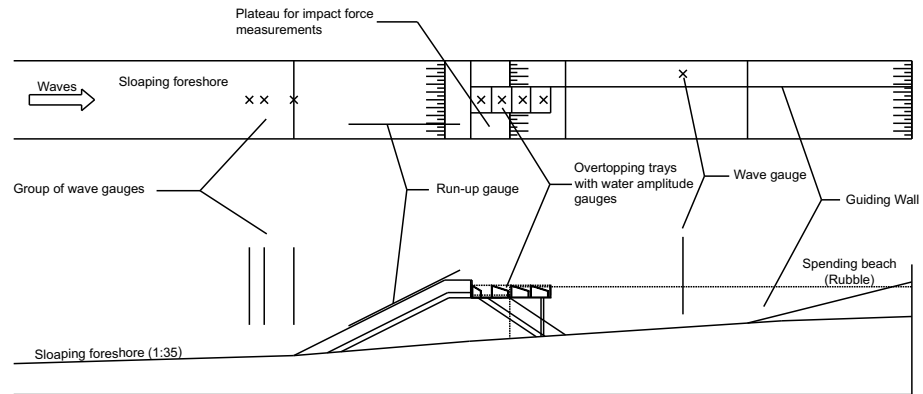


**Figure 10.1**  
*Layout in wave flume (top and side view).*

The size of the small scale model at Aalborg University corresponded to armour layer Reynolds numbers ( $Re_D$ ) just above  $3 \cdot 10^4$ . This was chosen as small scale model tests commonly are performed in this area of Reynolds numbers to avoid viscous scale effects on armour stability. The small scale tests are considered to correspond to scale 1:40 of prototype conditions. The size of the large scale model was as large as practical and economical possible, and corresponds to scale 1:7 of prototype. Hence, the large scale tests were performed in approximately 5.7 times larger scale than the small scale tests.

All data analysis has been performed with the WaveLab2 software package from Aalborg University [Aalborg University, 2005b]. In the small scale tests the WaveLab2 software package was further used for data acquisition with control of the pumps in the overtopping tanks in real time. In this way the state (on/off) of the individual pumps was stored in the data file. To give good time-resolution on the impact forces the sample frequency was 42 Hz in the large scale tests. The sample frequency in the small scale tests was 100 Hz, which means it was scaled according to Froude similarity law.

### 10.1.1 Bottom Configuration

A fixed concrete bottom was used both in the large and small scale tests. To rule out any differences resulting from different bottom configuration, completely identical bottom configurations were constructed in small and large scale, cf. Fig. 10.2. This involves also the length of the flume as the small scale flume was closed with a plate.

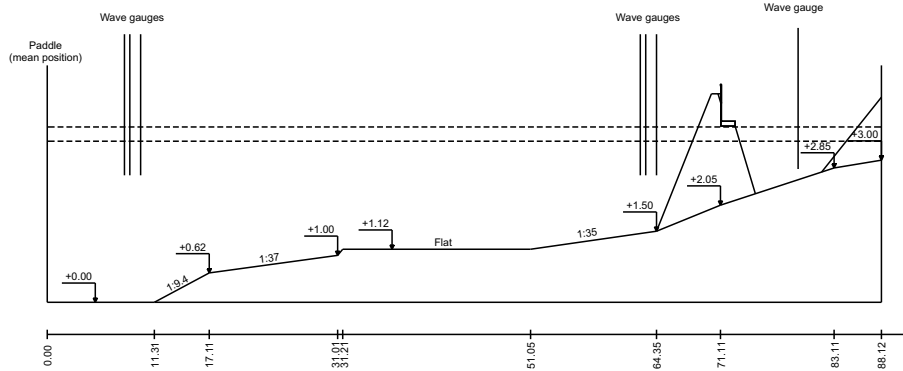


**Figure 10.2**

*Bottom configuration. Measures in meters and large scale. Note that vertical and horizontal scales are different.*

### 10.1.2 Breakwater Cross Sections

A very typical breakwater design with a superstructure was chosen for the investigations. Four breakwater cross sections were tested with only minimum rebuilding needed, cf. Fig. 10.3. The breakwater cross sections are commonly used types of a conventional two-layer rock armoured rubble mound breakwaters with a front slope of 1:2 and a superstructure.

## 10.1 Test Set-Up & Data Analysis

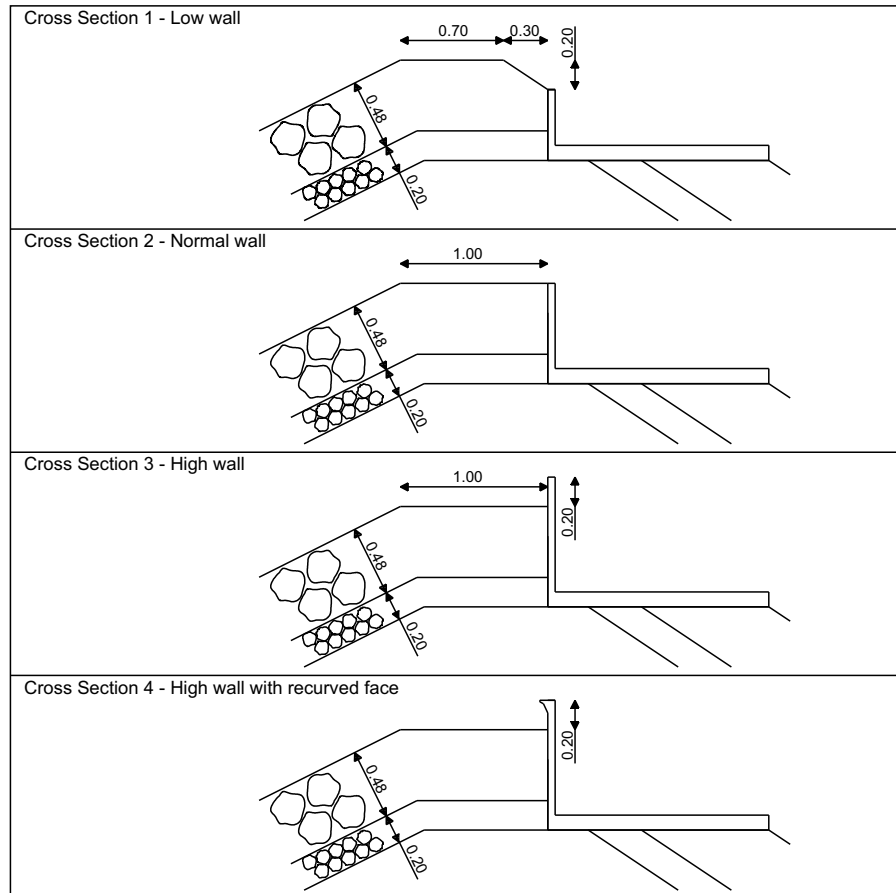
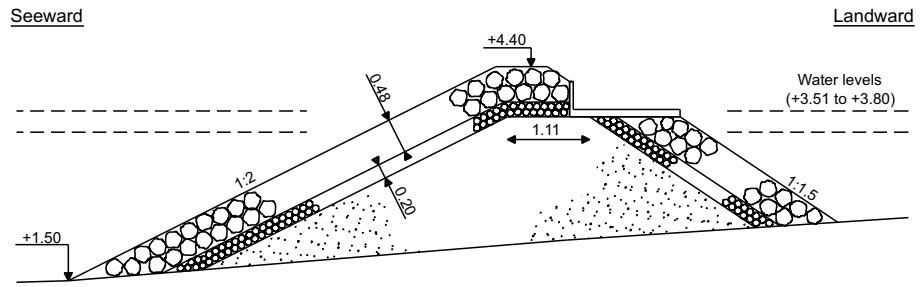


**Figure 10.3**

*Cross sections. Measures in large scale and meters.*

To ensure a fast change of the height of the superstructure, it was made as a modular structure, see Fig. 10.4. To give more storage volume in the overtopping tank, the superstructure was constructed with a thinner promenade section at the location of the overtopping tanks, cf. Fig. 10.4.

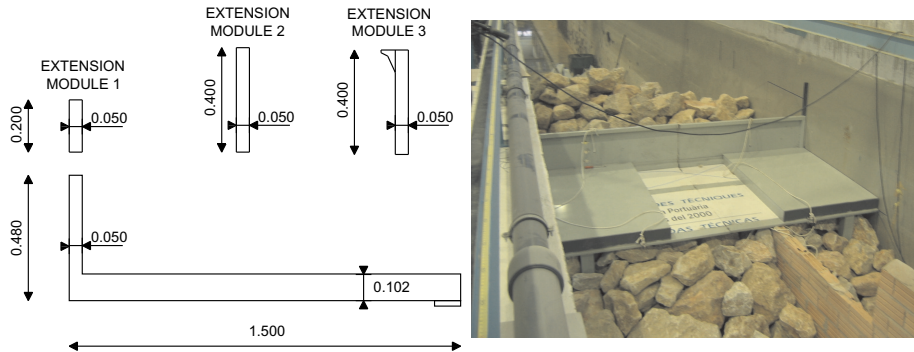


**Figure 10.4**

*Tested types of superstructures. Measures in large scale and meters. The picture on the right is from the large scale tests and shows the superstructure without extension module installed. For installing the structure, it had to be cut in the middle and welded together again in the flume.*

### 10.1.3 Quarry Materials for the Breakwater

The armour stones on the front side had the grain size distribution given in Fig. 10.5. The grain curves are when scaled according to Froude almost completely identical in small and large scale and are based on weighing every stone in the front armour layer. By doing so also differences in armour layer porosity between small and large scale were prevented. The armour on the rear side was constructed primary of stones not fitting into the weight interval used for the front side armour.

The grain size of the filter material in the small scale model corresponds approximately to a linear scaling according to Froude. The filter grain curves given in Fig. 10.6 are based on sample distributions.

As mentioned in section 9.3.2, the core material may have a large influence on the amount of water flowing through the core and the amount staying on the slope. Therefore two different core materials were tested in small scale to clarify this influence. Core material 1 corresponds to 1.5 times the diameter calculated from a linear scaling of the large scale core material. Core material 2 is more coarse as the filter material was used for the core as well and corresponds to 3.6

times the diameter a linear scaling imply. The size calculated by the method of Burcharth et al., 1999 to give similar flow fields in the two scales gives a diameter in between the two.

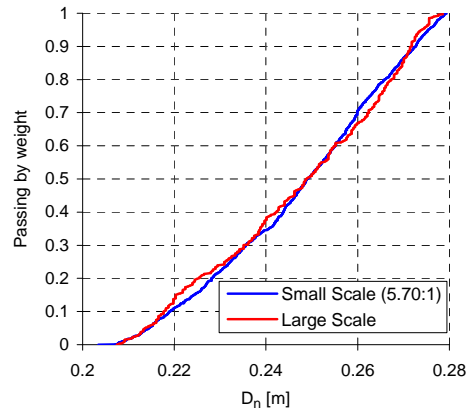


**Figure 10.5**  
Grain size distribution of armour stones (values in large scale).

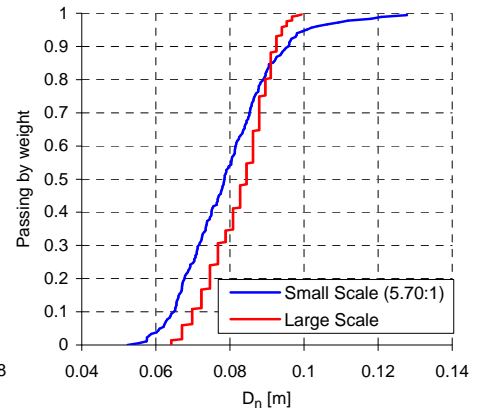


**Figure 10.6**  
Grain size distribution of filter stones (values in large scale).

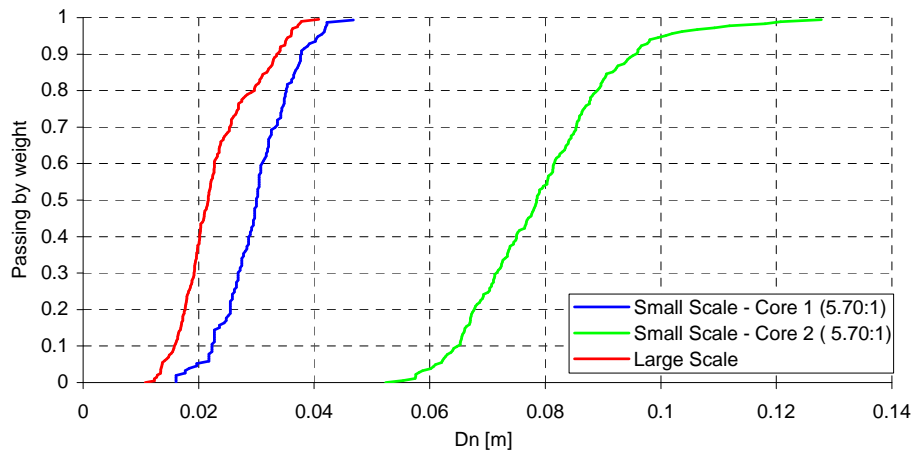


**Figure 10.7**  
Grain size distribution of core material (values in large scale).

The permeability of the the two different core materials was measured using the setup shown in Fig. 10.8. By measuring simultaneously stationary values of

pressure drop ( $\Delta h$ ) and flow discharge the results in Fig. 10.9 were obtained. It can be seen that the more coarse Core 2 material is as expected much more permeable.

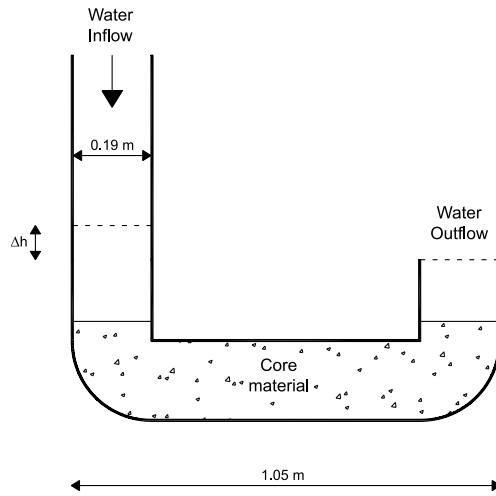


**Figure 10.8**  
Setup for measuring core material permeability.

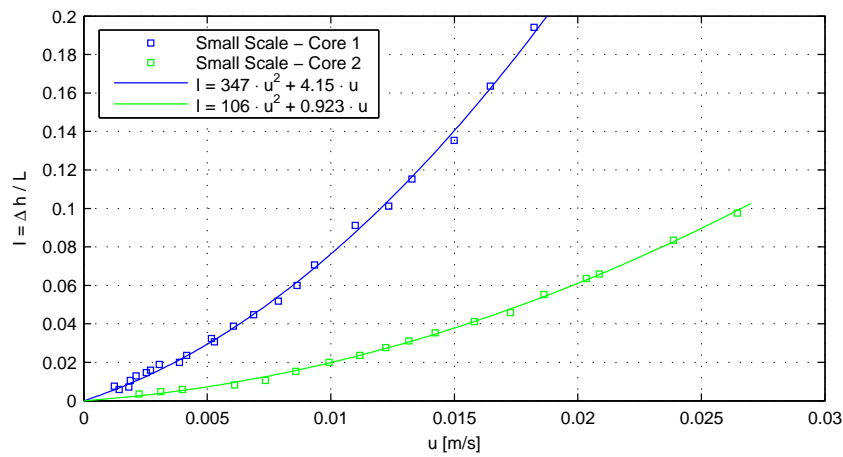


**Figure 10.9**  
Measured relationship between discharge velocity ( $u$ ) and hydraulic gradient ( $I$ ).

The porosity of the core materials was also measured, which made it possible to calculate the  $\alpha$  and  $\beta$  coefficients in the Forchheimer equation (Eq. 9.3). This was done from the coefficients of the fitted polynomials given in Fig. 10.9. In this calculation the equivalent sphere diameter ( $D_{s,50}$ ) was used as diameter ( $D$ ) in Eq. 9.3. These calculated  $\alpha$  and  $\beta$  coefficients together with other characteristics parameters of the used materials are given in Table 10.1.

	Small scale				Large scale		
	Armour	Filter	Core 1	Core 2	Armour	Filter	Core
$W_{50}$ [kg]	0.212	0.0070	0.0044	0.007	39.9	1.60	0.0268
$\rho$ [kg/m <sup>3</sup> ]	2590	2700	2700	2700	$\approx 2600$	$\approx 2650$	$\approx 2650$
$D_{n50}$ [m]	0.0434	0.0137	0.0052	0.0137	0.249	0.084	0.0216
$f_g$	1.19	1.37	1.56	1.37	1.22	1.26	1.85
Porosity $n$	0.38	0.37	0.40	0.37	0.38		
$\alpha$		351	314	351			
$\beta$		1.49	2.41	1.49			

**Table 10.1**  
*Material properties.*

### 10.1.4 Wave Measurements

The waves were measured both near the paddle and at the toe of the breakwater. The positions of the wave gauges were identical in the small and large scale tests, cf. Fig. 10.2. In both cases resistance type twin-wire wave gauges were used. In the large scale tests the wave gauges were calibrated during filling and take out of water. The calibration curves were due to the large volume of water assumed to stay rather constant for some days, because the temperature of the water changes very slowly due to the large volume of water and because the water was filtered by sandfilters when not performing tests. By sending the exact same regular wave signal to the paddle, this assumption was tested at least once per day, and a variation coefficient of 1.7% was found on the wave height. In small scale the wave gauges were calibrated once per day during filling of the flume. In both small and large scale the non-linearity of the wave gauges were taken into account by using a non-linear calibration curve. This was done in order to have very accurate wave measurements which is extremely important when studying overtopping. Errors of approximately 10% on the wave heights can occur for the used wave gauges, when applying a linear calibration curve and a non-central estimate with 2 calibration points.

Due to the high sample frequency used in the tests, time series were subsampled for the wave analysis by using every third data point in the sampled time



series. A bandpass filter with cut-off frequencies  $1/3 \cdot f_p$  and  $3 \cdot f_p$  was applied. The Mansard and Funke, 1980 method was used for separation in incident and reflected waves both in frequency and time domain.

### 10.1.5 Wave Set-Up Measurements

On the rear side of the breakwater water levels and waves generated by overtopping and penetration through the breakwater were measured. For this a guiding wall and a surface elevation gauge were installed, cf. Fig. 10.1.

The basins behind the breakwater were identical in small and large scale. In addition to the drainage through the breakwater there were used PVC tubes placed at the flume bottom, which reduced set-up. In the large scale model four PVC tubes (two in each side of the flume) with an inner diameter of 0.102 m were used. For the small scale tests one PVC tube in each side with an inner diameter of 0.058 m were used. Using classical pipe hydraulic formulae led to the  $\Delta h$ - $Q$  relationships given in Fig. 10.10 for large and small scale. It can be seen that the set-up will drain slower trough the pipes in large scale compared to small scale. A stationary simple calculation of the porous flow in the core, showed that the discharge trough the core is dominating over the discharge in the tubes, which will reduce the influence of this model effect.

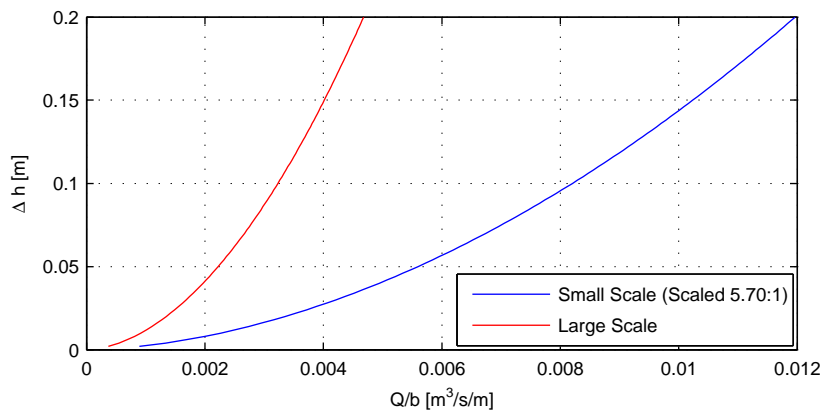


**Figure 10.10**

*Calculated relation between return flow discharge in tubes per meter flume width and setup behind breakwater. Values given in large scale.*

### 10.1.6 Overtopping Measurements

Significant overtopping scale effects are only expected for rather low overtopping discharges. Target overtopping discharges are in the prototype range 0.01 litre/ms - 10 litre/ms for the present study, which is the area typically used for design of breakwaters. The wave parameters were on each water level and cross-section chosen so overtopping discharges within this interval were reached. The large scale model was considered to be around scale 1:7 and the small scale model 1:40 of the prototype. The above given interval of prototype discharge corresponds then to 0.0007 litre/ms - 0.7 litre/ms for the large scale tests and 0.00004 litre/ms - 0.04 litre/ms for the small scale tests.

Identical method of overtopping measurements were applied in the two scales. To be able to measure the spatial distribution of the overtopping water the overtopping tank contained four chambers with a water level gauge and a pump in each chamber. The water level measurements in the overtopping chambers were slightly different in the two scales, as pressure sensors were used in large scale and resistance type water surface amplitude gauges were used in small scale. The length of the upper part of the chambers that collects the overtopping water was for each of the four chambers 0.75 m in the large scale model, cf. Fig. 10.11. The bottom part of chambers was narrower than the upper part. The main part of the overtopping volume will end in the first chamber (50-90%). To have enough storage volume in this chamber, it was relatively wide at the bottom. To give good resolution also on the last three chambers which collect less overtopping water these were much narrower at the bottom.

## Overtopping Scale Effects, New Large Scale Tests

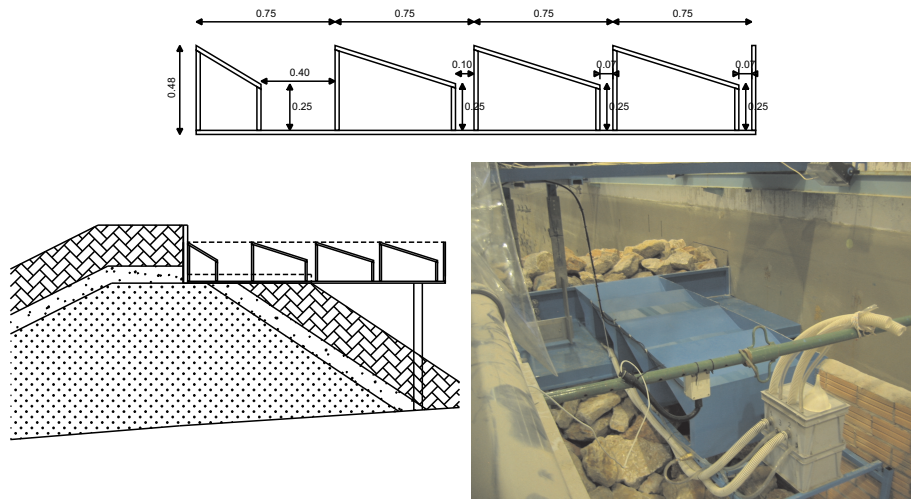


**Figure 10.11**

*Overtopping tank. Measures in large scale and meters. The picture on the right is from the large scale tests.*

The chambers were equipped with permanent pumps that were configured to stop and start automatically when the water levels in the chambers reached certain levels, this was done using digital outputs of the data acquisition system and a relay box. The tanks were designed to give high accuracy also for low overtopping discharges, as this is the area of suspected scale effects. As a consequence the tank layout could only be applied up to 6 litre/ms in prototype scale. Above that discharge the chamber could in some cases be filled within some few waves which makes it impossible for the pumps to remove the water in time. The tests with prototype overtopping discharges around 0.01 l/ms corresponds in small scale to only 0.7 mm raise in water level in the first chamber if all overtopping water is assumed to go into this chamber. Therefore, relatively large uncertainties on especially the spatial distribution of the overtopping water can be expected for these tests. The calibration curve for the chambers were obtained by filling the chambers with water after the set-up was completed. Pump discharges were also measured as these were needed for the data analysis.

Construction of overtopping time series were performed from time series of the level in the chambers and the pump state, cf. Fig. 10.12. Tank water level time series was filtered using an averaging filter.

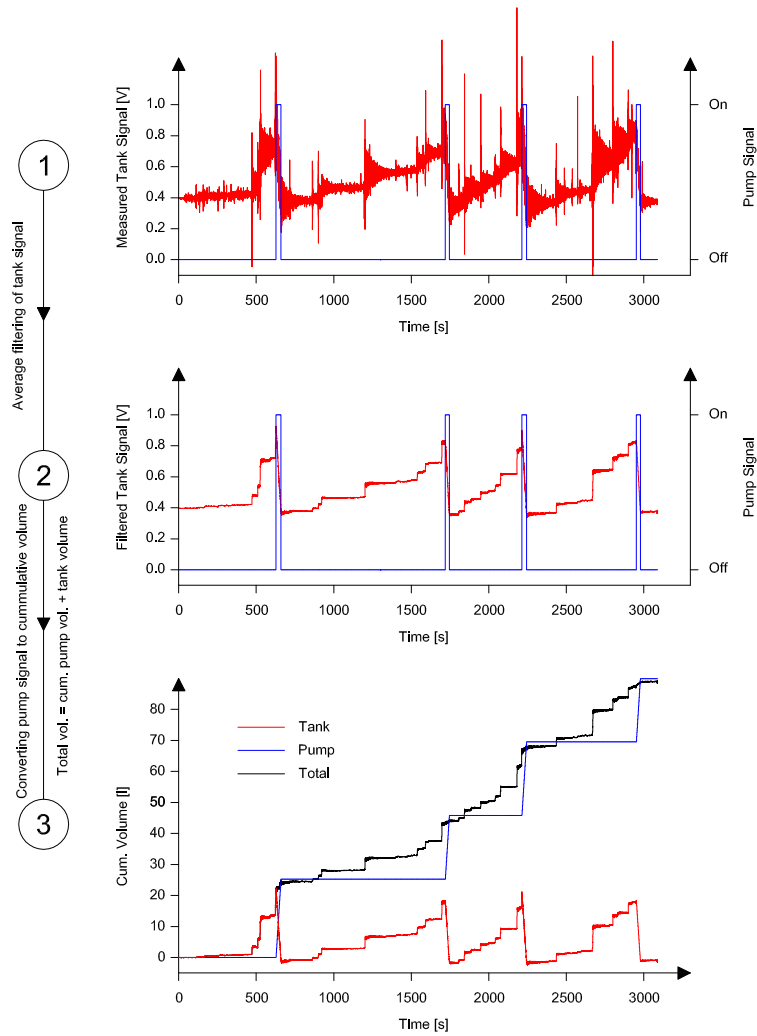


**Figure 10.12**  
Construction of overtopping time series.

### 10.1.7 Wave Run-Up Measurements

To measure wave run-up heights a wave gauge was in both scales placed on the top of the armour layer along the slope. The run-up gauge was placed as close

to the armour layer as possible without touching any of the armour stones.

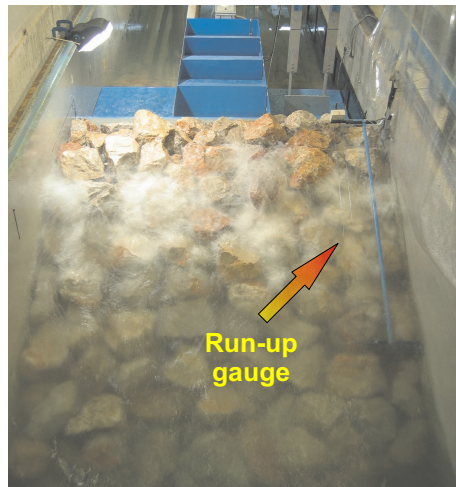


**Figure 10.13**  
*Run-up gauge.*

### 10.1.8 Overtopping Impact Force Measurements

Impact forces on a plate (dummy car), with the dimensions  $0.514 \text{ m} \times 0.229 \text{ m}$  in the large scale model, were measured by a strain gauge based force transducer constructed at Aalborg University. The elasticity and mass of the force transducer was scaled to give identical displacements and eigenfrequencies in the two scales. If the dimensions of the support were scaled linearly according to the Froude law using the same material, the displacements will scale with the square of the length scale. Therefore, the support sections with strain gauges were thicker in large scale than a linear scaling of the small scale dimensions imply.

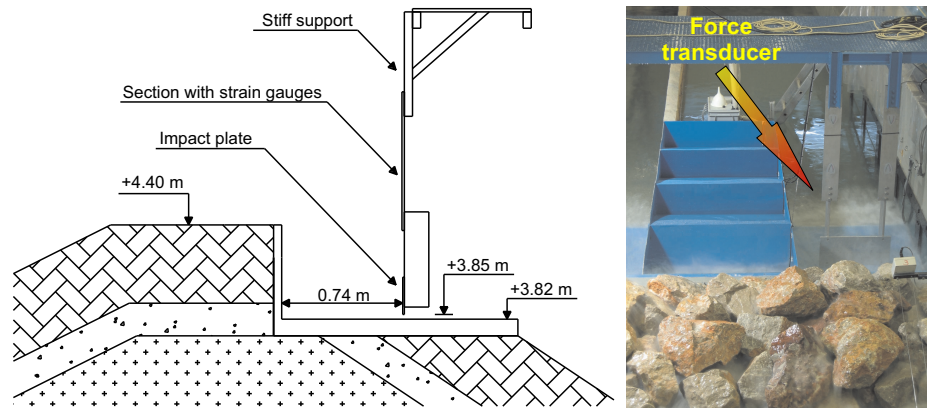


**Figure 10.14**  
 Force transducer for measuring impact forces on a plate. The picture on the right is from the large scale tests.

The eigenmode of the transducer is shown in Fig. 10.15. The eigenfrequency and damping ratio were calculated using the WaveLab2 software package. The eigenfrequencies corresponds approximately to a Froude scaling, but the damping ratio in the large scale is only half of the one in small scale.

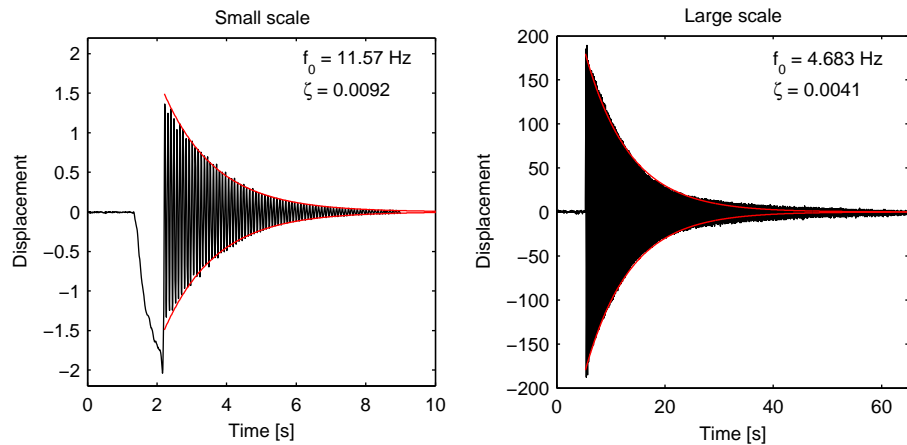


**Figure 10.15**  
 Measured force transducer eigen mode in small and large scale. Red lines are calculated displacements amplitude envelope function using the calculated eigen frequency and damping ratio and assuming a linear viscous damped system.

For the force measurements corrections for dynamical amplifications were performed using the WaveLab2 software package, which is based on FIR filtering of the data using the inverse of the dynamic amplification function for a linear viscous damped single degree system, which is given in most vibration theory books (e.g. Nielsen, 1998).

$$\begin{aligned} Gain &= \sqrt{\left(1 - \left(\frac{f}{f_0}\right)^2\right)^2 + \left(2 \cdot \zeta \cdot \frac{f}{f_0}\right)^2} \\ Phase &= -\arctan\left(\frac{2 \cdot \zeta \cdot \frac{f}{f_0}}{1 - \left(\frac{f}{f_0}\right)^2}\right) \end{aligned} \tag{10.1}$$

Because the gain function, given in Eq. 10.1, gives large gain for high frequencies (noise), there has been applied a cut-off at 1.5 times the eigenfrequency. Fig. 10.16 and 10.17 shows two examples of application of the filter. In the first example the filter is applied to a eigenmode test, where the plate was given an initial displacement. It can be seen that only the initial quasi-static force remains unchanged by the filter. At the time the applied force is removed the system continues vibrating, but this part is removed by the filter, as the force drops to and remains almost constant at zero. The second example is from one of the model tests. After filtering only positive impact forces are in the signal. The magnitude of the forces are changed due to removal of dynamic amplification. These two examples demonstrates that the filter has the desired effect.

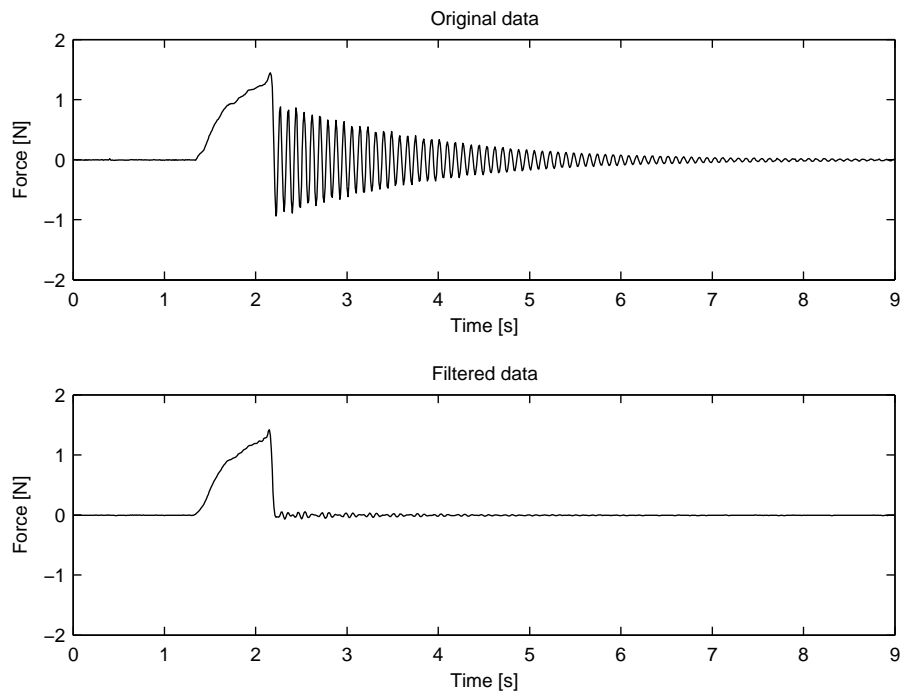


**Figure 10.16**  
*Examples of application of dynamic amplification filter on eigen mode data.*



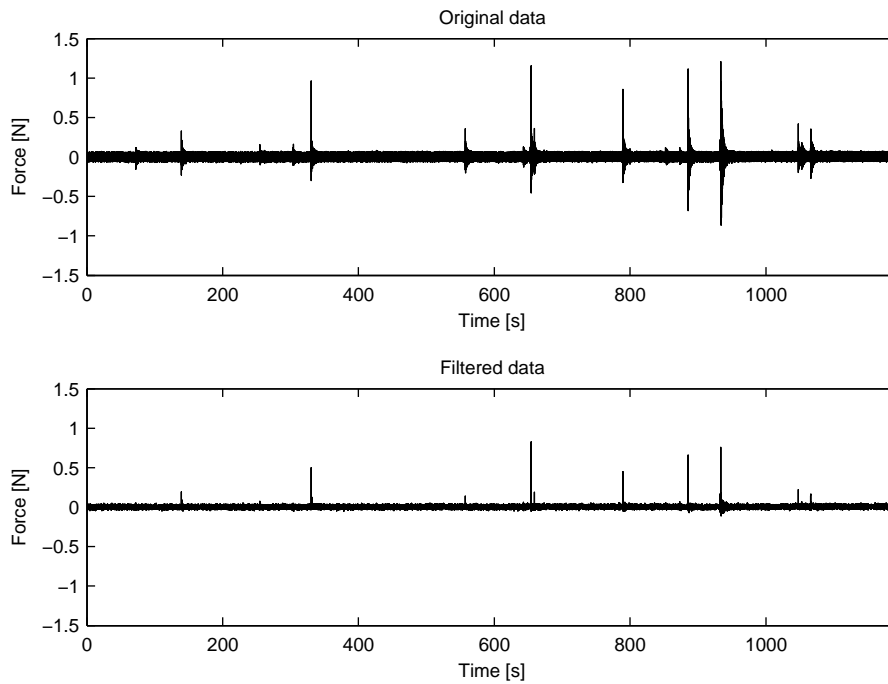


**Figure 10.17**  
*Examples of application of dynamic amplification filter on real data.*

## 10.2 Test Programme

51 large scale tests and 170 small scale tests were performed (85 on each of the two core configurations).

Tests were performed on two different water levels. At the highest water level the core was completely saturated and porous flow scale effects are believed to be small. On the lower water level the influence of the core material is greater.

Fresh water was used in the large scale tests and in most of the small scale tests. In addition to the 170 small scale tests performed with fresh water, 35 tests were performed to study the influence of surface tension and air content. To reduce the surface tension 50 ppm 1-pentanol was added to the water. 1-pentanol acts as a surfactant that reduces the surface tension so the air bubbles will be much smaller and even sized around 1 mm in diameter, as reported by So et al., 2002.

### 10.3 Comparison of Generated Waves in Large and Small Scale Experiments

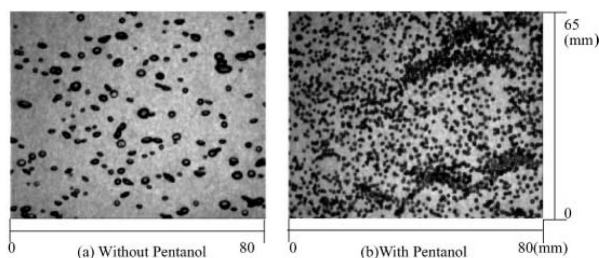


**Figure 10.18**

*Photos of the bubbles without pentanol and with pentanol [So et al., 2002].*

Much more air entrainment is observed in prototype and large scale when the waves impact and break on the slope. Therefore, some small scale tests were performed with air added on the lower part of the breakwater from a perforated tube both with and without the surfactant added to the water. 1-pentanol generates some foam when the air is added from the tube, but much less than soap will do. The foam disappears immediately when the waves stop.

The JONSWAP spectrum with a peak-enhancement factor of 3.3 was used in all tests. The length of the tests was 1000 peak periods corresponding to approximately 1200 waves.

Table 10.2 shows the ranges of sea state parameters tested and the corresponding armour Reynolds numbers. It can be seen that the large scale tests are performed in the area where the drag coefficient is approximately independent on the Reynolds number, cf. Fig. 9.2.

	Large scale	Small scale
$H_{m0,toe}$ [m]	0.31 - 0.65	0.054 - 0.119
$s_{0p,toe}$	0.017 - 0.049	0.018 - 0.051
$Re_D$	$4.3 \cdot 10^5$ - $6.3 \cdot 10^5$	$3.2 \cdot 10^4$ - $4.7 \cdot 10^4$

**Table 10.2**

*Investigated ranges of parameters.*

### 10.3 Comparison of Generated Waves in Large and Small Scale Experiments

In this section the generated waves in large and small scale are compared with respect to wave spectra, wave height distributions, wave skewness and wave

groupiness.

### 10.3.1 Wave Spectra and Wave Height Distributions Examples

In this section the incident wave spectra and the incident wave height distributions are compared for four tests, see Fig. 10.19 - 10.22. The tests have been chosen such that similar up-scaled deep water wave parameters  $H_{m0}$  and  $T_p$  exist in the two scales.

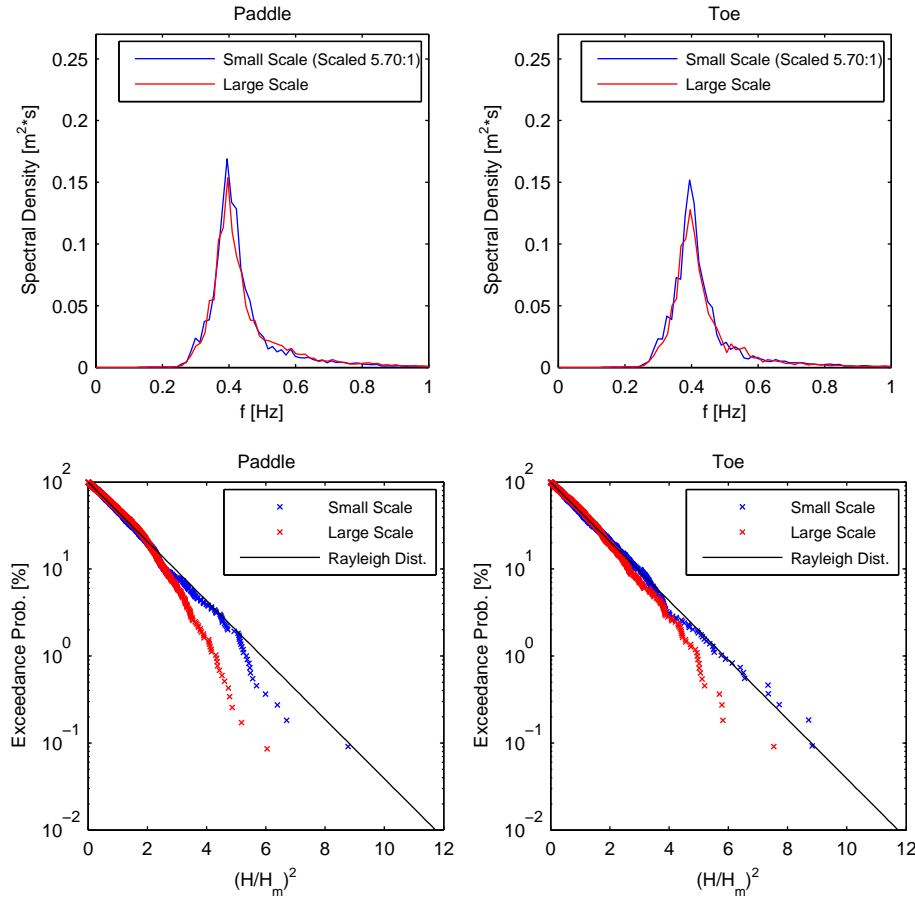


**Figure 10.19**

*Ex. 1: Comparison of incident waves near paddle and at the toe.*

### 10.3 Comparison of Generated Waves in Large and Small Scale Experiments

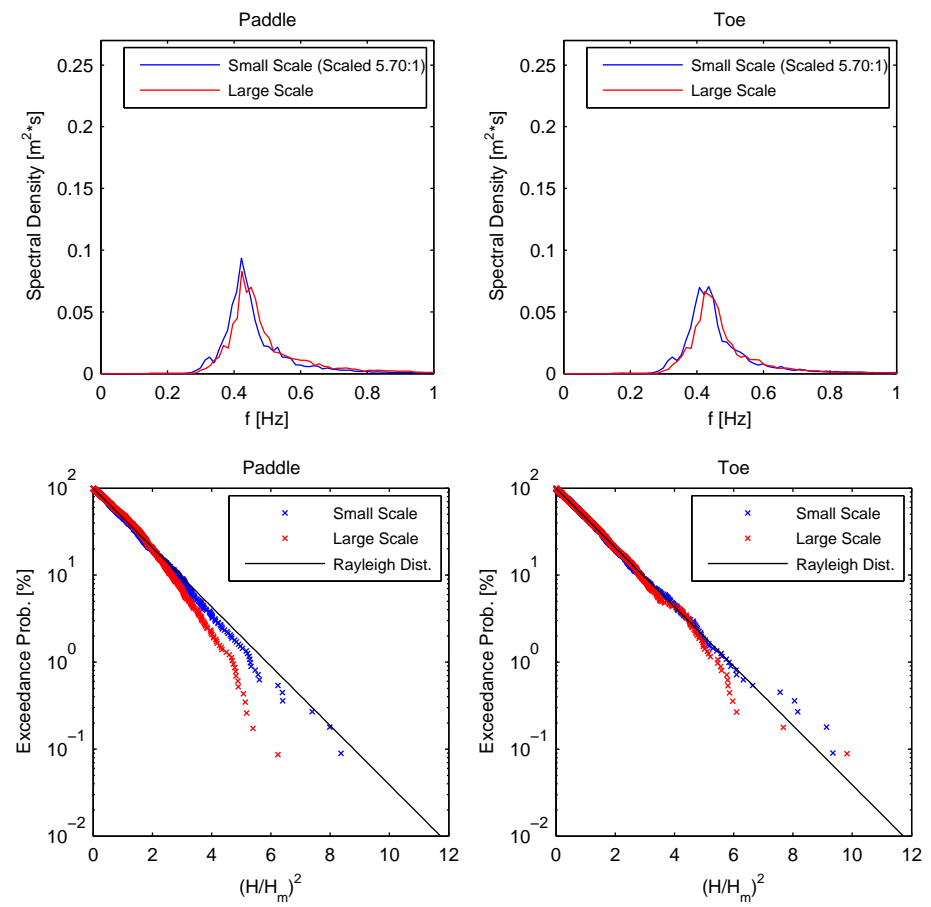


**Figure 10.20**

*Ex. 2: Comparison of incident waves near paddle and at the toe.*

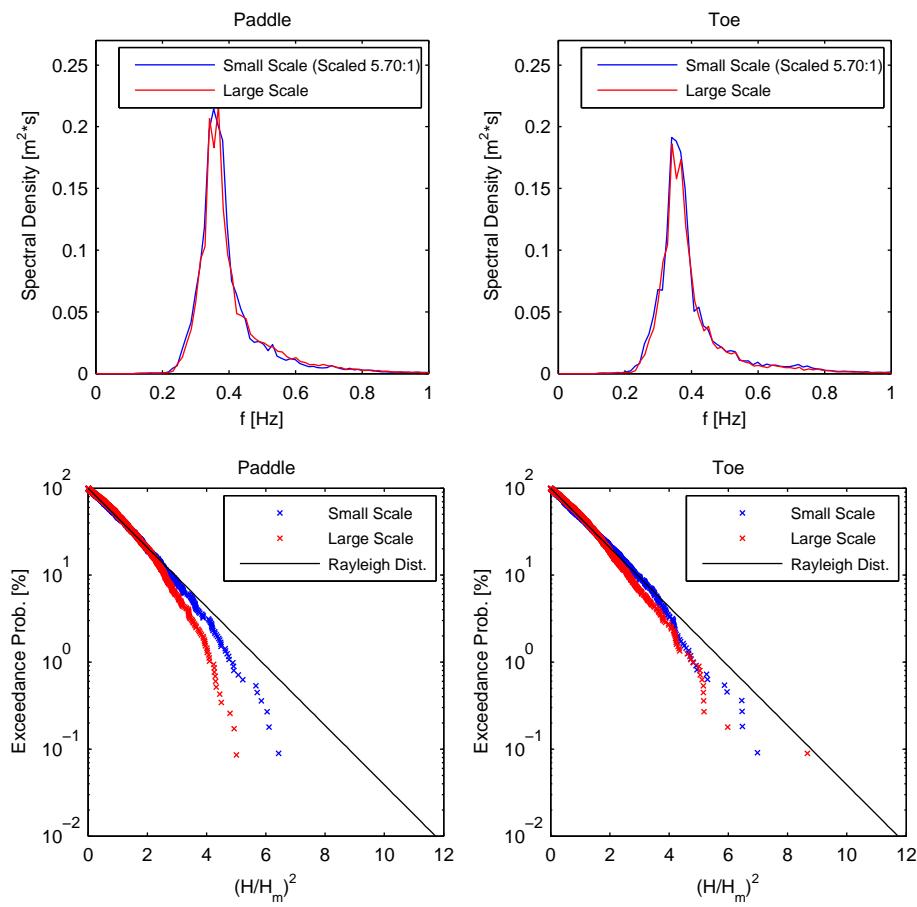


**Figure 10.21**

*Ex. 3: Comparison of incident waves near paddle and at the toe.*

### 10.3 Comparison of Generated Waves in Large and Small Scale Experiments

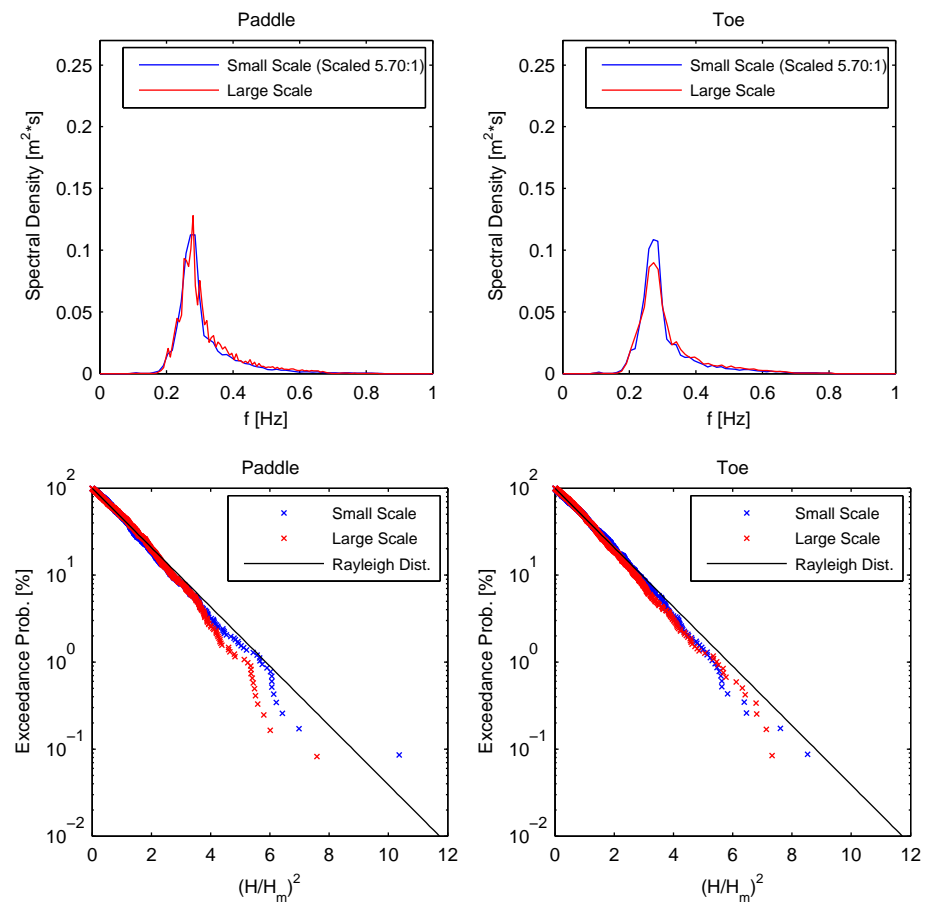


**Figure 10.22**

*Ex. 4: Comparison of incident waves near paddle and at the toe.*

It can be seen that in all four tests the generated waves are closer to Rayleigh distributed in the small scale compared to the large scale. The extreme waves are smaller in the large scale although strange enough is the largest wave in the two scales quite similar. However, the differences clearly is an important model effect. This difference is most probably due to different wave generation hardware and software in the two scales. In the large scale is used a wedge type wave generator and in small scale a piston type. At the toe of the structure the differences are clearly smaller, but still there are important differences. These differences in wave height distributions makes it much more difficult to conclude

on scale effects related to low to medium overtopping discharges for which the wave height distribution is very important.

### 10.3.2 Wave Height Distributions from all Tests

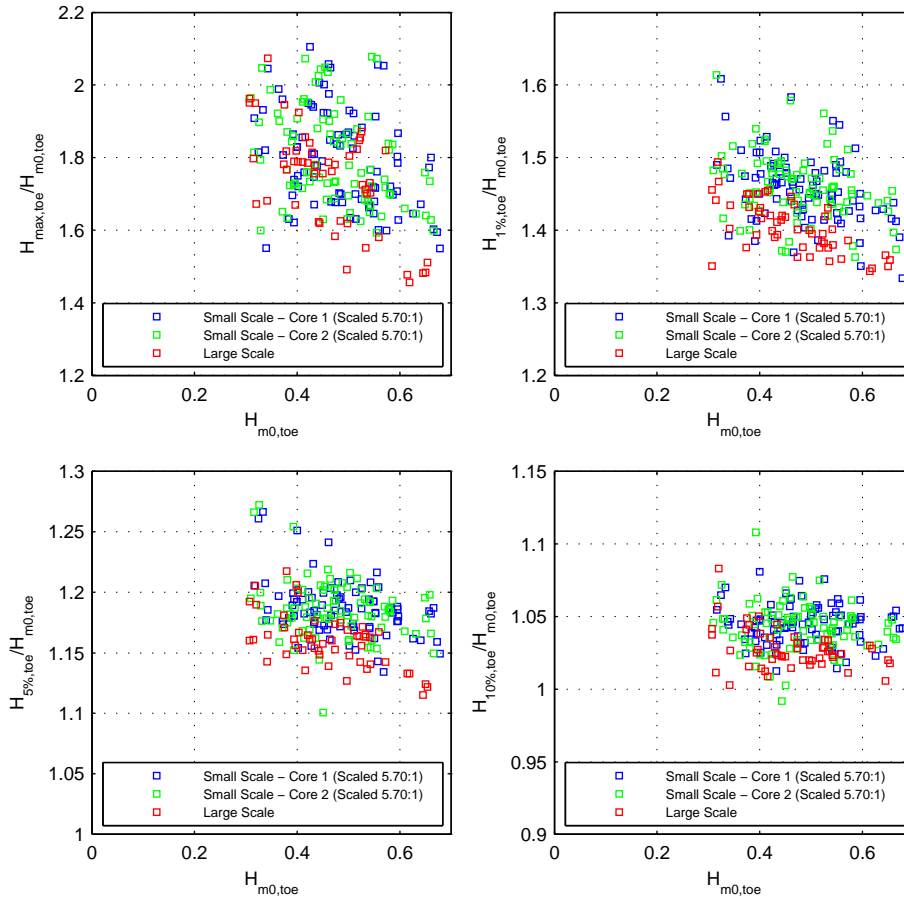


**Figure 10.23**  
*Comparison of incident wave height distributions at the toe.*

Fig. 10.23 shows comparison of the extreme wave heights measured in the two scales. The figure confirms the findings in the previous section.  $H_{max}$  is almost identical in the two scales, but  $H_{1/100}/H_{m0}$  is in average 1.57 in the small scale

### 10.3 Comparison of Generated Waves in Large and Small Scale Experiments

tests and 1.50 in the large scale tests, which means 4% larger in small scale. The influence of these differences in  $H_{1/100}/H_{m0}$  can be estimated from the berm breakwater tests to be a factor of approximately 3 on the overtopping discharge, cf. Fig. D.9.

#### 10.3.3 Wave Skewness

From Fig. 10.24 it can be seen that the incident vertical wave skewness both near the paddle and at the toe is much higher in small scale than in large scale. This is probably a result of the different wave height distributions observed.

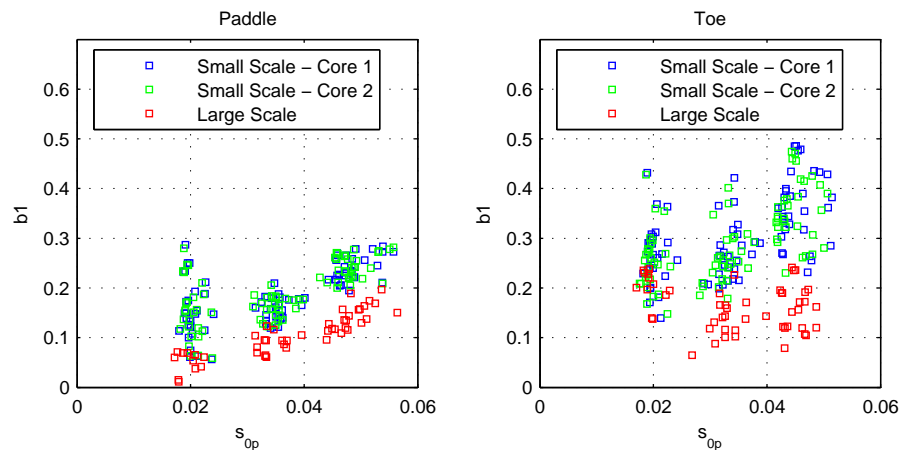


Figure 10.24

Comparison of incident vertical wave skewness near paddle and at the toe.

#### 10.3.4 Wave Groupiness

Table 10.3 shows a comparison of the groupiness factors ( $GF$ ) near the paddle. If the phases of the individual components are random the groupiness factor should be 1.0 in average. One can see that this is only true for the small scale tests while the wave groupiness is smaller in large scale. This can explain the different wave height distributions as more groupiness leads to higher extreme waves.



	<b>Small Scale</b>	<b>Large Scale</b>
Minimum	0.911	0.856
Maximum	1.06	0.956
Average	0.995	0.916

**Table 10.3**  
*Wave groupiness factors (GF) near the paddle.*

At the toe the wave groupiness in both small and large scale has in average increased as shown in Table 10.4.

	<b>Small Scale</b>	<b>Large Scale</b>
Minimum	0.959	0.892
Maximum	1.17	1.04
Average	1.04	0.965

**Table 10.4**  
*Wave groupiness factors (GF) at the toe.*

## 10.4 Model Effects

As demonstrated in the previous section the generated waves are not identical in the small and large scale tests even though the spectra are close to be identical. The distributions of the larger wave heights are significantly different, which is an important model effect. This model effect is most probably due to different types of wave generation hardware and software applied in the two scales. As the wave generator types are different, an exact reproduction of the wave time series (the complex wave spectrum) is difficult. An iterative procedure to reproduce the exact same wave field near the paddle could would maybe be a solution, but it was not done in the present study and will require a lot of calibration tests.

Even though the set-ups have been made to rule out as many model effects as possible, there besides the model effect related to the waves still remain some small differences between the set-ups.

The width of the overtopping tank was 1 m in large scale and 0.30 m in small scale. The CIEM flume used for the large scale tests is 3.00 m wide and the small scale flume is 1.50 m wide. The width of the flume and the chambers were when scaled linearly more narrow in the large scale model than the linear scaling implies. These effects are expected to be of no importance as in any case the width of the tanks were several times the typical side length of the armour stones.

The flow discharge in the tubes used to minimize setup behind the breakwater was calculated to be relatively smaller in large scale, leading to more set-up and overtopping in large scale. However, the influence of this is small as it was found that the flow through the core was the main contributor to the return flow.

## 10.5 Results

In the following sections the large and small scale results are compared with respect to:

- Wave propagation and breaking.
- Wave reflection.
- Wave run-up.
- Wave overtopping.
- Impact forces from overtopping.

### 10.5.1 Wave Propagation and Wave Breaking

Very good agreement in transformation of wave heights from the deeper part of the flume to the toe of the breakwater is observed between the two scales, cf. Fig. 10.25. The change in wave height is due to shoaling, breaking (and dissipation due to friction at walls and at the bottom). For the largest wave steepness quite some wave breaking took place on the foreshore.

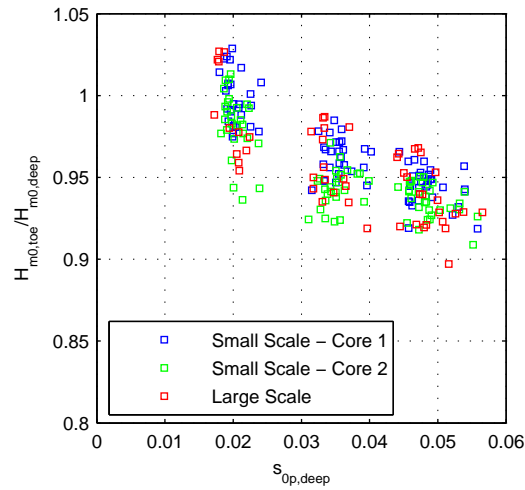


**Figure 10.25**

*Comparison of wave heights near the paddle and at the toe.*

### 10.5.2 Wave Reflection

Fig. 10.26 shows a comparison of the reflection coefficients ( $C_r$ ) obtained in large and small scale. The reflection coefficients are calculated as the ratio of reflected wave height ( $H_{m0,r}$ ) near the paddle and incident wave height ( $H_{m0,i}$ ) at the toe of the structure. This approach was chosen because the bottom is sloping at the toe, and the waves are more non-linear and breaking at the toe. Moreover, at the toe there will be a phase interaction due to the structure.

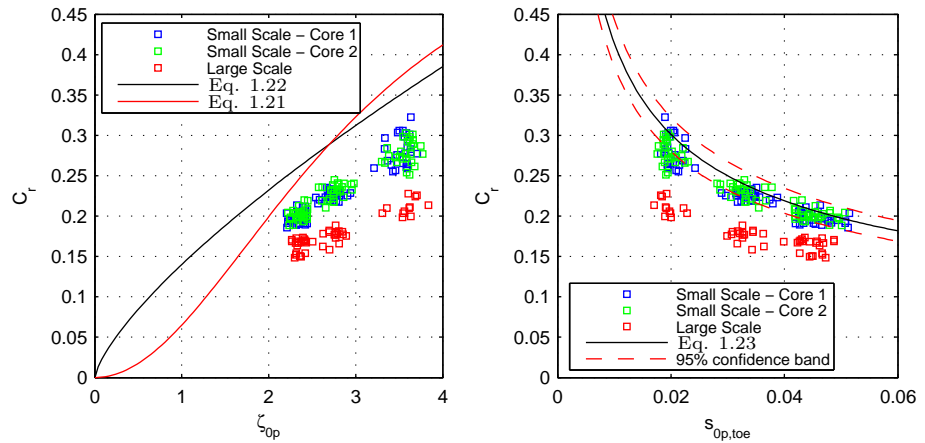


**Figure 10.26**

*Comparison of measured wave reflection coefficients in the two scales. The curves are the formulae of Seeling, 1983 (Eq. 1.21) and Postma, 1989 (Eq. 1.22 & 1.23).*

It can easily be seen that the reflection coefficients are clearly lower in large scale than in small scale. The more coarse Core 2 material applied in some small scale tests did not lead to less reflection as expected, but is the same as in tests with finer Core 1 material. The reflection coefficients obtained in small scale are in reasonable agreement with the improved Postma, 1989 formula (Eq. 1.23). Significant lower reflection coefficients are measured in large scale, which most likely is due to more energy dissipation in the run-up flow. It was visually observed that much more air is entrained in large scale when the waves impact on the slope. However, the difference in reflection coefficients could also be due to the differences in wave height distributions in the two scales, cf. section 10.3. However, this deviation is not expected to give such a big difference in reflection coefficients.

### 10.5.3 Wave Set-Up and Wave Transmission

Fig. 10.27 shows a comparison of time averaged dimensionless wave set-up behind the breakwater against the mean wave period  $T_{0,1}$ . The wave period has a large influence on the wave set-up. The data in Fig. 10.27 is for each type of test clustered in three groups corresponding to the three different wave steepnesses tested. More set-up is observed in large scale, as no significant difference is observed between Core 1 and Core 2 tests this is expected to be a model effect rather than a scale effect. The drainage through the tubes is one model effects

that partly could cause this, but is not expected to be the main contributor as the drainage through the structure was calculated to be the dominating part. Larger overtopping in large scale could be another factor. The difference in set-up is only 1% to 2% of the  $H_{m0}$  wave height and is thus expected to have very little influence on the overtopping.

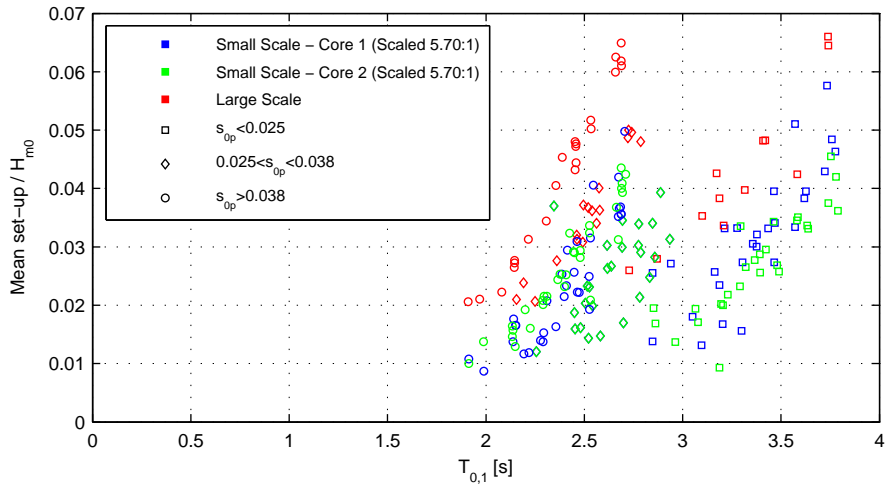


**Figure 10.27**

*Time averaged wave set-up behind the breakwater as function of the wave period (given in large scale).*

Fig. 10.28 shows a comparison of wave transmission coefficients which were found to be a function of the wave period. The wave transmission coefficients for tests with Core 2 are approximately twice the ones obtained with Core 1, which is due to less energy dissipation in the porous flow. The large scale tests are in between the two, but very close to Core 1 results. It could be seen that each of data series are separated in two groups reflecting the two water levels. As expected more transmission was measured in case of the high water level.

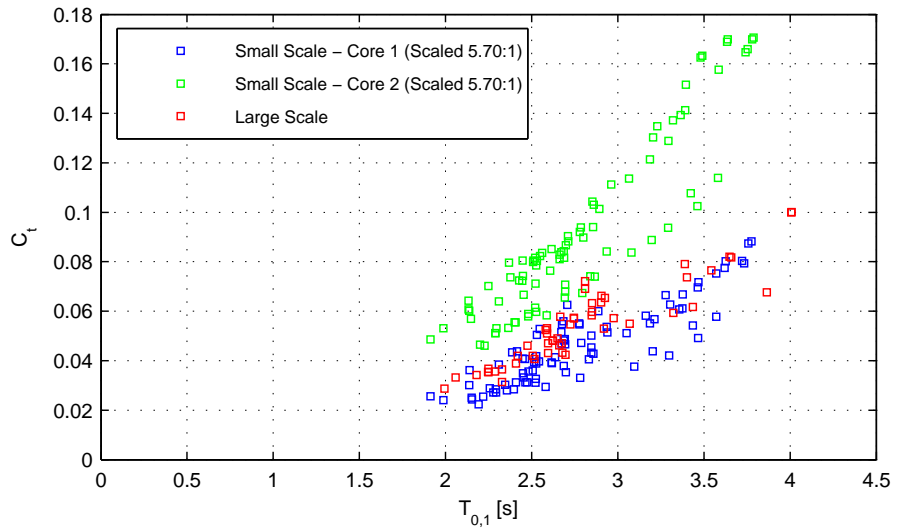


**Figure 10.28**

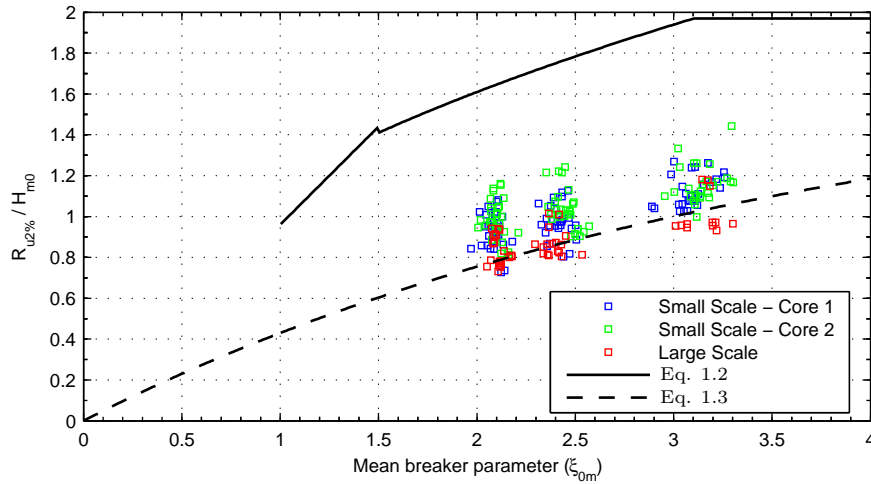
*Transmission coefficient as function of the wave period (given in large scale).*

#### 10.5.4 Run-Up

In Fig. 10.29 the measured relative run-up heights are plotted against the mean breaker parameter. The data shows much less run-up than the Delft Hydraulics, 1989 formula (Eq. 1.2) valid for rock armoured permeable slopes in relatively deep water. The reason for this large deviation is probably due to different ways of measuring run-up levels. The data are in excellent agreement with the formula of Murphy and Kingston, 1996 (Eq. 1.3), which as the present investigations is based on measurements with wave probes along the slope. Using a wave gauge along the surface of the armour layer leads to underestimation of the run-up heights due to the small layer thickness in the upper part of the run-up wedge. If the run-up heights instead were measured with a step gauge, which has shown to be excellent to measure run-up heights along an uneven surface, higher measured run-up levels could be expected.

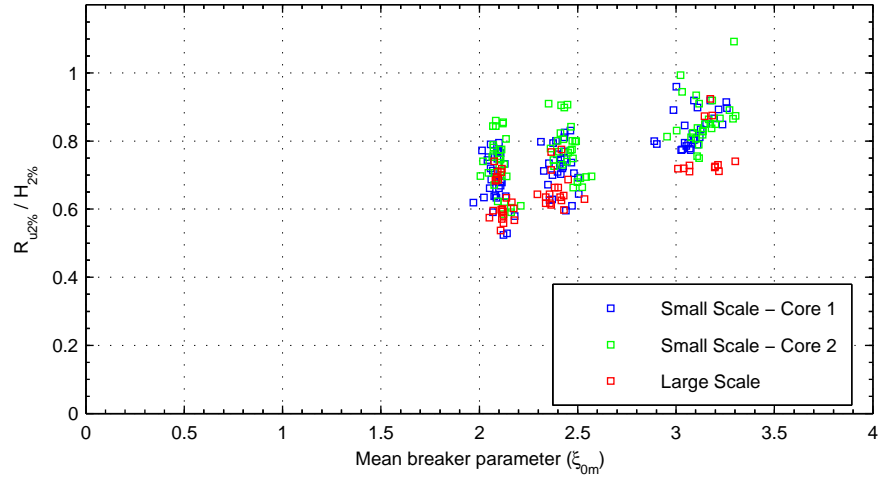
The large scale tests are approximately 10% lower than the small scale tests. However, an explanation for this might be the different wave height distributions observed in the two scales. What also can influence this is the exact placement of the run-up gauge and maybe the higher air content in large scale. Using a

resistance type gauge to measure run up with air entrainment in the water is questionable. The tests with the more coarse core material (Core 2) do not show lower run-up heights as might be expected, but are in the same range as for the tests with Core 1. Delft Hydraulics, 1989 found only differences in 2% run-up heights between impermeable and permeable slopes for large values of the surf similarity parameter ( $\xi_{0m} \gtrsim 3$ ).



**Figure 10.29**  
 Comparison of dimensionless wave run-up heights  $R_{u2\%}/H_{m0}$ .

$R_{u2\%}/H_{m0}$  is not a good parameter to conclude on scale effects due to the observed differences in the wave height distributions. Instead it might be better to relate the same exceedance probability for wave height and run-up height  $R_{u2\%}/H_{2\%}$ , cf. Fig. 10.30. However, it can be seen that also in this case the data show higher run-up in small scale compared to large scale. This plot does not account for the different wave skewnesses observed. Waves with higher skewness are expected to give larger run-up heights.


**Figure 10.30**

*Comparison of dimensionless wave run-up heights  $R_{u2\%}/H_{2\%}$ .*

### 10.5.5 Overtopping

It was observed that both the small and large scale data, with some scatter mainly for very low overtopping discharges, follow the exponential distribution:

$$\frac{q}{\sqrt{g \cdot H_{m0}^3}} = a \cdot \exp\left(-b \cdot \frac{R_c}{H_{m0}}\right) \quad (10.2)$$

The  $a$  coefficient is fixed to 0.2 as given in the non-breaking wave formula by Van der Meer and Janssen, 1994. The  $b$  coefficient is selected to 2.6 and a reduction factor  $\gamma$  is introduced as in the Van der Meer and Janssen, 1994 formula. The  $\gamma$ -value is a product of reduction factors where the roughness factor ( $\gamma_f$ ) is the main contributor for the present conditions. An additional scale reduction factor ( $\gamma_s$ ) is introduced to describe the expected decreased flow resistance in larger scale due to the larger Reynolds numbers.

$$q^* = a \cdot \exp\left(-b \cdot R^* \cdot \frac{1}{\gamma_f \cdot \gamma_s}\right) \quad (10.3)$$

where  $R^* = R_c/H_{m0}$  and  $q^* = q/\sqrt{g \cdot H_{m0}^3}$  have been introduced.  $\gamma_s$  is equal to unity for the prototype conditions. In the present analysis is used  $\gamma_s = 1.0$



for the large scale tests as no scale effects is assumed for  $Re > 4 \cdot 10^5$ . A value smaller than unity is expected in small scale due to higher flow resistance in the upper run-up wedge. A value of 0.90 indicates fictitious run-up heights in the small scale model to be approximately 90% of those in large scale.

The relationship between  $\gamma_s$  and a multiplication factor on  $q$  from small scale to prototype can be calculated as:

$$\begin{aligned}
 f_{scale} &= \frac{q_{prototype}}{q_{model} \cdot N_L^{1.5}} = \frac{q_{prototype}^*}{q_{model}^*} = \frac{\exp\left(-b \cdot R^* \cdot \frac{1}{\gamma_f}\right)}{\exp\left(-b \cdot R^* \cdot \frac{1}{\gamma_f \cdot \gamma_s}\right)} \\
 &= \left[ \exp\left(-b \cdot R^* \cdot \frac{1}{\gamma_f}\right) \right]^{1-1/\gamma_s} = \left[ \frac{q_{prototype}^*}{a} \right]^{1-1/\gamma_s} = \left[ \frac{q_{model}^*}{a} \right]^{\gamma_s-1}
 \end{aligned} \tag{10.4}$$

$a = 0.20$  is selected as in the Van der Meer and Janssen, 1994 formula. With this formula it is possible to calculate the multiplication factor between small and large scale when either the small scale or prototype conditions are known. In Fig. 10.31 the variation of  $f_{scale}$  with  $q_{model}^*$  is given (model values known). In the figure is also given the recommendations given in the CLASH guidelines (Eq. 9.6 and 9.8) calculated for a significant wave height in prototype of 3 m. In the CLASH project only rather small overtopping discharges were measured. The present tests where both small and large overtopping discharges have been measured verifies the exponential trend in both scales in the entire range. Therefore, the present suggested type of correction is expected to be better than the CLASH recommendations. To be discussed are the actual values of  $\gamma_s$  and the influence of the wind.

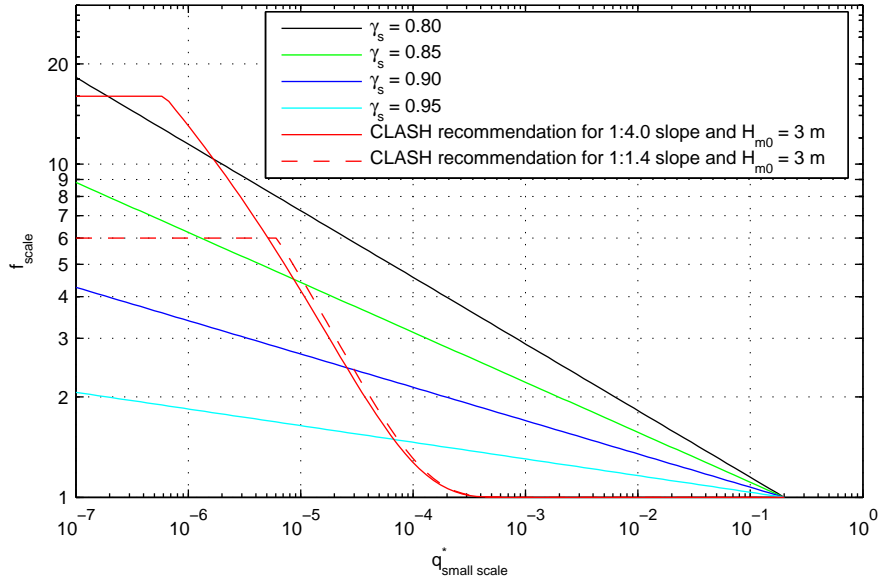


**Figure 10.31**  
*f<sub>scale</sub>* for different values of  $\gamma_s$  compared with the expression proposed in the CLASH project for  $H_{m0} = 3$  m (Eq. 9.6).

In the following figures the overtopping measurements in the two scales are compared for the four different cross-sections defined in Fig. 10.3. Typically this is done in the dimensionless plot  $R_c/H_{m0}$ ,  $q/\sqrt{(g \cdot H_{m0}^3)}$ . However, the wave height distributions are not identical in the present case (model effect) and thus a different approach is chosen here. Here the wave height used for the normalization is chosen to  $H_{1/100}$  as the biggest differences in the wave height distributions have been observed in this range. Also around 1% of the waves were in average overtopping. The results when using the typical dimensionless plot ( $R_c/H_{m0}$ ,  $q/\sqrt{(g \cdot H_{m0}^3)}$ ) is given in the figures in appendix H on the CD-Rom, for which the  $\gamma_s$ -values generally are higher as expected (underprediction of scale effects). However, even using this normalization leads to  $\gamma_s$ -values significantly below 1.0 for the low and normal wall. This clearly demonstrates that there are scale effects, as for identical  $H_{m0}$  the extreme waves are significantly larger in small scale. A more realistic and more conservative estimate of the scale effects is given by the figures in the following sections.

10.5.5.1 Low Wall

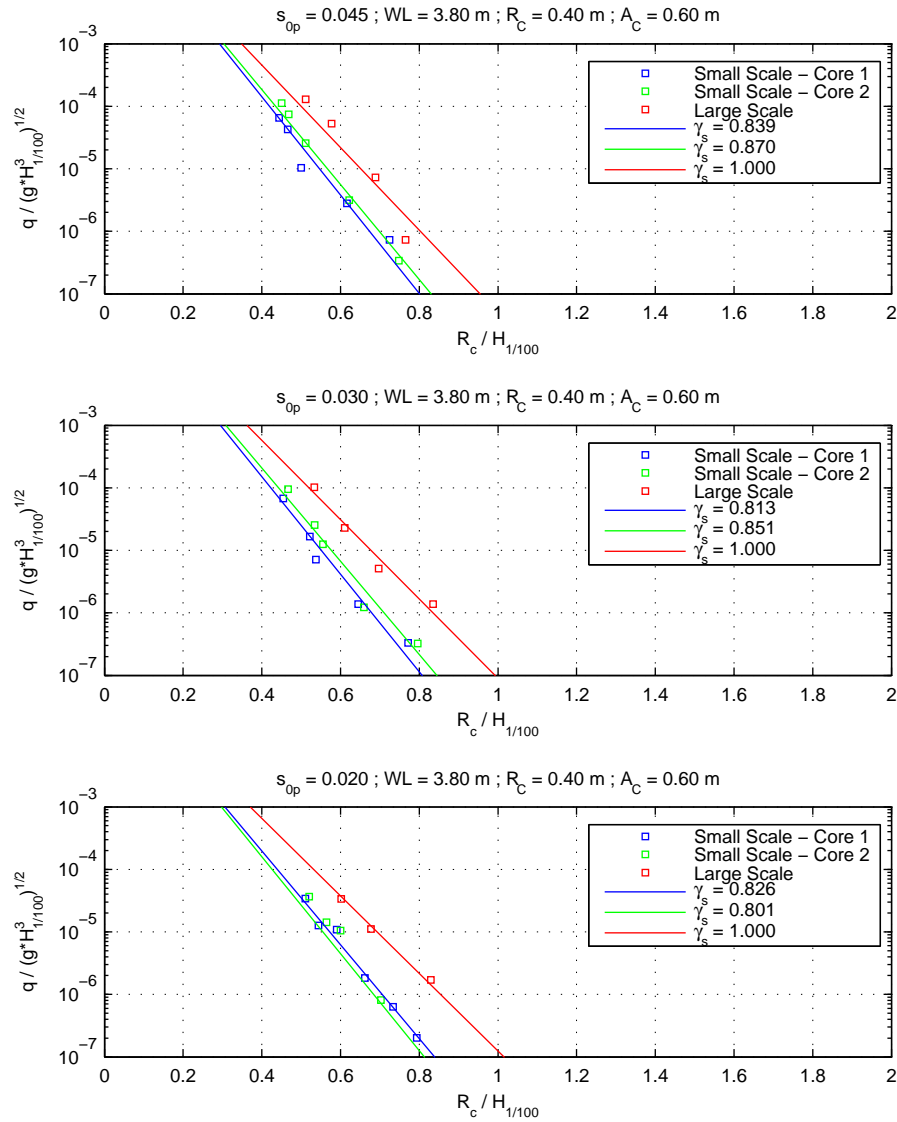
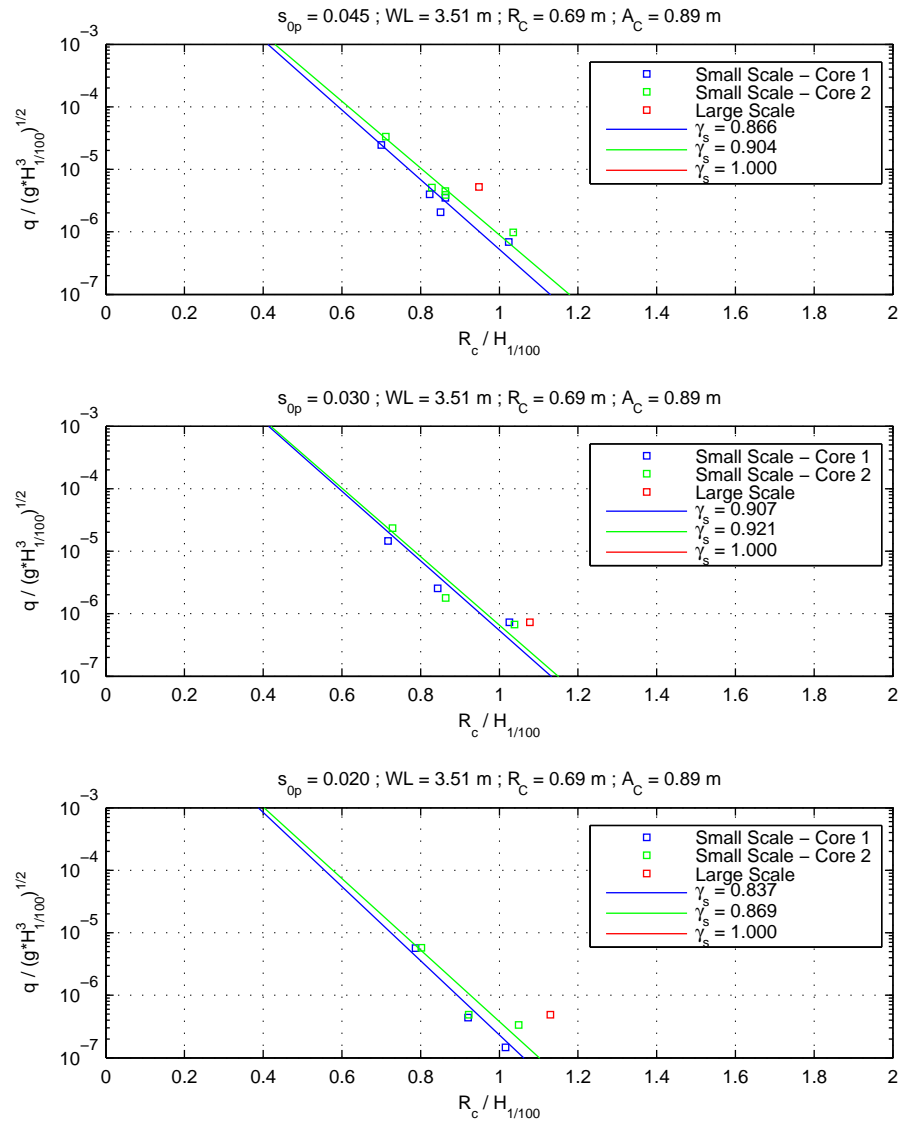
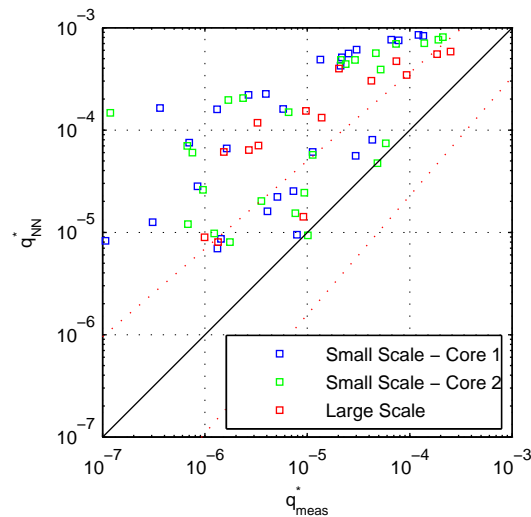


Figure 10.32

Comparison of dimensionless overtopping for high water level (small freeboard) and low wall.



**Figure 10.33**  
 Comparison of dimensionless overtopping for low water level (large freeboard) and low wall.



**Figure 10.34**

*Comparison of wave overtopping and the CLASH NN-model for the low wall case. Dashed lines show the overall 95% confidence band for the NN-model.*

Less overtopping in case of the more coarse Core 2 material was expected. However, from Fig. 10.32 and 10.33 very surprisingly it can be seen not to be the case as only very small differences between Core 1 and Core 2 were observed for this cross-section. The tests with Core 2 are repetition of tests with Core 1 with identical steering signals sent to the paddle.

Large scale overtopping discharges are in all cases with low wall larger than the small scale discharges showing fitted  $\gamma_s$  values in the range 0.80 to 0.92. The differences increases with decreasing wave steepness. An explanation for the larger differences for low wave steepness could be the way the waves impact on the slope. The steep waves breaks on the slope and overtopping is thrown over mainly as spray. For the low wave steepness much more water flows through the armour, and is thus much more influenced by viscous effects in the run-up flow. For the low water level, corresponding to a large freeboard, only few large scale data points are available. Therefore, the  $\gamma_s$ -values in the cases with low water level are very uncertain.

From Fig. 10.34 it can be seen that the CLASH NN-model not can describe overtopping on a low wall where  $R_c < A_c$ . This is probably due to a too little amount of data used in the training of the NN for this type of structure. The uncertainty of the NN estimate is also an output result from the NN model,

## 10.5 Results

---

where different confidence values of the overtopping discharge are given. These values show a much greater uncertainty for this structure than indicated by the average confidence band from all data used in the training, which is the one shown in Fig. 10.34.

10.5.5.2 Normal Wall

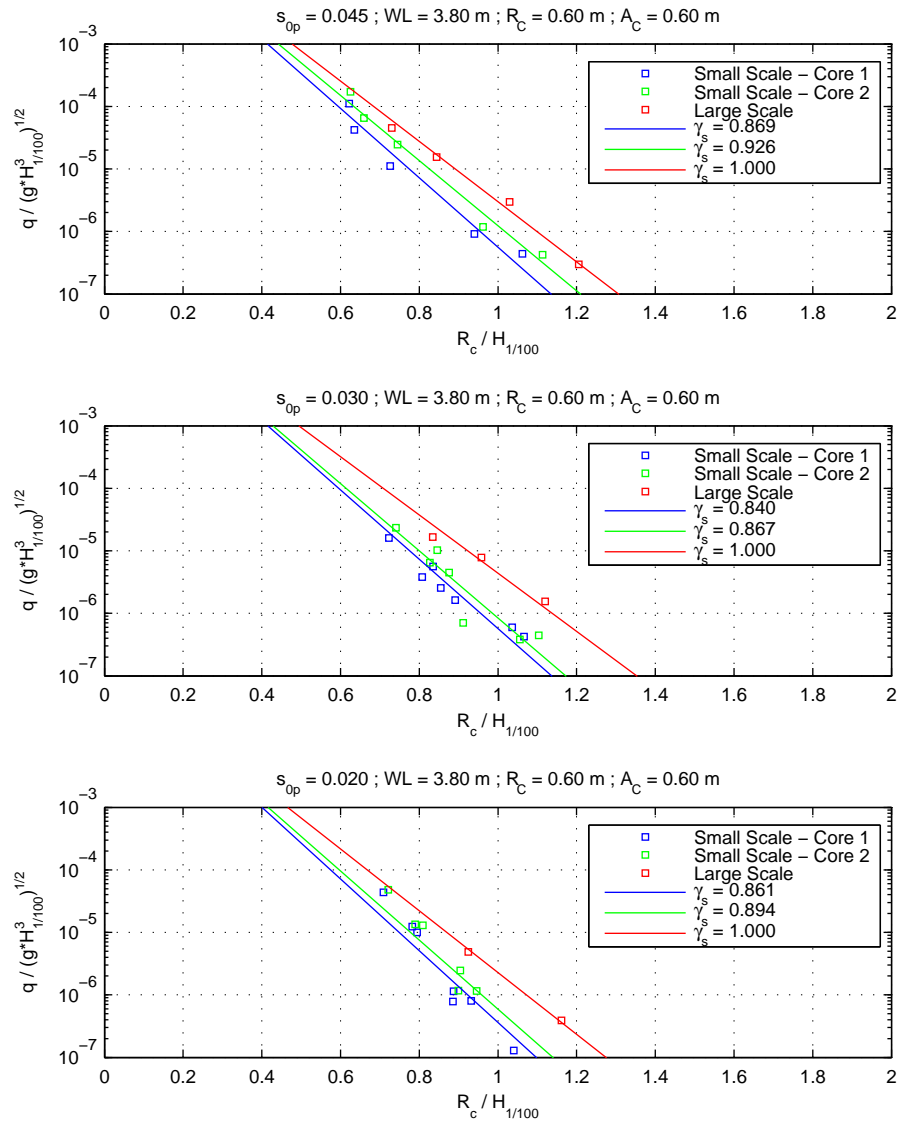
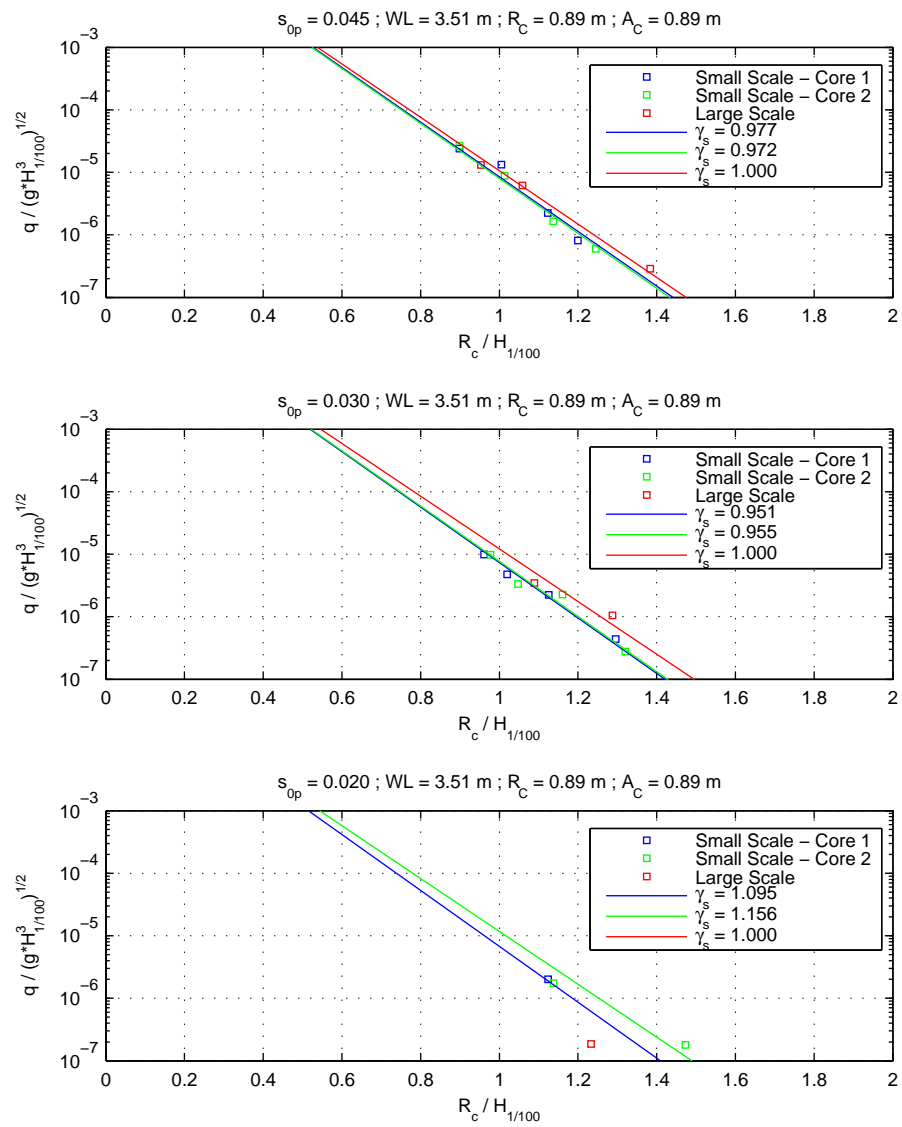


Figure 10.35

Comparison of dimensionless overtopping for high water level (small freeboard) and normal wall.



**Figure 10.36**  
 Comparison of dimensionless overtopping for low water level (large freeboard) and normal wall.



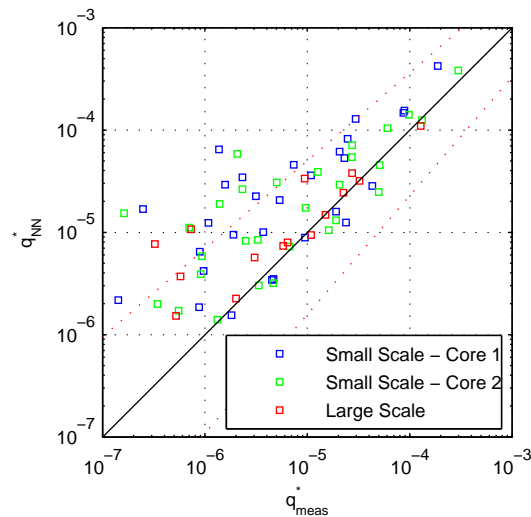


**Figure 10.37**

*Comparison of wave overtopping and the CLASH NN-model for the normal wall case. Dashed lines show the overall 95% confidence band for the NN-model.*

In the normal wall case the coarse Core 2 material does not give less overtopping than Core 1 material, but is within the range of scatter in most cases. When comparing to large scale tests the deviations are much smaller than for the low wall case, but are also for this cross-section very significant in case of high water level.  $\gamma_s$  values are in the range 0.84 to 1.16. For the high water level the same trend as for the low wall is observed, while for the low water level no significant deviations could be identified. It seems as if the water level, and hence the freeboard, has a big influence on the differences between large and small scale results.

The CLASH NN-model performs much better for this structure. Actually the main part of the large scale tests are right on the prediction line. For the small scale tests there is more scatter, but most of the data are also close to the prediction line. The reason for the more scatter is due to more tests performed on the low water level in small scale, because also for the large scale tests the deviations are also larger for this water depth. It is important to be aware that the CLASH NN-model is based on the  $H_{m0}$  wave height and no information on the wave height distribution is included. Therefore, the NN-model is difficult to use for estimating scale effects in the present case.

10.5.5.3 High Wall

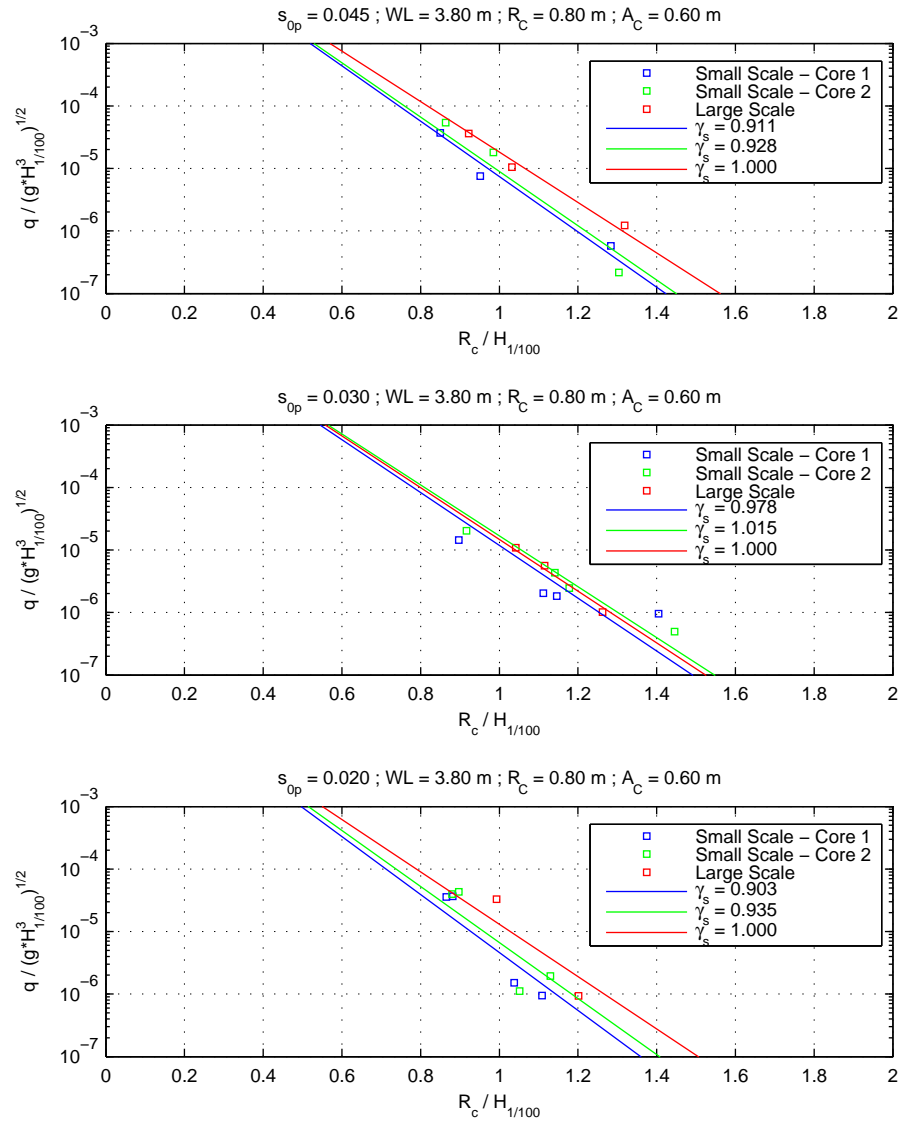


**Figure 10.38**

*Comparison of dimensionless overtopping for high water level (small freeboard) and high wall.*

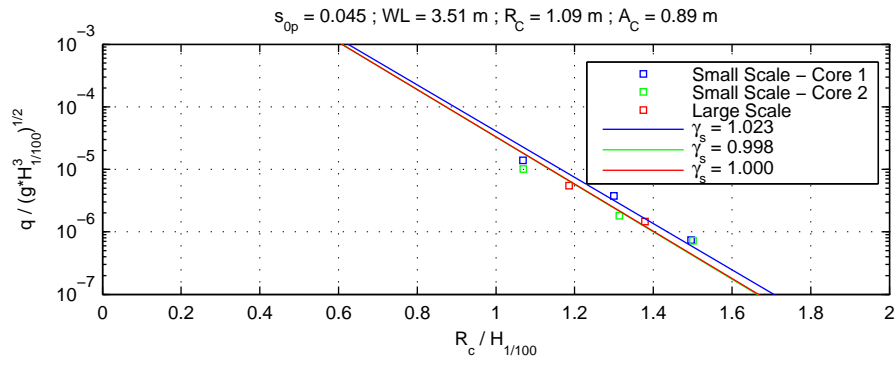


**Figure 10.39**

Comparison of dimensionless overtopping for low water level (large freeboard) and high wall.

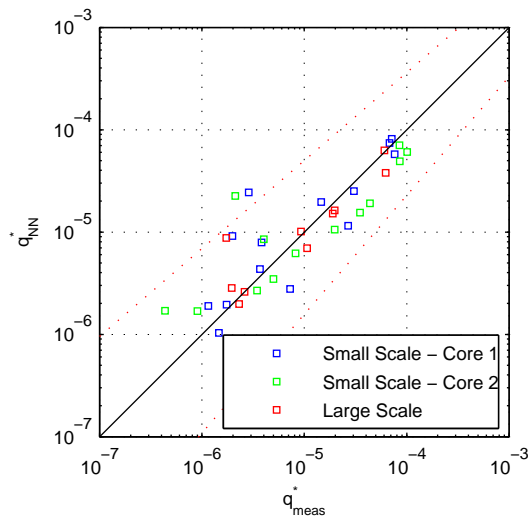


**Figure 10.40**

Comparison of wave overtopping and the CLASH NN-model for the high wall case. Dashed lines show the overall 95% confidence band for the NN-model.

In many cases all data are in good agreement for the high wall case. However, for the high water level slightly higher discharges have been measured in large scale.  $\gamma_s$  is in the range from 0.90 to 1.03. Also for the high wall case the CLASH NN-model performs very well with most data very close to the prediction line.

10.5.5.4 High Recurved Wall

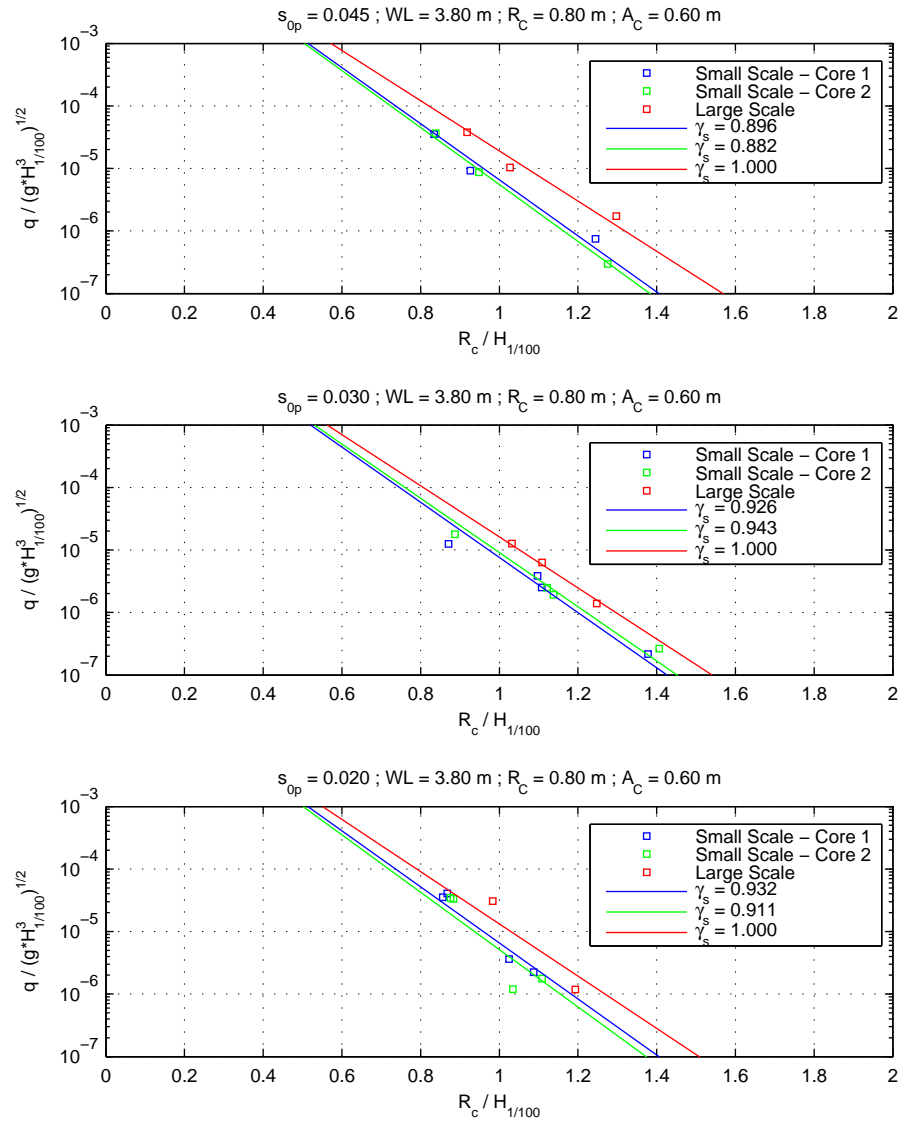
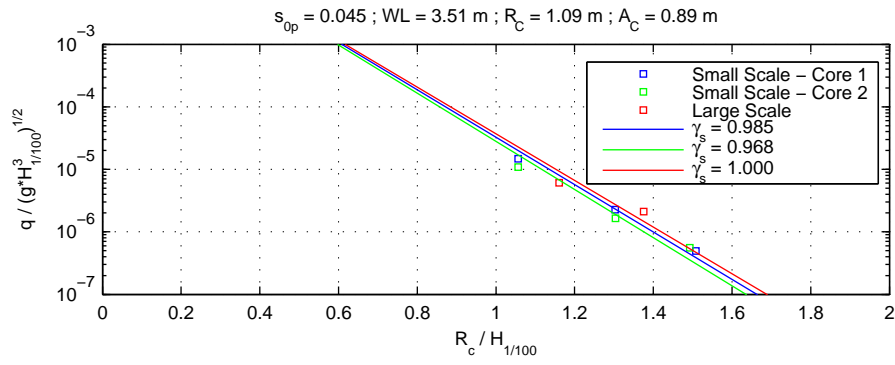


Figure 10.41

Comparison of dimensionless overtopping for high water level (small freeboard) and high recurved wall.



**Figure 10.42**

Comparison of dimensionless overtopping for low water level (large freeboard) and high recurved wall.

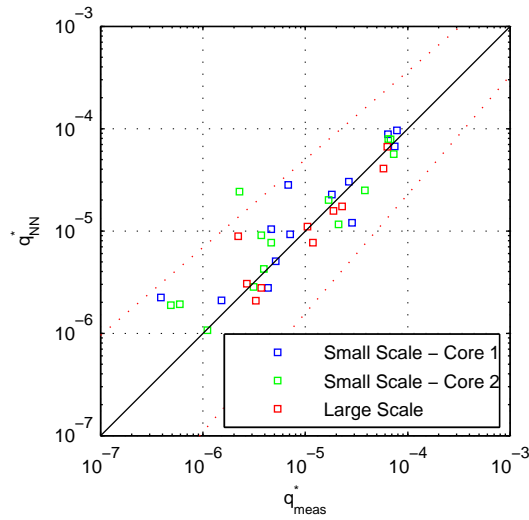


**Figure 10.43**

Comparison of wave overtopping and the CLASH NN-model for the high recurved wall case. Dashed lines show the overall 95% confidence band for the NN-model.

No significant differences were found between the high wall with and without recurve.

### 10.5.6 Influence of Surface Tension and Air Entrainment

The tests with air and pentanol are replay of tests with fresh water by sending the same steering signal to the paddle. The results of these tests are shown in Fig. 10.44. It can be concluded that the effect of adding pentanol and air is in most cases insignificant, indicating that the air content has little influence on the overtopping discharge. Visually the water appears to be much more white during run-up in large scale, which does not necessarily indicate more air in large scale, as smaller bubbles appear more white.

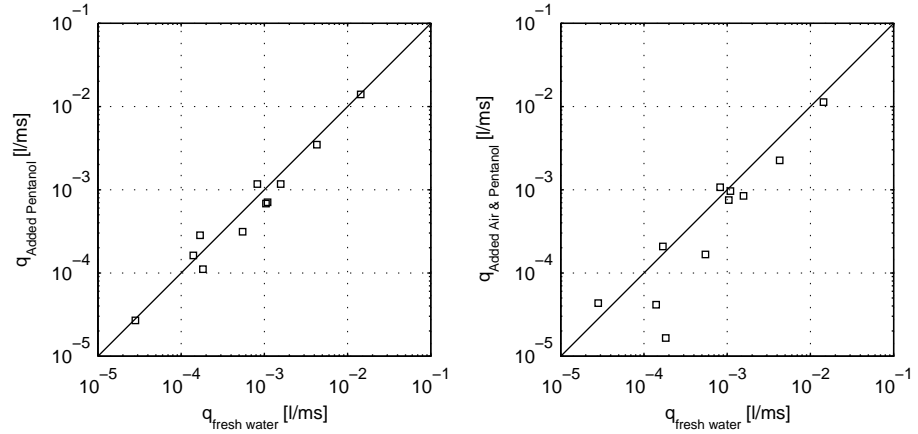


**Figure 10.44**  
*Influence of surface tension and air entrainment.*

### 10.5.7 Spatial Distribution of Overtopping Behind the Shoreward Edge of the Breakwater Crest

In the following sections results on the measured spatial distribution of the overtopping water are presented. More than 1000 overtopping tests including the present data resulted in the distribution function presented in Lykke Andersen and Burcharth, 2006:

$$\frac{x}{\cos(\beta) \cdot L_{0p}} = -\frac{\ln(F) \cdot s_{0p}^{1.05}}{+} 2.7 \cdot \frac{h_{meas}}{L_{0p}} \cdot s_{0p}^{0.15} \quad (10.5)$$

$F$  is the exceedance probability of the travel distance  $x$ , cf. Fig 10.45.  $h_{meas}$  is a parameter signifying the dependence of the distribution of the overtopping water

on the splash down elevation.  $h_{meas}$  is the vertical distance from the crown wall crest level to the splash down level (or level of interest). The definition of the parameter and four examples are shown in Fig. 10.45. Eq. 10.5 is correct in the limit  $x = 0$ ,  $F = 1$  only for  $h_{meas} = 0$ . For  $h_{meas} > 0$  the formula is not correct in this limit as it gives  $x > 0$ , as in reality there will be a little overtopping for  $x$  slightly bigger than zero.

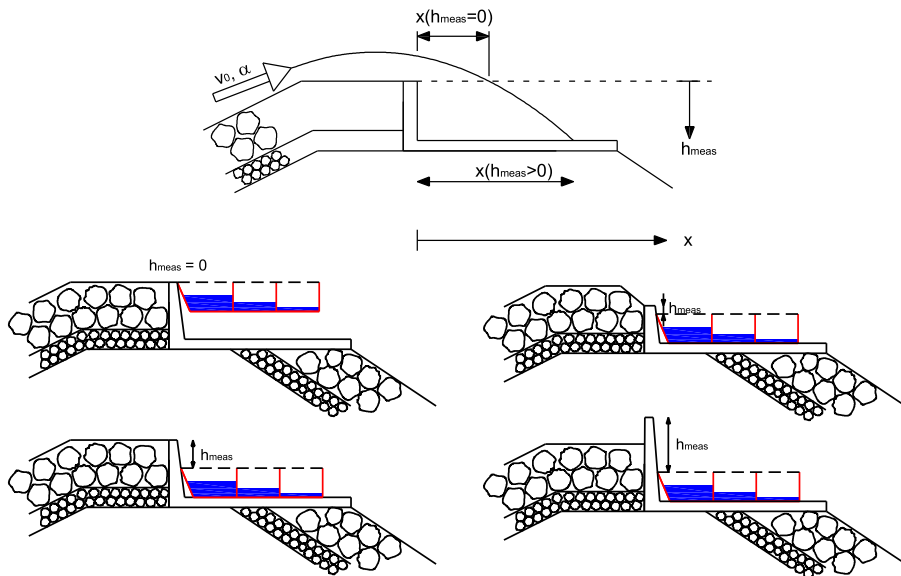


**Figure 10.45**  
Definition of  $h_{meas}$ .

Some distributions have fully or partially been discarded in the present analysis due to very large scatter, mainly related to very small average overtopping discharges typically less than 0.1 l/sm in prototype scale. Only the part of the spatial distribution where the water level raise in the chambers are larger than a specified value during a test is used. This limit is set to approximately 3 mm and 11 mm for the small scale and large scale tests, respectively. For smaller increases in water level the signal/noise ratio is too low.

10.5.7.1 Low Wall

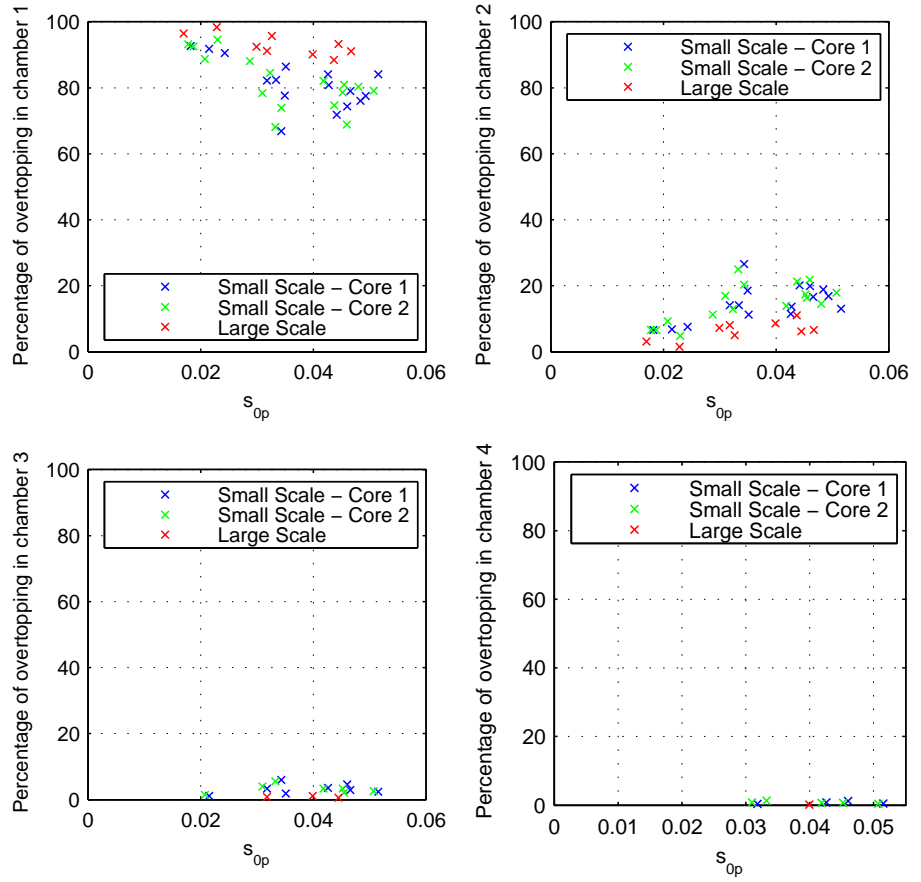


**Figure 10.46**  
Horizontal spatial distribution of overtopping water for the low wall case.



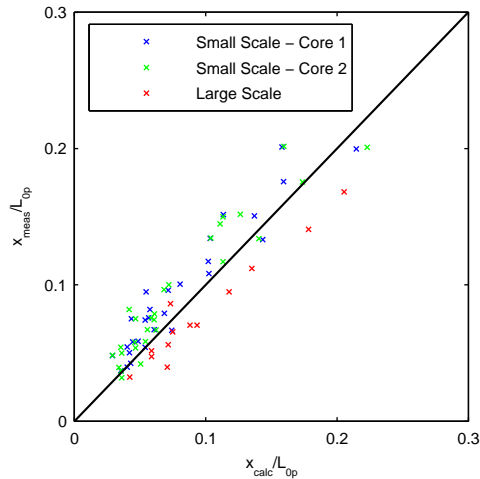


**Figure 10.47**

*Comparison of measured and predicted (Eq. 10.5) dimensionless travel distance  $x$  for the low wall case.*

From Fig. 10.46 is seen that the wave steepness has an influence on the spatial distribution of overtopping, as the travel distance increases with increasing wave steepness. This could also easily be observed visually during the tests. For the low wall there is clearly a difference in the distribution of the overtopping water between the two scales, cf. Fig. 10.46 and 10.47. A larger percentage of overtopping water ends up in chamber 1 in large scale, which indicates that the travel distance is relatively larger in small scale than in large scale. This difference could be expected, as the observed difference in overtopping discharges might have an impact on the spatial distribution. Furthermore, the extreme waves are larger in small scales than in large scale, which also could be expected to influence the distribution of the overtopping water quite significantly. No differences in spatial distribution between small scale tests with Core 1 and Core 2 material are observed.

10.5.7.2 Normal Wall

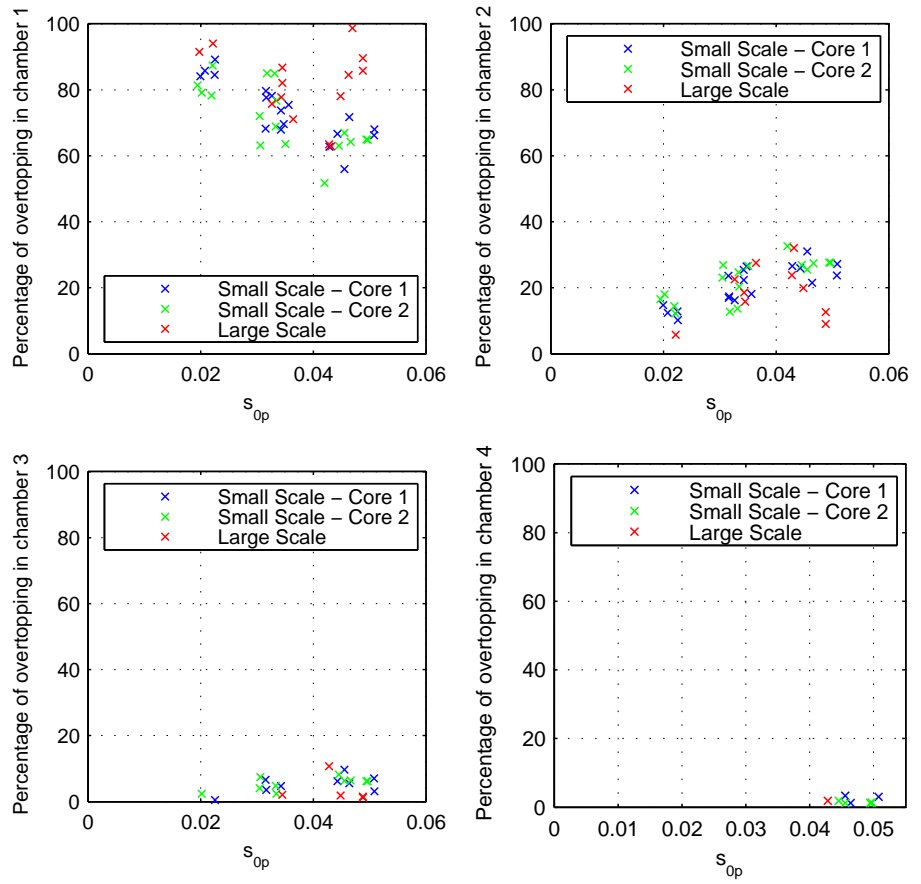


**Figure 10.48**  
Horizontal spatial distribution of overtopping water for the normal wall case.

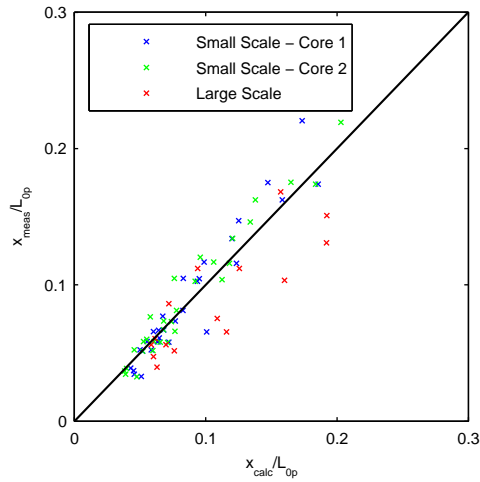


**Figure 10.49**

*Comparison of measured and predicted (Eq. 10.5) dimensionless travel distance  $x$  for the normal wall case.*

For the normal wall the travel distance is clearly larger than for the low wall, which is due to the increased crest freeboard. For the normal wall case the difference between large scale and small scale is less than for the low wall case. This is in excellent agreement with the observed smaller difference in overtopping discharges. In average no significant differences between tests with Core 1 and Core 2 are observed.

10.5.7.3 High Wall

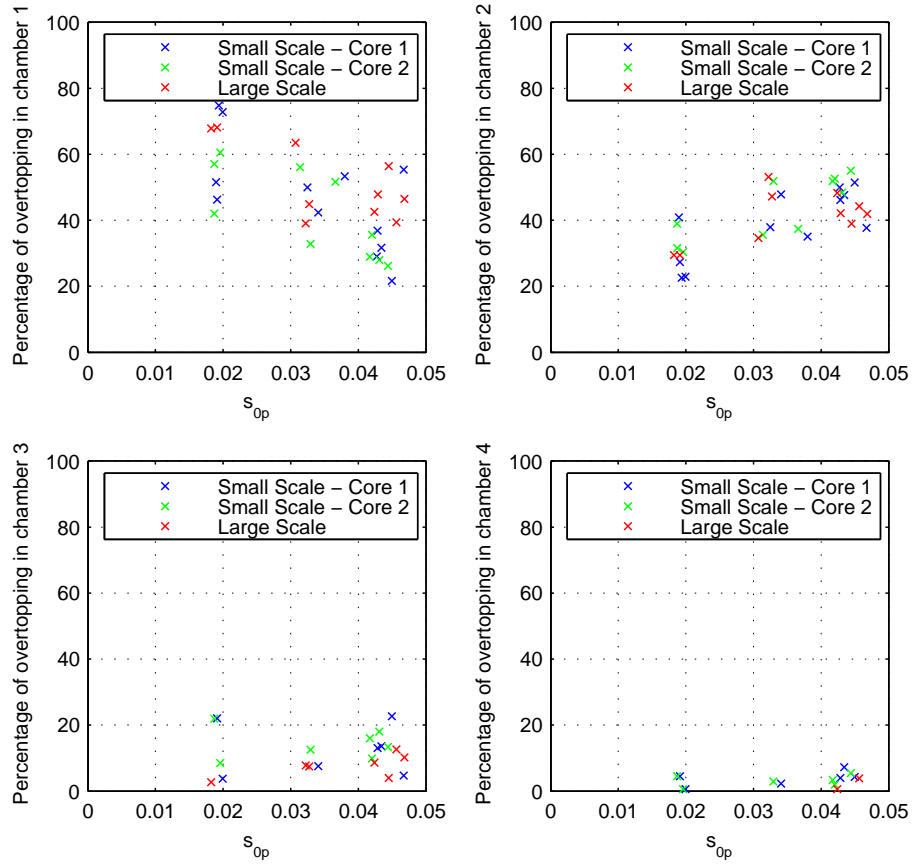


**Figure 10.50**  
Horizontal spatial distribution of overtopping water for the high wall case.

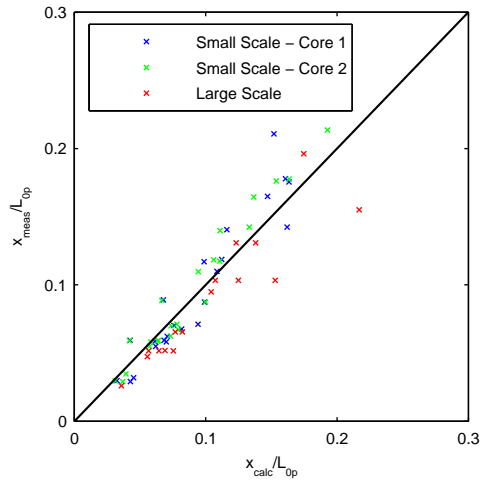


**Figure 10.51**

*Comparison of measured and predicted (Eq. 10.5) dimensionless travel distance  $x$  for the high wall case.*

For the low and normal wall the main part of the overtopping water ends up in the front chamber. Due to the increased freeboard in the high wall case, the distribution changes significantly, and only around half of the overtopping water ends up in chamber 1 and a larger percentage ends up in chamber 2, 3 and 4 in this case. For the high wall case no differences in measured spatial distribution of overtopping water between the two scales are observed. No differences between tests with Core 1 and Core 2 are observed.

10.5.7.4 High Recurved Wall

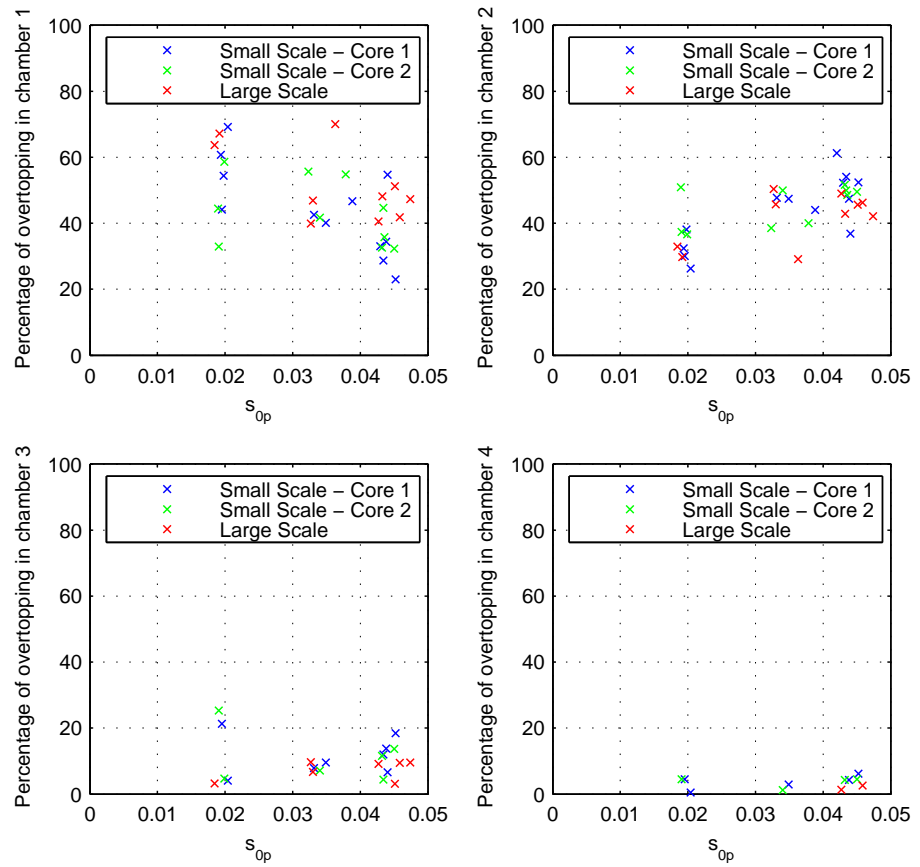


**Figure 10.52**  
 Horizontal spatial distribution of overtopping water for the high recurved wall case.

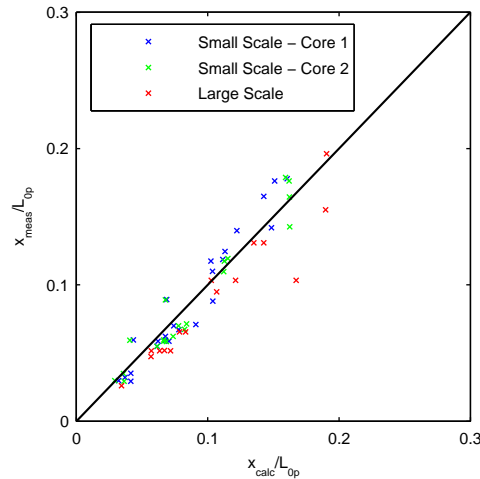


**Figure 10.53**

*Comparison of measured and predicted (Eq. 10.5 ) dimensionless travel distance  $x$  for the high recurved wall case.*

The high wall and the high recurved wall give similar distributions of the overtopping water.

### 10.5.8 Forces from Overtopping

In Fig. 10.54 and 10.55 are given the measured force on the dummy car (plate) as function of the mean overtopping discharge and the maximum single wave overtopping volume, respectively. In both cases are the data scaled to prototype values. The small and large scale tests are in very good agreement. This was also expected assuming that identical overtopping discharges leads to identical overtopping jet velocities, combined with the fact that viscosity is not important for a slim plate with sharp edges. The forces are largest for the two lowest walls, which is due to the fixed position of the plate. The location of the plate was selected to be in the splash zone for the two lowest walls. For the higher wall the main part of the overtopping jet flow above the plate. The forces seems very large, but the duration of the impacts is very small.

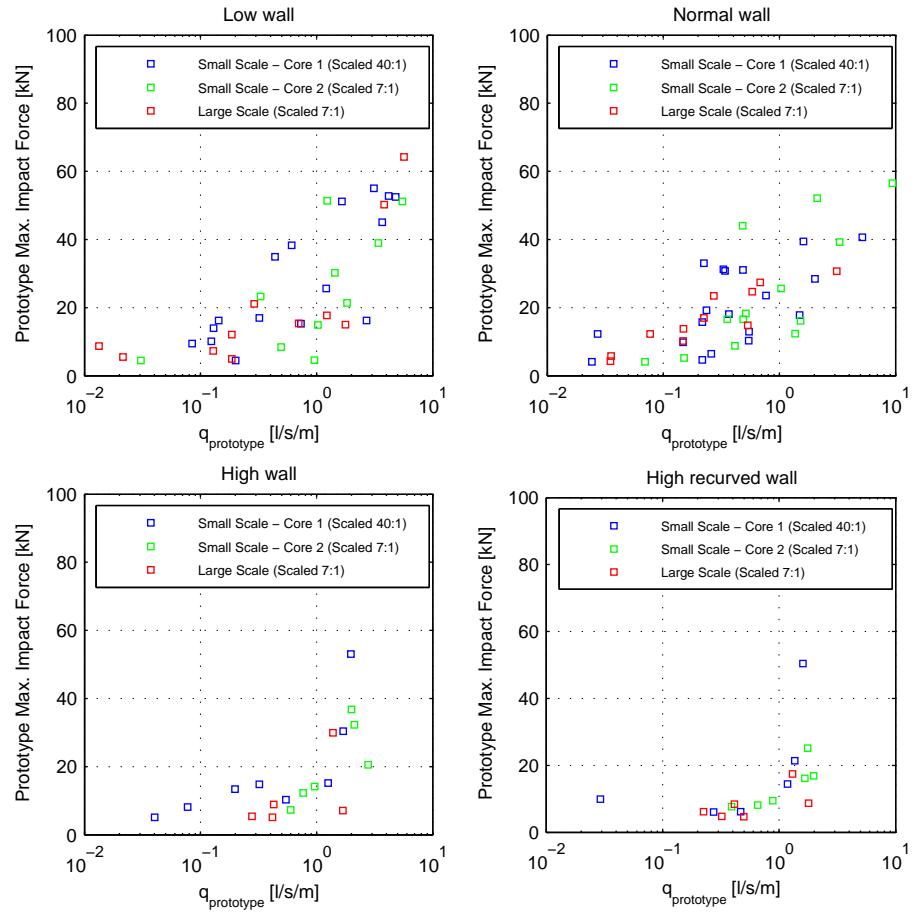


**Figure 10.54**  
*Maximum prototype overtopping impact forces on a plate against prototype mean overtopping discharge.*



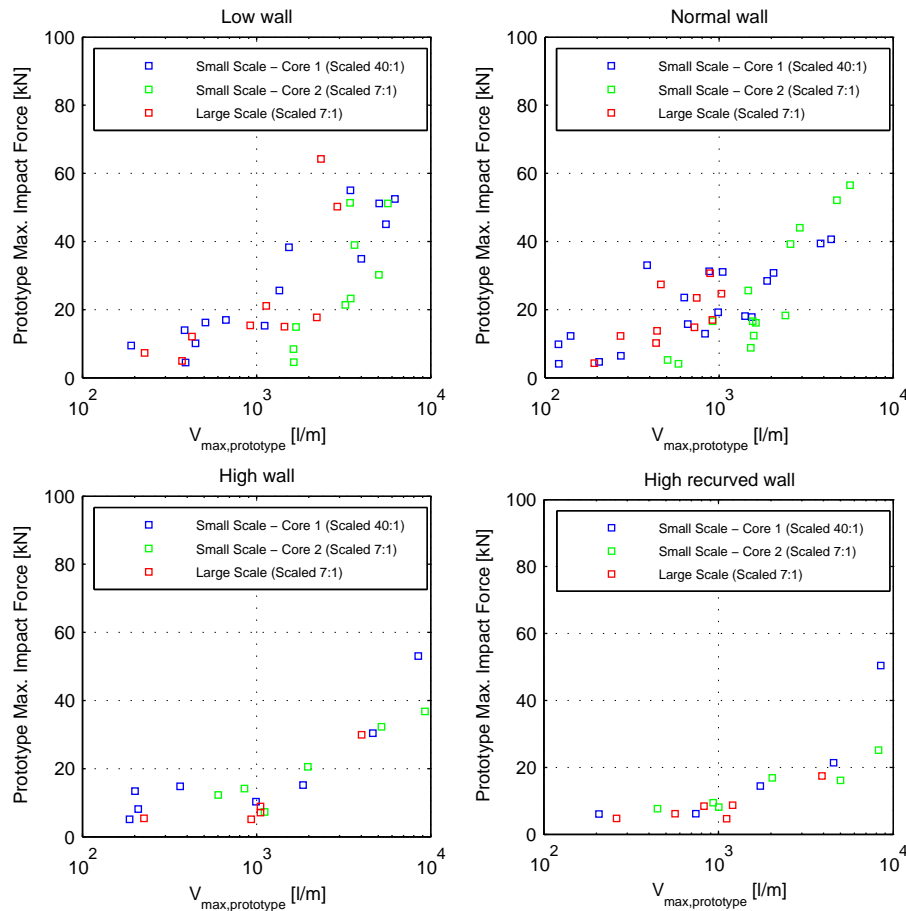


**Figure 10.55**

*Maximum prototype overtopping impact forces on a plate against prototype maximum single wave overtopping volume.*

## 10.6 Summary on Scale Effects related to Overtopping

Comparison of average overtopping discharges in large and small scale tests have been performed. Both the small and large scale tests are performed in fresh water with no wind.

Model effects caused by differences in wave height distributions, wave skewness and wave set-up were identified. Because the wave characteristics are very important for small overtopping discharges, it is difficult to separate these model effects from scale effects. Consequently only some rough estimates on overtopping scale effects can be given.

In a small scale model porous flow scale effects are present and no complete correction can be performed. Two core materials were tested in small scale to study the influence of this effect. The only measurable difference between the two tested core materials was on wave transmission, where the more permeable and coarse material gave approximately twice the amount of transmission measured for the less permeable core material. Wave reflection, water level set-up behind the structure, run-up and overtopping are all very close to be identical for the two core materials. This demonstrates that the porous flow in the core has only little influence on the run-up flow. This is even though the permeability of the two tested cores is significantly different.

Because of the model effects related to the wave characteristics, two different set of dimensionless overtopping plots were considered. In the conventional dimensionless plot, the freeboards and the overtopping discharges are made dimensionless using the  $H_{m0}$  wave height. This gives an underestimation of the scale effects as for identical  $H_{m0}$  wave heights the extreme waves are significantly larger in small scale. Even using this dimensionless plot, which underestimates the scale effects, there were identified larger dimensionless overtopping discharges in large scale for the low and normal wall. This shows clearly a scale effect is present for these cross-sections. The difference is most significant in the case of small armour crest freeboards (high water level).

A more realistic estimate of the scale effects is found by using  $H_{1/100}$  to make the freeboard and overtopping discharge dimensionless. This analysis method leads to more conservative estimates of the scale effects. Also this analysis shows that the difference between large and small scale overtopping discharges is most pronounced in case of small freeboards (high water level). The difference is most significant when the wall is low, where more of the overtopping water flows through the armour crest, which gives more influence of drag. The wave steepness also significantly influences the overtopping flow. For high wave steepness the main part of the overtopping water is thrown over as spray when the wave impact and breaks on the slope. For the low wave steepness much more water flows through the armour layer. This has an influence also on the observed differences, with larger differences for the low wave steepness. For the high wall case the crest berm has, especially for low wave steepness, to be more or less filled with water before overtopping occurs. This reduces the influence of viscosity, and is probably

the reason for only identifying small differences in overtopping discharges for this cross-section. The conclusion is that the magnitude of the scale effects is very dependent on the top geometry of the structure.

The run-up results are subjected to considerable model effects, due to the position of the run-up gauge and using a resistance type gauge, which is less reliable when air is entrained in the water. Therefore, no conclusions on run-up scale effects can be given.

By comparing small and large scale measurements of overtopping generated impact forces on a thin plate, it can be concluded that no significant differences in prototype impact forces on the plate were identified. This was also expected as viscosity is of no importance for a thin plate with sharp edges.

A significant model or scale effect was identified on wave reflection, as significant less reflection was measured in large scale. This is probably due to the wave dissipation on the slope (scale effect), but could also (partly) be due to the different wave kinematics in the two scales (model effect). Clearly the uprushing water appears more white in large scale compared to small scale.



## CHAPTER 11

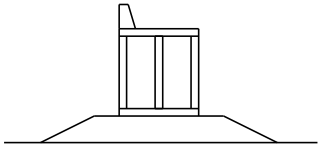
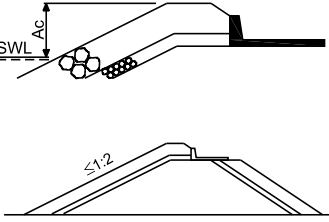
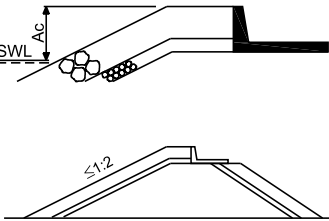
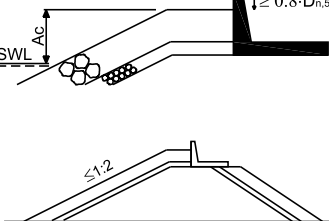
# Guidelines on Scale Effects

Mainly based on the new results presented in chapter 10, and partly on the existing results presented in chapter 9, the guidelines on scale effects in Fig. 11.1 are proposed. The concept of introducing an additional roughness factor is preferred compared to the methodology adopted in the CLASH project, as the new overtopping results show exponential trend both in large and small scale, even for very small overtopping discharges. Because of some model effects it is only possible to give rough guidelines on the size of the scale effects. Moreover only four specific cross sections has been tested, and a quite large variation in size of scale effects has been identified for those four. Therefore, the list of  $\gamma_s$ -values possibly has to be updated when more large scale data are available.

In many of the existing overtopping formulae the influence of roughness is dealt with as a roughness factor. These existing formulae which are based on small scale tests, the roughness factor  $\gamma_f$  should be divided by the  $\gamma_s$  value from Fig. 11.1 to take into account scale effects. For correcting overtopping discharges measured in small scale to prototype values and vice versa, the method given in section 10.5.5 has to be applied. This gives a multiplication factor ( $f_{scale}$ ) on the discharge to take into account scale effects, which can be calculated from  $\gamma_s$  as:

$$f_{scale} = \left[ \frac{q_{prototype}^*}{0.20} \right]^{1-1/\gamma_s} = \left[ \frac{q_{model}^*}{0.20} \right]^{\gamma_s-1} \quad (11.1)$$

The influence of wind is not included in the  $\gamma_s$ -values suggested in Fig. 11.1.

Structure	Overtopping	Wave reflection																		
Vertical wall 	No significant scale effects $\gamma_s = 1.00$	No significant scale effects																		
Rubble mound breakwater with a low crown wall 	<ul style="list-style-type: none"> <li>- Too small overtopping discharges measured in small scale.</li> <li>- Too large travel distance in small scale</li> </ul> <table border="1"> <thead> <tr> <th></th> <th colspan="2"><math>A_c/D_{n,50}</math></th> </tr> <tr> <th></th> <th>2.5</th> <th>3.5</th> </tr> </thead> <tbody> <tr> <td><math>S_{0p}</math></td> <td>0.045</td> <td>0.84</td> <td>0.88</td> </tr> <tr> <td></td> <td>0.030</td> <td>0.82</td> <td>0.92</td> </tr> <tr> <td></td> <td>0.020</td> <td>0.82</td> <td>0.85</td> </tr> </tbody> </table> $\gamma_s$ -values		$A_c/D_{n,50}$			2.5	3.5	$S_{0p}$	0.045	0.84	0.88		0.030	0.82	0.92		0.020	0.82	0.85	Less reflection in prototype
	$A_c/D_{n,50}$																			
	2.5	3.5																		
$S_{0p}$	0.045	0.84	0.88																	
	0.030	0.82	0.92																	
	0.020	0.82	0.85																	
Rubble mound breakwater with a normal crown wall 	<ul style="list-style-type: none"> <li>- Too small overtopping discharges measured in a small scale model, but mainly if the freeboard is small compared to the roughness.</li> <li>- In some cases too large travel distance in small scale</li> </ul> <table border="1"> <thead> <tr> <th></th> <th colspan="2"><math>A_c/D_{n,50}</math></th> </tr> <tr> <th></th> <th>2.5</th> <th>3.5</th> </tr> </thead> <tbody> <tr> <td><math>S_{0p}</math></td> <td>0.045</td> <td>0.90</td> <td>1.00</td> </tr> <tr> <td></td> <td>0.030</td> <td>0.85</td> <td>0.95</td> </tr> <tr> <td></td> <td>0.020</td> <td>0.87</td> <td>1.00</td> </tr> </tbody> </table> $\gamma_s$ -values		$A_c/D_{n,50}$			2.5	3.5	$S_{0p}$	0.045	0.90	1.00		0.030	0.85	0.95		0.020	0.87	1.00	Less reflection in prototype
	$A_c/D_{n,50}$																			
	2.5	3.5																		
$S_{0p}$	0.045	0.90	1.00																	
	0.030	0.85	0.95																	
	0.020	0.87	1.00																	
Rubble mound breakwater with a high crown wall 	<ul style="list-style-type: none"> <li>- Too small overtopping discharges measured in a small scale model, but only if the freeboard is small compared to the roughness.</li> </ul> <table border="1"> <thead> <tr> <th></th> <th colspan="2"><math>A_c/D_{n,50}</math></th> </tr> <tr> <th></th> <th>2.5</th> <th>3.5</th> </tr> </thead> <tbody> <tr> <td><math>S_{0p}</math></td> <td>0.045</td> <td>0.92</td> <td>1.00</td> </tr> <tr> <td></td> <td>0.030</td> <td>0.95</td> <td>1.00</td> </tr> <tr> <td></td> <td>0.020</td> <td>0.93</td> <td>1.00</td> </tr> </tbody> </table> $\gamma_s$ -values		$A_c/D_{n,50}$			2.5	3.5	$S_{0p}$	0.045	0.92	1.00		0.030	0.95	1.00		0.020	0.93	1.00	Less reflection in prototype
	$A_c/D_{n,50}$																			
	2.5	3.5																		
$S_{0p}$	0.045	0.92	1.00																	
	0.030	0.95	1.00																	
	0.020	0.93	1.00																	

**Figure 11.1**

Guidelines for scale effects.  $D_{n,50}$  is the Equivalent cube length exceeded by 50% of the armour stones. In case of concrete armour units  $D_{n,50}$  should be selected on the basis of having equivalent roughness as an armour layer consisting of two layers of rock with diameter  $D_{n,50}$ .

### 11.1 Evaluation of Guidelines on Zeebrugge data

The Zeebrugge breakwater is an antifer cube armoured rubble mound breakwater with a low superstructure, where full scale run-up and overtopping measurements have been performed, cf. section 9.7.2.

The wave steepness ( $s_{0p}$ ) for the obtained overtopping measurements is approximately 0.04.  $A_c/D_{n,50}$  is in the range 3.1 to 3.6. Thus Fig. 11.1 gives a correction factor ( $\gamma_s$ ) between 0.82 and 0.92 with an expected value close to 0.88.

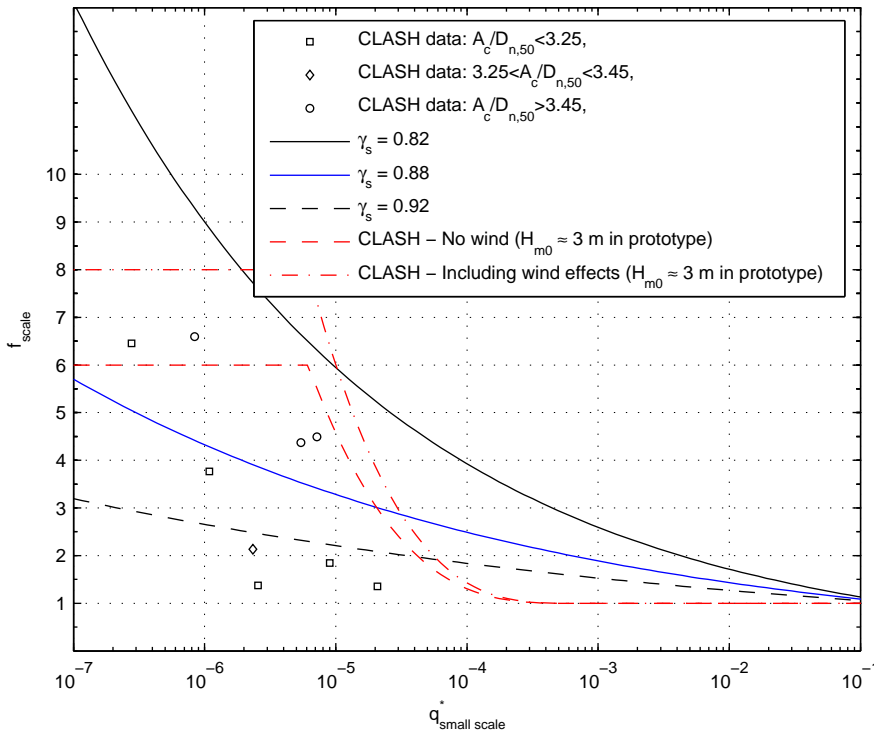


**Figure 11.2**

Comparison of data from Zeebrugge as reported De Rouck et al., 2005 compared to the CLASH revised scaling function for steep slopes (Eq. 9.9) and the present proposed scaling function.

Reasonable agreement between the data obtained for the Zeebrugge breakwater and the proposed guidelines is observed, cf. Fig. 11.2.  $\gamma_s = 0.82$  is a conservative upper limit for the needed correction and  $\gamma_s = 0.92$  is close to the lower limit

of the correction needed.  $\gamma_s = 0.88$  is close to an average correction needed. However, the data does not confirm that the biggest correction is needed for small values of  $A_c/D_{n,50}$ , which maybe could be explained by larger influence of the wind for a large freeboard. The influence of wind is not included in the present proposed correction factors. Therefore, either the influence of wind is not that significant for the prototype data from Zeebrugge, or more likely the proposed correction is conservative for a steep breakwater.

## 11.2 Evaluation of Guidelines on Ostia data

The Ostia breakwater is a rock armoured rubble mound breakwater with a front slope of approximately 1:4. The crest level of the crown wall is identical to the crest level of the armour crest.

For the obtained prototype data in the CLASH project  $A_c/D_{n,50}$  is between 3.2 ad 3.6. The wave steepness is in the range 1% to 2.5%.

The guidelines proposed in Fig. 11.1 gives  $\gamma_s = 0.85$  to 1.00 for a slope 1:2 or less. From the guidelines an expected value of  $\gamma_s$  is found to be close to 1.0. The data from Ostia corresponds to  $\gamma_s = 0.85$ , cf. Fig. 9.5. This deviation can be due to larger scale effects on flatter slopes, wind effects and/or model effects. Much larger possible model effects were identified for the Ostia data compared to the Zeebrugge data.



## CHAPTER 12

# Conclusions

An introduction to the principles and fundamentals of designing rubble mound breakwaters, led to the definition of two important white spots in designing rubble mound breakwaters. These were selected for further investigations in the present thesis.

1. *Design of berm breakwaters:* A generally lack of data and design formulae was identified, but especially wave overtopping was detected as an enormous white spot.
2. *Overtopping scale effects:* The motivation for the CLASH project was an expected scale effect on overtopping of rubble mound structures, leading to unsafe results obtained in a physical model. In the CLASH project comparisons of prototype and model results were performed, which confirmed the expected scale effect as more overtopping was measured in prototype. However, many possible model effects were identified, and it could not be ruled out that the differences observed were due to model effects only. Therefore, one of the main conclusions of the CLASH project was that large tests were needed, in order to obtain reliable recommendations on overtopping scale effects. These have been performed in the present project.

### 12.1 Berm Breakwaters

In the present thesis the results of a large physical model test programme with berm breakwaters were presented. A total of 695 tests were performed with homogeneous berm breakwaters covering the entire interval from non-reshaping to dynamically stable profiles. The test programme led to new design formulae

for front slope stability, rear slope stability and wave overtopping. Further results on wave reflection has been presented and discussed.

The developed overtopping formula has been compared to the little amount of data available from other researchers. Very good agreement was observed in most cases, which verified that the formula could be applied to both homogeneous and multi-layer berm breakwaters. The uncertainty of the formula has been discussed and should be taken into account for design purposes. In contrary to what many expect, the model test study showed more overtopping on reshaped profiles compared to non-reshaped profiles.

Front slope stability of berm breakwaters was not considered as a white spot, but the results of the test programme showed that there was room for big improvements. The most important parameter describing the stability of a homogeneous berm breakwater is the recession of the berm. A design formula was developed to calculate the berm recession. Very good agreement was observed between the developed formula and the main part of the available data. The uncertainty of the formula has been discussed and should be taken into account for design purposes.

A simple conservative design rule for rear slope damage was developed. This is valid for rear slopes 1:1.25 and gives the stability of the rear side as function of the overtopping discharge, rear armour stone size and density.

Results on wave reflection, quantified by the wave reflection coefficients, has been given. The data points are in the area of those for conventional rubble mound structures. However, because reshaping breakwaters have a gentle slope around the water level, berm breakwaters give less reflection than a steeper conventional breakwater do.

## 12.2 Overtopping Scale Effects

To investigate overtopping scale effects comparative small and large scale model tests were performed. 51 large scale tests were performed in the CIEM flume in Barcelona and 170 small scale tests were performed at Aalborg University. The tests were setup to rule out as many sources for model effects as possible. Nevertheless, some important differences in the wave kinematics were identified.

To rule out differences due to porous flow scale effects two different core materials were tested in small scale. A significant difference was found between the two core materials only with respect to wave transmission. Only insignificant differences were found in overtopping discharges, wave run-up heights, wave reflection

coefficients and wave induced set-up behind the breakwater.

The comparison of small and large scale results showed that wave reflection coefficients are significantly lower in large scale compared to small scale. The small scale tests are in pretty good agreement with the improved formula of Postma, 1989, which is based on small scale results. The difference is probably due to different wave-structure interaction in small and large scale (scale effects), but could also be partly or fully due to the different wave kinematics in the two scales (model effects). It was visually observed that much more air was entrained in large scale.

Even though an important model effect was identified, it seems reasonable to conclude that overtopping scale effects are most pronounced for the wall lower than the armour crest and close to non-existent for the wall higher than the armour crest. A simple method to take into account overtopping scale effects has been proposed. The method has been tested against prototype data from Zeebrugge and Ostia. The conclusion is that the proposed guidelines are in pretty good agreement, but slightly conservative, for the data from Zeebrugge, and unsafe for the data from Ostia. This could be due to wind effects, model effects or larger scale effects for a very flat front slope.

Further, the test results showed that overtopping generated impact forces on a plate with sharp edges is not subjected to any scale effects. This was also expected, if no scale effects on overtopping velocities exist.



# Bibliography

- Aalborg University (1995). *Heraklion Airport. Hydraulic Model Test of Slope Protection*. Department of Civil Engineering, Aalborg University.
- Aalborg University (2005a). Erosion profiler. <http://hydrosoft.civil.aau.dk/epro/>.
- Aalborg University (2005b). Wavelab2 homepage. <http://hydrosoft.civil.aau.dk/wavelab>.
- Abecasis, C. and Ferreira da Costa, A. (2004). Funchal airport extension berm breakwater - design, construction and monitoring. *ICCE2004*.
- Alikhani, A. (2000). *On Reshaping Breakwaters*. Ph.D. thesis, Hydraulics & Coastal Engineering Laboratory, Aalborg University.
- Andersen, F. J. and Poulsen, C. (1991). *MAST Berm Breakwaters*. Danmarks Ingeniør Akademi, Lyngby, Copenhagen, Denmark. Thesis carried out at DHI.
- Andersen, O., Juul, J., and Sloth, P. (1992). Rear side stability of berm breakwaters. *International Conference on Coastal Engineering, Venice, Italy*.
- Archetti, R., Franco, L., Muttray, M., Passoni, G., Tautenhain, E., and Zimmermann, C. (1995). Large scale model tests on wave overtopping on rubble mound breakwaters. *International Conference on Coastal and Port Engineering in Developing Countries, Brazil*, pages 1219–1231.
- Archetti, R. and Lamberti, A. (1996). Parametrizzazione del profilo di frangiflutti berma. *Proc. Congresso AIOM, Padova*.
- Ayyub, B. M. and McCuen, R. H. (1997). *Probability, Statistics, & Reliability for Engineers*. CRC Press LLC.

## BIBLIOGRAPHY

---

- Besley, P. (1999). *Wave Overtopping of Seawalls - Design and Assessment Manual*. HR Wallingford, R&D Technical Report W178.
- Biesel, F. (1949). *Calcul de l'ammortissement d'une houle dans un liquide visqueux de profondeur finie*. Houille Blanche, no. 4.
- Bolatti Guzzo, L. and Marconi, R. (1991). Flume tests on a physical model of a berm breakwater. *3rd International Conference on Coastal and Port Engineering in Developing Countries, Mombasa, Kenya*.
- Broderick, L. L. (1983). Riprap stability a progress report. *Proceedings of Coastal Structures '83, American Society of Civil Engineers*,, pages 320–330.
- Brodertick, L. L. and Ahrens, J. P. (1982). *Riprap stability scale effects*. CERC Technical Paper No. 82-3, USA.
- Bullock, G. N., Crawford, A., Hewson, P., Walkden, M. J. A., and Baird, R. A. D. (2001). The influence of air and scale on wave impact pressures. *Coastal Engineering*, 24(4):291–312.
- Burcharth, H. F. (1993). *The Design of Breakwaters*. Chapter 28, Coastal and Harbour Engineering Reference Book, Edited by: Abbott, M. B. and Price, W. A.. E & FN SPON, UK.
- Burcharth, H. F. (2004). *On Scale Effects Related to Run-Up and Overtopping for Rubble Mound Structures*. Department of Civil Engineering, Aalborg University.
- Burcharth, H. F. and Andersen, O. H. (1995). On the one-dimensional steady and unsteady porous flow equations. *Coastal Engineering* 24, pages 233–257.
- Burcharth, H. F. and Christensen, C. (1991). *On Stationary and Non-Stationary Porous Flow in Coarse Granular Materials*. MAST G6-S, Project I, Department of Civil Engineering, Aalborg University.
- Burcharth, H. F. and Frigaard, P. (1990). On 3-dimensional stability of reshaping breakwaters. *Proc. 22th International Conference on Coastal Engineering, Delft*.
- Burcharth, H. F. and Hughes, S. A. (2003). *Coastal Engineering Manual (draft)*.
- Burcharth, H. F., Liu, Z., and Troch, P. (1999). Scaling of core material in rubble mound breakwater model tests. *Proc. Fifth Int. Conf. on Coastal and Port Engineering in Developing Countries, Cape Town, South Africa*, 2:1518–1527.

- Dai, Y. B. and Kamel, A. M. (1969). *Scale Effect Tests for Rubble Mound Breakwaters*. U. S. Army Engineer Waterway Experiment Station, Corps of Engineers, Vicksburg, Mississippi, Research Report H-69-2.
- De Rouck, J. (2005). *CLASH - D46: Final Report*. Ghent University, Belgium.
- De Rouck, J., Boone, C., and Van de Walle, B. (2001). *OPTICREST - FINAL REPORT - Detailed Scientific and Technical Report*. Ghent University, Belgium.
- De Rouck, J., Geeraerts, J., Troch, P., Kortenhaus, A., Pullen, T., and Franco, L. (2005). New results on scale effects for wave overtopping. *ICE2005, London*.
- De Rouck, J., Troch, P., Van de Walle, B., Van der Meer, J. and Van Damme, L., Medina, J., Willems, M., and Frigaard, P. (2000). Wave run-up on a rubble mound breakwater: Prototype measurements versus scale model tests. *Proceedings 27th International Conference on Coastal Engineering (ICCE), ASCE, Sydney, Australia*.
- Delft Hydraulics (1985). *St. George Harbor, Alaska. Two-dimensional tests on scale effects. Three-dimensional tests on breakwater stability*. Delft Hydraulics Laboratory, The Netherlands.
- Delft Hydraulics (1989). *Slopes of Loose Materials: Wave Run-Up on Statistically Stable Rock Slopes*. Report M 1983 (in Dutch), Delft Hydraulics Laboratory, The Netherlands.
- DHI (1995). *EU MAST II Berm Breakwater Structures. Report on the Three-Dimensional Model Tests. Draft Report*. DHI (Danish Hydraulic Institute).
- DHI (1996). *EU MAST II Berm Breakwater Structures. Influence of Permeability and Stone Gradation. Draft Report*. DHI (Danish Hydraulic Institute).
- Frigaard, P. and Brorsen, M. (1995). A time-domain method for separating incident and reflected irregular waves. *Coastal Engineering*, 24.
- Frigaard, P., Jensen, M. S., and Hald, T. (1996). *Berm Breakwater Design - Influence of Rock Shape*. Hydraulics & Coastal Engineering Laboratory, Aalborg University.
- Gilman, J. (2001). St. George harbor - berm breakwater construction issues. *Paper presented at the Fifth Regional Symposium of Pacific Congress on Marine Science and Technology (PACON), San Francisco, California, USA*.

## BIBLIOGRAPHY

---

- Goda, Y. and Suzuki, Y. (1976). Estimation of incident and reflected waves in random wave experiments. *Proc. of the 15th International Conference on Coastal Engineering, Honolulu, Hawaii*, 1:828–845.
- Hall, K. (1994). Influence of wave groups on stability of berm breakwaters. *ASCE Journal of Waterway, Port, Coastal and Ocean Engineering*, 120(6).
- Hall, K. and Kao, S. (1991). A study of the stability of dynamically stable breakwaters. *Canadian Journal of Civil Engineering*, 18:916–925.
- Hall, K. R. (1991). *Report # 1 - Hydraulic Model Test Results - A Study of the Stability of Berm Breakwaters*. Queen's University Coastal Engineering Laboratory.
- Hedar, P. A. (1960). *Stability of Rock-Fill Breakwaters*. Akademiförlaget-Gumperts, Göteborg.
- Helgason, E. (2006). *The influence of rock density on the stability of rubble mound breakwaters*. Aalborg University, unpublished.
- Helgason, E. and Burcharth, H. F. (2006). Comparison between overtopping discharge in small and large scale models. *Abstract for the 30th International Conference on Coastal Engineering, San Diego, California, USA*.
- Holthuijsen, L. H., Booij, N., Ris, R. C., Haagsma, I. G., Kieftenburg, A. T. M. M., Kriezi, E. E., Zijlema, M., and van der Westhuysen, A. J. (2004). *SWAN User Manual - SWAN Cycle III version 40.31*. Delft University of Technology.
- Hudson, R. Y. (1958). *Design of Quarry-Stone Cover Layers for Rubble-Mound Breakwaters, Research Report No. 2-2*. Waterways Experiment Station, CERC, Vicksburg.
- Hughes, S. A. (1993). *Physical Models and Laboratory Techniques in Coastal Engineering*. World Scientific Publishing Co. Pte. Ltd.
- Instanes, A. (1987). *Molostabilitet*. Institut for Marin Byggeteknikk, Trondheim, Norway.
- Jensen, O. J. and Klinting, P. (1983). Evaluation of scale effects in hydraulic models by analysis of laminar and turbulent flows. *Coastal Engineering*, 7:319–329.



- Juhl, J., Van der Meer, J. W., Burcharth, H. F., d'Angremond, K., Sigurdarson, S., Holmes, P., Tørum, A., and Lamberti, A. (1997). *Berm Breakwater Structures. Final Report. MAST contract MAS2-CT94-0087*. DHI (Danish Hydraulic Institute).
- Kajima, R. and Sakakiyama, T. (1994). Review of works using criepi flume and present work. *Proc. Coastal Dynamics, Barcelona, Spain*, pages 614–627.
- Kamphuis, J. W. (1975). *Physical Modeling*. in Handbook of Coastal and Ocean Engineering, J.B. Herbich, Vol. 2, Gulf Publishing Company, Houston, Texas.
- Kao, J. S. and Hall, K. R. (1990). Trends in stability of dynamically stable breakwaters. *Proc. 22th International Conference on Coastal Engineering, Delft*, pages 1730–1741.
- Kudale, M. D. and Kobayashi, N. (1996). Hydraulic stability analysis of lee-side slopes of overtopped breakwaters. *Proceedings of the 25th International Conference on Coastal Engineering, Orlando, Florida*, pages 1721–1734.
- Kuhnen, F. (2000). *Scour and Scour Protection Around Berm Breakwaters*. The Foundation of Industrial and Technical Research (SINTEF), Norwegian University of Science and Technology (NTNU), Trondheim, Norway.
- Le Mehauté, B. (1976). Similitude in coastal engineering. *Journal of Waterways, Harbors and Coastal Engineering Division*, 102(WW3):317–335.
- Lissev, N. (1993). *Influence of the Core Configuration on the Stability of Berm Breakwaters. Experimental Model Investigations*. Report No. R-6-93. Department of Structural Engineering, University of Trondheim, The Norwegian Institute of Technology.
- Lissev, N. and Daskalov, K. (2000). Berm type breakwater - an alternative solution for new east breakwater for port of burgas. *Varna conference, 2000*.
- Losada, M. A. and Gimenez-Curto, L. A. (1981). Flow characteristics on rough permeable slopes under wave action. *Coastal Engineering*, 4:187–206.
- Lykke Andersen, T. and Burcharth, H. F. (2006). Landward distribution of wave overtopping for rubble mound breakwaters. *Proceedings of the First International Conference on the Application of Physical Modelling to Port and Coastal Protection*.
- Mansard, E. P. D. and Funke, E. R. (1980). The measurement of incident and reflected spectra using a least squares method. *Proc. 17th Coastal Engineering Conference, Sydney, Australia*.

## BIBLIOGRAPHY

---

- Menze, A. (2000). *Stability of Multilayer Berm Breakwater*. University of Braunschweig, Germany. Diploma Thesis Carried out at SINTEF/NTNU, Trondheim, Norway, under supervision of Alf Tørum.
- Miller, R. L. (1972). The role of surface tension in breaking waves. *Proceedings 13th International Conference on Coastal Engineering, ASCE, Vancouver, Canada*, 1:433–449.
- Mol, A., Ligteringen, H., Groeneveld, R. L., and Pita, C. R. A. M. (1983). West breakwater-sines. study of armour stability. *Proc. Speciality Conference on the Design Maintenance and Performance of Coastal Structures, Arlington, Virginia, U.S.A.*
- Montgomery, R. J., Hofmeister, G. J., and Baird, W. F. (1987). Implementation and performance of berm breakwater design at racine. *Unconventional Rubble-Mound Breakwaters, Ottawa, Canada*.
- Murphy, J. and Kingston, K. (1996). *Full Scale Dynamic Load Monitoring of Rubble Mound Breakwaters (MAST 2) - Thematic report, B. Wave run-up/run-down*. University College, Cork, Ireland, MAS02/1-893/PTH.
- Nielsen, S. R. K. (1998). *Vibration Theory, Vol. 1 - Linear Vibration Theory*. Aalborg tekniske Universitetsforlag.
- Owen, M. W. (1980). *Design of Seawalls Aallowing for Wave Overtopping*. Hydraulic Research, Wallingford, Report No. EX 924.
- Pearson, J., Bruce, T., Allsop, W., and Gironella, X. (2002). Violent wave overtopping - measurements at large and small scale. *Proceedings 28th International Conference Coastal Engineering, ASCE*, 2:2227–2238.
- PIANC (2003). *PIANC MarCom Report of Working Group No 40. State-of-the-Art of Designing and Constructing Berm Breakwaters*. International Navigation Association. PIANC General Secretariat, Brussels, Belgium. ISBN 2-87223-138-2.
- Porarinnsson, J. S. (2004). *Porlákshöfn-harbour*. Aalborg University. Ms. thesis carried out at Aalborg University under supervision of Peter Frigaard.
- Postma, G. M. (1989). *Wave Reflection from Rock Slopes under Random Wave Attack*. Delft University of Technology, Faculty of Engineering, Delft. M.Sc. Thesis.
- Rauw, C. I. (1987). Berm type armor protection for a runway extension at unalaska. *Presented at Seminar for Berm Breakwaters: Unconventional Rubble-Mound Breakwaters, Ottawa, Canada*.

- Resio, D. T. (1987). *Assesment of Wind Effects on Wave Overtopping of Proposed Virginia Beach Seawall*. Tech. Memo to CERC., OCTI.
- Sakakiyama, T. and Kajima, R. (1998). Scale effects on wave overtopping of seawall covered with armour units. *26th International Conference Coastal Engineering, Copenhagen, Denmark*.
- Sakakiyama, T., Kajima, R., Imai, S., Shimizu, T., and Katayama, H. (1997). Field measurements of wave overtopping on seawall covered with armour units. *Proc. Waves'97*.
- Sarpkaya, T. and Isaacson, M. (1981). *Mechanics of Wave Forces on Offshore Structures*. Van Nostrand Reinhold Company Inc.
- Schüttrumpf, H. (2002). *Wellenüberlaufströmung bei Seedeichen*. ISSN: 0343 - 1223. Leichtweiss-Institut für Wasserbau, Der Technischen Universität Braunschweig.
- Seeling, W. N. (1983). Wave reflection from coastal structures. *Proc. of Coastal Structures '83, ASCE*.
- Sharp, J. J. and Khader, M. H. A. (1984). Scale effects in harbour models involving permeable rubble mound structures. *Symposium on Scale Effects in Modelling Hydraulic Structures, Esslingen, Germany*, pages 7.12-1 – 7.12-5.
- Shiraishi, N., Numata, A., and Endo, T. (1968). On the effect of armour block facing on the quantity of wave overtopping. *Proc. 11th International Conference on Coastal Engineering, London, England*, pages 853-869.
- Sigurdarson, S., Bjornsson, B. J., Skulason, J., Viggosson, G., and Helgason, K. (1999). A berm breakwater on a weak soil extension of the port of hafnarfjörður. *COPEDEC V, South Africa*, 2:1395-1406.
- Sigurdarson, S., Viggosson, G., and Benediktsson, S. (1995). Berm breakwaters and quarry investigations in iceland. *International Conference on Coastal and Port Engineering in Developing Countries, Brazil*, pages 1204-1218.
- Slauenwhite, D. E. and Johnson, B. D. (1996). The effect of organic matter on bubble surface tension in fresh water and sea water. *Journal of Geophysical Research*, 101:3769-3774.
- So, S., Morikita, S., and Takagi, S. and Matsumoto, Y. (2002). Laser doppler velocimetry measurement of turbulent bubbly channel flow. *Experiments in Fluids*, 33(1):135-142.

## BIBLIOGRAPHY

---

- Stive, M. J. F. (1985). A scale comparison of waves breaking on a beach. *Coastal Engineering*, 9:151–158.
- TAW (2002). *Technical Report Wave Run-up and Wave Overtopping at Dikes*. Technical Advisory Committee on Flood Defence, Delft.
- Tørum, A. (1998). On the stability of berm breakwaters in shallow and deep water. *Proc. of the 26th International Conference on Coastal Engineering, Copenhagen, Denmark, ASCE.*, pages 1435–1448.
- Tørum, A., Arntsen, . A., Mathiesen, M., and Bjørdal, S. (2003). *Sirevåg Berm Breakwater. Comparison Between Hydraulic Model and Prototype behaviour*. Norwegian University of Science and Technology, NTNU, Department of Civil and Transport Engineering.
- Tørum, A. and Krogh, S. R. (2000). *Berm Breakwaters. Stone Quality. SINTEF Report No. STF22 A00207*. SINTEF, Civil and Environmental Engineering.
- Tørum, A., Krogh, S. R., and Bjørdal, S. (1999). Design criteria and design procedures for berm breakwaters. *Proc. of Coastal Structures'99*, 1:331–341.
- Tørum, A., Mathiesen, B., and Escutia, R. (1977). *Scale and Model Effects in Breakwater Model Tests*. Port and Ocean Engineering under Arctic Conditions (POAC), Norway.
- Tørum, A., Næss, S., Instanes, A., and Vold, S. (1988). On berm breakwaters. *Proc. 21st Coastal Engineering Conference, Spain, 1988*.
- Van de Walle, B. (2003). *Wave run-up on rubble mound breakwaters*. Ghent University.
- Van der Meer, J. W. (1988). *Rock Slopes and Gravel Beaches under Wave Attack*. Delft Hydraulics Communication No. 396.
- Van der Meer, J. W. (1992). Stability of the seaward slope of berm breakwaters. *Coastal Engineering*, 16:205–234.
- Van der Meer, J. W. (2004). Influence of roughness on wave run-up: Scale effect? *Note for CLASH project, Workpackage 7, 3pp*.
- Van der Meer, J. W. and Janssen, J. P. F. M. (1994). Wave run-up and wave overtopping at dikes. *Wave forces on inclined and vertical wall structures, ASCE*.

- Van der Meer, J. W. and Veldman, J. J. (1992). Singular points at berm breakwaters: scale effects, rear, roundhead and longshore transport. *Coastal engineering*, 17.
- Van Gent, M. R. A. (1995). *Wave Interaction with Permeable Coastal Structures*. Delft University of Technology.
- Van Gent, M. R. A. and Pozueta, B. (2004). Rear side stability of rubble mound structures. *Proc. of the 29th International Conference on Coastal Engineering, Lisbon, Portugal*, 4:3481–3493.
- Verhagen, H. J., Van Dijk, B., and Nederpel, A. (2003). Riprap stability of the inner slope of medium-height breakwaters. *Proceedings of Coastal Structures 2003, Portland, Oregon*, pages 213–222.
- Vidal, C., Losasa, M. A., Medina, R., Mansard, R., and Gomez-Pina, G. (1990). Universal analysis for the stability of both low-crested and submerged breakwaters. *Proc. of the 23th International Conference on Coastal Engineering*, pages 1679–1692.
- Viggosen, G. (1990). Rubble mound breakwaters in iceland. *Journal of Coastal Research, Special Issue 7*, pages 41–61.
- Viggosson, G., Sigurdarson, S., and Halldorsson, A. (1993). *Keilisnes Harbour Project, Hydraulic Model Tests, Wave Disturbance Tests of Moored Ships, Breakwater Stability Tests*. Icelandic Harbour Authority.
- Walker, J. R., Palmer, R. Q., and Dunham, J. W. (1976). Breakwater slope stability. *Proc. Civil Engineering in Oceans*, pages 879–898.
- Ward, D. L. (1994). Wind effects on runup and overtopping. *Proc. of the 24th International Conference on Coastal Engineering, Kobe, Japan, ASCE.*, pages 1687–1699.
- Ward, D. L., Zhang, J., Wibner, C. G., and Cinotto, C. M. (1996). Wind effects on runup and overtopping. *Proc. of the 25th International Conference on Coastal Engineering, Orlando, Florida, USA, ASCE.*, pages 2206–2215.
- Zelt, J. A. and Skjelbreia, J. (1992). Estimation incident and reflected wave fields using an arbitrary number of wave gauges. *Proc. 23th International Conference on Coastal Engineering, Venice, Italy*, 1:777–789.